



Biomedical Applications of Nucleic Acid-based Nanoparticles: Gene Regulation and Biosensing

by

Hassan Hussam Fakh

Department of Chemistry, McGill University

Montréal, QC, Canada

December 2021

First Published: April 3rd, 2023

A thesis submitted to McGill University in complete fulfillment of the requirements

for the degree of

Doctor of Philosophy

© Hassan H. Fakh, 2021

Abstract

Nucleic acid therapeutics, such as small interfering RNA (siRNA) and antisense oligonucleotides (ASO), offer unique potential for gene therapy due to their ability to silence disease-associated genes with high selectivity and efficacy. However, significant challenges have impeded their translation into clinical applications, such as instability in biologically relevant media, off-target effects, poor cellular uptake and *in vivo* biodistribution. An attractive solution to these challenges is the use of drug delivery systems that protect and deliver nucleic acid therapeutics to their desired target site, such as liposomes or polymeric nanoparticles. However, approval of these systems has been slow due to hurdles blocking their translation to the clinic, such as polydispersity, toxicity, and off-target effects. Nucleic acid nanotechnology offers a promising alternative, where the nucleic acids themselves are used as a material to build nanostructures for targeted drug delivery. In particular, nucleic acids conjugated to sequence-controlled polymers are a promising class of building blocks: they spontaneously self-assemble into DNA and RNA-based particles (called “spherical nucleic acids” or SNAs) that are monodisperse, bio-degradable, non-toxic, easily functionalized and can themselves be therapeutic. This thesis examines the fabrication and properties of these systems, specifically tailoring them to overcome barriers to nucleic acid therapeutic delivery and to improve their efficacy.

First, we examine improving the selectivity of spherical nucleic acids, by making it stimuli-responsive. We designed these particles to activate their cargo in the presence of a specific intracellular cue, or otherwise they are dormant to avoid off-target effects. Detailed investigation of assembly, stability, and controlled activity *in vitro* was conducted to showcase the promise of such particles. Second, we focus on optimizing the therapeutic activity we can achieve using sequence-controlled spherical nucleic acids, specifically by interfacing nucleic acid nanoparticles with chemical modifications. Specifically, we assemble 2'-Fluoroarabino modified spherical nucleic acids and study the structural parameters necessary for superior activity *in vitro*. A cleavable spacer was demonstrated to be a necessary feature of the design for maximal activity, multiple genes were targeted to showcase the modularity of the system, as well as the superior activity reached with free uptake when we fuse chemical modifications

with spherical nucleic acids. Third, we investigate another sequence-controlled nucleic acid conjugate for the delivery of nucleic acid therapies. The dendritic conjugate exhibits nanomolar affinity to albumin, the most abundant protein in circulation, as shown previously in *in vitro* experiments. In this chapter, we explore the effects of such strong binding *in vivo*, where biodistribution and efficacy are studied. Binding albumin improved therapeutic efficacy in specific organs through systemic administration, and enhanced cell-specific activity when injected locally. The promise of controlling the protein corona using such conjugates and its effect on activity is highlighted. Lastly, in the appendices, we shift focus to producing minimal DNA nanostructures that are adaptable to deliver nucleic acid therapeutics, but also enhance fluorescence readouts in biosensing applications. Design, assembly and optimization of various shapes and sizes is described, highlighting the importance of precise DNA nanostructure control.

Overall, this thesis aims at producing and studying the next generation of nucleic acid nanoparticles for the delivery of nucleic acid therapeutics. We focus on critical parameters that need to be considered in fabricating such particles that will enable nucleic acid therapeutics fulfill their potential, without compromising simplicity and safety.

Résumé

Les thérapies à l'acide nucléique(NA),telles que les petits ARN interférents et oligonucléotides antisenses, offrent un potentiel unique pour la thérapie génique grâce a leur capacité à arrêter l'expression de gènes d'intérêt avec sélectivité et efficacité élevée. Cependant, des défis entravent leur traduction en clinique, tels que leur instabilité dans des milieux biologiques, effets hors cible, faible absorption cellulaire et distribution in vivo. Une solution intéressante est l'utilisation de systèmes d'administration de thérapies tels que les liposomes ou nanoparticules polymères qui protègent et délivrent des NA thérapeutiques aux sites cibles. L'approbation de ces systèmes est lente à cause d'obstacles, tels que la polydispersité, toxicité et effets hors cible. La nanotechnologie des NA offre une alternative prometteuse, où les NA sont utilisés comme matériaux pour construire des nanostructures pour l'administration ciblée de thérapies. En particulier, les NA conjugués à des polymères à séquence contrôlée constituent une classe prometteuse:ils s'auto-assemblent spontanément en particules à base d'ADN et d'ARN(appelées« acides nucléiques sphériques »ou SNA)qui sont monodispersées, biodégradables, non toxiques, facilement fonctionnalisées et peuvent être thérapeutiques en soi. Cette thèse examine la fabrication et propriétés de ces systèmes, en les adaptant pour surmonter les obstacles à l'administration thérapeutique et améliorer leur efficacité.

Tout d'abord, nous examinons l'amélioration de la sélectivité des SNA, en les rendant sensibles. Nous avons conçu ces particules pour activer leur cargaison en présence d'un signal cellulaire spécifique pour éviter les effets hors cible. Une étude détaillée de l'assemblage, stabilité et activité contrôlée in vitro a été menée pour mettre en valeur la promesse de telles particules. Deuxièmement, nous nous concentrons sur l'optimisation de l'activité thérapeutique de ces SNA, en particulier en adaptant des nanoparticules d'NA avec des modifications chimiques. Plus précisément, nous assemblons des SNA modifiés au 2'-Fluoroarabino et étudions les paramètres structurels nécessaires à une activité supérieure in vitro. Nous avons démontré qu'une entretoise clivable est une caractéristique nécessaire du design pour une activité maximale. Plusieurs gènes ont été ciblés pour mettre en valeur la modularité du système, ainsi que son activité supérieure atteinte avec l'absorption libre.

Troisièmement, nous étudions un autre conjugué d'NA à séquence contrôlée pour l'administration de thérapies à base d'NA. Ce conjugué dendritique présente une affinité nanomolaire pour l'albumine, la protéine la plus abondante en circulation, comme montré précédemment dans des expériences in vitro. Dans ce chapitre, nous explorons les effets de cette liaison forte in vivo, ainsi que sa distribution et efficacité. La liaison à l'albumine a amélioré l'efficacité thérapeutique dans des organes spécifiques quand administré systémiquement et a amélioré l'activité de cellules spécifiques lorsque le conjugué est injectée localement. La promesse de contrôler la couronne protéique à l'aide de ces conjugués et l'effet sur l'activité sont mis en évidence. Enfin, nous nous concentrons sur la production de nanostructures d'ADN minimales et adaptables pour fournir des thérapies à l'NA et améliorer les lectures de fluorescence pour des applications de biodétection. La conception, l'assemblage et l'optimisation de différentes formes et tailles sont décrits, soulignant l'importance d'un contrôle précis de la nanostructure d'ADN.

Dans l'ensemble, cette thèse vise à étudier la prochaine génération de nanoparticules d'NA pour l'administration de thérapies d'NA. Nous nous concentrons sur les paramètres critiques à considérer dans la fabrication de telles particules qui permettront aux thérapies à base d'NA de réaliser leur potentiel, sans compromettre ni simplicité ni sécurité.

Acknowledgments

First, I would like to start by thanking my mentor and supervisor Dr. Hanadi Sleiman who has been instrumental to my career over the past 5 years. I am eternally grateful for her believing in my capabilities to become a scientist and welcoming me into her lab. She has provided unconditional support, kept me motivated and believed in me when I did not even believe in myself. She has supported me with various letters for awards and conferences; without here I would have never imagined to be where I am today. Most importantly, I would like to thank her for being an amazing human being, for her understanding of the emotional difficulties that I went through being apart from my family in tough times.

Then, I would like to extend my thank you to staff and faculty of the chemistry department at McGill, for their help and warm welcoming of all international students and assisting us in doing great science. Specifically, I would like to thank my review committee members Prof. Cosa and Prof. Wiseman for the fruitful discussion we had and their productive feedback. A special thank you for Prof. Damha who became another mentor for me and a pivotal element in shaping my career into nucleic acid therapeutics. Your kindness and support I shall cherish forever. A huge thank you goes out to Chantal Marotte who is always there for me and fellow students. Violetta Toader, a huge thank you to you as well for constant support in my syntheses. Adam katolik, i appreciate your constant help with synthesis during our collaboration as well!

I would like to also extend my gratitude to Pof. Pierre Karam and all members of his lab who worked with me at the time. Without Prof. Karam, I would have never been introduced to the exciting world of research and pursue a PhD in chemistry thank you for believing in me and supporting my journey. Ghinwa Darwish, thank you for believing in my abilities as a young scientist; it paid off!

A big appreciation and gratitude towards the NSERC-CREATE program and the Molson & Hilton Hart Fellowship for providing me with scholarships and awards to support my studies.

I also would like to thank the UMASS Medical School crew and the Lab of Prof. Anastasia Khvorova for being such a beautiful chapter in my career. You guys have welcomed me with open arms twice and made my stay so pleasant. Thank you, Prof. Khvorova and Prof. Watts, Marybeth, Matt, Dimas, Qi, Chantal, David and the rest of the group.

Another round of appreciation goes to Quantum Si. Inc, specifically Jeremy Lackey and Xinghua Shi for believing in me and collaborating with us on a very exciting project.

Friends are the bread and butter of life, they are the extended family you choose to add to your own. I have made so many friends during my stay here in Montreal, and without them it would have been so dull. It will be so hard to name each and every person so I will start by thanking every single friend I came across, do know you played a part in my journey one way or another. My beautiful coworkers, the Sleimanellas and Sleimanellos, thank you for being such an awesome crew! Katherine Bujold, thank you for being my lab mom, training me and working with me on exciting projects; you laid a great foundation for me which led me to this thesis! Johans Fakhoury, if Katherine is the mom, you are certainly the dad figure here. I truly appreciate your constant support and for believing in me, even after you have departed the lab you stayed close. I will miss all the good debates and laughs we had inside and outside the lab, I am sure we will carry on when I visit you, Sabrina, Leo and Bismark! Emparsita et Oreo!!! You guys were the best labmates to spend the majority of my years with, I certainly miss all the brunches, hikes and trips for coffee across the street (salade de fruizzzz)! Danny Bousssss, “Wahde chocolate glazzeeee” my lab and gym buddy as well as my neighbor! Your friendship made feel I never left home, thank you boss for all the good memories and the new ones! ASHOOOO, Jathavan Asohan, I am so glad I was around when you joined the lab, our friendship grew over the past two years, and I am so proud to be the one who trained you; you are an amazing scientist and friend, looking forward to seeing what the future holds for you! Thank you so much for being a shoulder to lean on in the lab especially during the toughest periods of the pandemic and thesis-writing. Casey and Felix, my sassy roommates during CSC in Quebec city, thank you both for being amazing friends and colleagues, for being there for me with good advice and support; so proud of both of you! To the rest of the Sleiman lab members: Nicole, Donatien, Micheal, Tuan, Xin, Alex, Pongphak the dragon!, Justin, Alex Rossina, Chris, Dani, Sean Shayne and Shuan, Sepideh and everyone who I might have forgot:

thank you so much for making my stay pleasant, fun and productive! I extend my regards to all the friends I made as well from outside our lab. Amani Hariri and Hala Bou Assi, thank you for taking care of me when I first got here and becoming such a comfort to hang out with.

To my friends who made Montreal feel like home. To Rola, who will have dedicated section solely for her later, thank you for first being my friend and being the amazing person you are. Lara (pampa), Nadim (nadiks), Anastasia (faro buddy!), Andrew (el 3omda), Sarah, Yasmine Naji and Rachad (hike hike!), Olivia (livliv), elie (Elios) thank you for all the amazing nights we danced away, and the amazing food we tasted around Montreal. Thank you specifically to Lara and Rola for being there for me during tough times as well. Hiba (basketball buddy!), thank you for being my friend from day 1 since I met you with Amani, and for keeping my basketball passion alive. A special thank you goes out to Kyril and my Basketball crew (safe space/brunch at kobe's) for the many years we played along side each other, it was a pleasure to play with you and become friends a long the way. I also would like to thank Chuong (Waterboii) for being one of the first people to befriend me and introduce me to the culture in Montreal.

To my friends back home, Thank you Saad, Mohamad-Ali (Panda), Amer, Afif, Tarek, Hicham, Ibrahim, and the saida crew, for staying connected while I am abroad. You guys kept me alive and provided comfort when I needed it the most. Thank you to all my friends I met at AUB as well!

I also would like to thank the city of Montreal for providing amazing local coffee shops and food scene, without these two I certainly wouldn't have been able to stay up and write all these pages.

To my family, I will try to hold back my tears while I write this. To my Father Hussam and Mother Wafaa, there is nothing in this world that I can do to repay you for what you have done for me and continue doing. You invested all your love, energy and resources to raise us to be decent people and provide me and my siblings with the best education possible, knowing that this is the way to survive in the conditions we lived in. For that, I love you both forever and I will do my best to keep making you proud, by trying to be just a fraction of what amazing

people and parents you both are. To my siblings, Mohamad, Nour and Jana, you have no idea how much I missed you all these years I was away and I want you to know that I love you and I hope that I have made you proud. I extend my gratitude to my grandparents, uncles, aunts, cousins, and extended family, for all the love and support.

Last but not least, to the love of my life and partner Rola Hamed. I don't know where to start really, your name and presence is all over the past 4 years. I would first like to thank you for your unconditional love throughout the thick and thin, fun and dark times. Thank you for loving me on my best and on my worst, especially when I get hangry or stressed. Thank you for lifting me up when I was down, when I felt that I cannot do this or I wasn't meant to have a PhD; you motivated me and reminded me of all the work I have put in. Thank you for your caring gestures and kind heart, from providing me with comfort mood (literally she just cooked for me while I was writing this), to supplying hugs and self-care days. Thank you, for simply being you, the amazing, loving, caring soul you are. From the day that I met you, I told you that you are a Gem, and since then you did nothing but be such a valuable and one-of-a-kind person. Without your support and love during the failure of many of my experiments, my internship at Boston, and your care during the pandemic, I am not sure I could have made it. I am so glad that we got hitched this year, and I can't wait to continue spending the rest of my life with you.

Finally, I would like to thank me. Thank you to the younger version of myself who believed in himself. Thank you for working so hard and believing in science. Thank you for being resilient and motivated, which found you a way to come here and escape the destructive environment you were once living in. Thank you for not giving up no matter how many hardships you faced, from being away from your loved ones to all the failures you encountered during your studies. Thank you for choosing to focus on bettering yourself and career instead of wasting your time. Thank you for also appreciating life and giving time for self-care and having a life outside your career with a beautiful balance. Thank you for remaining humble when you succeeded and being a genuinely positive human being. I want to thank me for doing all this hard work, for never quitting, and trying to always do right than wrong.

الْحَمْدُ لِلَّهِ

“It is going to get hard, keep your head strong

If I quit now, then I'm dead wrong

Fighting off this hunger for hours

Big stepper, don't get stepped on

The money might fade, but respect don't

Still going t be me when success gone

I don't speak the language of cowards

I walk through the flame like I'm Teflon.

Can't be afraid of sunlight

Spotlights when it glows

All the pain you hold

Makes you worth your weight in gold”

Jermaine Cole.

“It's beauty in the struggle, ugliness in the success”

Table of contents

Abstract	2
Résumé	4
Acknowledgments	6
Table of contents	11
List of figures	18
List of tables	32
List of abbreviations	33
Contributions	36
1 Introduction	38
1.1. Preface	39
1.2. The Central Dogma of Life and Onset of Disease	39
1.3. Conventional Pharmacotherapeutics and Their Limitations	41
1.4. Nucleic Acid Therapeutics to The Rescue	43
1.4.1. Solid Phase Synthesis of Nucleic Acids	43
1.4.2. Types and Mechanisms of NATs.....	46
1.4.3. Challenges of NATs.....	52
1.5. Chemical Advances in NATs; “Keep Calm and Do Chemistry!”	59
1.5.1. Chemical modifications:	60
1.5.2. Conjugation.....	63
1.5.3. Drug delivery systems.....	66
1.6. Nucleic Acid Nanotechnology: Nucleic Acids Delivering Themselves	84
1.6.1. Taking nucleic acids out of their biological milieu	84

1.6.2.	Structural strategies to build NANPs for NAT delivery	86
1.6.2.1.	Tile-based assembly	86
1.7.	Spherical Nucleic Acids	95
1.7.1.	First reported SNAs: The gold standard	95
1.7.2.	SNAs' attractive properties for the delivery of NATs	97
1.7.3.	Sequence-controlled SNAs (sc-SNAs)	102
1.8.	Scope and Context of This Thesis.....	104
1.9.	References	108
Preface 1	123
2 Minimalist Design of a Stimuli-Responsive Spherical Nucleic Acid for Conditional Delivery of Oligonucleotide Therapeutics	124
2.1.	Abstract	125
2.2.	Introduction	125
2.3.	Results and Discussion.....	128
2.3.1.	Design and assembly of RSNA.....	128
2.3.2.	Characterization of the RSNA loaded with antisense or siRNA cargo	129
2.3.3.	Two keys, one lock	132
2.3.4.	Stability in biological conditions	135
2.3.5.	Unhindered silencing ability and activation on demand.....	136
2.4.	Conclusion.....	138
2.5.	Materials and methods	139
2.6.	Acknowledgement.....	142
2.7.	Supporting Information	142
2.7.1.	General.....	142

2.7.2.	Instrumentation	143
2.7.3.	Design and Synthesis	144
2.7.4.	SNA's loading capacity with bridge strand	148
2.7.5.	SNA's loading capacity with bridge strand	149
2.7.6.	Loading with a different-sized bridge.....	150
2.7.7.	Transfecting cells with trigger strands	152
2.7.8.	Cellular uptake of SNA.....	153
2.7.9.	Specificity of release and targeting.....	154
2.8.	References	156
Preface 2		160
3 Design and Enhanced Gene Silencing Activity of Spherical 2'-Fluoroarabinose Nucleic Acids (FANA-SNAs)		161
3.1.	Abstract	162
3.2.	Introduction	162
3.3.	Results and Discussion.....	166
3.3.1.	Antisense oligonucleotides (ASOs)	166
3.3.2.	Synthesis and characterization of FANA-modified SNAs (FANA-SNAs).....	167
3.3.3.	Gene silencing activity of the SNAs.....	168
3.3.4.	Steric vs stability of spacer	169
3.3.5.	Assessing the cellular uptake of SNAs with varying spacer structure.....	171
3.3.6.	Duration of effect.....	172
3.3.7.	FANA SNA exhibits greater activity compared to free FANA ASO.....	173
3.3.8.	Serum stability	174
3.3.9.	Testing against different mRNA targets	175

3.3.10.	SNA improves transfection-free delivery (gymnosis)	177
3.3.11.	Discussion	179
3.4.	Acknowledgement.....	181
3.5.	Supporting Information	182
3.5.1.	General.....	182
3.5.2.	Instrumentation	183
3.5.3.	Synthesis and purification.....	184
3.5.4.	Table of oligonucleotide sequences	185
3.5.5.	Methods.....	187
3.5.6.	Viability assay.....	190
3.5.7.	Testing Hexaethylene glycol as a spacer	191
3.5.8.	Flow cytometry uptake assessment of SNAs with different spacers	192
3.5.9.	Titration with various concentration of modSurvivin-SNA	194
3.5.10.	Characterization of FANA-(PS-dN4)-SNA	195
3.5.11.	Silencing controls	195
3.5.12.	Agarose gel of SNA assembly	196
3.6.	References	198
Preface 3	203
4 The <i>In Vivo</i> Properties of Albumin-Binding, Dendritic-Lipid Conjugated siRNA		204
4.1.	Abstract	205
4.2.	Introduction	205
4.3.	Materials and methods	208
4.3.1.	Oligonucleotide synthesis	208
4.3.2.	Injection of lipid-conjugated siRNAs into mice	210

4.3.3.	In vivo mRNA silencing experiments.....	210
4.3.4.	Peptide nucleic acid (PNA) hybridization assay.....	210
4.3.5.	Fluorescence microscopy.....	211
4.3.6.	Lipoprotein size exclusion chromatography.....	211
4.3.7.	CD47 protein expression assessment in specific cell-types in the lung via flow cytometry.....	212
4.3.8.	Reverse Phase HPLC analysis of D-siRNA vs DCA-siRNA.....	212
4.4.	Results.....	213
4.4.1.	Protein binding profile of dendritic-modified oligonucleotides.....	213
4.4.2.	Assessment of biodistribution and efficacy of D-oligonucleotides.....	214
4.4.3.	Increase in cell-specific uptake of D-siRNA in local injection site.....	216
4.5.	Discussion.....	219
4.6.	Conclusion.....	222
4.7.	Acknowledgment.....	222
4.8.	Supporting information.....	223
4.8.1.	Hydrophobicity difference between D-siRNA and DCA-siRNA.....	223
4.8.2.	SEC on mice plasma following injection with conjugated oligonucleotides.....	224
4.8.3.	Liver tissue imaging of DCA-siRNA and D-siRNA.....	225
4.8.4.	Preliminary toxicity screening of D-siRNA.....	226
4.9.	References.....	227
5 	Discussion and Conclusions.....	231
5.1.	Discussion, conclusion, and contributions to knowledge.....	231
5.2.	Suggestions for future work.....	235
5.3.	Publications' List.....	238

5.4. References	239
Preface 4.....	243
Appendix I Size-controlled, fully modified minimal-NANPs for therapeutics delivery... 244	
AI.1. Abstract.....	245
AI.2. Introduction	245
AI.3. Results and Discussion	247
AI.3.1. Design.....	247
AI.3.2. Assembly test	248
AI.3.3. Assembly at higher concentration and cleanup:.....	249
AI.3.4. In vivo scale assembly and siRNA loading:	251
AI.3.5. In vivo Biodistribution profile and toxicity:	254
AI.3.6. Silencing activity of siRNA loaded structures:	256
AI.4. Conclusion	258
AI.5. Experimental.....	259
AI.5.1. Oligonucleotide synthesis, purification, MS analysis and assembly	259
AI.5.2. Gel electrophoresis characterization of structures	260
AI.5.3. Animal injections	260
AI.5.4. Fluorescence microscopy	261
AI.5.5. In vitro gene silencing	261
AI.6. References	262
Appendix II Ultrabright DNA Nanostructures for Biosensing.....	264
AII.1. Abstract.....	265
AII.2. Introduction	265
AII.3. Results and Discussion	268

AII.3.1.	Design.....	268
AII.3.2.	Assembly optimization and sequencing with triangle.....	269
AII.3.3.	Square 1 (S1) assembly.....	273
AII.3.4.	Eliminating excess strands by centrifugation filtration.....	275
AII.3.5.	Design of Square 2 (S2) for lower deletion rates.....	276
AII.4.	Conclusion.....	279
AII.5.	Experimental.....	280
AII.5.1.	Oligonucleotide synthesis, purification, and assembly.....	280
AII.5.2.	Gel electrophoresis characterization of structures.....	281
AII.5.3.	Fluorescence spectroscopy.....	281
A1.6	References.....	282

List of figures

Figure 1. 1. A) Crick’s Central Dogma of molecular biology. Solid lines represent natural phenomenon, dotted lines represent special phenomenon (adapted from Ref. ¹) B) The production of protein based on the central dogma, where DNA is transcribed into RNA, which is then translated into protein (adapted from Ref. ⁴).	40
Figure 1. 2. Various drug modalities and what step they target from the protein production pathway (adapted from Ref. ⁵).	42
Figure 1. 3. DNA synthesis cycle on solid support (adapted from eurogentec).	46
Figure 1. 4. Gene regulation with A) ASOs and B) RNAi (adapted from Ref. ²⁵).	48
Figure 1. 5. Genome Editing with CRISPR-Cas9 system (adapted from New England Biolabs Inc.).	50
Figure 1. 6. Oligonucleotides folding into 3D structured Aptamers and the SELEX cycle for their selection. A nucleic acid pool is incubated with its target. Then, unbound nucleic acids are removed from those that folded and bound the target. Afterwards, the binders are eluted from their target and amplified. The process is repeated many times to obtain the best binders. (Adapted from IDT. ³⁷).	52
Figure 1. 7. Pathway of NATs toward their target, and the challenges they face (in red) (Adapted with modification from Ref. ³⁹).	53
Figure 1. 8. Fate of oligonucleotide following systemic administration First, the oligonucleotide should be stable enough to not be degraded and circulate. Then, it should avoid glomerular filtration, which is renal clearance via the kidney. The oligonucleotide is also challenged by the reticuloendothelial system (liver,kidney, bone marrow), which is the macrophage sequestering of the therapeutic. If the oligonucleotide extravasated through the endothelium, it faces another challenge of cellular uptake and lysosome degradation. (adapted from Ref. ⁵¹).	56
Figure 1. 9. A) Uptake pathways reported for oligonucleotides and the key markers used to track the various compartments are shown (adapted and reproduced from Ref. ⁵⁹), B) Depurination and degradation of a DNA strand in acidic conditions (adapted and reproduced from from Ref. ⁶²). ..	58

Figure 1. 10. NATs are informational drugs, which allow the independent optimization of the dianophore without affecting specificity of the drug (adapted from Ref. ¹⁶).....	59
Figure 1. 11. A) Various chemical modifications to nucleic acids at various positions (adapted from Ref. ⁷), B) 2'-Fluoro-ribose (FNA) vs 2'-Fluoro-arabinose modification (FANA). FANA has the fluoro substitution at the 2' position pointing upwards, whereas FNA has it pointing downwards. This results in a more DNA-like structure and puckering for FANA where it has a C2 endo pucker, and a more RNA-like structure and puckering for FNA that adopts a north C3 endo pucker. ⁶⁹⁻⁷¹	62
Figure 1. 12. Various conjugates appended to NATs for improved biodistribution and delivery. a) Cholesterol-conjugated siRNA, b) GalNAc conjugated ASO, c) antibody conjugated siRNA, d) aptamer conjugated siRNA, and peptide-conjugated PMO ASO (adapted and reproduced from Ref. ⁷).	65
Figure 1. 13. Various classes and drug delivery systems, with their advantages and limitations (adapted from Ref. ¹⁰⁴).....	67
Figure 1. 14. A) Structure of liposome-based approved drug Doxil, and lipid nanoparticle (LNP)-based approved drug Onpattro, and their composition. (adapted from Ref. ¹¹¹). B) Onpattro's LNP mechanism of action. (1) After intravenous administration of patisiran, PEG2000-C-DMG dissociates from the LNP as it has a short lipid tail and can exchange with lipoproteins in circulation. Removal of the PEG coating allows endogenous ApoE to associate with the LNP, (2) facilitating uptake into hepatocytes via an ApoE-dependent process. (3) upon internalization via endocytosis, the ionizable DLin-MC3-DMA lipid is protonated (positively charged), as the pH decreases in the endosome. (4) The positively charged DLin-MC3-DMA lipid interacts with the negatively charged endosomal lipid, resulting in disintegration of the LNP, destabilization of the endosome membrane, and release of therapeutic into the cytoplasm. (5) the siRNA therapeutic binds to RISC, leading to the targeted degradation of TTR mRNA and subsequent reductions in the target protein levels. (Adapted from Ref. ⁴⁵).	70
Figure 1. 15. Examples of polymers used to build various vehicles for the delivery of oligonucleotides, as well as modifications that can be appended for additional functionality (PEG for immune stealth, pH-sensitive moieties, and antibodies for targetability) (adapted from Ref. ¹¹⁷).	72

Figure 1. 16. Structure and biodegradation of PLGA (adapted from Ref. ¹¹⁹)	73
Figure 1. 17. Various structural assemblies from amphiphilic block copolymers based on the variation of the critical packing parameter (adapted from Ref. ¹²¹).....	75
Figure 1. 18. multifunctional polymeric micelle that sheds its PEG corona in the environment of the tumor, followed by enhanced uptake and siRNA release in cancer cells (adapted from Ref. ¹²⁷).	77
Figure 1. 19. various structures of cationic dendrimers used for NAT delivery A) polyamidoamine B) phosphorous C) carbosilane and D) polypropylenimine (Adapted from Ref. ¹³³).....	78
Figure 1. 20. Important design factors to consider in engineering the next generation of DDS that can produce promising translational carriers for the delivery of NAT (adapted from Ref. ¹⁰⁴). ...	84
Figure 1. 21. A) DNA duplex double helix structural parameters, showing the specific hydrogen bonding between A-T and C-G, the antiparallel orientation of strands, and dimensions of the helix (adapted from Ref. ¹⁵⁷). B) Holiday junction with sticky ends that assembles into an array (adapted and reproduced from Ref. ¹⁵⁸)......	85
Figure 1. 22. A) Various tile-based assemblies with control over shape and size (adapted from Ref. ¹⁶⁴). B) tile-based star that can deliver functional miRNA in vitro (adapted from Ref. ¹⁶³). ..	87
Figure 1. 23. Toehold mediated strand displacement mechanism which introduces stimuli-responsive and dynamic behavior to NANPs (adapted from Wikipedia)......	88
Figure 1. 24. Design of a multifunctional tubular DNA nanodevice. (a) Illustration of the construction of a siRNAs/drug co-loaded tubular nanodevice based on DNA origami technique. (b) Schematic representation of utilizing the nanodevice for combined cancer therapy (adapted from Ref. ¹⁶⁸)......	89
Figure 1. 25. A) DNA NANPs constructed via wireframe assembly (adapted from Ref. ¹⁷⁵). B) examples of wireframe assemblies for the delivery of NATs: tetrahedron carrying siRNAs and trigonal prisms carrying ASOs with varying amounts (adapted and reproduced from Ref. ¹⁶¹). ..	92
Figure 1. 26. Various structures made from DNA amphiphiles. A) DNA-drug conjugate that assembles into sphere or rod (adapted from Ref. ¹⁵⁹). B) micelles that can be further assembled into rods (adapted from Ref. ¹⁸⁰). C) ASO-PEG and positively charged KALA forming a spherical	

complex to enhance delivery (adapted from Ref. ¹⁸¹). D) Pyrene-DNA amphiphile assembling into a helical ribbon (adapted from Ref.). E) DNA amphiphile that assembles into a vesicle (adapted from Ref. ¹⁸²).....	94
Figure 1. 27. SNA formation by incubating thiol-modified DNA strands with passivated AuNP surface, in aqueous solutions with high salt concentration (adapted from Ref. ¹⁴²).....	96
Figure 1. 28. Schematic diagram showcasing the variety of SNAs that can be made from different material (adapted from Ref. ¹⁴³).....	97
Figure 1. 29. A) Hollow SNAs were synthesized by crosslinking the DNA on the surface of AuNP followed by dissolution of the AuNP. B) schematic representation of the hollow SNA interacting with scavenger receptors that facilitate the uptake of polyanionic ligands (adapted from Ref. ^{142,189}).	99
Figure 1. 30. Examples of SNAs used for the delivery of NATs. A) AuNP SNA that crosses the BBB and delivers siRNAs to treat glioblastoma (adapted from Ref. ¹⁹¹). B) antibody functionalized SNAs for cell-selective delivery (adapted from Ref. ¹⁹³). C) SNAs delivering siRNAs that can restore wound healing in mice (adapted from Ref. ¹⁹⁴). D) immunomodulatory SNAs able to improve on delivery and immunostimulation resulting from CpG motifs (adapted from Ref. ¹⁹⁵).	100
Figure 1. 31. Polymeric SNAs for the delivery of NATs. A) LNP based SNA changes the biodistribution profile and mRNA delivery locus (adapted from Ref. ¹⁹⁸). B) Brush-like DNA amphiphiles assembling into dense SNAs with enhanced uptake and gene regulation (adapted from Ref. ²⁰¹). C) poly(norbornyl) based SNAs, made from both ASOs and siRNAs (adapted from Ref. ^{199,200}).....	101
Figure 1. 32. Sequence controlled conjugates and SNAs produced on the DNA synthesizer and their promising applications. A) The stepwise manner of building a variety of polymers from their monomers in a high-yielding and efficient manner (adapted from Ref. ²⁰³), B) 12 units of hexaethylene conjugated in a sequential manner produce well defined SNAs that show C) enhanced silencing activity when carrying an ASO (adapted from Ref. ²⁰⁵), as well as D) promising biodistribution profile in mice models (adapted from Ref. ⁴²).....	103

- Figure 2. 1.** Schematic representation of the responsive Spherical nucleic acid (RSNA). **A.** The components that assemble to form RSNA. Two ‘pillar’ amphiphilic strands assemble with a ‘bridge’ strand and the oligonucleotide therapeutic (Green) is hybridized to the horizontal portion of the bridge strand. **B.** Strand displacement by two cytoplasmic genetic markers (‘triggers’) releases the bridge strand and the therapeutic cargo, resulting in the responsiveness of the system (hydrophobic part not shown for simplicity) 128
- Figure 2. 2. A.** Scheme of the different states of SNA loaded with Bridge and therapeutic. **B.** Characterization by DLS. **C.** fluorescence/FRET measurements along with agarose gel electrophoresis. Samples are prepared at 5uM concentration of SNA in 1xTAMg buffer. DNA ladder used is GeneRuler DNA Ladder Mix (100-10,000 bp/mass). Gel lanes: 1) SNA, 2) SNA loaded with bridge, 3) RSNA with both bridge and therapeutic, 4) released RSNA after addition of triggers (green star = Cy3, red star = Cy5, arrow indicates FRET)..... 131
- Figure 2. 3.** Specificity of RNSA. Both triggers must be present simultaneously (lane 4) in order to release the cargo. Lane 1: RSNA; lane 2: RSNA with one trigger; lane 3: RSNA with second trigger. lane 4: RSNA with both triggers; lane 5: DNA ladder, GeneRuler DNA Ladder Mix (100-10,000 bp/mass); lane 6: RSNA without cargo. All SNA’s were assembled at 5 μ M and loaded on agarose gel. 133
- Figure 2. 4.** Atomic Force Microscopy characterization of SNA and RSNA. Samples prepared at 5uM SNA concentration in 1xTAMg buffer. 134
- Figure 2. 5.** Serum stability assessment of RSNA and its ability to improve the half-life of the cargo. Aliquots loaded on a 20% denaturing polyacrylamide gel electrophoresis (PAGE). First set of lanes are the denatures RSNA at different incubation times with serum, the second set is for the bridge+ therapeutic. Band intensities were normalized and then fitted with an exponential decay fit to estimate the half-life of the bridge strand. DNA ladder used is GeneRuler Ultra Low Range DNA Ladder (15-300 bp/mass). 135
- Figure 2. 6. A.** Firefly Luciferase knockdown activity of different samples containing ASO. Firefly luciferase activity was measured after 24 hours incubation and normalized to MTT results and ASO-free control. **B.** MTT cell viability assay for cytotoxicity of samples, normalized to ASO-free control. Error bars are SD for triplets of each sample. 137

Figure 2. 7. Testing the importance of the SNA in shutting down the activity of the cargo until released compared to monomeric SNA. Monomeric SNA is the DNA portion of the fully loaded SNA, but lacking the hydrophobic chains.	138
Supplementary Figure 2. 1. design and sequencing of the RSNA. The bridge arms are complementary to the pillars with 14 bases (red and blue), leaving a 7-base toehold for strand displacement (black). The bridge strand's variable and constant regions are shown on the right.	145
Supplementary Figure 2. 2. Agarose gel showing mobility of SNA loaded with different equivalents of bridge strand. SNA assembled at 5 μ M. DNA ladder used is GeneRuler DNA Ladder Mix (100-10,000 bp/mass).	148
Supplementary Figure 2. 3. testing different equivalents of triggers at different timepoints. A. after 5-10 mins incubation. B. after 1-2 hours incubation. gels are 2.5% agarose. All SNAs were prepared at 5 μ M.. DNA ladder used is GeneRuler DNA Ladder Mix (100-10,000 bp/mass)..	149
Supplementary Figure 2. 4. A. Scheme of the different states of SNA loaded with bridge B. Cy5 during characterization using DLS measurements, fluorescence/FRET measurements, and agarose gel electrophoresis. C. Samples prepared at 5uM SNA concentration, in 1xTA buffer. DNA ladder used is GeneRuler DNA Ladder Mix (100-10,000 bp/mass).	151
Supplementary Figure 2. 5. Testing the different transfection times of trigger strands (T) before adding the RSNA. A. Firefly Luciferase knockdown activity of different samples containing ASO. Firefly luciferase activity was measured after 24 hours incubation and normalized to B. MTT.	152
Supplementary Figure 2. 6. Flow Cytometry histogram showing the uptake of naked vs transfected SNA in HeLa Cells after 4-hour incubation.	153
Supplementary Figure 2. 7. Testing the specificity of release of cargo from SNA in the presence of complementary (2XT) and noncomplementary (m 2XT) trigger strands using Firefly Luciferase knockdown assay. (A)Firefly luciferase activity was measured after 24 hours incubation and normalized to the MTT measurement (B).	154

Supplementary Figure 2. 8. Testing the specificity of cargo using Firefly Luciferase knockdown assay. A. Firefly luciferase activity was measured after 24 hours incubation and normalized to the B. MTT measurement.	155
Figure 3. 1. Design and assembly of FANA SNA. Conjugating twelve dodecanediol units to FANA ASO gapmer 18 nt in length results in the formation of an SNA with low polydispersity and well-defined size and shape. The spacer region is modulated to optimize activity. N represents nucleotides, n represents the number of nucleotides. PO and PS represent phosphodiester and phosphorothioate backbone, respectively.	165
Figure 3. 2. Dynamic light scattering and atomic force microscopy characterization of A) FANA-SNA (no spacer) and B) FANA-(PO-dN4)-SNA.	168
Figure 3. 3. Firefly luciferase knockdown activity comparison between various free FANA-ASO and FANA-SNA (see Table 1 for description of the different strands). A. Luciferase activity was measured after 24 h incubation and normalized to CellTiter-Blue and Control (no ASO). B. fluorescence measurement of CellTiter-Blue cytotoxicity results normalized to Control (no ASO). Error bars represent SD of triplicate experiments for each sample. ASO final concentration is 150 nM for all samples.	169
Figure 3. 4. A. Assessing steric versus cleavability of SNAs. The improved activity of mod-(PO-dN4)-SNA could be due to having increased flexibility away from the hydrophobic core, or due to its cleavability and release once in the cytoplasm. B. The new designs with variable spacers. C. Luciferase activity was measured after 24 h incubation and normalized to CellTiter-Blue and Control (no ASO). Error bars represent SD for triplets of each sample. ASO final concentration is 150 nM (in strands) for all samples.	170
Figure 3. 5. Flow cytometry experiment to assess the uptake of various samples in different cell lines. Cells were incubated at 0.5 μ M final concentration of sample (in strands) for 24 hours, followed by detachment and assessment. Samples were made in duplicates. 10,000 cells count was collected for all samples in HeLa and MCF-7 cells, and 1,000 cells count was collected in MDA-453 cells. one duplicate is shown for simplicity.	172

- Figure 3. 6.** Duration of effect: Luciferase activity after 24, 48, or 72 h incubation, and normalized to CellTiter-Blue and Control (no ASO). Error bars represent SD for triplets of each sample. ASO final concentration is 150 nM strands for all samples. 173
- Figure 3. 7. A.** Relative gene silencing activity of SNAs and free ASOs at 150 nM (in strands).
B. Firefly luciferase knockdown assay for a titration of different concentrations of FANA-(PO-dN4)-SNA compared to FANA-(PO-dN4)-ASO, where at 50 nM (in strands) the SNA performs better. Luciferase activity was measured after 24 h incubation and normalized to CellTiter-Blue and Control (no ASO). Error bars represent SD for triplets of each sample. Concentrations tested are: 150, 100, 50 and 10 nM (in strands). 174
- Figure 3. 8.** Serum stability of cleavable vs non-cleavable SNAs over time. Aliquots at different timepoints were treated with Proteinase K and loaded on a A) 20% denaturing polyacrylamide gel electrophoresis (PAGE). Arrows points to fragment moving similarly to the free ASO. B) Plot of relative band intensity for each sample over time. Each sample was normalized to the initial intensity at time 0 h). 175
- Figure 3. 9. A.** CellTiter-Blue cytotoxicity assay comparison between free FANA-ASO and FANA-SNA targeting Survivin. Metabolic activity was measured after 24 h incubation and normalized to Control (no ASO). ASO final concentration is 500 nM (of strands) for all samples
B. qRT-PCR Gene-silencing comparison between free FANA-ASO and FANA-SNA targeting APOB mRNA in HepG2 cells. Knockdown was measured by qRT-PCR after 24 h incubation and normalized to Control (no ASO) and to GAPDH as reference mRNA. Error bars represent SD for triplets of each sample. ASO final concentration is 150nM (of strands) for all samples. FANA-ASO/SNA targeting luciferase was used as a non-targeting control here in both experiments as indicated. 176
- Figure 3. 10.** Gymnotic gene silencing of FANA-SNA, FANA and DNA ASO. Luciferase activity of various samples at 72 h incubation, normalized to CellTiter-Blue and Control (no ASO). Error bars represent SD for triplets of each sample. ASO final concentration is 1 μ M (in strands) for all samples. 178
- Supplementary Figure 3. 1.** Viability assay data for multiple samples in HeLa cells. 190

Supplementary Figure 3. 2. A. Firefly luciferase knockdown activity comparison between various samples normalized to B. MTT results and AON-free control. Error bars represent SD for triplets for each sample.	191
Supplementary Figure 3. 3. Flow cytometry experiment to assess the uptake of various samples in different cell lines. Cells were incubated at 0.5 μ M final concentration of sample for 24 hours, followed by detachment and assessment. Samples were made in duplicates. 10,000 cells count was collected for all samples in HeLa and MCF-7 cells, and 1,000 cells count was collected in MDA-453 cells.	193
Supplementary Figure 3. 4. CellTiter-Blue cytotoxicity assay at various concentrations of NAT. metabolic activity was measured after 24 h incubation and normalized to AON-free control. Error bars represent SD for triplets for each sample.	194
Supplementary Figure 3. 5. Dynamic light scattering and additional atomic force microscopy characterization of A) FANA-SNA (no spacer), B) FANA-(PO-dN4)-SNA and C) FANA-(PS-dN4)-SNA.	195
Supplementary Figure 3. 6. Firefly luciferase knockdown activity comparison between various free FANA-ASO and FANA-SNA. A. Luciferase activity was measured after 24 h incubation and normalized to CellTiter-Blue and Control (no ASO). B. fluorescence measurement of CellTiter-Blue cytotoxicity results normalized to Control (no ASO). Error bars represent SD of triplicate experiments for each sample. ASO final concentration is 150 nM for all samples.....	196
Supplementary Figure 3. 7. 2.5% agarose gel showing the assembly and mobility of Cy3 modified FANA-(PO-dN4)-SNA and FANA-(PS-dN4)-SNA under cy3 emission. Gel was run at 100V for 1hr45mins in 1xTAMg buffer at 4oC.....	197
Figure 4. 1. Structure of the dendritic moiety studied, termed "D" for short.	208
Figure 4. 2. Tabulated retention times of various samples following injection on size exclusion chromatography (SEC). Plasma proteins were monitored at 280 nm and Cy3 labeled oligonucleotides were monitored at 570nm. Plasma samples are collected from mice (n=2) 15 mins after IV injection. Retention times of the various proteins in plasma are assigned as previously demonstrated. ²⁸	214

Figure 4. 3. Comparing in vivo silencing activity of the dendritic conjugate to the standard DCA conjugate targeting Htt mRNA in mice. **A.** structure and chemical modification of the compared samples, **B.** measurement of mRNA levels of Huntington gene in various organs using QuantiGene® (Affymetrix), normalized to a housekeeping gene, Hprt (Hypoxanthine-guanine phosphoribosyl transferase) and presented as percent of NTC control (mean \pm SD) **C.** Bar graph showing accumulation of conjugate siRNA from part B. mRNA levels and siRNA accumulation were from the same experiment, where female mice (20 mg/kg; n = 5–6 mice per group \pm SD) were injected a single subcutaneous injection of each compound and analyzed following 1 week. Data analysis: multiple comparisons = one-way ANOVA, Dunnett test (****p < 0.0001, ***p < 0.001, **p < 0.01, *p < 0.05). n.s., non-significant. 216

Figure 4. 4. Comparing in vivo silencing activity in local injection site of the dendritic conjugate to the DCA conjugate at 20 and 5 mg/kg doses 1 week post injection. CD47 protein levels in lungs of mice were measured using Flow Cytometry following fluorescent antibody staining. Measurement of CD47 protein levels via fluorescent labeling, normalized to a housekeeping gene, Hprt (Hypoxanthine-guanine phosphoribosyl transferase) and presented as percent of NTC control (mean \pm SD). Female mice (n = 4-8 mice per group \pm SD) were injected a single intratracheal injection of each compound and analyzed. Various cell types were separated by fluorescent antibody tagging and gating. 20 mg/kg DCA-siRNA injected mice did not survive, and no data points are available. Data analysis: multiple comparisons = one-way ANOVA, Dunnett test (****p < 0.0001, ***p < 0.001, **p < 0.01, *p < 0.05). n.s., non-significant. Only 20mg/kg D-siRNA statistical significance from 20mg/kg NTC-D-siRNA is shown (5mg/kg statistics is shown in the next figure). 217

Figure 4. 5. Comparing in vivo silencing activity in local injection site of the dendritic conjugate at various time points post injection (1 week vs 2 weeks). CD47 protein levels in lungs of mice were measured using Flow Cytometry following fluorescent antibody staining. Measurement of CD47 protein levels via fluorescent labeling, normalized to a housekeeping gene, Hprt (Hypoxanthine-guanine phosphoribosyl transferase) and presented as percent of NTC control (mean \pm SD). Female mice (5 mg/kg l; n = 5-8 mice per group \pm SD) were injected a single intratracheal injection of each compound and analyzed following A)1 week and B) 2 weeks. Various cell types were separated by fluorescent antibody tagging and gating. Data analysis:

multiple comparisons = one-way ANOVA, Dunnett test (****p < 0.0001, ***p < 0.001, **p < 0.01, *p < 0.05). n.s., non-significant. 218

Supplementary figure 4. 1. Reverse phase HPLC trace following the injection of D-siRNA or DCA-siRNA, showcasing the difference in hydrophobicity between them. 223

Supplementary figure 4. 2. Chromatograms from size exclusion chromatography of plasma from mice that were injected with various conjugates (n = 2, 15 mins post i.v. injection) where proteins were monitored at 280 nm and Cy3-oligonucleotides at 570 nm. 224

Supplementary figure 4. 3. Microscopy images of Liver tissue to get a closer look at the liver delivery differences between DCA-siRNA and D-siRNA. Female mice (10 mg/kg; n = 2 mice per group) were injected with a single subcutaneous injection of each Cy3 labeled compound, and livers were collected after 48 hours. Bottom row is a zoom in image of the upper row. Blue = DAPI nucleus staining, Red = Cy3 fluorescence signal. A more even distribution and cellular uptake is seen for D-siRNA, with evident uptake in hepatocytes (tetrapod large nuclei by DAPI staining) 225

Supplementary figure 4. 4. Initial toxicity screening of D-siRNA via CBC and blood chemistry counts, showing no significant changes in any reading in comparison to DCA-siRNA. Female mice (n=3) were injected with one dose of siRNA (20mg/kg) and blood was collected after 1 week for analysis..... 226

Figure AI. 1. Design, assembly, and parameters of A) triangle, square, and B) cube..... 248

Figure AI. 2. 8% Polyacrylamide native gel showing the sequential assembly of triangle, square and cube at 1uM. samples were Run for 1.5 hr at 130V in 1xTAMg. Lane 1: A1, Lane2: A1+A3, Lane 3: A1+A3+A5, lane 4: A1+A3+A6+A7, lane 5: C1, lane 6: C1+C2, lane 3: C1+C2+C3, lane 4: C1+C2+C3+C4. 249

Figure AI. 3. 8% Polyacrylamide native gel showing assembly of triangle, square and cube at 1 μ M and 5 μ M. samples were run for 1.5 hr at 130V in 1xTAMg. Lane 1: triangle against SFLT1, HTT, and PPIB, Lane2: triangle against HTT, Lane 3: square against SFLT1, HTT, and PPIB, lane

4: square against HTT, lane 5: cube. Orange arrows indicate misfolded structures and leftover strands. 250

Figure AI. 4. Filling of the triangle with increasing amounts of sense strand, as well as assembling the structures at concentrations representative 20nmoles of siRNA. 8% Polyacrylamide native gel showing assembly of various structures assembled at 5 μ M (lanes 1 to 6). samples were run for 1.10 hr (to see left over, time was decreased) at 130V in 1xTAMg. NOTE: we used a Cy3 labeled A4 strand to visualize in both Cy3 and DNA stain channels..... 252

Figure AI. 5. 8% Polyacrylamide native gel showing the triangle and square becoming fully double stranded with 1:1 sense strands, and no need for higher amounts. the addition of the sense strands was done at room temperature following the annealing of the structures, proving that the filling can be done without annealing. samples were run for 1.5 hr at 130V in 1xTAMg 253

Figure AI. 5 Fully assembling the structures at high concentration (20nmoles of antisense strand). 8% Polyacrylamide native gel showing assembly of various structures assembled 20nmoles of antisense strand (lanes 1,2,3), followed by addition of the sense strands in a 1:1 ratio (lanes 4,5) and quick anneal test (lanes 7,8,9). samples were run for 1.5 hr at 130V in 1xTAMg. NOTE: we used a Cy3 labeled A4 strand to visualize in both Cy3 and DNA stain channels 254

Figure AI. 6. In vivo study on the biodistribution and toxicity of various sized structures. A) the samples that were prepared and injected in mice (black6, male, 6-8 weeks old, n=3) via tail vein injection. B) CBC and blood chemistry counts after 24 hours of injection (only significant statistical difference is plotted) and C) representative microscopy images of various organs from different mice groups (blue = DAPI nucleus stain, red = Cy3 fluorescent signal). CBC and blood chemistry abbreviations are defined in experimental data..... 255

Figure AI. 7. 7-point dose response curve to measure gene silencing activity following RNAimax transfection of various samples into HeLa cells, and gene expression via mRNA quantification using Quantigene bDNA assay 2.0. A) 10nM starting dose and B) 100nM starting dose. All concentrations indicate the final amount of siRNA per sample. 257

Figure AII. 1. Scheme of the A) the DNA nanostructures developed to incorporate fluorescently labeled strands and nucleotide carrying strands (multiple dye strands are randomly represented with yellow circles) B) sensing system being used: a DNA sequencing of a target (black) is

happening by synthesizing its complementary (green). Nucleotides are attached to the fluorescent DNA nanostructures (triangle); when that nucleotide is being incorporated to the growing sequence (green), the triangle enters the fluorescence field (such as total internal reflection evanescence field) and the dyes are excited to emit a fluorescent signal that is being captured to report on the incorporation of that specific nucleotide. 267

Figure AII. 2. Design of triangle and square that can carry multiple fluorescent probes..... 268

Figure AII. 3. 6% Polyacrylamide native gel showing the sequential assembly of triangle and its loading with D strands at 1 μ M, under different conditions (RT= room temperature, annealed, following 3-day storage at 4 degrees after annealing). samples ran for 1.5 hr at 130V in 1xTAMg. 269

Figure AII. 4. Loading triangle with nuc strands sequentially. 6% Polyacrylamide native gel showing the sequential assembly addition of nuc strands to the triangle at 1 μ M. Samples were annealed for 2 hours and ran for 1.5 hr at 130V in 1xTAMg. 270

Figure AII. 5. A) 6 % Polyacrylamide native gel showing the assembly of the triangle with fluorescently labeled probe strands Q3 and Q4 at various conditions. B) the fluorescent signal increase between a triangle containing 1 labeled strands vs 3 labeled strands, measured on a fluorescence plate reader following 25-fold dilution of 1 μ M samples (n=2). Yellow circles indicate the strands that are labeled with fluorescent dyes. 271

Figure AII. 6. testing the assembly of fluorescently labeled triangle (Q4) with nucleotide functionalized strands (dC). 6 % Polyacrylamide native gel showing the mobility shift of various samples listed in the figure. Samples were annealed for 2 hours at 1 μ M and ran for 1.5 hr at 130V in 1xTAMg..... 272

Figure AII. 7. Testing the assembly of the square S1 design with dye and nucleotide strands. 6 % Polyacrylamide native gel showing the mobility shift of various samples listed in the figure. Samples were annealed for 2 hours at 1.5 μ M and ran for 1.5 hr at 130V in 1xTAMg. 274

Figure AII. 8. Testing the ability to clean up the square S1 assembly sample by size-exclusion centrifugation filtration by checking assembly on A) 6% native polyacrylamide gel, and B) 10% native polyacrylamide gel to check removal of excess strands. Samples were annealed for 2 hours at 1.5 μ M and ran for 1.5 hr at 130V in 1xTAMg. filtered samples are purified based on size.

Samples indicated with “ ’ ” are resuspended to their original volume and concentration using 1xTAMg buffer. Cy3 channel is used to image the fluorescently labeled samples..... 276

Figure AII. 9. Difference in design between S1 and S2. S1 has 4 regions to bind 4 nucleotide carrying strands, while S2 can only bind one nucleotide strand..... 277

Figure AII. 10. Testing the assembly of Square 2 design, where it carries only 1 nucleotide strand. Samples were annealed for 2 hours at 1.5 μ M and ran for 50 mins at 130V in 1xTAMg. Lane 7 is the eluted buffer from sample 6..... 278

List of tables

Table 2. 1. Sequences of strands and polymers used, color-coded similarly to strands in figures. Complementary strands are of same color. (special amidites/nucleotides: X= dodecane-diol, lower case = phosphorothioated)	147
Table 3. 1. Variation of the ASO or SNA based on their base modification, target, spacer region and conjugation. FANA = 2'-Fluoroarabino nucleic acid with phosphothioate (PS) linkages. ASO = antisense oligonucleotide with PS linkages against firefly luciferase. SNA = strand with 12 units of dodecanediol that assembles into spherical nucleic acid. PO-dN4/8 = 4 or 8 nucleotide spacer with phosphate linkages (PO). PS-dN4/8 = 4 or 8 nucleotide spacer with PS linkages. Survivin = FANA antisense oligonucleotide with PS linkages against Survivin. NegativeASO = non-targeting sequence with PS linkages. mmASO = antisense oligonucleotide against firefly luciferase with 3 mismatches and PS linkages. APOB = FANA antisense oligonucleotide against APOB with PS linkages.	166
Table 3. 2. sequence ID table of all oligonucleotides used in this manuscript. Bold nucleotides are FANA modified bases. D represents dodecane-units. Underline is phosphorothioate linkages, while non-underlined are regular phosphate linkages.	186
Table 3. 3. primers used RT-qPCR experiment for the APOB in HepG2 cells.	189
Table 4. 1. Oligonucleotide sequences synthesized and used.....	209
Table AI. 1. Table containing all the sequences used in this appendix, with MS data.....	260
Table AII. 1. Table containing all the sequences used in this appendix. Similar color-highlighted sequences are complementary to each other. (NNN)n represents the sequence complementary to the dye strands, and (MMM)m represents that complementary to the nucleotide strands.....	281

List of abbreviations

1D	One dimensional
2D	Two dimensional
3D	Three dimensional
A	Adenine
Å	Angstrom
Ab	Antibody
AGE	Agarose gel electrophoresis
AFM	Atomic force microscopy
AS	Antisense
ASO	Antisense Oligonucleotide
AON	Antisense OligoNucleotide
AuNP	Gold nanoparticle
Bp	Base pair
CRISPR	Clustered Regularly Interspaced Short Palindromic Repeats
Cy3	Cyanine 3
Cy5	Cyanine 5
C	Cytosine
C ₁₂	Dodecane
CPG	Controlled pore glass
CMC	Critical micelle concentration
Dh	hydrodynamic diameter
DNA	Deoxyribonucleic acid
DDS	Drug delivery system
D-DNA	Dendritic Deoxyribose nucleic acid
D-siRNA	Dendritic small interfering ribonucleic acid
ds	Double stranded
DMEM	Dulbecco's modified eagle's medium
DMT	Dimethoxytrityl
DLS	Dynamic light scattering
DTT	Dithiothreitol
DX	Double crossover
EDTA	Ethylenediaminetetraacetic acid
et al.	et alia (Latin) – and others (English)
EPR	Enhanced permeability and retention effect
FANA	2'-Fluoroarabino nucleic acid
FACS	Fluorescence-activated cell sorting
FBS	Fetal bovine serum
FDA	Food and Drug Administration

FBS	Fetal bovine serum
FRET	Förster resonance energy transfer
g	Grams
G	Guanine
G4	Guanine quadruplex
HeLa	Henrietta Lacks immortal cells (cell line)
HE	hexaethylene
HEG	Hexa(ethylene)glycol
hrs	hours
HPLC	High performance liquid chromatography
Rh	Hydrodynamic radius
H-bond	Hydrogen bond
i.e.	id est (Latin) – in other words (English)
kg	kilograms
LC-ESI-MS	Liquid chromatography-electrospray ionization mass spectrometry
LNA	Locked nucleic acid
LNP	Lipid nanoparticles
[Mg ²⁺]	Magnesium ion concentration
m/z	Mass-to-charge ratio
mRNA	Messenger RNA
miRNA	Micro RNA
MW	Molecular weight
μL	Microlitre
μM	Micromolar
mL	Millilitre
mM	Millimolar
min	Minute
mol	Moles
NAT	Nucleic acid therapeutics
NTC	Non targeting control
nt	Nucleotide
nM	Nanomolar
OD	Optical density
PAGE	Polyacrylamide gel electrophoresis
PBS	Phosphate-buffered saline
PCR	Polymerase Chain Reaction
PO	Phosphodiester
PS	Phosphorothioate
RNA	Ribonucleic acid

RSNA	Responsive Spherical Nucleic Acid
RPMI	Roswell Park Memory Institute medium
RT	Room temperature
SELEX	Systematic evolution of ligands by exponential enrichment
s	Seconds
SD	Standard deviation
SNA	Spherical nucleic acids
siRNA	Short interfering RNA
ss	Single-stranded
TEMED	Tetramethylethylenediamine
TAMg	Tris-acetate-magnesium
Tris	Tris(hydroxymethyl)aminomethane
T	Thymine
mol	Moles
UV-Vis	Ultraviolet-visible

Contributions

Prof. Hanadi F. Sleiman (HFS) provided funding, research objectives, experimental design and intellectual guidance for all the projects described in this thesis.

Chapter 1 was written by **Hassan H. Fakh (HHF)** with comments and edits from **HFS**.

Chapter 2 is a published manuscript with **HHF** as first author. **HHF** co-designed and was the major contributor to all experimental data and analysis. **Johans J. Fakhoury (JJF)** provided feedback and discussion on *in vitro* results. **Danny Bousmail (DB)** conducted the AFM imaging to provide the first evidence that the responsive SNAs assemble into the expected structure, from samples that **HHF** synthesized, prepared, and provided to **DB**. **HFS** co-designed the project with **HHF**, where she provided guidance and discussion of the overall work. **HHF and HFS** co-wrote the manuscript.

Chapter 3 is a published manuscript with **HHF** as first author. **HHF** co-designed the project and was the major contributor to all experimental data and analysis. This project was a collaboration with the lab of **Masad J. Damha (MJD)**. Specifically, **HHF** started collaborating with **Elise Malek-Adamien (EMA)**, where she synthesized the first FANA modified oligonucleotide and provided to **HHF** who later functionalized it with a polymer for further studies. The initiation of the collaboration was by **JJF**, with the approval from **MJD and HFS**. **Adam Katolik (AK)** then took over providing the FANA modified material to **HHF** following the graduation of **EMA**. **HFS** co-designed the project with **HHF** and input from **MJD**, where she provided guidance and discussion of the overall work. **HHF and HFS** co-wrote the manuscript with edits from **MJD**. **Sepideh Kaviani (SK)** provided AFM imaging when it was requested by reviewers.

Chapter 4 is a manuscript in preparation where **HHF** as first author. **HHF** co-designed the project and was the major contributor to all experimental data and analysis. This project was a collaboration with the lab of **Anastasia Khvorova (AKh)** and was sponsored by PROMOTE CREATE NSERC funding. Specifically, **HHF** visited the lab of **AKh** at the RNA Therapeutics Institute at UMass Medical School, Massachusetts. Previously, **HHF** worked with **Aurelie**

Lacroix (AL) on this conjugate, and they co-published a paper in the journal of controlled release on the *in vitro* studies of this material. **HHF** designed this project and exchange visit to investigate the *in vivo* properties of the albumin-binding dendritic conjugate, where **AKh** has the facilities for such project. At UMASS, **Qi Tang (QT)** was the postdoc working directly with **HHF** to provide guidance on mice experimental design, and aid in mice handling. **HHF** synthesized all the material and designed the *in vivo* experiments with **QT**, where both co-injected the mice and analyzed the data. **Minwook Shin (MS)** a post-doc under the supervision of **Jonathan Watts (JW)** both developed a novel technique for intratracheal injections and cell-type segregation. **MS** performed the lung experiments with the materials and samples that **HHF** provided. **HFS** co-designed the project with **HHF** and input from **AKh**, where both provided guidance and discussion of the overall work. **HHF and HFS** co-wrote the manuscript with edits from all authors.

Appendix I was also a collaboration with **AKh** as well, where the work is still to be completed due to return of **HHF** due to COVID, funding, and graduation. In this appendix, **HHF** was the primary contributor in terms of design, synthesis, analysis, and experimental planning. **QT** aided with animal experiments. **HFS** co-designed the project with **HHF** and input from **AKh**, where both provided guidance and discussion of the overall work.

Appendix II is collaborative work with Quantum Si Inc (QSi), a company based in Guilford CT, USA, that provides next generation sequencing services. The Collaboration was initiated between **HFS** from McGill University, and **Jeremy Lackey (JL)** and **Xinghua Shi (XS)** from QSi. **HHF** was the primary student leading the collaboration, and contributed to the design, production and conducted all experiments performed at McGill University. **Haidong Huang and Robert Boer** synthesized and provided the fluorescent DNA strands and phosphate functionalized DNA strands used in the assemblies. **Quantum Si team (Xinghua Shi and others)** conducted the sequencing experiments, which are confidential and not included in this chapter due to IP purposes.

1 | Introduction



“Cellular landscape cross-section through a eukaryotic cell.”

- The most detailed model of a human cell to date. By Evan Ingersoll and Gael McGill.

“The universe is within you; you are the universe”

1.1. Preface

Nucleic acid therapeutics (NATs) have the potential to treat thousands of known genetic diseases, malignancies, among several ailments. This is accomplished via their ability to modulate gene expression and immune reactions *in vivo*. Unlocking the full potential of these therapeutics is hindered by the obstacles they face when introduced inside the body. Drug delivery strategies are being studied and employed to aid in their translation from lab prototypes to applicable therapies. Nucleic acid-based nanoparticles (NANPs), are nanocarriers built from the nucleic acids themselves, are a promising modality for delivery due to their biocompatibility, programmability, and intrinsic activity (made from therapeutics themselves). This thesis examines a range of designs of nucleic acid nanoparticles to aid in their translation to the clinic. The first chapter provides an overview on the onset of disease and why NATs have the potential to revolutionize medicine. We then preview how NATs are made, their various mechanisms, and the challenges for their application. Then, we discuss the strategies that are employed to overcome these challenges, including chemical modifications and drug delivery systems, such as NANPs, and their biological applications.

1.2. The Central Dogma of Life and Onset of Disease

The central dogma of molecular biology and life was formulated in 1957 by Francis Crick which states that Deoxyribonucleic acid (DNA) encodes genetic information and is transcribed into Ribose nucleic acids (RNA), which in turn is translated into proteins. The flow of sequence information is unidirectional going from nucleic acids to proteins, and not the other way around.¹ This is how the cell encodes and produces all proteins that are responsible for thousands of functions (**Figure 1. 1**).

The DNA code is made from four nucleotides, where a deoxyribose phosphate sugar is connected to one of the nucleobases: (A)denine, (C)ytosine, (G)uanine or (T)hymine. Three sequential DNA nucleotides are termed “codons”, and together they code for one specific amino acid. A series of these codons in DNA that usually code for a functional protein are termed “genes”. To produce the protein, the gene is transcribed from the DNA code to the RNA code, which utilizes ribose phosphate sugar connected to the

same nucleobases, except that (T) is substituted by (U)racil. The product, termed pre-messenger RNA, then goes through a series of modifications to become a messenger RNA (mRNA), before being ultimately translated into a sequence of amino acids that form the protein that was originally encoded. These gene-encoded proteins are the workhorses of cells, where they carry critical essential work for the life of the cell such as metabolizing nutrients and making new cellular constituents.²

When there is a defect in the production of the protein, this leads to the production of a mutated version of the protein that leads to the onset of diseases, such as sickle cell disease, cystic fibrosis, huntingtin disease, muscular dystrophy and many more. This could be due to a loss or gain of function of the mutant in reference to the original protein, which affects the essential work it performs in the cell.³

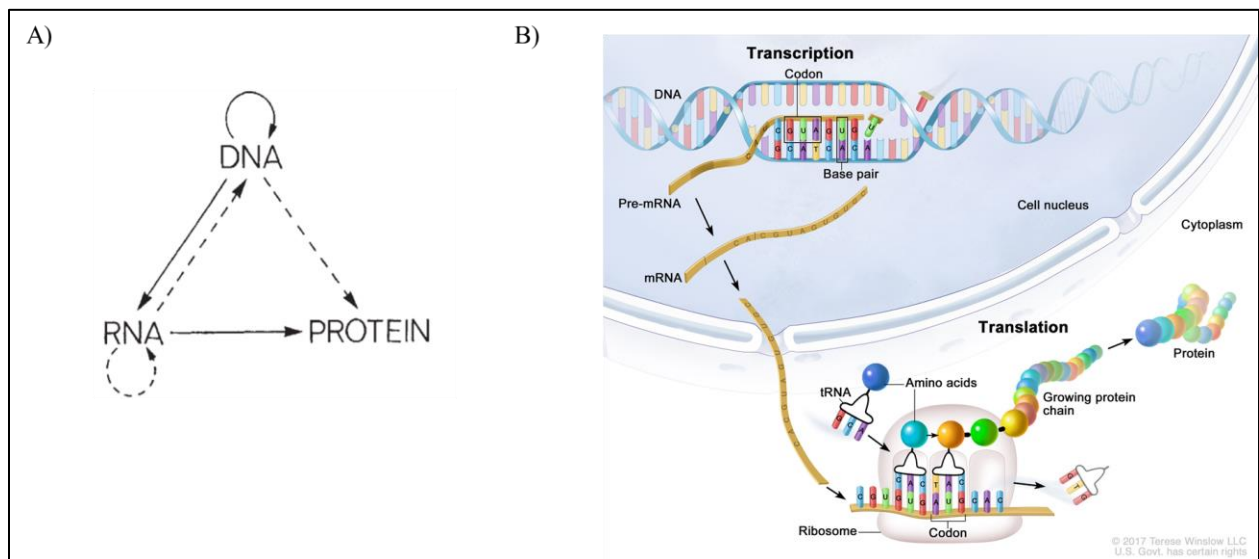


Figure 1. 1. A) Crick's Central Dogma of molecular biology. Solid lines represent natural phenomenon, dotted lines represent special phenomenon (adapted from Ref.¹) B) The production of protein based on the central dogma, where DNA is transcribed into RNA, which is then translated into protein (adapted from Ref⁴).

1.3. Conventional Pharmacotherapeutics and Their Limitations

Pharmacotherapy relies on treating diseases by the development of pharmaceutical chemicals that aim to control the disease, rather than physical intervention such as radiation and surgery.⁵ The most common target for these therapeutics are proteins: The pharmaceutical agents binds to a protein and alters its behaviour – either neutralizing its disease-specific function, or activating it to restore healthy function.⁵ These agents are mostly made of small molecule drugs, that are optimized in chemistry and molecular weight to allow them to pass through cell membranes and bind their target protein in very specific sites (**Figure 1. 2.**).⁶ To ensure specificity, this requires extensive and iterative screening effort followed by chemistry optimization of the small molecule drug candidate so that it binds its target protein and induces the desired function.⁵⁻⁷ Examples of small molecule inhibitors are colchicine, that binds tubulin and inhibits microtubule assembly leading to cell death (usually cancer cells are the target).⁸ Paclitaxel, another drug that targets the same protein (tubulin) is an activator in this case, where it makes microtubule formation constant, which signals cancer cell apoptosis.⁹

The other class of therapeutics are proteins such as antibodies, that revolutionized drug development at the time of their introduction.¹⁰ The most known example is the development of monoclonal antibodies that bind target proteins specifically and induce a therapeutic effect. An example of such a modality is Trastuzumab, which binds overexpressed HER2 protein on cancer cells, causing a decrease in the abnormal excessive division of cancerous cells.^{10,11}

The main challenge with these approaches can be split in two categories. First, not all proteins have target binding sites that can be utilized by these therapies (small molecule and antibodies), making many of them undruggable. In fact, the approved small molecule drugs currently interact with only 2% of human proteins. Second, it is approximated that only a maximum of 15% of proteins are disease modifying, and that only about 15% of proteins are actually druggable; meaning around 2.25% of disease-causing proteins have the chance to be targeted by protein-binding and altering strategies.^{6,7,12} In addition, 95% of our genome actually does not code for protein production, rather it is mostly non-protein

coding sequences. Yet, these sequences can produce many functional non-coding RNAs that are involved in regulating protein production for crucial tasks in the cell (**Figure 1. 2**).^{13,14} Other challenges for these modalities include instability, shelf-life, low solubility and immunogenicity, especially for protein-based therapeutics.

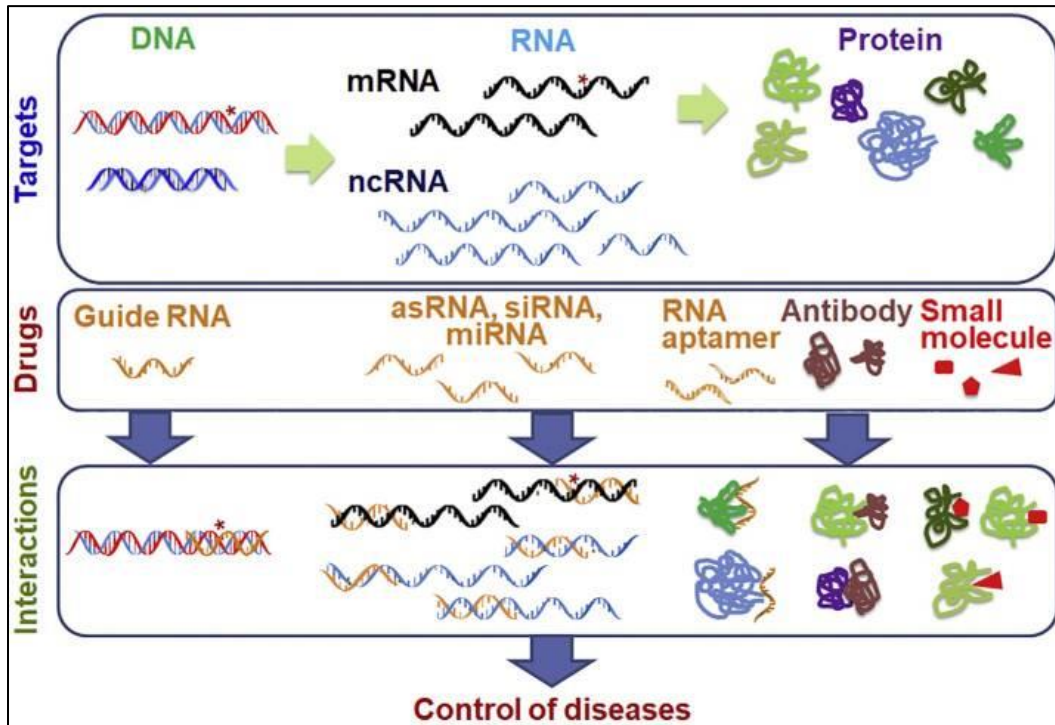


Figure 1. 2. Various drug modalities and what step they target from the protein production pathway (adapted from Ref.⁵).

1.4. Nucleic Acid Therapeutics to The Rescue

If we revisit central dogma presented by Crick, we see that we can target a diseased protein by taking a step back and targeting its coders: RNA, specifically mRNA. For example, if one can degrade the mRNA that is being translated into the mutated protein, we will halt its production and hence get the same effect of the inhibiting drug that targets it. This is precisely the function of nucleic acid therapeutics. This does not only resolve the issue of work-intensive optimization of small molecule drugs to bind a specific pocket of a protein, but also opens the ability to target non-coding sequences that play a role in disease progression.

Nucleic acid therapeutics (NATs) are made from nucleic acids - DNA or RNA- and modulate gene expression. The first discovery of such a class of therapeutics was in 1978, when Zamecnik and Stephenson reported that a short synthetic DNA sequence, termed antisense oligonucleotide (ASO), was able to block viral replication in chicken fibroblasts.¹⁵ This was due to the ability of the ASO to bind its target, mRNA, via complementary Watson-Crick base pairing, and halt the production of the targeted protein. This discovery has ushered the development of the field of nucleic acid therapeutics, where nucleic acids can be used to modulate gene expression and progression. A variety of NATs have been discovered, developed and approved since, with various functionalities and mechanisms of actions (ASOs, RNAi, CRISPR-Cas, aptamers, etc.) (**Figure 1. 2.**)^{7,16}

1.4.1. Solid Phase Synthesis of Nucleic Acids

Like any other pharmaceutical, we need to produce NATs in a high yielding synthesis to employ it as a therapeutic. Previously, nucleic acids were synthesized by relying on nature's machinery and developing molecular biology methods, such as Polymerase chain reaction (PCR) to produce DNA enzymatically, starting from a template.¹⁷ However, PCR faces major issues, especially that the enzyme is error-prone and we cannot replicate the cell's proof-reading mechanisms in a test-tube, which is too complex.¹⁷ Additionally, it is labor intensive and requires multiple steps.

Solid phase synthesis of DNA and nucleic acids was a revolutionary discovery, that allowed the production oligonucleotides in a high-yielding sequence-controlled manner.¹⁸

The two main components of the synthesis cycle of oligonucleotides are: phosphoramidite chemistry and solid phase synthesis.

The sequence of the therapeutic is extremely essential, as it dictates what target it will bind.¹⁶ Hence, chemists needed a methodology to couple the building blocks of oligonucleotides in a sequence controlled manner.^{19,20} The discovery of the highly reactive nucleoside phosphoramidite coupling in 1981, which is still in use today, resolved that issue. Chemists needed to iteratively perform coupling reactions in a fast and easy stepwise manner with minimal waste. This is where solid-phase synthesis comes into the picture, where the building block molecules are covalently bound on solid support and coupled in a stepwise manner relying on orthogonal protective groups. When the product is immobilized, this allows for by-products to be washed away, enabling more efficient and speedy synthesis without multi-purification steps.²¹ Combining these seminal developments as well as automation, the “Gene Machine” was developed in the 1980s that provided the tools to make these new therapeutics modalities in an accessible, scalable and user-friendly process.^{20,22}

A typical automated DNA synthesizer today can synthesize oligonucleotides on a controlled pore glass (CPG) solid support, up to 250 bases in length, at a high rate (around 10 bases/hr) where each base addition has a yield of >99%. The nucleoside monomers are first protected with a dimethoxytrityl group (DMT) on their 5'-end and equipped with a phosphoramidite unit on their 3'-end. The amino groups of A, C, and G are protected as their amide derivatives. These nucleoside phosphoramidites are added in a sequential manner to a growing DNA strand on the solid support. The strand is grown from 3' to 5' end., and the protocol follows these major cycle steps: 1. Deblocking or deprotection, 2. Coupling, 3. Capping, 4. Oxidizing (**Figure 1. 3**).²³ In short, the 5'-hydroxyl is deprotected by cleavage of the DMT group with dichloroacetic acid, which gives an orange color indicating success of trityl cleavage (or detritylation). Then, the next nucleoside of the desired sequence is added, and its phosphoramidite moiety is attacked by the freshly deprotected 5'-hydroxyl of the previous base in the presence of an activator (from the tetrazole family). Following this, capping agents are used to block off any 5'-hydroxyl groups that did not react, so they do not grow further during the next cycle. Lastly, the

phosphorus (III) is oxidized to phosphorous (V), the more stable and inert form, with iodine water and pyridine. Then, this cycle repeats until the desired sequence and length of oligonucleotide is made. This is then cleaved from the solid support and deprotected in the presence of ammonia to yield the oligonucleotide. Further purification of the resulting oligonucleotide is performed via gel electrophoresis or high-performance liquid chromatography.

The automated DNA synthesizers operate at scales ranging between 0.5-10 μmol scale, but large-scale industrial production of oligonucleotides is also possible. The current commercial cost from vendors is around 0.05\$/base for a (natural, unmodified base up to 100 nmol).²³

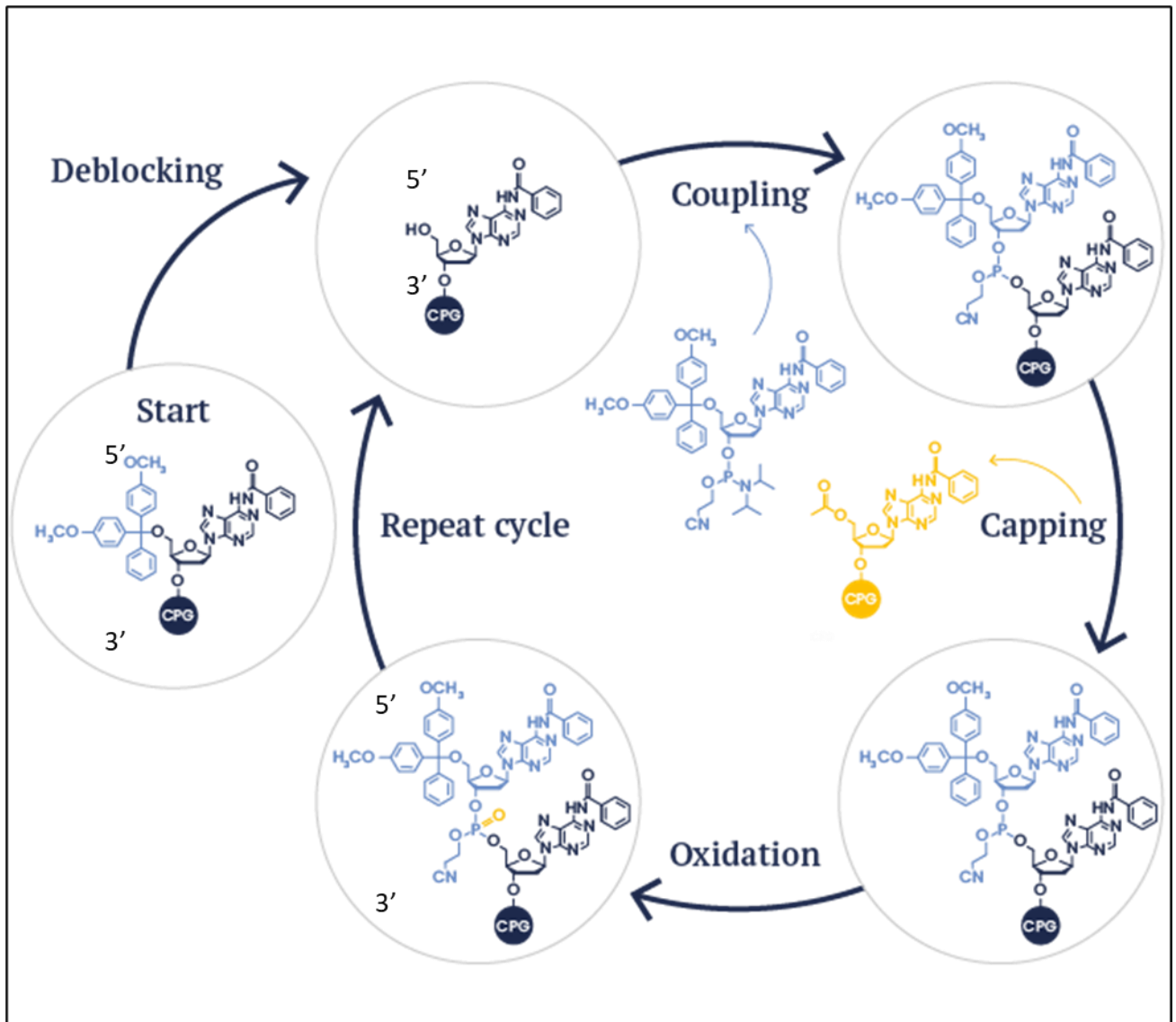


Figure 1. 3. DNA synthesis cycle on solid support (adapted from eurogentec).

1.4.2. *Types and Mechanisms of NATs*

Many types of NATs have been developed over the years since their discovery, that are made from various nucleic acids and act in various mechanistic pathways to control gene expression and onset of disease. They are divided into three major subgroups: Gene silencing and regulatory NATs, gene editing NATs, and protein targeting Aptamers. The versatility of NATs allowed them to target all stages of protein production in the central dogma.

1.4.2.1. *Gene silencing and regulatory NATs*

As mentioned, DNA is the carrier of genetic information, which is transcribed into a long RNA (mRNA). This mRNA is transported from the nucleus to the cytoplasm, where it gets translated into an amino acid chain that folds into the protein destined for a pre-determined function. If the DNA is mutated (not the correct sequence or code of bases), this results in misfolded and dysfunctional RNA and proteins involved in diseases. The first and most used class of NATs are the ones that act on the mutated mRNA to down-regulate the production of the diseased protein, which is coined “gene silencing”.

The NAT utilized by Zamecnik in 1978 was an antisense oligonucleotide (ASO): These are single-stranded DNA oligonucleotides of a length between 13-30 nucleotides.^{7,15} They are designed to have a specific sequence complementary to part of the target mRNA, which leads to binding and inhibition of translation either via steric blockage, or via the more powerful and catalytic destruction of the mRNA by Ribonuclease H (RNase H) recruitment (**Figure 1.4. A**). RNase H binds RNA:DNA heteroduplexes, such as the ASO:mRNA, and catalyzes the degradation of the RNA strand, which means that the ASO can be recycled and hence this is a more favorable mechanism for downregulation (up to 95%). ASOs are also capable of modulating the splicing of pre-mRNA to mRNA, where it restores the natural inclusion or omission of certain regions in the RNA transcript to restore function of a dysfunctional protein. The ASOs also were the first approved NATs by the FDA (such as Vitravene in 1998 and Kynamro 2013) and many are in clinical trials.^{7,24}

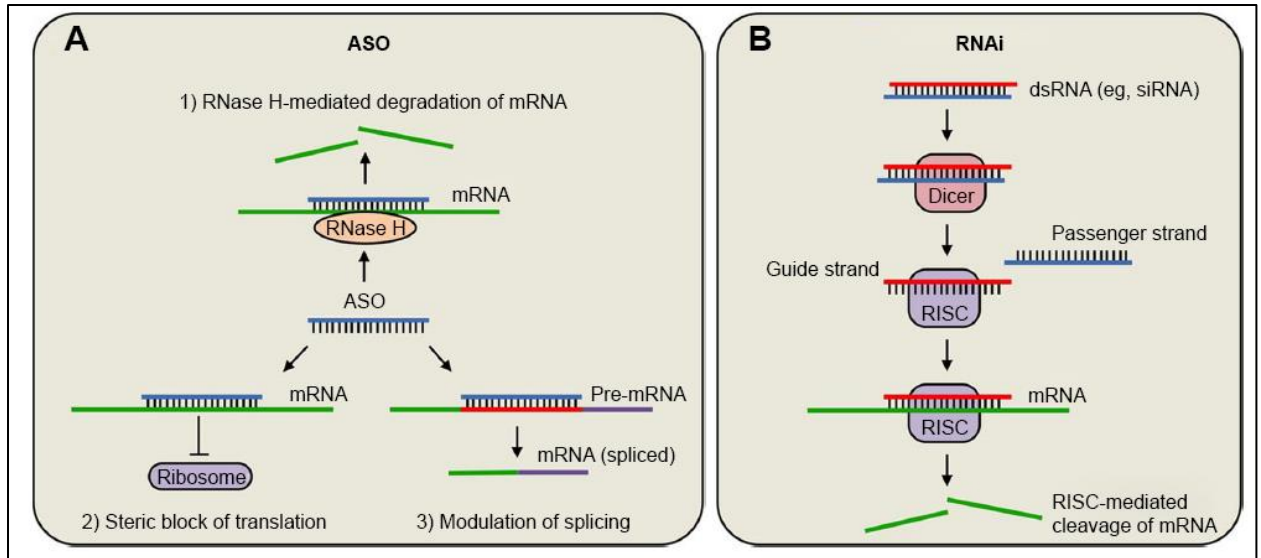


Figure 1. 4. Gene regulation with A) ASOs and B) RNAi (adapted from Ref.²⁵).

The second widely used NATs use the RNA interference (RNAi) mechanism, and this includes small interfering RNA (siRNA) and micro RNAs (miRNA) (**Figure 1. 4. B**). Discovered by Fire and Mello in 1998 which won them the Nobel Prize in 2006, RNAi took the center stage for its very high effectiveness. For RNAi, double-stranded RNA strands of around 20 nucleotide long are utilized. Inside the cell, they are loaded into the RNA-induced silencing complex (RISC) in the cytoplasm, leading to the association of one of the strands (antisense strand) with the target mRNA that gets cleaved/degraded. This is done via Agronaute2 (Ago2) protein for siRNAs, which then is free to bind another mRNA and cleave it (catalytically). Whereas for miRNA (not shown) the sequence is not fully complementary to the target mRNA, so Ago2 is not recruited for degradation, but translation blockage still occurs. The first siRNA drug to be approved was 3 years ago (ONPATRO, 2018) which then was followed quickly by others (currently 6 approved RNA drugs).²⁴

It is worth mentioning that there are also therapeutics that act on the increased production of a certain protein, such as the famous COVID-19 mRNA vaccine. These mRNA-based NATs focus on delivering a whole mRNA piece that codes for a lacking protein, so the cell can translate it and produce the needed

protein (such as the spike protein in case of COVID-19). This a relatively recent field with a great deal of promise in curing many difficult diseases, as well as developing vaccines, as shown with the pandemic that hit in 2019 and still on-going.^{26,27}

We can see how ASOs, RNAi, and mRNA therapeutics are valuable new modalities of pharmacotherapy, whereby simply designing the right sequence, one can virtually target any gene of interest. This is especially advantageous over small molecule drugs and antibodies, as they can target undruggable proteins that lack a well-defined binding site, as well as genes that code for transcription factors and other key players in diseases.^{5,13,16}

1.4.2.2. *Genome editing NATs*

From their name, genome editing nucleic acid therapeutics take the approach even one step further back than RNA and target the DNA gene code itself. The most prevalent tool from this class is the CRISPR-Cas system, which is a protein-RNA complex capable editing chromosomal DNA by either removing, adding, or changing parts of a gene with high specificity.^{28,29} It can do a single-base addition, gene insertion, deletion or even translocation (moving of a certain base to another location).²⁹ The CRISPR-Cas system relies on having 2 main components: the Cas protein and a guide RNA strand. The former is a member of a nuclease protein family derived from bacteria (such as Cas9) that is capable to introduce nicks in the genome (**Figure 1. 5.**). The latter is a nucleic acid that incorporates into Cas protein on one end, and binds the desired target on the other end (sequence can be changed to bind desired target). Then, the cellular repair mechanisms are employed to repair this break, either via non-homologous end joining usually utilized for removing genes, or via homology-directed repair that is more used for introduction of genes (**Figure 1. 5.**). Within only few years of its discovery, the CRISPR-Cas system is now used around the world by scientists, won the Nobel Prize, as well as the first clinical trial testing its efficacy in human subject was done a few months ago with extremely promising success.³⁰

Another class of genome editing NATs also include viral vectors.³¹ This technique hijacks the ability of viruses to integrate their DNA into the host genome and utilize this mechanism to engineer harmless viruses that carry the desired functional gene of interest into the host cells.³¹ Concerns on this technique are prominent, as utilizing viruses have been shown to have immune responses and can have an increased risk of cancer. Examples include Adeno-Associated Viruses (AAV), such as the most expensive drug back in 2019 produced by Novartis, Zolgensma.³²

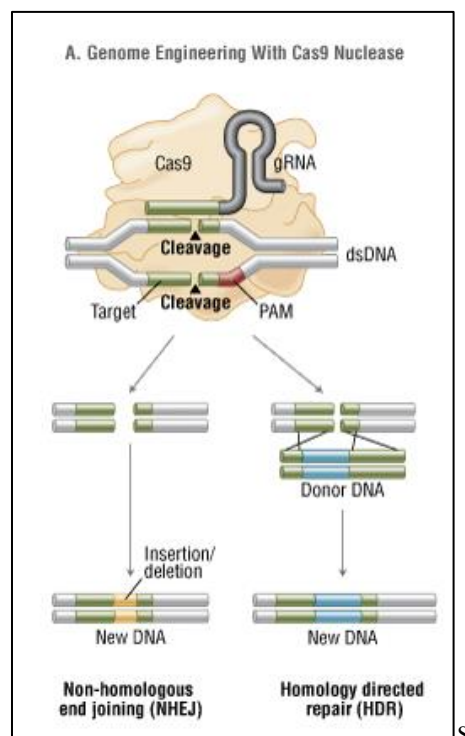


Figure 1. 5. Genome Editing with CRISPR-Cas9 system (adapted from New England Biolabs Inc.).

1.4.2.3. Target binding Aptamers

Nucleic acid therapeutics are so versatile that not only can they target the messenger code (mRNA via gene silencing and regulation) and the back-end code (DNA via genome editing), but also the front-end code, proteins. Aptamers are the third class of NATs, which are short sequences of RNA or DNA that fold into a

specific 3D shape that allows them to bind specific targets such as small molecules and proteins (Figure 1. 6).³³ They are often compared to antibodies in their 3D structural organization that allows specific binding of targets, but they are made from nucleotides instead of amino acids, which makes their production much easier, cheaper and also less toxic and immunogenic.³⁴ They are typically produced via a process called Systematic Evolution of Ligands by Exponential Enrichment (SELEX), which mixes large libraries of sequences with the desired target (molecule, protein, cell etc.) and then goes through an iterative cycle of washing the non-binders and enzymatically amplifying the binders (**Figure 1. 6.**)^{33,34}

The first FDA approved aptamer was Macugen, which targets vascular endothelial growth factor (VEGF) to treat macular degeneration due to aging.^{35,36} Many other aptamers are currently in the pipeline in clinical trials, where they either target small molecules, surface proteins, or intracellular proteins.³⁵ Aptamers can be used as therapeutics themselves by hindering protein-protein interactions (extremely difficult to achieve with small molecule drugs), or they can be used as targeting ligands for NATs (siRNA-aptamer complex for example) to guide them towards specific cells and targets.^{35,37}

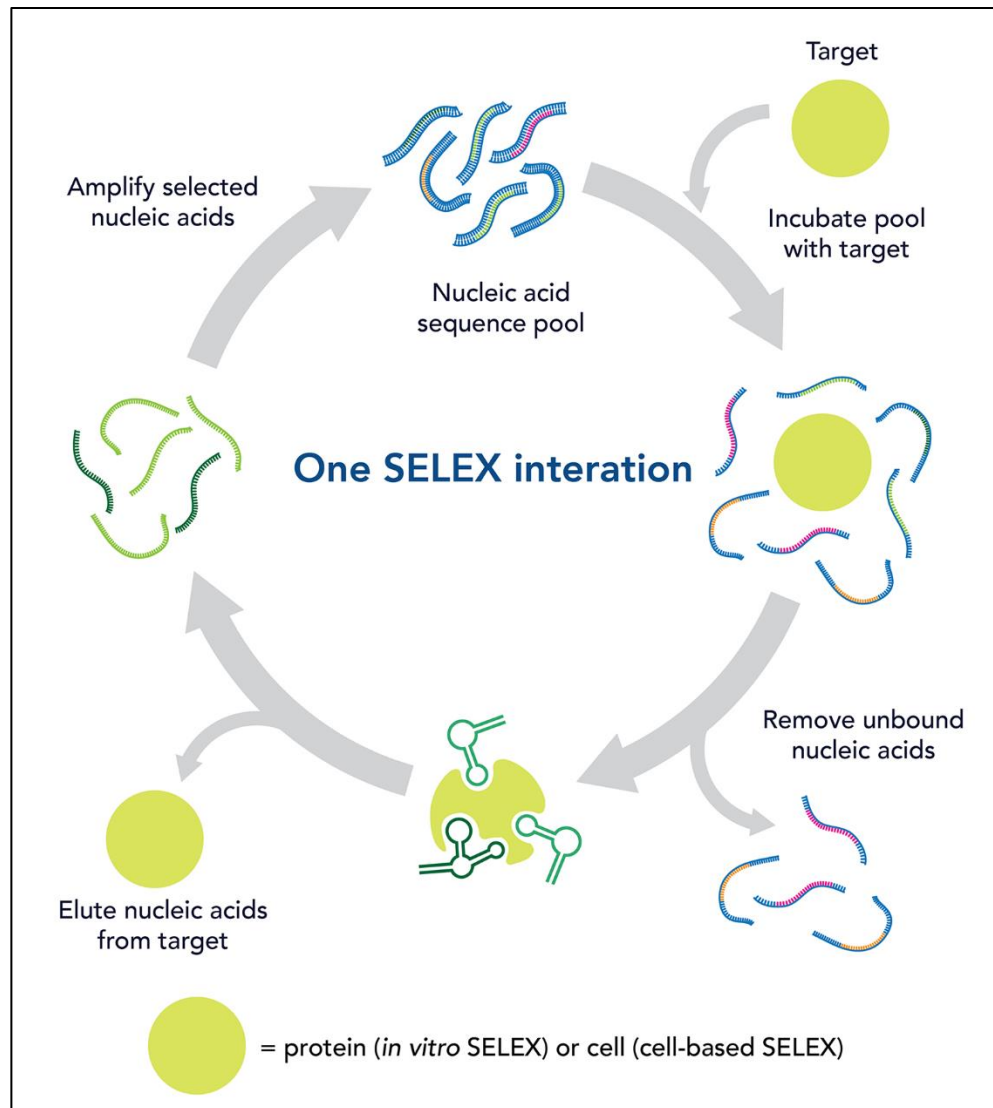


Figure 1. 6. Oligonucleotides folding into 3D structured Aptamers and the SELEX cycle for their selection. A nucleic acid pool is incubated with its target. Then, unbound nucleic acids are removed from those that folded and bound the target. Afterwards, the binders are eluted from their target and amplified. The process is repeated many times to obtain the best binders. (Adapted from IDT.³⁷).

1.4.3. *Challenges of NATs*

Since NATs hold enormous potential of treating virtually any disease, the million-dollar question (or even billion-dollar question) is: why are there not many NAT-based

drugs? Why did it take 20 years since the discovery of ASOs to get an ASO-based approved drug, with a similar process for siRNA? ^{38,39}

This is because NATs have to overcome many hurdles to get to their site of action, where they are effective against their target. We will focus on the challenges faced by gene silencing NATs. The journey towards the site of action (cytoplasm for siRNAs, nucleus, and cytoplasm for ASOs and gene editing) starts from the instant these oligonucleotides are injected into body fluids in the presence of many degradative components, diffusing towards their target organ, going inside their target cell-type and then finally binding their target in the correct intracellular compartment (**Figure 1. 7.**).³⁸ Challenges along this road to efficacy, specifically for gene silencing NATs are: stability in biological media, organ-selective biodistribution, cell-specific uptake, and endosomal escape.³⁹

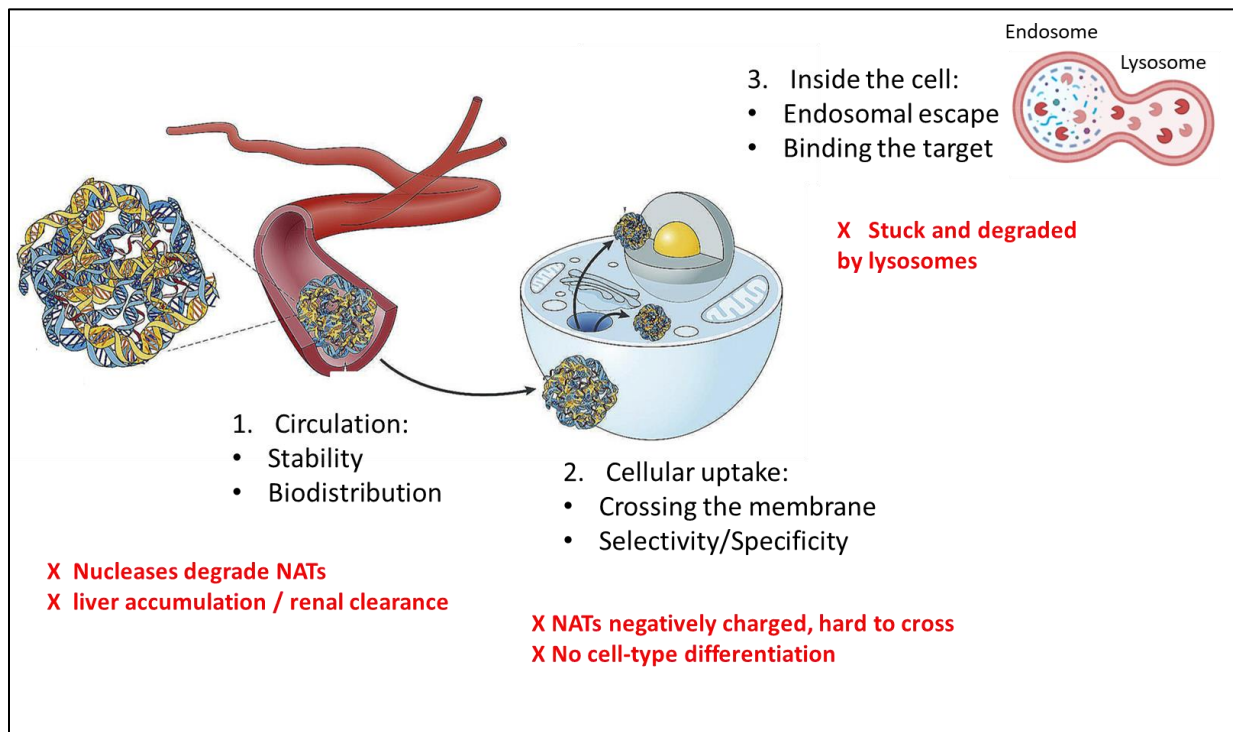


Figure 1. 7. Pathway of NATs toward their target, and the challenges they face (in red) (Adapted with modification from Ref.³⁹).

1.4.3.1. *Stability in biological media*

As soon as NATs are put into contact with biological fluids or biological media, such as cell culture media *in vitro* or blood *in vivo*, they are introduced to a very high level of nucleases with the sole purpose of degrading nucleic acids.³⁸ In fact, a short DNA oligomer will degrade within minutes in these conditions by nucleases.⁴⁰⁻⁴² These nucleases are critical to fight off virus infections and unwanted accumulation of nucleic acids. Various classes of nucleases exist, such as exonucleases that degrade oligomers from the 5' or 3' end, endonucleases that degrade from the middle of oligomers, as well as NA-specific oligomers that only degrade DNA or RNA selectively.^{43,44} It is worth noting that 3'exonucleases, that degrade from the 3' end to 5' end, are the most present and active extracellularly, while endonucleases activity becomes more pronounced intracellularly in the cytoplasm and endosomes/lysosome.⁴⁴ Thus, NATs must be made resistant to nucleases for their delivery.

1.4.3.2. *Organ-selective biodistribution*

Stability in biological media is a shared concern between *in vitro* and *in vivo* studies. However, for NATs to be tested critically as potential therapeutics, studies in animal models are a must, especially that it has been reported that results in cells do not always translate to animals, and vice versa.⁴⁵ In animal models, a major concern that arises for NATs is their biodistribution towards the correct organ where activity is desired.^{7,24,38} It was shown indeed that silencing activity is present in all tissues in different extents (excluding the brain) following systemic injection, indicating the promise of using NATs for many organs.⁴⁶ Yet, this is also problematic because if NATs go to unwanted organs, this results in off-target effects as well as degradation and clearance.⁷

Naked therapeutic oligonucleotides are negatively charged biopolymers, that once injected need to survive nucleases first, which can be achieved by improving the chemistry of NATs (will be discussed in the following sections).⁴⁷ Then, they should avoid renal clearance, which is what typically happens due to

their size (kidney clearance cut-off size is $< 6\text{nm}$).⁴⁸⁻⁵¹ If not cleared, they should evade non-productive sequestration and elimination (**Figure 1. 8.**)⁵² This happens either by plasma proteins binding to them and tagging them for elimination from the body, or via the reticuloendothelial system (RES), which includes phagocytes, macrophages, liver endothelial cells and Kupffer cells.^{7,49} This is unfortunately what was observed for the first generation of NATs tested, where the majority was cleared by the kidney, or directed towards the liver due to its discontinuous endothelium that favors the uptake of the free oligonucleotides. Indeed, due to this data, the first-generation NATs focused on liver-targeted and kidney-targeted diseases.⁷ (**Figure 1. 8.**)

Assuming the NAT is still in circulation, to cross into the organ of interest they need to extravasate from blood circulation into the organ, via the tight endothelial barrier around the blood vessels which is challenging.⁵³ This is not the case for example in tumors, where abnormal rapidly growing cells form a leaky vasculature/endothelium with large gaps that makes tumors more permeable to nanoparticles that are retained following passage. This is termed the Enhanced Permeability and Retention effect (EPR), which is being exploited to favor extravasation of drugs and molecules in tumors rather than other organs, due to these large endothelial gaps (around 12 nm) compared to healthy organs endothelial gaps (around 3 nm).⁵³

To this day, targeted distribution beyond the kidney and liver remains the major goal to achieve the untapped potential of the NAT field, where specific organs are targeted, based on the specific disease treatment (for example COVID-19 NAT therapies targeting the lungs, or delivering NATs to muscles for diseases like Duchenne muscular dystrophy).⁵⁴ There has been some improvement and recent advances for this hurdle which will be discussed in later sections, but more work is still needed and is ongoing in the field.²⁴

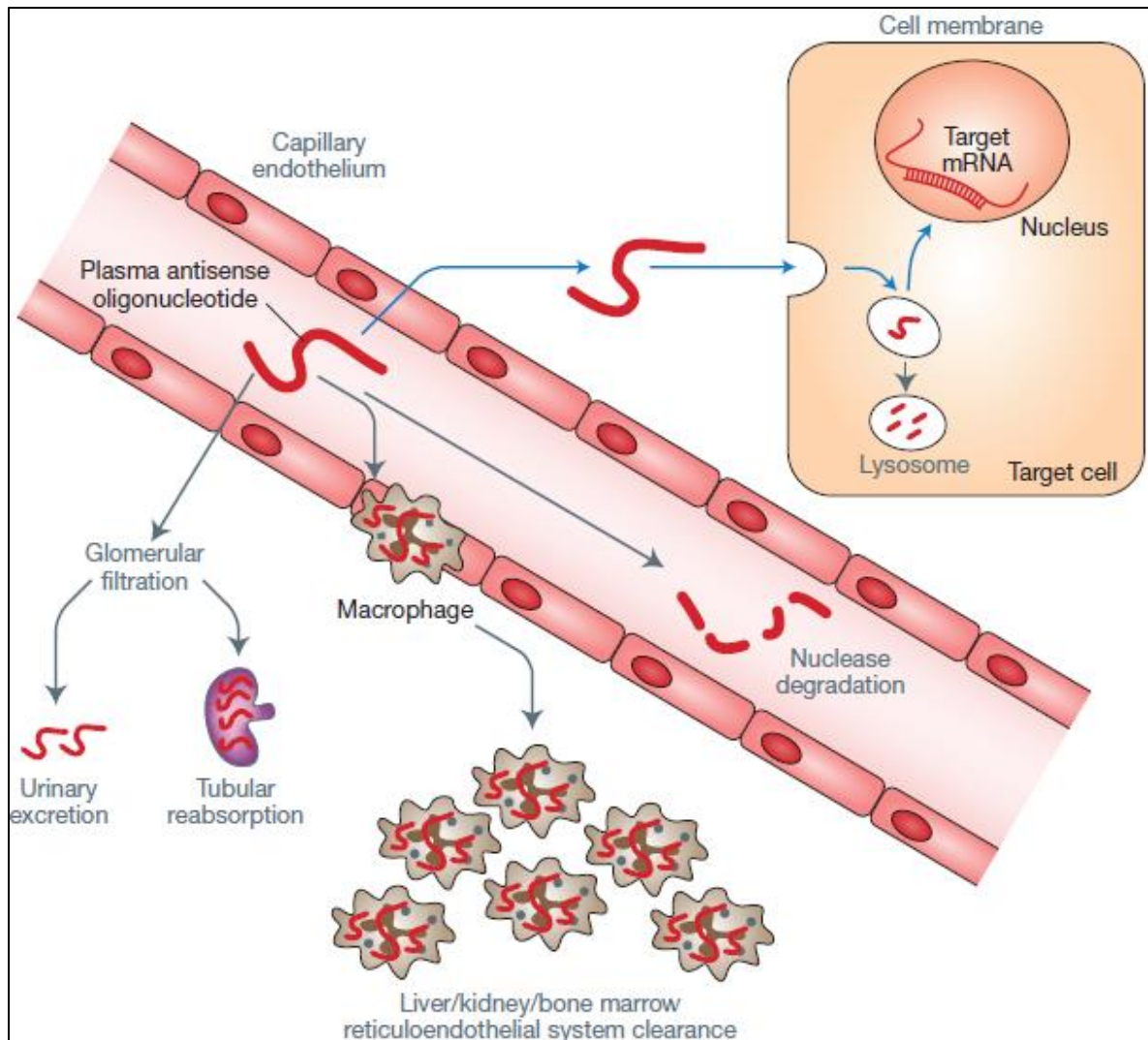


Figure 1. 8. Fate of oligonucleotide following systemic administration First, the oligonucleotide should be stable enough to not be degraded and circulate. Then, it should avoid glomerular filtration, which is renal clearance via the kidney. The oligonucleotide is also challenged by the reticuloendothelial system (liver,kidney, bone marrow), which is the macrophage sequestering of the therapeutic. If the oligonucleotide extravasated through the endothelium, it faces another challenge of cellular uptake and lysosome degradation. (adapted from Ref.⁵¹).

1.4.3.3. *Cell-specific uptake and endosomal escape*

If a fraction of the NATs circulating in the body make it to the target organ it is intended to treat, two other hurdles remain to resolve, which are cell-type specificity and cellular uptake. Organs are made from various cell types that exert different functions. For example the liver has Kupffer cells that are resident macrophages, endothelial cells line up the organ, and hepatocytes that are the parenchymal cells responsible for protein production and detoxification.⁵⁵ This means that, in a genetic defect in the hepatocytes, localization in the liver of NATs targeting that gene does not necessarily mean that it will be effective; rather it will require the therapeutics to be localized in hepatocytes specifically.⁵⁷ Hence, NATs not only need to be honed towards organs, but also towards specific cells.

Crossing the membrane of the target cell-type, termed endocytosis, is another challenge.⁵⁶ NATs are negatively charged, relatively large molecules that are repelled by the negatively charged cellular membranes, which are self-assembled lipid bilayers with embedded proteins and small molecules.⁵⁷ This limits their productive uptake and efficacy, as NATs rarely make it to the cytosol to bind their target. Most NATs that make it inside cells are taken up by endocytosis (**Figure 1. 9. A**). Endocytosis is an active transport mechanism that requires energy and has two main mechanisms: clathrin-dependent and clathrin-independent/caveolae-dependent endocytosis (**Figure 1. 9. A**).⁵⁸ For clathrin-mediated uptake, clathrin units polymerize and form a vesicle of around 150 nm in size on the membrane's surface, following a binding event to its receptor. Then this vesicle engulfs the material and sorts into an early endosome compartment that has a pH of around 6.⁵⁸ The early endosome then fuses with the acidic lysosome with a pH of 4.5-5, that leads to the degradation. Clathrin-independent endocytosis encompasses pathways that do not rely on clathrin, with Caveolae-mediated uptake being the most prominent. This pathway is less common but has been reported and it involves invagination using caveolin, cholesterol and lipids.⁵⁸ Uptake using this pathway does not always lead to lysosomal fusion and degradation. Last, there is increasing interest recently in pursuing macropinocytosis

for the delivery, which has been reported to avoid lysosome formation leading to a functional delivery of NATs.⁵⁸ If not digested by lysosomes or escaped into the cytoplasm, oligonucleotides can be recycled outside the cell via multi-vesicular bodies.⁵⁹

Lysosomes and their acidic pH (4.5-5) degrade NATs as such acidity induces depurination of the oligonucleotides (**Figure 1.9. B**).^{57,60,61} Hence NATs will also need to get around ending up in the lysosomal degradative environment and get to the cytosol for finally meeting and binding its target, which is seen as the final bottle neck for their productive delivery.

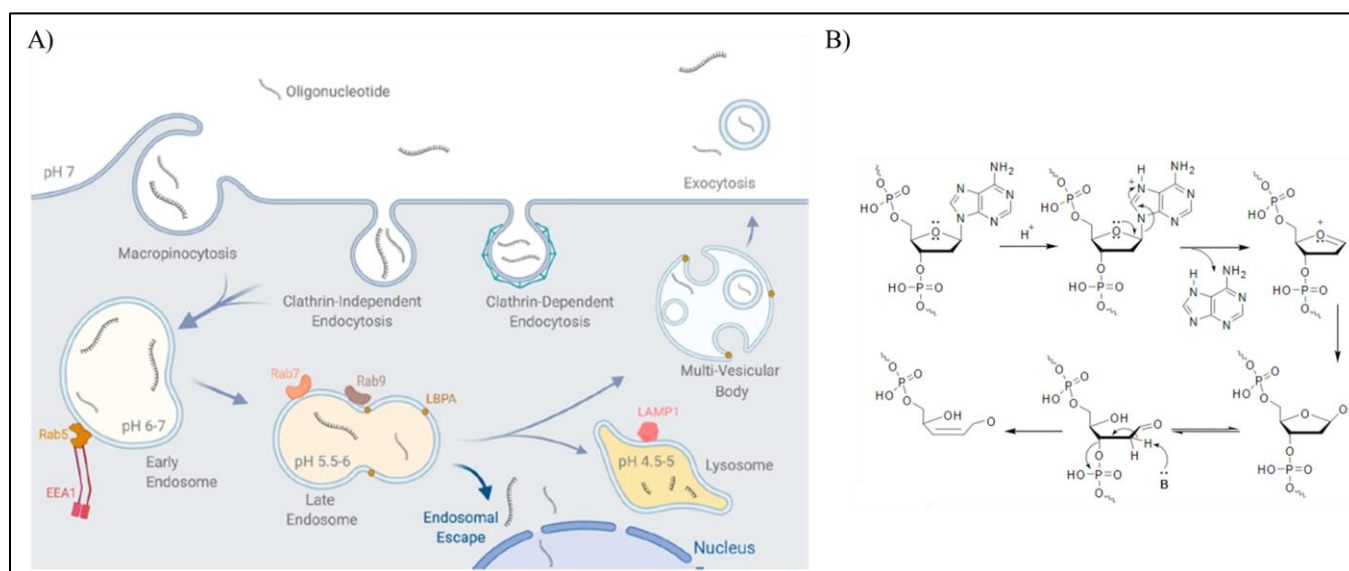


Figure 1.9. A) Uptake pathways reported for oligonucleotides and the key markers used to track the various compartments are shown (adapted and reproduced from Ref.⁵⁹), B) Depurination and degradation of a DNA strand in acidic conditions (adapted and reproduced from Ref.⁶²).

As outlined, NATs must surmount many hurdles and challenges to achieve efficacy, starting from stability upon injection, all the way to cell-specific uptake and endosomal escape. Keeping in mind as well that NATs will need to do that without evoking any toxicity or immune response, which has been observed.⁶³ The next section will outline the chemical advances in the field that yielded the birth of the first successful NA-based drugs on the market.

1.5. Chemical Advances in NATs; “Keep Calm and Do Chemistry!”

The challenges impeding the translation of NATs into clinically approved drugs (stability, biodistribution, selectivity and endosomal escape) sparked an enormous effort by chemists to resolve them. The beauty of nucleic acid-based drugs is that even if they have various mechanisms, they are informational drugs. This means that the sequence of the therapeutic is what it dictates what it is targeting (specific complementary mRNA); hence the sequence of NATs is what we call the pharmacophore (**Figure 1. 10.**). The chemistry of the NATs, such as the composition of the phosphate backbone, ligands and materials attached to it, are what determine its biological stability, metabolism, and distribution; in other words, the dianophore (**Figure 1. 10.**).¹⁶ This is not the case for traditional small molecule drugs where the structure dictates both efficacy and behaviour. This allows a huge room of chemical engineering of NATs with little alteration of effectiveness towards its target, as well as the possibility of applying the advancements of one NAT drug to all NATs.

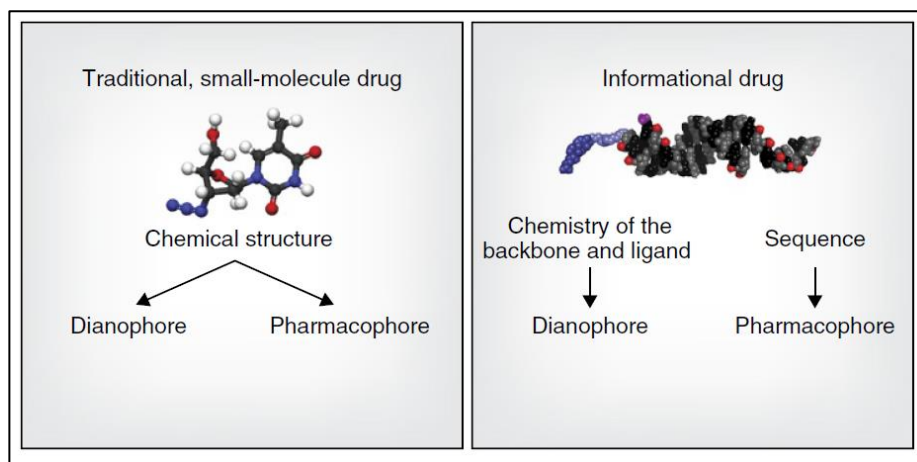


Figure 1. 10. NATs are informational drugs, which allow the independent optimization of the dianophore without affecting specificity of the drug (adapted from Ref.¹⁶).

In this section we will focus on the major chemical advancements that are enabling the translation of NATs from the lab to patients: Chemical modifications, conjugation, and drug delivery systems.

1.5.1. Chemical modifications:

The introduction of chemical modifications to the components of NATs was the first approach to enhance their stability and effectiveness. The very first modification employed was that of the phosphate backbone of nucleic acids, where one oxygen of the inter-nucleotide phosphate was replaced by a sulphur atom, i.e., having phosphorothioate (PS) backbone instead of a phosphodiester (PO) backbone, which did not hinder silencing activity (**Figure 1. 11**).^{64,65} PS-NATs showed increased nuclease stability due to the inability of nucleases recognize them, which increased their circulation time *in vivo*. They also improved cellular uptake resulting from the interactions of PS backbones with proteins and their increased hydrophobicity compared to PO.^{65,66} This has led to the extensive use of the PS modification, and it is to this day even after many decades of its discovery, the most used modification due to its simplicity.⁷ Indeed the first few approved NAT drugs had PS modifications that helped in increasing their stability, availability and activity (Vitravene and Kynamro).

However, with more research conducted on the PS modification, some drawbacks have been identified. First, the phosphorus of the PS is chiral, and adding PS linkages on the automated synthesizer results in a mixture of diastereomers. Stereospecific differences have resulted in different properties, where R isomers have been shown to be better substrates to RNase H but S isomers have better nuclease resistance.⁶⁵ Also, PS oligonucleotides have increased binding affinity to proteins that can lead to unintended side effects.^{66,67} In addition, having too many PS modifications has been shown to increase toxicity.⁶⁶ Last but not least, PS modification reduces the binding affinity towards the mRNA target. Hence, the newer generation of NATs are only including PS modifications on the extremities of oligonucleotides to increase their stability but limit their unwanted side effects.⁷

After discovery of the PS backbone, more chemical modifications have been synthesized and implemented, and are not limited to the backbone only. The most common modifications are those that modify the 2' position of the ribose sugar. Many modifications have been made and implemented in the currently 20 approved nucleic acid-based drugs, such as 2'-O-methyl (2'-OMe) and 2'-Fluoro (2'-F) modifications (**Figure 1. 11.A**).^{7,16} Modifications at this position have a wide variety of properties they can introduce, ranging

from extreme increase in stability towards nucleases, to increasing activity by improving binding. For example, a 2'-deoxy modification that represents the natural DNA is important to be present in the binding region of ASOs to their mRNA target, to maintain a DNA:RNA duplex recognizable by RNase H for degradation.^{68,69} Modifications that can increase binding affinity and resistance and maintain a DNA:RNA-like structure are favored in this case. This can be seen in subtle yet major difference between 2'-Fluoro mod that have a D-ribose configuration (termed FNA) and are more RNA-like, and 2'-Fluoro mods that have a D-arabinose configuration (termed FANA modification) and are more DNA-like (**Figure 1. 11. B**).⁶⁸⁻⁷¹ FANA modifications that mimic DNA, have higher stability, bind more strongly and form a DNA:RNA like duplex recognizable by RNase H and hence have a higher catalytic activity in gene silencing than their stereochemical sibling FNA.^{62,68,70,72}

Functionalization currently includes backbone, nucleobase, ribose sugar modifications and substitutions, as well as alternative chemistries altogether for nucleic acids (**Figure 1. 11**).^{7,16} While covering all these modifications is beyond the scope of this thesis, it is important to highlight that the field of chemical modifications to NATs is forever expanding, where laboratories around the world work on careful chemical engineering of NATs with various modifications, fine tuning their position and implementation to tune efficacy and stability. This huge toolbox has indeed ushered the approval of the first generation of NATs following 20 years from their discovery (first PS-ASO drug in 1998 and first modified siRNA drug in 2018) and has resolved the stability and activity challenge that was impeding NATs.^{7,24}

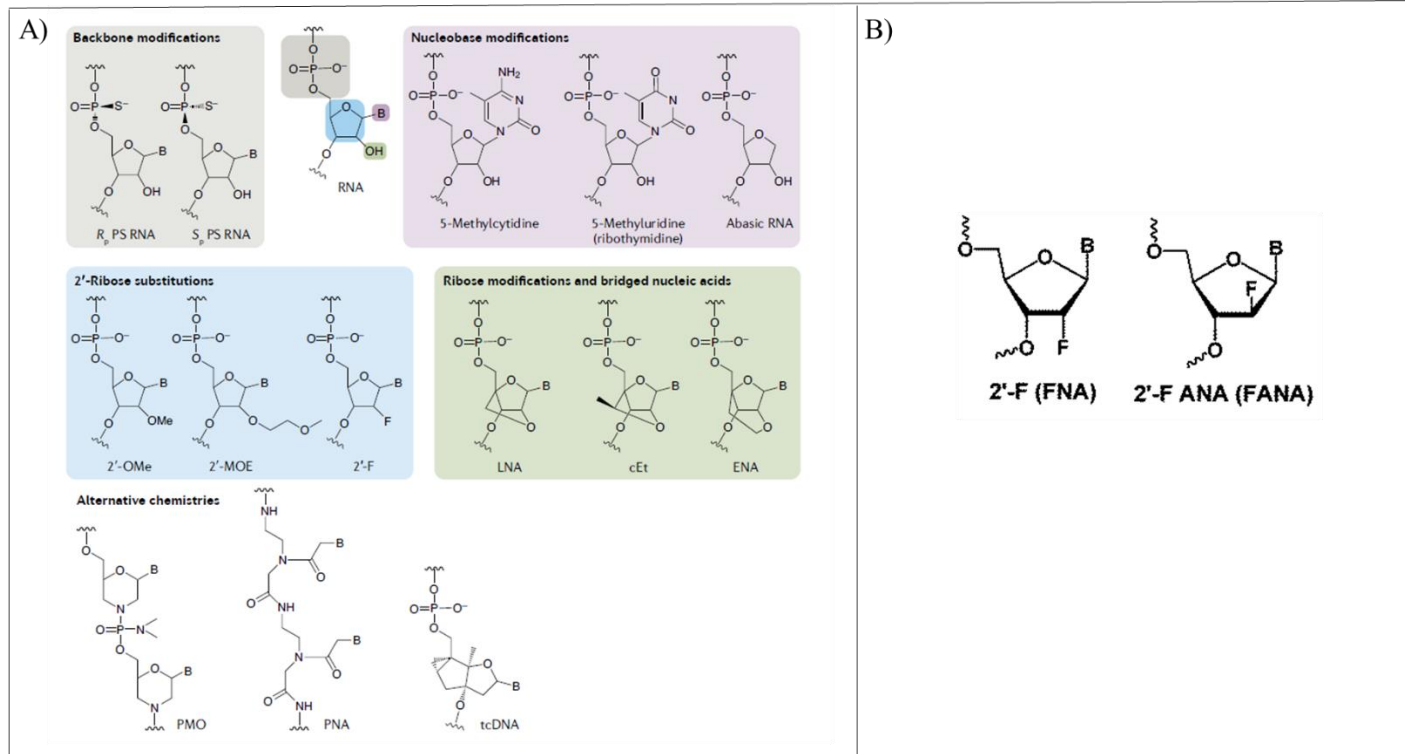


Figure 1. 11. A) Various chemical modifications to nucleic acids at various positions (adapted from Ref.⁷), B) 2'-Fluoro-ribose (FNA) vs 2'-Fluoro-arabinose modification (FANA). FANA has the fluoro substitution at the 2' position pointing upwards, whereas FNA has it pointing downwards. This results in a more DNA-like structure and puckering for FANA where it has a C2' endo pucker, and a more RNA-like structure and puckering for FNA that adopts a north C3' endo pucker.⁶⁹⁻⁷¹

While chemical modifications have resolved the issue of stability, and improved on target efficacy and bioavailability of NATs, these newly stable and active NATs move on to face the next challenge of biodistribution and clearance *in vivo*. Chemical modifications at certain positions can lead to a change in the biodistribution profile, which requires the careful design and assessment of insertions (3'/5' end modifications for increased nuclease resistance, PS modifications for improved cellular uptake, DNA like gapmer designs for RNase H activity). Nonetheless, chemical modifications by themselves do not resolve poor biodistribution nor RES clearance of NATs, which is unfortunately dictated by size and interactions with proteins in circulation.

1.5.2. Conjugation

Another major class of modifications implemented into NATs is appending them with conjugates that have added functionalities, such as improving their biodistribution *in vivo*, targeting them to specific cells/tissues, and stimulating cellular uptake.^{7,24} Conjugates are a single entity attached to NATs, which imparts well-defined pharmacokinetic (PK) properties.⁷ Conjugates appended to NATs can be divided into two groups: non-targeting and targeting conjugates.⁵⁷

Non-targeting conjugates are entities attached to NATs that can alter the biodistribution of the drug, but not necessarily actively target it to a specific location. Such ligands include polymers and hydrophobic conjugates.^{7,57} One of the most common conjugates used in this group are polyethylene glycol (PEG) chains.⁷³ These are hydrophilic polymer chains that give oligonucleotides longer stability and circulation times without reacting with entities in the body due to their inertness.^{73,74} However, reports on PEG inducing immune responses and accelerated clearance from the blood have recently appeared.^{74,75} Other ligands include the lipophilic cholesterol, which has been attached to both siRNAs and ASOs (**Figure 1. 12.**).⁷⁶ Cholesterol's hydrophobicity was able to eliminate the rapid renal clearance of oligonucleotides (usually within minutes) and to dictate their efficient distribution towards the liver.^{76,77} Other lipids have also been shown to be active in the liver, such as α -tocopherol conjugation, which allowed silencing of Apolipoprotein B (ApoB) in the liver.⁷⁸ The concept of hydrophobicity of conjugates being able to alter biodistribution was then further investigated and found to be due to preferential binding of the conjugates to various proteins present in circulation. These include high-density and low-density lipoprotein (HDL and LDL respectively), as well as albumin.⁷⁹ Less hydrophobic conjugates bind HDL which increases kidney accumulation, while binding LDL is due to increased hydrophobicity leading to liver accumulation.⁷⁹ Albumin is a particularly interesting serum protein, as it has an excellent systemic biodistribution profile with prolonged half-life, as well as passive accumulation in tumor tissues which is of extreme interest in cancer therapy.^{80,81} The extended half-life of albumin (around 20 days) is due to the neonatal Fc receptor (FcRn), that following cellular uptake via endocytosis, binds albumin and saves its from degradation by re-shuttling it outside the cell.⁸²⁻⁸⁴ The increased tumor localization of albumin is due to tumor cells digesting it as

a source of energy for their rapid growth, as well as its increased transcytosis via its receptor (gp60) that is overexpressed in tumor cells, and the elevated production of SPARC protein that has a high affinity to albumin. Systematic studies on various hydrophobic conjugates are being conducted, and some reported results show that these conjugates do not only improve biodistribution and circulation but also some of them can direct distribution to specific organs.⁵⁴

Targeting conjugates for oligonucleotides have attracted increasing attention in recent years, especially after liver and kidney delivery have been optimized, and the desire to target other organs is growing.⁵⁷ Targeting conjugates are capable of honing NATs towards specific tissues via various mechanisms. These conjugates include, but are not limited to, glycoconjugates, antibodies, aptamers, and cell-penetrating peptides (CPP) (**Figure 1. 12.**).^{7,24,57} They are attractive especially because they add targeted functionality as well as improved general pharmacokinetics (PK) of NATs. For example, coupling NATs to antibodies that bind specific proteins solely or overly expressed in cancer cells and tumors will lead to preferential steering towards those cells. Antibodies and aptamers can be designed to have both improved binding and distribution, as well as enhanced uptake (e.g., cell internalizing aptamers).^{86,87} This targeting will also decrease side effects associated with activity in regular or off-target cells in the body.^{7,88} Some targeted receptors include HER2, which is highly expressed in breast cancer cells, CD71 that is highly expressed in skeletal muscle, and EGFR in epithelial tumor cells.⁸⁹⁻⁹² Companies such as Avidity biosciences and Dyne therapeutics are currently developing antibody-NAT technologies for clinical applications. Aptamers and antibody conjugated NATs have not progressed well in clinical trials, mainly due to some difficulty in conjugating them, as well as stability and internalization ability. Aptamer/antibody conjugates are still a work in progress that have great potential once optimized.⁵⁷

Perhaps the most widely used targeting conjugate in the field is the GalNac conjugate (**Figure 1. 12. b**), which is a carbohydrate that binds to asialoglyco-protein receptor 1 (ASGR1) with nanomolar affinity.^{93,94} This receptor is highly expressed in the hepatocytes of the liver and is rapidly recycled to the cell membrane, hence binding it facilitates uptake of NATs into parenchymal liver cells (hepatocytes) and not non-parenchymal liver cells (Kupffer cells, macrophages, endothelial cells).⁹³ Following uptake via endocytosis, the NAT

dissociates from the receptor during acidification of the endosome, due to the pH-sensitive binding of GalNAc to its receptor.⁹⁵ This shows how powerful targeting this receptor is, where it not only facilitates liver targeting, but even induces sub-cellular population preference that is not observed in un-conjugated NATs, which are cleared by the liver non-parenchymal cells.⁹⁵ GalNAc is one of the leading strategies for NAT delivery and is the center of the work in many biotech companies. Indeed GalNAc-conjugated siRNA was the *second siRNA drug to be approved* in 2019 under the name Givosiran, where a chemically modified siRNA duplex was conjugated to GalNAc for the treatment of acute hepatic porphyria, a genetic disorder caused by the defect in enzymes involved in heme synthesis and causes devastating symptoms (seizures, psychosis, abdominal and back pain etc.).^{24,96}

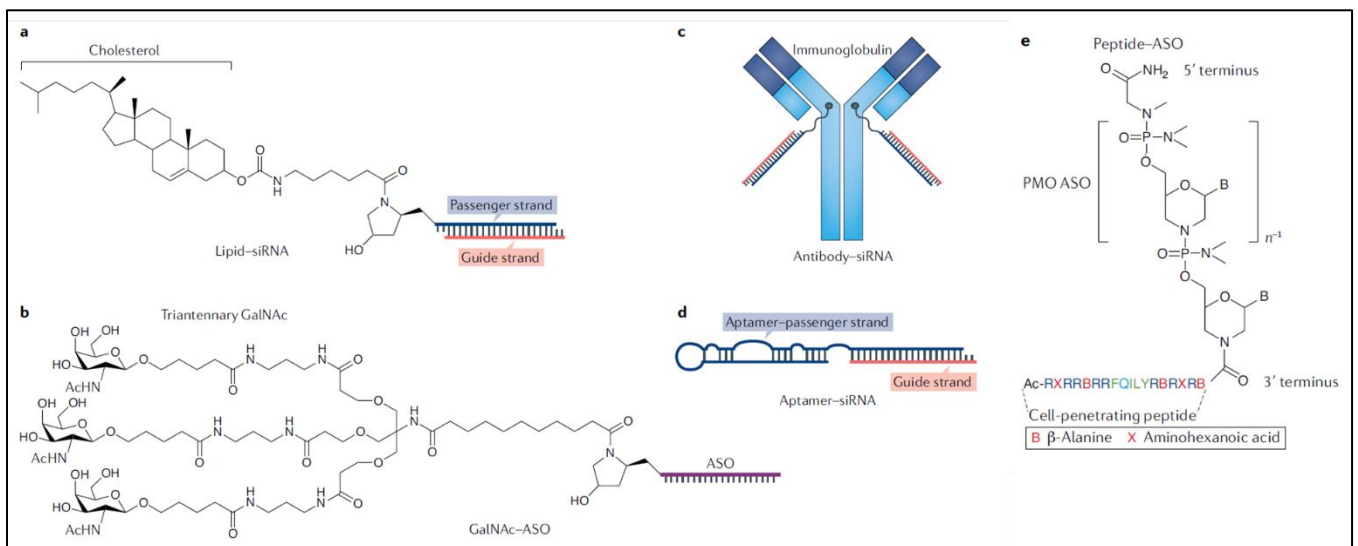


Figure 1.12. Various conjugates appended to NATs for improved biodistribution and delivery. a) Cholesterol-conjugated siRNA, b) GalNAc conjugated ASO, c) antibody conjugated siRNA, d) aptamer conjugated siRNA, and peptide-conjugated PMO ASO (adapted and reproduced from Ref.⁷).

Peptides are another class of conjugates that are gaining attraction in the field.⁹⁷ They are short amphipathic or cationic polymers of amino acids capable of tissue/cell targeting properties, as well as cell-penetrating capabilities with endosomal escape mechanisms (**Figure 1.12. c**). The use of positively charged amino acids allows these peptides to disrupt the endosome/lysosome membrane, leading to the release of the conjugated NAT into the cytosol

for it to be effective.⁹⁷ Recent advances in the development of these cell-penetrating peptides show that they can also be selected with a certain specificity towards target organs or cell types, such as muscle, brain, endothelial, and cancer cells.⁹⁸⁻¹⁰⁰ The ability to have all these properties in one conjugate is attractive. One key element to keep in mind is that these peptides are positively charged, thus most of them are conjugated to NATs that have a neutral backbone to avoid complexation and aggregation, such as morpholino oligonucleotides or peptide nucleic acids (charge of the phosphate backbone is neutralized).⁹⁷ This positive charge can also be associated with toxicity observed in animal models, causing renal damage at high doses and nephrotoxicity.^{101,102} Additionally, the positive charge can lead to the formation of a protein corona once in serum or in circulation, which impacts activity uptake and biodistribution.¹⁰² A lot of work needs to be done on CPP conjugates, but progress is happening, especially with Sarepta Therapeutics' Peptide-PMO conjugate undergoing clinical trials.^{24,103}

Conjugates, whether non-targeting or targeting, have aided in the next wave of approval of therapeutics nucleic acids, and offered potential for extra-hepatic activity.^{7,57} They are attractive as they are a well-defined small molecular entity with decent yield and well-established characterization techniques. Nonetheless, there are some disadvantages associated with such a strategy to modulate distribution.⁵⁷ First, they are still small which could still lead to their renal clearance. Second, a conjugate can only aid one copy of the therapeutic, which will require many events of correct accumulation and clearance avoidance to induce an efficacious distribution.⁵⁷ Also, since this involves direct conjugation of a molecular entity NATs, they should be well-designed so as to not interfere with the therapeutics ability to perform its function (for example hindering ASOs' binding to its target, or siRNA's ability to load into RISC).⁵⁷ Lastly, conjugates might provide a small degree of protection, but it might not be enough for therapeutics which are limited in their chemical modifications (siRNAs) and thus require an enhanced protection.^{16,57}

1.5.3. Drug delivery systems

While chemical modifications have led to the first approved NAT drug to enter the market, drug delivery systems and nanotechnology strategies are the ones that led to the approval of the first siRNA drug, Patisiran by Alnylam.²⁴ Drug delivery systems (DDS) are

nano-sized carriers that are capable of delivering NATs towards their action site.³⁸ A good analogy for DDS is FEDEX delivery, where the truck represents the DDS that delivers a package (NAT) to its destination precisely and safely. DDS can be designed to protect their cargo (NAT) from degradation and unwanted interactions and deliver it to a specific location via targeting ligands (organ and cell specific) where it is then dispatched. The power and beauty of such systems is that they allow for a complete, separate, and intricate design and optimization of the carrier with the desired properties, without affecting the properties of the cargo like conjugates and modifications do.³⁸ They are also attractive because one carrier is capable of delivering multiple copies of the NAT in comparison to 1-conjugate:1-NAT, and they can deliver multiple drugs in a combinatorial fashion. DDS have the potential to resolve many of the issues pertaining NAT delivery, and we will cover some of the most prominent DDS below.

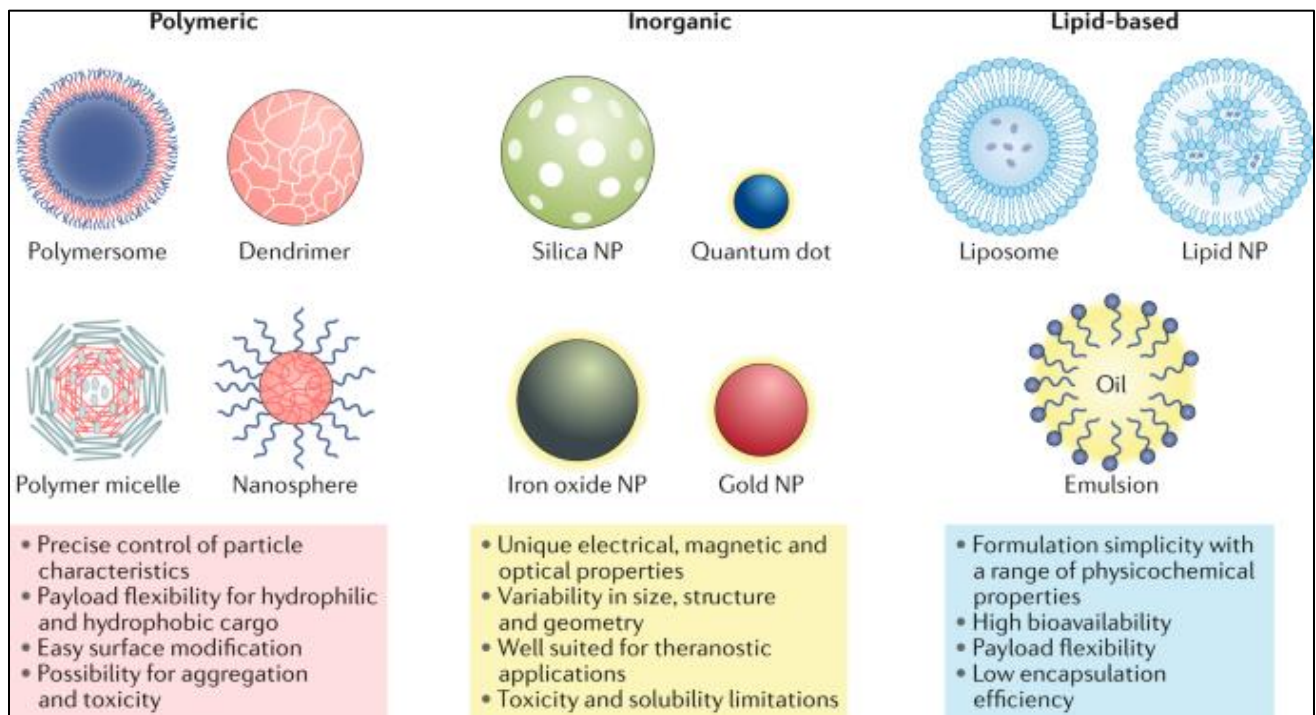


Figure 1. 13. Various classes and drug delivery systems, with their advantages and limitations (adapted from Ref.¹⁰⁴).

1.5.3.1. Lipid-based nanoparticles

Patisiran/Onpattro is based on encapsulating siRNA therapeutics in lipid nanoparticles (LNPs), one class of drug delivery systems made from lipid-based material.^{24,38} LNPs and liposomes are the most used and well-characterized class of DDS. Liposomes were first tested in the 1980s where they delivered DNA to kidney cells successfully.¹⁰⁵ The first approved liposome for clinical use was Doxil, where liposomes encapsulated the chemotherapeutic drug doxorubicin and improved on its drug's safety and efficacy (**Figure 1. 14. A**). Liposomes consist of self-assembled closed structures of phospholipids that form a spherical shape, where the inner phase is aqueous that is encircled by lipid bilayers (**Figure 1. 14. A**).^{105,106} NATs are usually encapsulated in the aqueous cavity due to their water solubility, which protects them from nucleases, minimizes unwanted interactions in circulation, and even offers protection from lysosomes once endocytosed into cells. Liposomes are versatile as they can also encapsulate hydrophobic drugs in between the hydrophobic tails that form the bilayer, which is advantageous for dual delivery.^{104,106} Unfortunately, these particles are rapidly taken up by the RES and cleared, which has led to the use of modifications on the surface of liposomes to extend their circulation and delivery, such as PEGylation.¹⁰⁴

Another notable subset of lipid-based nanoparticles is lipid nanoparticles (LNPs) (**Figure 1. 14. A**). The primary difference between liposomes and LNPs is that the latter forms micellar structures within the core rather than a continuous aqueous interior. LNPs are made from phospholipids for particle structure, PEGylated lipid for enhanced circulation, and cationic lipids to complex with the negatively charged NATs. LNPs are effective in crossing cell membranes mainly due to binding apolipoprotein E that interacts with the LDL receptor.^{7,57}

The most noteworthy design advancement of LNPs is the inclusion of fusogenic and ionizable lipids, that are capable of inducing endosomal escape of the LNP cargo into the cytosol of the cell, which enhances efficacy.¹⁰⁷ Patisiran's LNP design truly was special due to the inclusion of such ionizable lipids: Once

present in the acidic environment of the late endosome/lysosome, they are protonated and interact with the anionic membrane lipids to form a non-bilayer lipid phase with an inverted hexagonal shape.¹⁰⁸ This leads to increased permeability and bursting of the LNP hence releasing the cargo (**Figure 1. 14. B**).^{107,108}

Although liposomes and LNPs have numerous studies showing their safety, and some LNP-based therapeutics are approved, they still face significant challenges especially for NAT delivery. They are low-loading particles, and their systemic delivery is limited to liver and RES, as well as sites with fenestrated endothelium (such as tumor), due to their size which is usually around 100-200 nm. Hence most lipid-based particles have focused on liver delivery or local delivery.¹⁰⁹ Functionalizing these particles with targeting ligands (aptamers, antibodies etc.) is one promising way to modulate these DDS for extra-hepatic delivery, however this will increase the complexity of the particle as well as its toxicity, which complicates its manufacturing and utility. Nonetheless, lipid-based particles' advancements have allowed significant progress in the field and made it to the clinic, especially with the very recent use for mRNA delivery in the COVID-19 vaccine from Pfizer and Moderna, and they remain the most studied/used nucleic acid carrier today.^{24,110,111}

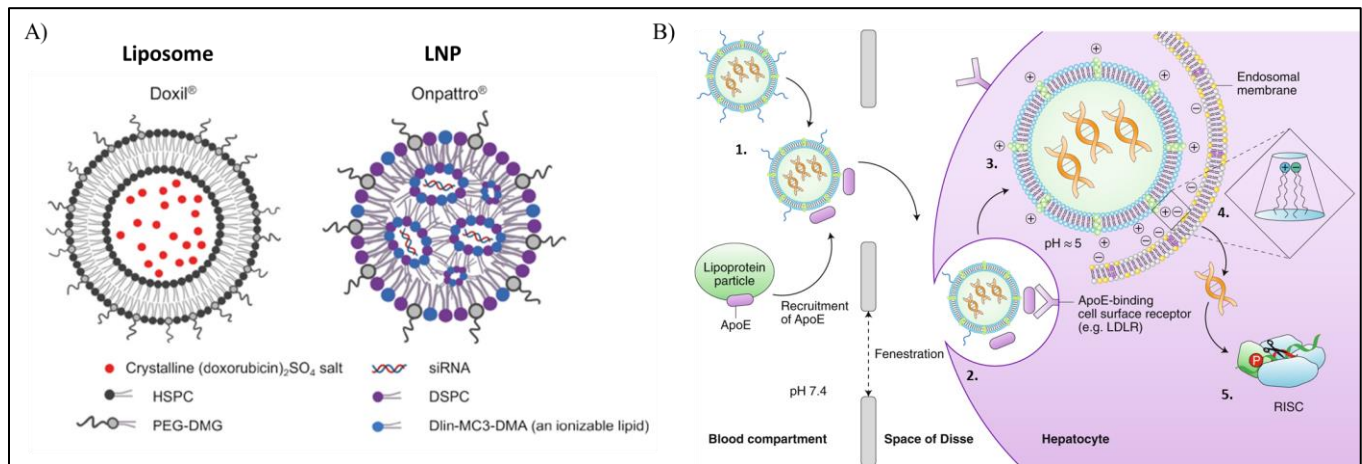


Figure 1. 14. A) Structure of liposome-based approved drug Doxil, and lipid nanoparticle (LNP)-based approved drug Onpattro, and their composition. (adapted from Ref.¹¹¹). **B)** Onpattro's LNP mechanism of action. (1) After intravenous administration of patisiran, PEG2000-C-DMG dissociates from the LNP as it has a short lipid tail and can exchange with lipoproteins in circulation. Removal of the PEG coating allows endogenous ApoE to associate with the LNP, (2) facilitating uptake into hepatocytes via an ApoE-dependent process. (3) upon internalization via endocytosis, the ionizable DLin-MC3-DMA lipid is protonated (positively charged), as the pH decreases in the endosome. (4) The positively charged DLin-MC3-DMA lipid interacts with the negatively charged endosomal lipid, resulting in disintegration of the LNP, destabilization of the endosome membrane, and release of therapeutic into the cytoplasm. (5) the siRNA therapeutic binds to RISC, leading to the targeted degradation of TTR mRNA and subsequent reductions in the target protein levels. (Adapted from Ref.⁴⁵).

1.5.3.2. Exosomes

Exosomes are a newly developed biotechnology technique for the delivery of cargo such as NATs¹¹². They are an endogenously produced nanoparticle with a size of 30-150nm, released by most cells in the body as well as other living organisms (plant-based and bacteria-based exosomes) and can be isolated from cells or body fluids. They have a similar structure to liposomes, but since they are produced from cells (endogenous) they contain many similar materials found in their parent cell.^{7,38,112} This is a key advantage because these proteins allow them

to be recognized as “self” entities like their mother cell, and label them as safe with low immunogenicity. Exosome’s protein composition can be manipulated to contain targeting ligands for improved biodistribution and enhance cellular uptake. An example of such manipulation is the functionalization with rabies virus glycoprotein (RVG) for enhanced brain penetration and uptake.^{7,38,113} The ability to cross the blood-brain-barrier (BBB) is a key feature of exosomes, as this had been a long-standing barrier for NAT delivery to the brain.^{7,113}

Exosomes’ main limitations include isolation/production and loading with NATs.¹¹⁴ Producing and collecting exosomes is still a time-consuming and less reproducible procedure, which introduces many variations and difficulties in their scale-up production for delivery.¹¹⁴ Loading exosomes with their NAT cargo efficiently is also still a challenge, despite a variety of methods being reported such as endogenous production of NAT in mother-cell, and exogenous techniques (electroporation, co-incubation, and sonication).¹¹⁴ Advances in systematic production and loading are in the exploratory phase, but exosomes undeniably have a promising future.³⁸

1.5.3.3. *Polymeric nanocarriers*

Another major class of DDS for NATs are those derived from polymers. This class includes, but not limited to, synthetic polymeric particles (polyplexes, block-copolymers), polymeric micelles, polymeric dendrimers, hydrogels, and natural polymers (chitosan, cyclodextrin) (**Figure 1. 15**).^{38,115-117} Polymeric nanocarriers are widely used due to the ease of manipulation of their physiochemical properties, and the ability to equip them with many functional groups.

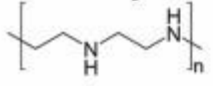
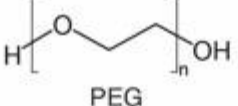
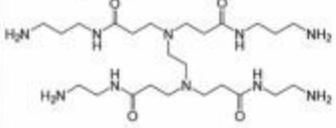
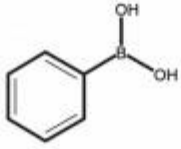
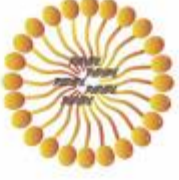
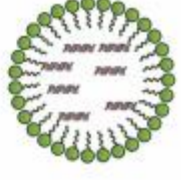
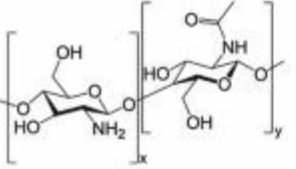
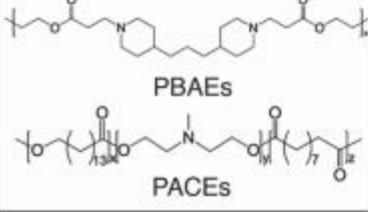
Polymers	Modifications	Vehicle Designs	
Linear Polycations  PEI	Immune System Stealth  PEG	Polyplex 	Nanoconjugate 
Amphiphilic/Nonlinear  PAMAM	Environmental Responsivity  Phenylboronic Acid (pH-sensitive)	Micelle 	Nanocapsule 
Natural Biodegradable  Chitosan		Targetability  Antibody	Dendrimer 
Synthetic Biodegradable  PBAEs PACEs	Sequence/Mw Defined 		

Figure 1. 15. Examples of polymers used to build various vehicles for the delivery of oligonucleotides, as well as modifications that can be appended for additional functionality (PEG for immune stealth, pH-sensitive moieties, and antibodies for targetability) (adapted from Ref.¹¹⁷).

One of the most popular and most used polymeric strategies for delivery of NATs is the use of polycationic polymers such as poly(ethylene imine) (PEI). These positively charged polymers complex with the negatively charged backbone of NATs to form what we call polyplexes, with a size of 50-300 nm and enhance their delivery and uptake into cells. Since its discovery in 1995, PEI is still used today

for this purpose.^{38,118} The abundance of protonation sites in PEI and similar cationic polymers (polyamid-oamine PAMAM, poly-lysines etc) increases their effective delivery of NATs, as they get protonated in the acidic medium of the lysosome which causes them to burst from water and chloride influx (this is known as the proton sponge effect), hence releasing the cargo.¹¹⁷ Although highly efficient, their positive charge causes toxicity and poses a challenge for use *in vivo*, where they induce blood coagulation, innate immune response, apoptosis of cells and inhibition of ATP synthesis.¹¹⁷ Coupling PEG to PEI and using it as a block copolymer improves the performance and decreases toxicity, but not enough for *in vivo* and clinic use.¹¹⁵

Another common polymeric nanoparticle used results from the assembly of polylactic-co-glycolic acid (PLGA) into polymeric particles.⁵⁷ PLGA is biocompatible and biodegradable and has received approval from the FDA as a DDS (**Figure 1. 16.**). However, it is anionic and hence is usually incorporated with PEI that is positively charged so it complex with NATs. PLGA particles have been challenging to use for NAT delivery as they have low loading which reduces their effectiveness.

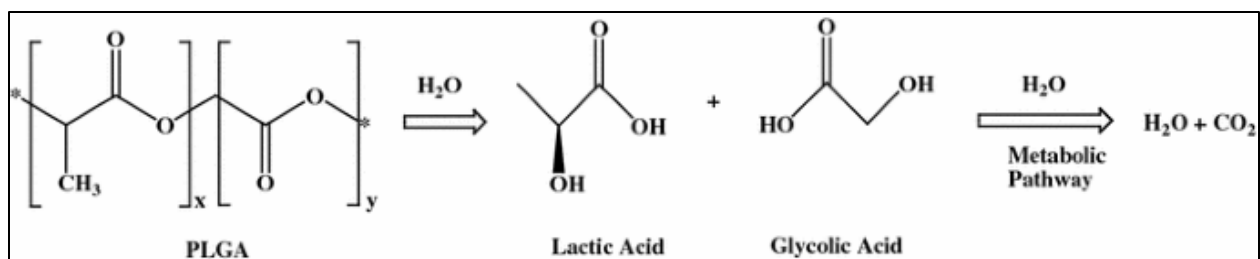


Figure 1. 16. Structure and biodegradation of PLGA (adapted from Ref. ¹¹⁹)

Poly(beta amino) esters (**Figure 1. 15.**) are another family of cationic degradable polymers that have improved properties over the previously mentioned polymers. This is due to its ability to encapsulate nucleic acids, promote cellular uptake, and act as a proton sponge for endosomal escape, while also being

biodegradable and easy to synthesize. Their only limitation is that the high amino content makes them susceptible to aggregate with anionic serum components.¹¹⁷

Polymeric micelles are another class of polymeric nanocarriers that has been extensively studied. They can be spherical with sizes of 10-200 nm, and arise from the self-assembly of amphiphilic block-co-polymers – polymers that possess hydrophobic and hydrophilic blocks (for example polystyrene-PEG or polylysine-PEG block co-polymers).^{115,120} The assembly is driven by the tendency of the hydrophobic entities to hide from the aqueous media around it by forming a hydrophobic core and a hydrophilic corona, especially when increasing the concentration of the amphiphile (**Figure 1. 15.**). The concentration at which micelles start forming is referred to the critical micelle concentration (CMC), at which the formation is driven by dehydration of the hydrophobic entities (releasing organized water molecules around them) and increasing van der Waals interactions between them.¹²⁰ The release of the ordered water molecules leads to the favorable increase in entropy, that overpowers the decrease in entropy from the hydrophobic chains alignments in the core.

Amphiphilic block copolymers can assemble to other structures than the spherical micelles, such as cylindrical micelles and nanosheets.¹²¹ This is dictated by the critical packing parameter (CPP) which depends on the ratio between the hydrophobic and hydrophilic component of the block copolymer's monomer. The more the hydrophobic tail increases in volume, the assembly will go from micelle to cylindrical micelle, all the way to a bilayer and inverted micelle (**Figure 1. 17.**).¹²¹

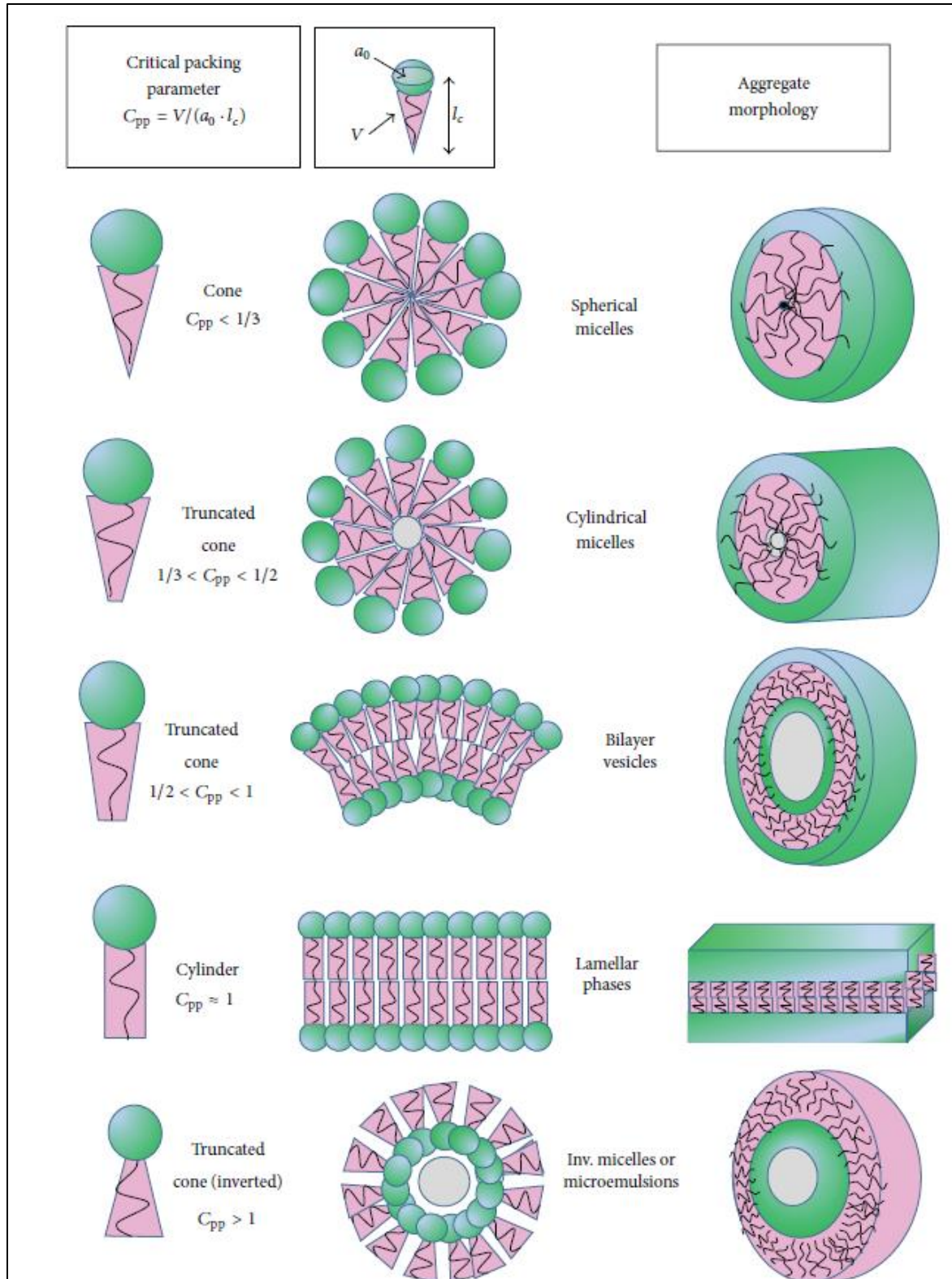


Figure 1. 17. Various structural assemblies from amphiphilic block copolymers based on the variation of the critical packing parameter (adapted from Ref.¹²¹).

Polymeric micelles are a promising DDS for the delivery of NAT. They are relatively straightforward in their design, scalable in production, easy to modify, and enhance the half-life of NAT both *in vitro* and *in vivo*.¹²²⁻¹²⁴ Having the polymeric core provides stability of the particle structure and can be utilized to co-deliver small molecule drugs and NATs for enhanced effects such as cancer.^{124,125} NATs usually electrostatically interact with micelles and small molecule drugs are encapsulated in the core due to their hydrophobicity. Some polymeric particles that have been used for such applications include PLGA-PEI and PEG-PEI based micelles.¹²⁶ Additionally, micelles can be made stimuli-responsive in their release and activation via stimuli-responsive cleavable bonds (disulfide bonds, acetals, esters, etc.).¹²⁶ For example, a block-copolymer shown below has an azobenzene moiety, that is cleaved in the hypoxic and enriched free radical environment of tumor, which leads to the shedding of the PEG corona of the micelle (**Figure 1. 18**).¹²⁷ This particle takes advantage of increased circulation via PEG but gets rid of it when in the tumor to enhance cellular uptake once in the right place.¹²⁷ Many variations of polymeric micelles are being explored by varying the hydrophobic and hydrophilic units, and they all are designed to ensure complexation of NAT by having a cationic character or by direct conjugation to the NAT. The common challenges this class of particles face are the variability in size and molecular weight of the particles produced, as well as some toxicity issues when there is an excess of cationic character as previously discussed.

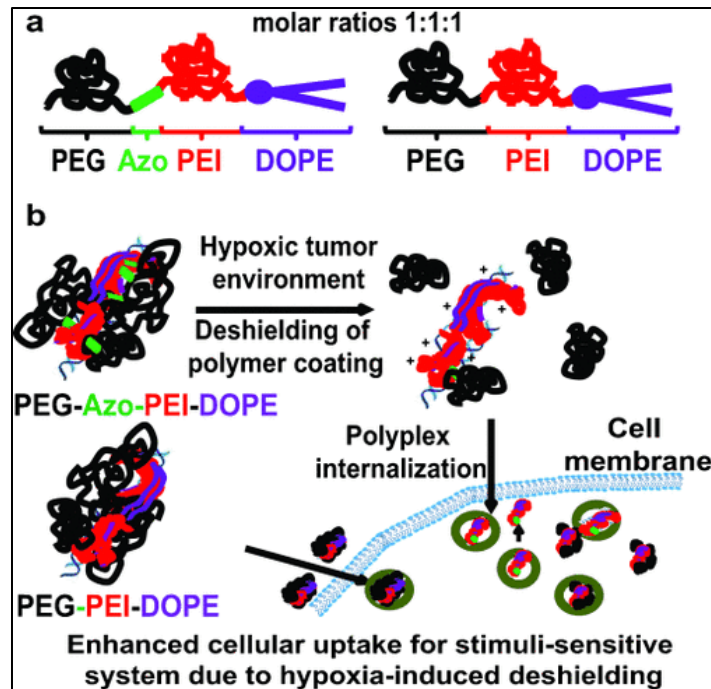


Figure 1. 18. multifunctional polymeric micelle that sheds its PEG corona in the environment of the tumor, followed by enhanced uptake and siRNA release in cancer cells (adapted from Ref. ¹²⁷).

Dendrimers are macromolecules with a branched architecture that is well-defined. A variety of dendrimers can be produced by changing the degree of branching and the polymer used, which produces various sizes and reactive entities.¹²⁸ Polyamid-oamine (PAMAMs), which we previously mentioned, are the most commonly used dendrimers, as they are rich in amines and allow for strong uptake and lysosomal release of NATs¹²⁸. Some examples of PAMAM for the delivery of NATs include work by Delong *et al.* using a 3rd generation PAMAM dendrimet to deliver ASOs to astrocytes, where they saw enhanced uptake comparable to transfection agents.¹²⁹ Another example is using PAMAM dendrimer to deliver 3 different ASOs to tumors *in vivo* showing improved tumor localization.¹³⁰ unfortunately, the richness of positive charge in PAMAMs induces similar toxicity profiles as seen in PEI, and their lack of biodegradability is a challenge for their use in advanced clinical setting.¹²⁸ To modulate toxicity, surface modification of PAMAM dendrimers is one common strategy, such as PEG and lauroyl chains.¹³¹ other strategies include acetylation and hydroxylation of the amines.¹³¹ However, neutralizing the cationic character of dendrimers will impact

the loading capacity of NATs, which necessitates careful design and balance between these two parameters (loading and toxicity).¹³¹ Other dendritic material is also used for NAT delivery, such as poly(propylene imine) (PPI) and poly-L-lysine (PLL), but PAMAM remains the most used and studied in the literature.¹³¹ One interesting new class of dendrimers that is being employed for NAT delivery are Carbosilane dendrimers with phosphonium as the cationic group instead of ammonium, which showed similar transfection capabilities and complexation with much lower toxicities.¹³²

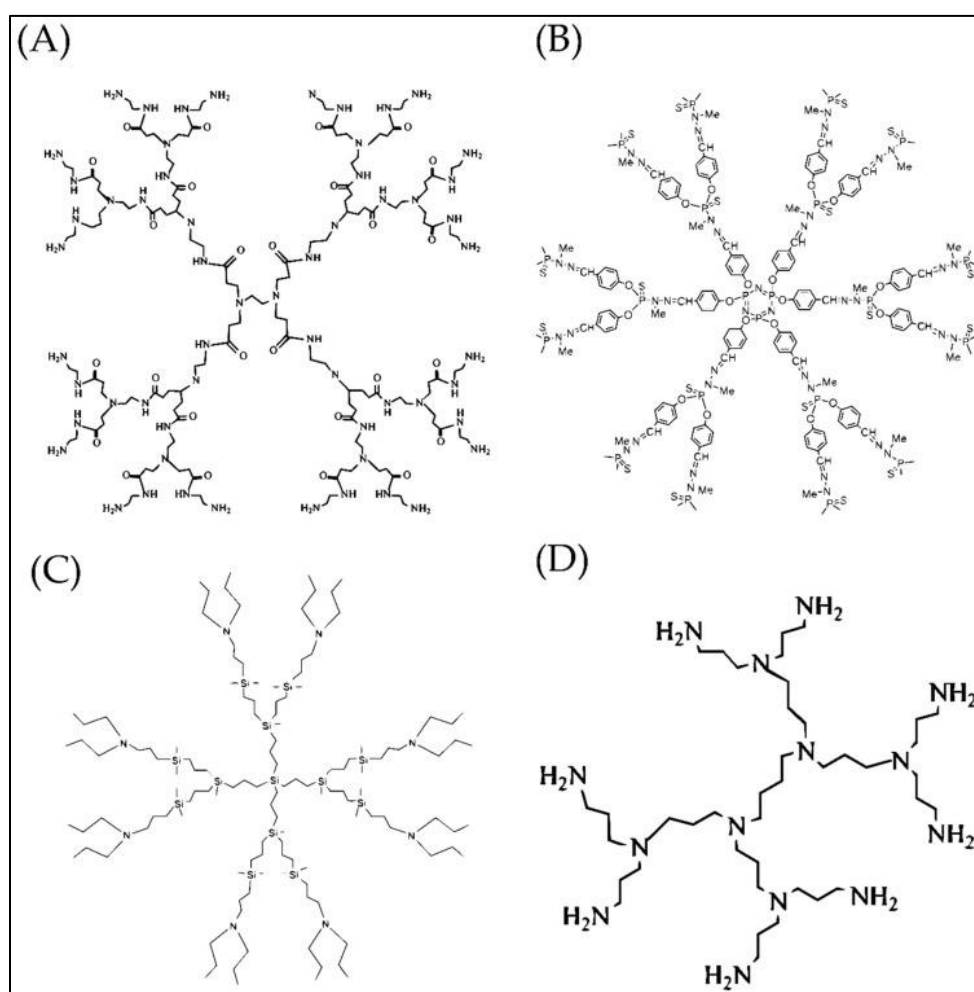


Figure 1.19. various structures of cationic dendrimers used for NAT delivery A) polyamidoamine B) phosphorous C) carbosilane and D) polypropyleneimine (Adapted from Ref. ¹³³)

Natural polymer and materials have also been used for the delivery of NATs.^{38,134} The very first use of nanotechnology for siRNA delivery was by complexing siRNAs with cyclodextrins that are modified with cationic polymers.¹³⁵ Cyclodextrin is a macrocyclic oligosaccharide that has a hydrophobic cavity and hydrophilic external that interacts and protects NATs. The use of cyclodextrin-based nanocarriers is attractive due to its ability to promote cellular uptake via membrane permeability, however toxicity reports have rendered its clinical application. Davis *et al.* demonstrated that cyclodextrin-based self assembled polymeric particles facilitated siRNA delivery in human, where cyclodextrin helped in cell permeability, and the particles showed effective siRNA delivery with significant decrease of the target mRNA in tumors of the patients.¹³⁶ Other natural polymers used for NAT delivery include chitosan, hyaluronic acid, and gelatin as well as hydrogels.^{137,138} Chitosan is cationic natural polymer and can complex with siRNA to form a polyplex particle, where low MW chitosan provided better intracellular release and high MW chitosan showed better stability.¹³⁹ hyaluronic acid-based formulation have also been reported to effectively deliver NATs to tumors.¹⁴⁰

Many other variations of polymeric nanocarriers and materials are being developed and studied for the delivery of NATs, and this area remains an exciting avenue to resolve NATs' challenges. Advantages of polymeric material is that they offer encapsulation of small molecule drugs, we can produce various sizes and shapes with precise control over these parameters, as well as ease of surface modification and functionalization.¹⁰⁴ These are attractive properties for vehicles that deliver NATs, as we can vary physical parameters (size and shape that influence biodistribution and uptake) and add functionalities (targeting ligand, stimuli-responsive behaviour), without altering the therapeutic itself and impacting its activity.¹⁰⁴

1.5.3.4. *Inorganic and hybrid nanoparticles*

Inorganic nanoparticles (NPs) have attracted increasing attention recently for the delivery of NATs. What is attractive about such particles is the ability to control the size and surface properties to a higher degree than the previously mentioned systems, as well as the high drug loading efficiency. Some of the most used inorganic NPs include metallic NPs (gold, silver, iron), quantum dots, calcium-based and silica-based NPs (**Figure 1. 13.**)^{38,141}

Gold NPs (AuNPs) are the most used members of this class as they are easily fabricated in various sizes and are readily functionalized with NATs. The most common strategy is by decorating the surface of AuNPs with thiol-modified oligonucleotides, via the strong interaction of Au with thiols. These particles, which were termed Spherical nucleic acid (SNAs) by Mirkin *et al.*, have been shown to have excellent biodistribution, naturally penetrate skin and pass cellular membranes without the need of transfection agents.^{142,143} SNAs, particles of a solid core and oligonucleotide corona have tremendously expanded to a field of their own by varying their composition and chemistry, and will be discussed in later sections. Other metal NPs include Iron oxide NPs, which have magnetic properties that can be controlled for targeted biodistribution and bioimaging.¹⁴⁴

Quantum dots have unique optical features with tunable sizes and shapes, which can be exploited not only for delivery of NATs but also tracking their fate *in vivo*. These NPs are made from semiconductor nanocrystals and have long-term stability and broad excitation/narrow emission spectrum with high quantum yields of fluorescence.¹⁴⁵ Complexing NATs with cationic quantum dots enables improved stability and activity, as well as near-infrared fluorescent imaging in live animal models.¹⁴⁵⁻¹⁴⁷ Nonetheless, examples of these particles to deliver NATs are very limited, due to the increasing reports and concern on their toxicity.¹⁴⁶

Calcium based NPs can be utilized as well to deliver NATs, as they complex with the negatively charged phosphate backbone of DNA, which have been reported to transport easily through cellular membranes via ion channel-mediated

endocytosis.¹⁴¹ For example, Calcium phosphate nanoparticles have high binding affinity to NATs, where electrostatic interactions occur between the Calcium ions in the carrier and the negatively charged oligonucleotides.¹⁴⁸ Calcium phosphates are easily endocytosed by cells and can escape the lysosome, by dissolving and increasing the positive charge inside with similar effect to the proton sponge.¹⁴⁸ ¹⁴⁹Calcium based nanoparticles are particularly interesting to deliver NATs for bone repair applications, where calcium and phosphate are involved in bone resorption and bone deposition.¹⁵⁰ Hence, dual delivery of calcium ions and NATs that can modulate these phenomena in bones is attractive and under investigation.^{148,151}

Common concerns for inorganic NPs are the toxicity associated with using some of these materials. Metallic structures are not biodegradable and can lead to toxicity in high amounts, as well as increased calcium from calcium-based NPs.^{148,151} In addition, clearance of such particles is not yet well understood, and sometimes too much increased stability will render their clearance from they system and induce toxic effects.^{144,152}

1.5.3.5. *Stimuli-responsive DDS*

Considerable interest in the field is being directed towards the next generation of DDS, especially those with stimuli-responsive behavior. A stimuli-responsive DDS is a dynamic nanocarrier that interacts and responds to cues from the microenvironment around it, that signal it to perform behaviours such as protonation, cargo release, and conformational changes.^{7,38} This is extremely attractive for the delivery of NATs, as it can improve specificity by only releasing the drug in the correct location, thus allowing activation of NATs in the targeted organ or cell.

Stimuli-responsive DDS are a wide class of materials and covering them in detail is beyond the scope of this thesis.^{38,104,138} Nonetheless, it is essential to highlight that all the DDS mentioned above are capable having that stimuli-responsiveness property, thanks to the ease of functionalization of DDS without

modifying the pharmacophore (NATs). Some stimuli that are being studied include pH-response (cationic lipids for endosomal release, acid-labile bonds in tumor microenvironment), temperature-responsive (iron oxide NPs), and redox-responsive (disulfide-based material and azobenzene moieties) DDS.¹⁴¹

1.5.3.6. *The “Valley of Death” for DDS*

Drug delivery systems have enormous potential to resolve the bottleneck issues hindering NATs from reaching their potential in precision medicine. The ability to protect, selectively and effectively deliver large amounts, and minimise toxicity of NATs with little modification of the pharmacophore is indeed the future of the field. However, there is a large imbalance between lab-discovered nanocarriers and the ones that make it to the clinic. This is termed the “valley of death” for the field of drug delivery, where many of promising particle prototypes fail in *in vivo* models and clinical trials. It was reported for example that only 0.7% of the administered nanoparticle dose of all nanoparticle types designed for tumor delivery, ended up in the tumor site.¹⁵³ NATs have already a plethora of challenges, and this statistic will definitely discourage the use of DDS for their delivery.

As more research was conducted in the field, it became clear that design of DDS is not as trivial as it sounds. Structural and chemical properties play a critical role in determining DDS behaviour in biological environment (**Figure 1. 20**).^{7,38,104}

- 1) *The material composition* that makes up the DDS is important in defining the toxicity and immunogenicity profile, as mentioned for PEI and AuNPs earlier. PEGylation and “self” conjugates on the surface could be used to mask immunogenic responses and toxicity-inducing interactions.
- 2) *Architecture (size, shape, and charge)* of the DDS was also shown to have great influence on its behaviour. For example, sizes smaller than 5 nm are renally cleared while larger than 150 nm can no longer benefit from the EPR effect.^{7,104,117} Uniformity in size is also critical, to ensure there is no behavioral variation. This is a challenge for many of the DDS discussed earlier. Various shapes also have different behaviours, where spherical and pointy/sharp particles had better uptake locally in organs and

cells, but rod-shaped particles had better extravasation while in blood circulation.^{104,153,154} 3) *Targeting DDS* as previously mentioned can be obtained via functionalization with ligands that *actively* target them towards specific organs and cells. DDS indeed improve biodistribution by avoiding premature clearance, but they also localize in the liver and kidneys. Hence, careful engineering of which targeting ligand and how much of it to use is essential to ensure beneficial delivery for NATs. Additionally, *stimuli-responsive DDS* are indeed the more promising generation of nanocarriers, which adds another layer of specificity and targeting in delivery.¹⁰⁴

Finally, a very important factor to keep in mind is the ease of manufacturing of the DDS. DDS are modifiable and modular in their design which is attractive, however adding all the necessary properties for a successful delivery can lead to a very complex design, which has a difficult or non-trivial production methodology. This complexity is highly disfavored for clinical translation of the DDS, as it will make it harder to produce it in big quantities needed for pre-clinical and clinical studies, as well as making it challenging for quality control.^{7,38}

The drug delivery field holds the potential to resolve all the major issues that are hindering NATs (stability, specificity/selectivity, biodistribution), however rational and careful design with control over properties via simple strategies is necessary.

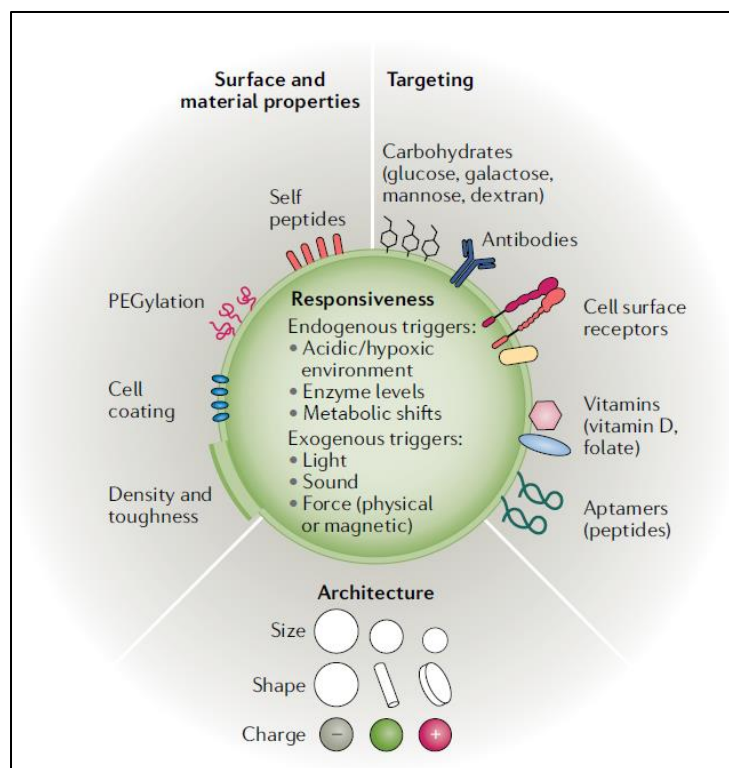


Figure 1. 20. Important design factors to consider in engineering the next generation of DDS that can produce promising translational carriers for the delivery of NAT (adapted from Ref.¹⁰⁴).

1.6. Nucleic Acid Nanotechnology: Nucleic Acids Delivering Themselves

Nucleic acids are so versatile that they have found roles to play in genetics, medicine, and in materials chemistry. This section will discuss how nucleic acids are taken out of their biological context to be used as building blocks in supramolecular chemistry, the birth of DNA nanotechnology, and its application in the delivery of NATs.

1.6.1. Taking nucleic acids out of their biological milieu

Nucleic acids have critical roles in the central dogma of life, where DNA carries and stores genetic information and RNA translates this genetic information into functional proteins. They are also being exploited as medicinal entities as outlined so far (NATs). Nonetheless, the utility of such informational material is not limited to its biological context. From a chemist's point of view, DNA is seen as a biopolymer of nucleotide

monomers that has unique features.¹⁵⁵ Due to the high specificity of its code (A binding T and C binding G) and rigidity of DNA duplexes with well-defined parameters, DNA is a promising building block of materials via self-assembly (**Figure 1. 21. A**).¹⁵⁵ This was envisioned by Ned Seeman in early 1980s, where his group used DNA as a building block to form four-way branched DNA junctions of significant stability, inspired by the naturally occurring Holliday junctions (**Figure 1. 21. B**), which can further assemble into larger arrays via extended complementary arms termed “sticky ends”.^{155,156} This was the birth of the DNA nanotechnology field (and afterwards RNA nanotechnology).

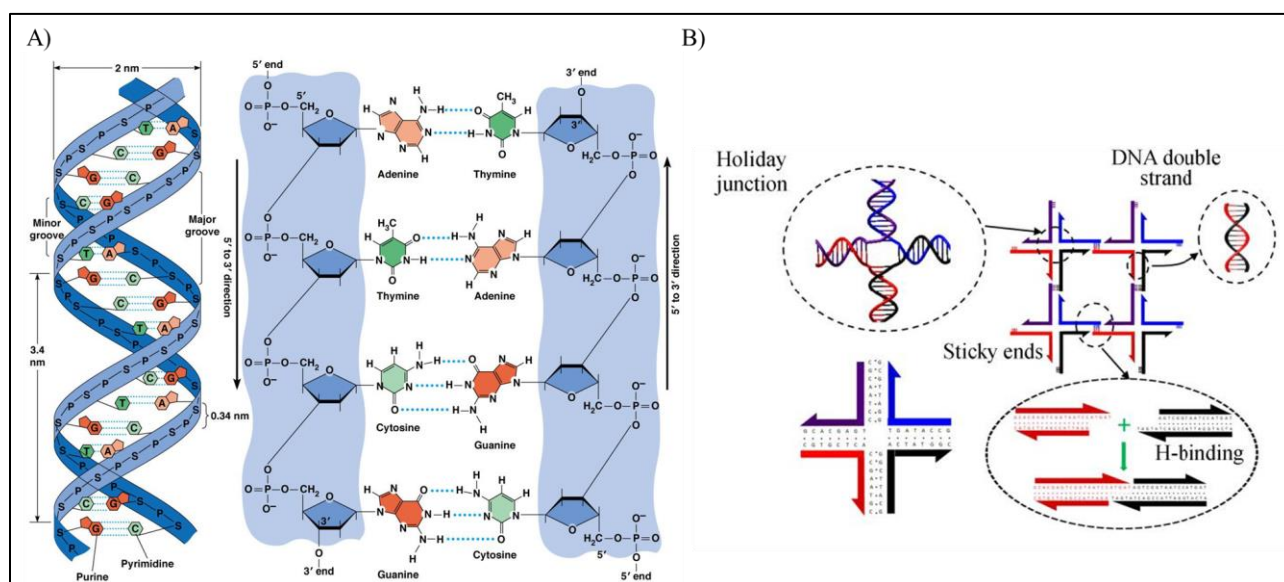


Figure 1. 21. A) DNA duplex double helix structural parameters, showing the specific hydrogen bonding between A-T and C-G, the antiparallel orientation of strands, and dimensions of the helix (adapted from Ref.¹⁵⁷). B) Holliday junction with sticky ends that assembles into an array (adapted and reproduced from Ref.¹⁵⁸).

The interest in the field skyrocketed due to the many advantageous characteristics of DNA as building block: rigidity, programmability, water solubility, and ease of synthesis (automated). Subsequently, a variety of structures were engineered and termed Nucleic Acid Nanoparticles (NANPs), with controlled physiochemical properties and inherit biological activity owed to the defined molecular features of the building blocks.¹⁵⁵ NANPs

are being utilized to a variety of applications such as biosensing, nanoscale organization of materials and biocomputing.^{159,160}

NANPs are also excellent candidates for drug delivery, and they are emerging as a promising DDS.¹⁶¹ They intrinsically overcome many challenges hampering DDS from crossing the “valley of death”: they are biocompatible, programmable with precisely controlled sizes and shapes, easily functionalized with targeting ligands, and easy to make thanks to automated synthesis.¹⁵⁹ Many small molecule drugs can be bound to DNA duplexes, and improved delivery and efficacy of these drugs has been reported (most famously doxorubicin).^{155,159,160} But more interestingly for this thesis, nucleic acid nanoparticles are modular drug delivery vehicles as they incorporate NATs as part of their design.¹⁵⁹

One might wonder why nucleic acids, that are unstable and have difficulties crossing cellular membranes, can be used to resolve these same issues. This is due to new properties NANPs gain when they are organized into specific structures. In comparison to stand alone nucleic acids, NANPs have increased nuclease stability; some NANPs display enhanced cellular uptake owing to their 3D structure and avoid renal clearance due their increased size.^{7,40,155,159,162} The synthesis and properties of NANPs will be the discussion of the next section.

1.6.2. Structural strategies to build NANPs for NAT delivery

The three main strategies to build NANPs are: 1) tile-based assembly, 2) DNA origami, and 3) wireframe assemblies.¹⁵⁹ later, DNA amphiphiles became a prominent strategy as well, which expanded on the DNA language for assembly. Each strategy will be briefly introduced, with specific examples in NAT delivery.

1.6.2.1. Tile-based assembly

The tile-based assembly strategy of NANPs is based on the stable and immobile Holliday junction developed by Seeman’s group, which is made from

two DNA duplexes that crossover to each other. The stiffness is double that of linear DNA, which led to the construction of more complex and rigid structures from this starting material. Later, double, and triple crossovers were developed with great structural variations. With single-stranded regions (sticky ends) at the extremities of these “tiles”, arrays of tiles can be formed that can assemble into a variety of structures (**Figure 1. 22. A**).

These structures have been shown to be more stable in biological conditions due to sterically shielding nucleases from binding and degrading the components. For example, these assemblies have been utilized to protect and deliver miRNAs that are incorporated into the NANP, allowing for a significant gene regulation and inhibiting cancer cell growth *in vitro*, that is otherwise absent when no NANP is used. (**Figure 1. 22. B**).¹⁶³

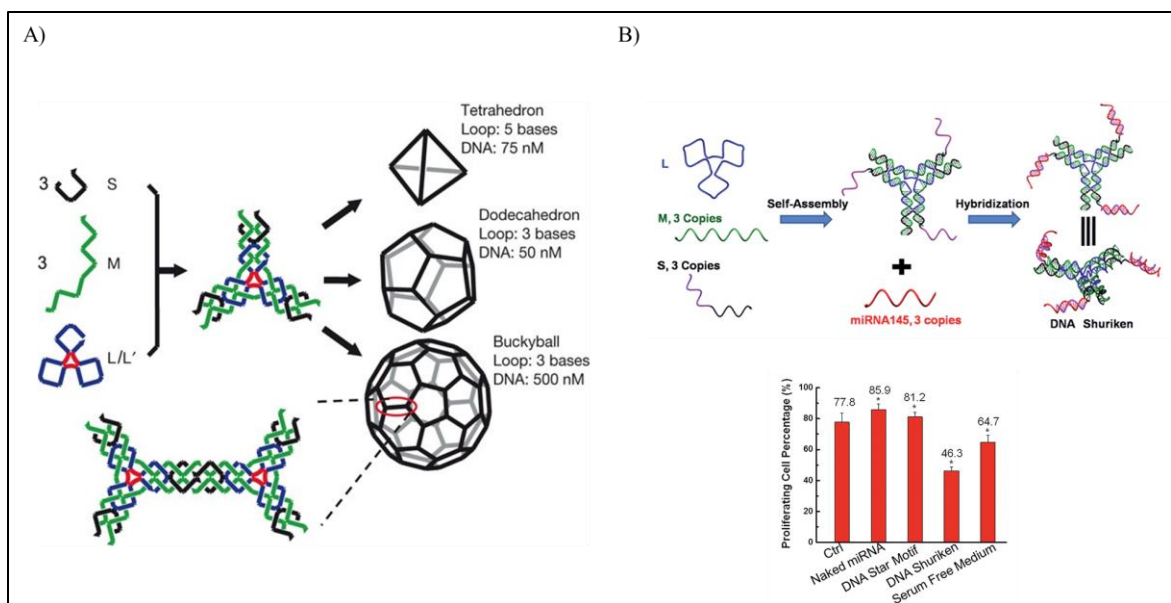


Figure 1. 22. A) Various tile-based assemblies with control over shape and size (adapted from Ref.¹⁶⁴). **B)** tile-based star that can deliver functional miRNA *in vitro* (adapted from Ref.¹⁶³).

DNA tile-based assembly was also the first modality to show that dynamic structures can be formed from such material, when Seeman *et al.* showed that they can switch between two forms of DNA (B and Z DNA) on a DX tile. This was the

basis for exploring dynamic NANPs, where NANPs were developed to respond to various stimuli (pH, temperature, light).¹⁵⁹ One unique stimuli-responsive property that is exclusive to NANP is toehold mediated strand displacement. In this method, a fully complementary strand (strand 2-3 in **Figure 1.23.**) can invade a partially duplexed strand (1-2:2*-3*) via a toehold region (3*), leading to the release of the less-favored partially bound strand and formation of the fully complementary and more favorable duplex (**Figure 1. 23.**).¹⁶⁵ This strategy is extensively employed in stimuli-responsive NANPs.^{159,166}

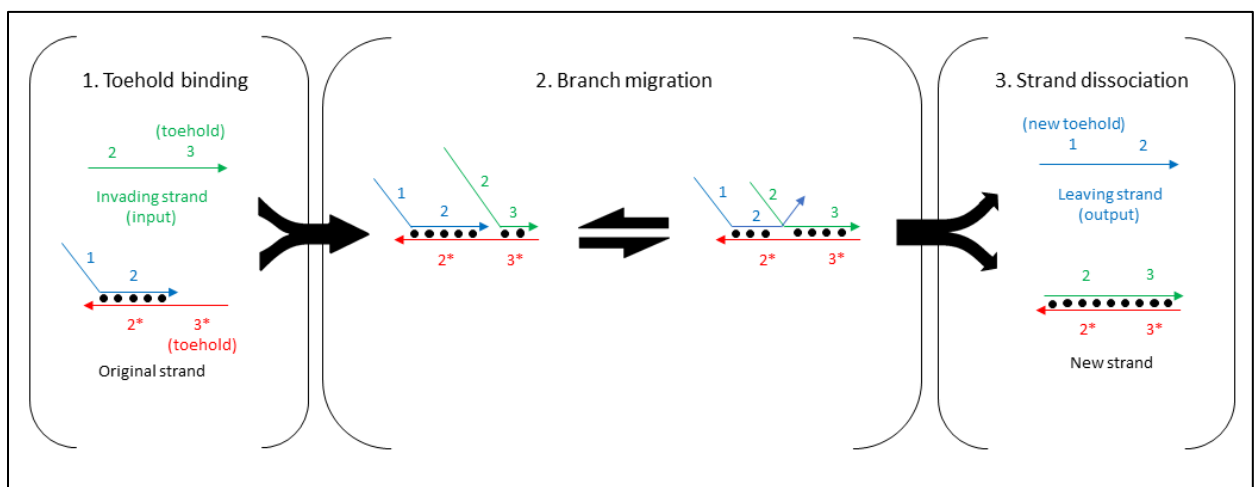


Figure 1. 23. Toehold mediated strand displacement mechanism which introduces stimuli-responsive and dynamic behavior to NANPs (adapted from Wikipedia).

1.6.2.2. DNA Origami

Another hallmark in DNA nanotechnology was the development of DNA origami. Discovered and developed solely by Paul Rothemund in 2006 in a seminal paper, it applies the principles of origami (folding of a scaffold to form structures) to DNA, where a very long DNA scaffold strand is molded into a variety of shapes with hundreds of short staple strands (**Figure 1. 24. A**).¹⁶⁷ The computer-aided design and variety of binding positions of the staple strands to the scaffold will sculpt the latter into the desired shape.¹⁶⁷ Rothemund showcased the versatility of the system by making smiley faces, stars, and triangles. The field gained immense

traction and various origami-inspired methods were developed, yielding assemblies with precisely controlled structure and function.¹⁵⁵

Origami-based NANPs have also been utilized for the delivery of drugs, including NATs.¹⁶¹ One example that showcases the modularity, physical parameters control, and ease of functionalization of NANPs is shown below (**Figure 1. 24**). An origami-based tubular NANP was formed to deliver two different siRNA and small molecule drug, in a targeted/enhanced (tumor-penetrating peptide) and stimuli-responsive (labile S-S bond) manner.¹⁶⁸ The NANP is rigid, has the predicted size and shape with low polydispersity, and successfully accumulated in tumors *in vivo* with silencing of the genetic target.¹⁶⁸

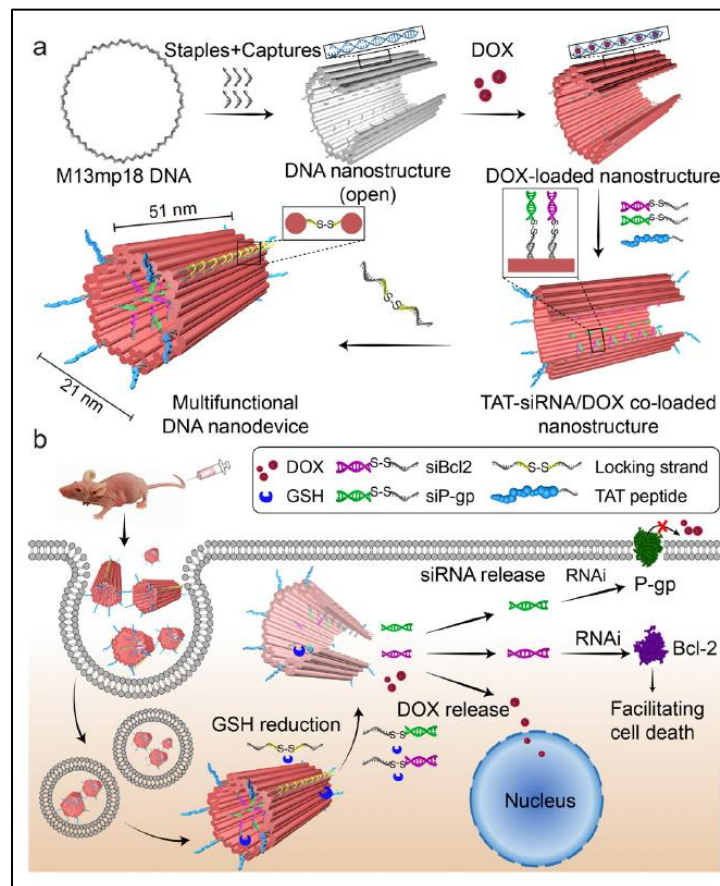


Figure 1. 24. Design of a multifunctional tubular DNA nanodevice. (a) Illustration of the construction of a siRNAs/drug co-loaded tubular nanodevice based on DNA origami technique. (b) Schematic representation of utilizing the nanodevice for combined cancer therapy (adapted from Ref.¹⁶⁸).

While DNA origami NANPs are dense and robust particles, and even with advancements in production of oligos, it is impractical to use such many nucleic acids (hundreds) which is limiting in manufacturing and can lead to many unwanted side effects and toxicity.^{159,160} This is especially prominent in origami structures, as CpG motifs (a C base followed by G base, where the C is unmethylated as in genomic DNA) will be very common due to the increased number of strands used.^{159,160}

1.6.2.3. Wireframe assembly

Perhaps the most economic, versatile, and attractive method to develop NANPs for drug delivery is wireframe assembly.¹⁵⁵ This method focuses on “DNA minimal” approaches and assembles hollow structures, where a specific shape is designed and made by assembling the wireframe of that shape in 3D.¹⁶⁹ This was first demonstrated by Seeman *et al.* when they formed a wireframe DNA cube, and then other structures were developed (**Figure 1. 25. A**).^{155,170} Wireframe NANPs have been a focus in the Sleiman lab, and a large variety of structures were made with varying sizes and geometries with using as low as 4-8 strands.^{155,169} Such strategy makes the production of NANPs inexpensive and synthetically simple in comparison to the previously discussed methods, a key factor to consider for drug delivery. Their simplicity however does not take away from their functionality, as these structures still have all the benefits mentioned earlier: robustness, dynamicity, and addressability.¹⁵⁵

Examples of wireframe assembled NANPs for the delivery of NATs are numerous and some are highlighted below. In one instance, a DNA tetrahedron was functionalized with siRNAs and folate as a cancer-specific target ligand (**Figure 1. 25. B**). Such design allowed the study of how many targeting ligands, and which spatial orientation is necessary for enhanced *in vivo* delivery and accumulation in tumor. This shows the versatility and level of control that NANPs allow (size, shape, orientation, functionalization) in a simple and effective way.¹⁷¹ Another

example are triangular prisms from our lab that were hybridized to ASOs and delivered to cells (**Figure 1. 25. B**).¹⁷² Being part of NANPs allowed for control of how many copies of the therapeutics are delivered, enhanced stability as well as increased cellular uptake and efficacy.¹⁷²

Another example that showcases the power of wireframe assemblies was reported by our laboratory, where a DNA “nanosuitcase” was designed to engulf an siRNA and release it in a stimuli responsive manner (**Figure 1. 25. C**).¹⁷³ The siRNA is partially hybridized to the suitcase, and only in the presence of two over-expressed cancer genomic markers (double the specificity), toehold strand displacement will occur and release the cargo.¹⁷³ Many other examples of stimuli-responsive NANPs have also been reported, such as DNA-minimal nanotubes via aptamer switches reported by Ju *et al.*¹⁷⁴

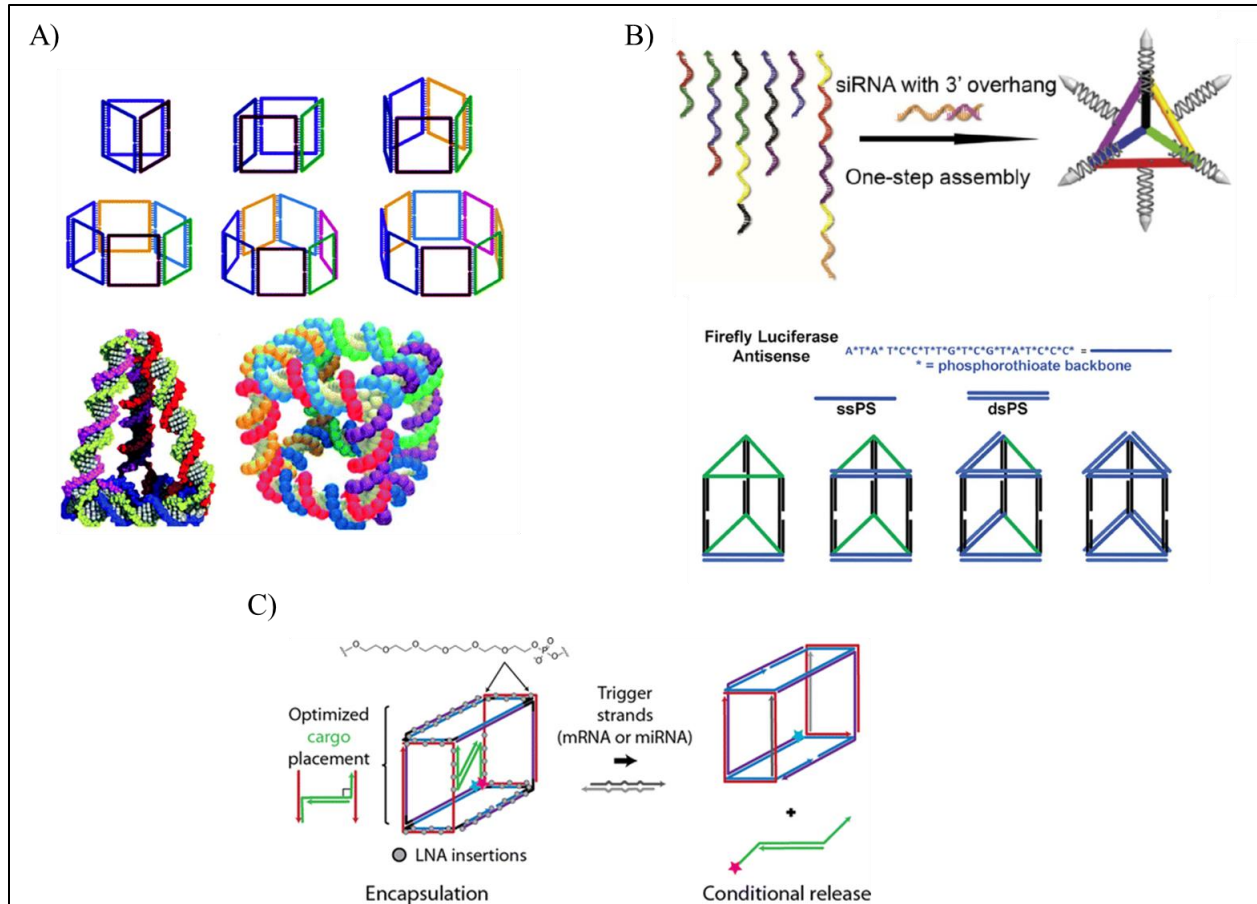


Figure 1. 25. A) DNA NANPs constructed via wireframe assembly (adapted from Ref.¹⁷⁵). B) examples of wireframe assemblies for the delivery of NATs: tetrahedron carrying siRNAs and trigonal prisms carrying ASOs with varying amounts (adapted and reproduced from Ref.¹⁶¹).

While wireframe assemblies of NANPs are extremely promising DDS, they are not as robust and rigid as other particles (origami based particles and tile-based). They are more dynamic in size/shape as well as accessible to nucleases, which will necessitate strategies to improve the stability, especially for *in vivo* studies and long-term effects. Such challenges also apply in general to all DNA-based materials; DNA origami structures pose the additional challenge of being unstable in physiologically relevant, magnesium reduced environments.¹⁶⁰ Strategies to mitigate these issues include chemical modifications of nucleic acids as described earlier, as well as insertion of chemical moieties and polymeric shells.¹⁶⁰ Any modifications to NANPs should not become too complicated, which would negate

their simplicity in production and manufacturing/scale-up. Another important point is that NANPs over the years have been heavily studied *in vitro* only. Only recently have some NANPs been thoroughly studied *in vivo*.¹⁷⁶ Not many successful reports are available on NANPs *in vivo*, and the more we conduct studies on all the variants available, the more the field will inch towards clinical applications.^{159,160,176}

1.6.2.4. DNA amphiphiles

All the previously mentioned strategies to build NANPs are made solely from nucleic acids and mostly rely on their assembly via Watson-crick non-covalent base-pairing. However, chemists wanted to further expand the language in which NANPs assemble from and started incorporating other supramolecular interactions.¹⁵⁵ DNA-amphiphiles, which are made from a hydrophilic DNA strand and hydrophobic unit (small molecule, polymer), are an important area of research that has gained increasing attention.^{177,178} DNA amphiphiles self-assemble into a variety of structures when placed in aqueous solutions, mainly to shield the hydrophobic entities from the aqueous phase (hydrophobic effect).¹⁷⁷ In these core-shell structures, the core is composed of hydrophobic units and the outer shell (corona) is composed of DNA strands. The formation of hydrophobic pockets is attractive for the delivery of small molecule drugs that suffer from poor solubility where they can be encapsulated in the hydrophobic core, while the nucleic acid portion is still addressable and potentially used for therapy or stimuli-responsive behaviour.¹⁵⁵

Control over structures generated from DNA amphiphiles is achieved by varying the ratio of the hydrophilic and hydrophobic components, as well as mixing them with other materials of interest that can interact with the nucleic acid handle.^{159,177,179} Spherical micelles, rods, ribbons, and vesicles, as well as amphiphiles that can switch between two different shapes have been generated (**Figure 1. 26.**), and these assembled DNA amphiphiles have been applied for the delivery of both hydrophobic drugs and NATs.^{159,177} Indeed the ability to form various structures of different sizes and shapes is attractive for the delivery of

NATs, as it allows to investigate the physiochemical properties that impact delivery and efficacy.¹⁸⁰ For instance, rod-shaped polymeric particles were internalized in cells to a different extent than spherical particles, even when both are made from the same material.¹⁸⁰

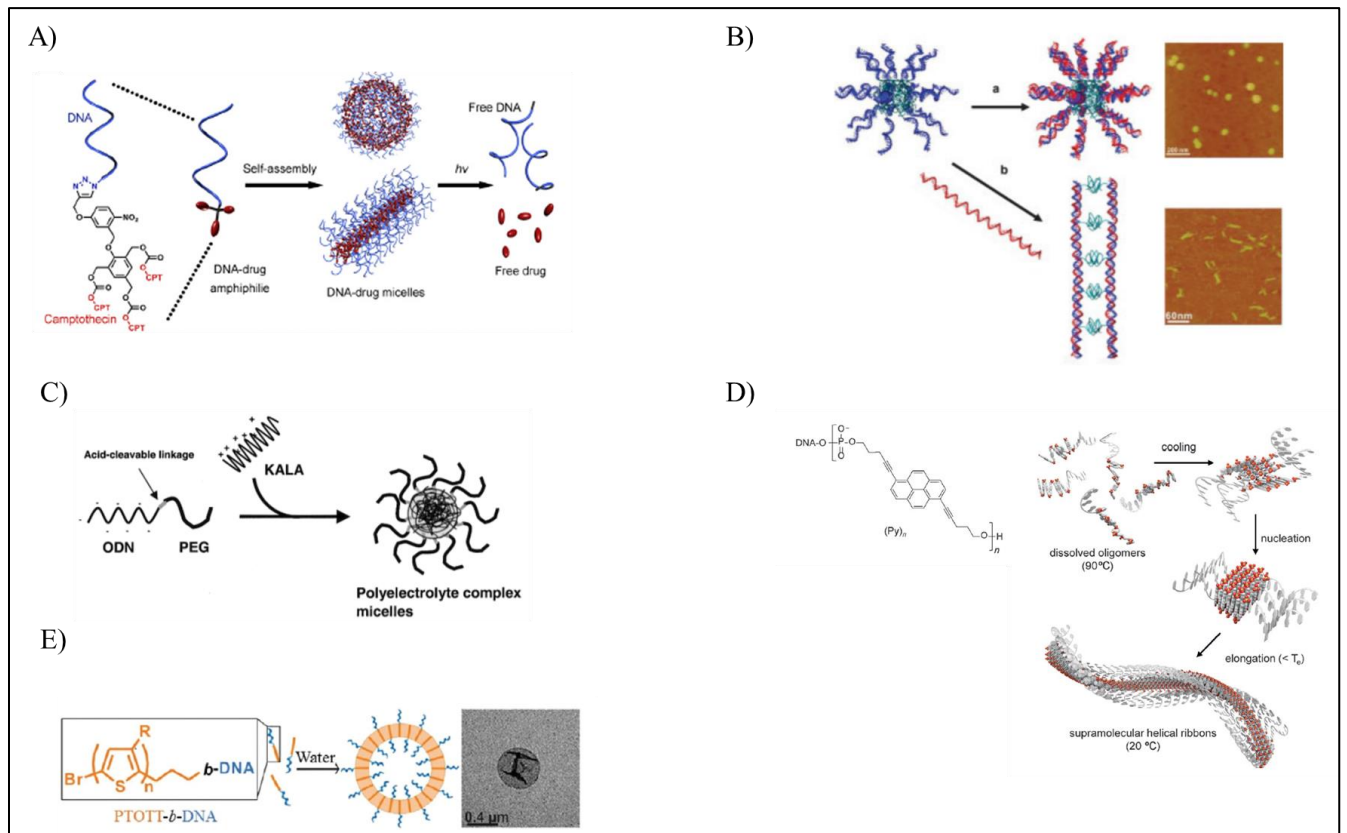


Figure 1. 26. Various structures made from DNA amphiphiles. A) DNA-drug conjugate that assembles into sphere or rod (adapted from Ref.¹⁵⁹). B) micelles that can be further assembled into rods (adapted from Ref.¹⁸⁰). C) ASO-PEG and positively charged KALA forming a spherical complex to enhance delivery (adapted from Ref.¹⁸¹). D) Pyrene-DNA amphiphile assembling into a helical ribbon (adapted from Ref.). E) DNA amphiphile that assembles into a vesicle (adapted from Ref.¹⁸²).

One of the most promising NANP for the delivery of NATs to this date are spherical nucleic acids (SNAs). SNAs are composed of a metallic or hydrophobic core, and a radiant dense nucleic acid corona.^{142,179} Many variations of SNAs are being studied and developed.^{143,183} Due to the exponential advancements on SNAs

in recent years, their promising properties, and the work reported by this thesis on sequence controlled SNAs, the next section will discuss SNA's origin, advancements, and applications in delivering NATs.¹⁴³

1.7.Spherical Nucleic Acids

Nucleic acid nanotechnology has great promise in producing the next generation of DDS that will enable the full capacity of NATs. Out of the variety of NANPs generated, SNAs are the most clinically advanced class due to their advantageous properties. In this section we will introduce SNAs and why they are a promising candidate for clinical advancement for the delivery of NATs, and we will discuss SNAs developed in our lab via sequence-controlled polymers.

1.7.1. First reported SNAs: The gold standard

SNAs are a subgroup of nucleic acid-based particles that is characterized by having a densely packed, radially oriented nucleic acid outer shell, and a solid core than can be made from various starting materials.^{142,143} It is important to make the distinction between SNAs and other NANPs, where the shape and orientation of the nucleic acid portion is determined solely by the shape of the core and the chemical linkage between the core and nucleic acid, and not by the recognition properties of DNA (hybridization).¹⁴² The first reported SNA was a gold-nanoparticle (AuNP) core functionalized with DNA strands via thiol linkages.¹⁸⁴ The attachment of DNA to the gold core was optimized where a passivated AuNP surface was bound to thiol-modified DNA strands to produce a dense and uniform DNA outer corona (**Figure 1. 27.**).¹⁴²

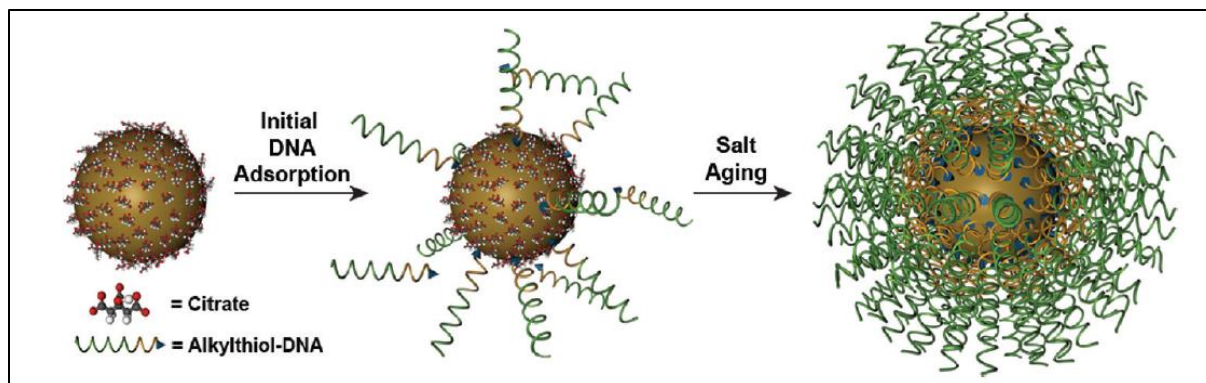


Figure 1. 27. SNA formation by incubating thiol-modified DNA strands with passivated AuNP surface, in aqueous solutions with high salt concentration (adapted from Ref.¹⁴²).

Gold nanoparticles were used as a suitable core material due to the ease synthesis with good control over size and shape, as well as their unique optical properties.¹⁴² A variety of SNAs were also developed by varying the core from gold to other metallic (iron, platinum) and non-metallic nanoparticles (silica, liposomes, micelles, polymers, quantum dots), where each had their own additional unique properties, but still possess SNA features (**Figure 1. 28.**)¹⁴³ Functionalizing these SNAs requires unique chemistry dependent on the core used.

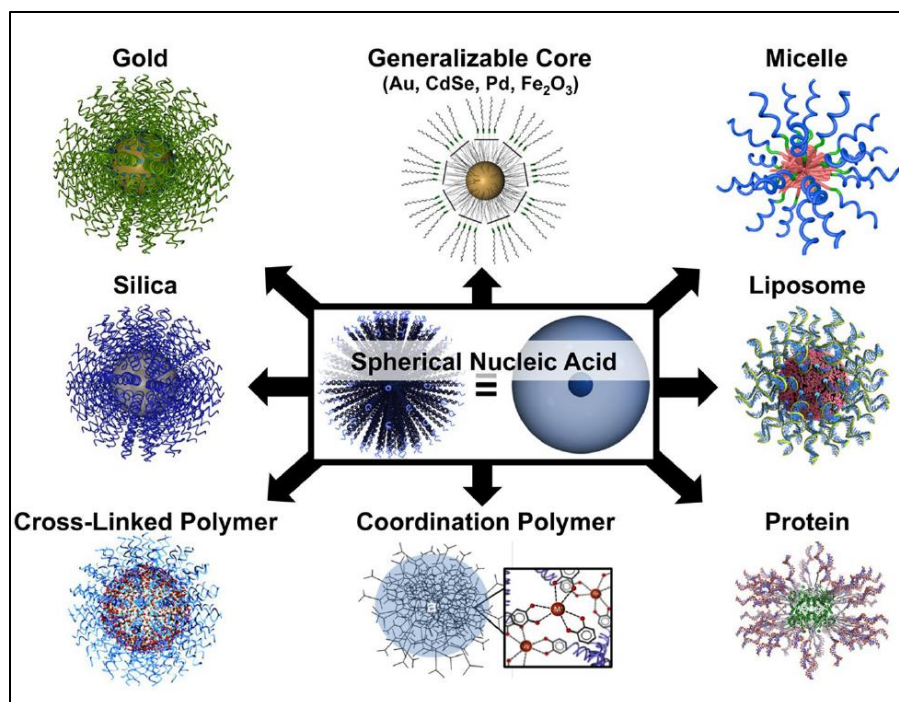


Figure 1. 28. Schematic diagram showcasing the variety of SNAs that can be made from different material (adapted from Ref.¹⁴³).

These structures were applied to a variety of applications such as assembly, diagnostics, and materials chemistry.^{142,143} Of interest to this thesis, SNAs were utilized as drug delivery vehicles to improve on the delivery of NATs, where the outer shell is made from either ASOs or siRNAs.

1.7.2. *SNAs' attractive properties for the delivery of NATs*

SNAs became a promising modality to deliver gene-regulating NATs due to some unique characteristics, in addition to being a simple and adaptive nanoparticle.¹⁸⁵ First, SNAs have been shown to have higher binding affinity towards their target, which would increase efficacy of NATs in binding and degrading their target.^{186,187} Second, SNAs are nuclease resistant in comparison to the free NAT, even if the nucleic acids are exposed.¹⁸⁸ This stability is mainly due to dense packing on the surface and increased local salt

concentration, which sterically hinders nucleases from degrading them.¹⁸⁸ Third, they readily penetrate cells at a high rate (more than 50 cell types tested) without the use of any aiding transfection agent (cationic polymers or liposomes).^{185,189} Last, SNAs have little observed toxicity and have low immunogenic response in comparison to standalone NATs and allow for additional functionalities derived from the nanoparticle core.^{142,189}

All these unique properties of SNAs that are advantageous for NAT delivery are indeed derived from the structural features of having a solid core and a radiant nucleic acid corona. No matter what core is utilized to make SNAs, if the shape is spherical with a dense nucleic acid corona, then these SNAs will have nuclease stability, enhanced cellular uptake and improved binding towards their target sequence, with only minor variability based on the material used in terms of chemistry.¹⁴² An interesting study provided evidence for the importance of SNA structure conferring their function, where AuNP SNA was formed, and then the gold core was dissolved, leaving a hollow SNA that kept its radiant structure of dense nucleic acid shell (**Figure 1. 29.**). The study showed that this structure was still able to enter many cell lines, via a common pathway for many SNAs: cell surface scavenger receptors that perform endocytosis of polyanionic ligands, such as the densely packed nucleic acid corona of SNAs.¹⁸⁹

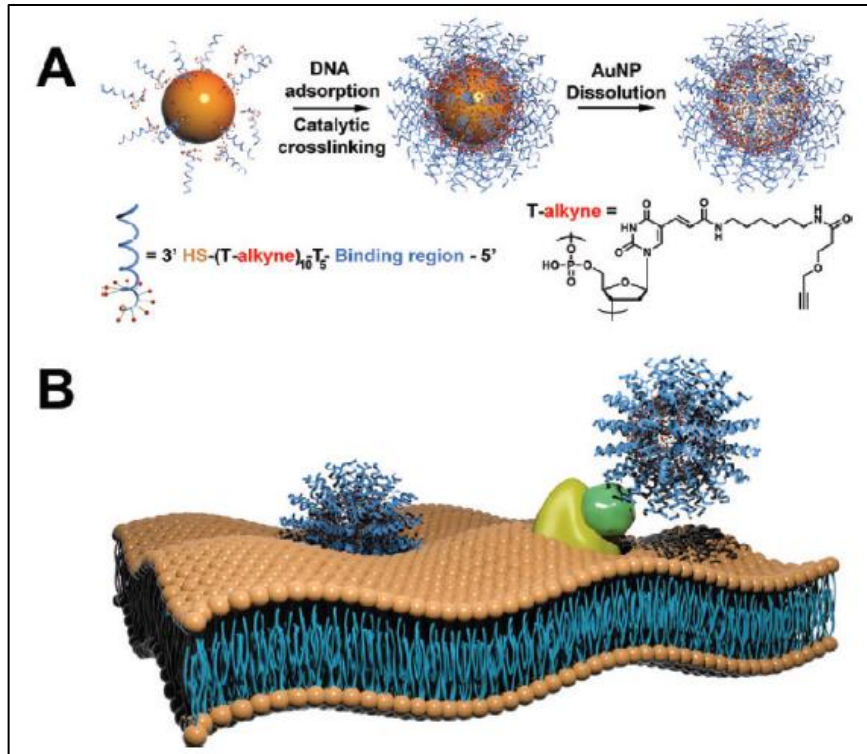


Figure 1. 29. A) Hollow SNAs were synthesized by crosslinking the DNA on the surface of AuNP followed by dissolution of the AuNP. B) schematic representation of the hollow SNA interacting with scavenger receptors that facilitate the uptake of polyanionic ligands (adapted from Ref.^{142,189}).

SNAs offer a new paradigm for the delivery of NATs, where negatively charged, nucleic acids do not necessarily have to be packaged inside positively charged carriers to enable their protection and uptake. Instead, using nucleic acids as building blocks and controlling their density and orientation as in SNAs, allows for the use of a single entity carrier with the desired characteristics.^{142,143}

The first application of SNAs for NAT delivery was published over a decade ago, where AuNP SNA functionalized with ASOs were able to silence the expression of green fluorescent protein in cells.¹⁸⁵ Following this, SNAs made from various materials were used to deliver ASOs and siRNAs to regulate a variety of genes both *in vitro* and *in vivo*.^{143,190} For example, SNAs were used to deliver siRNAs targeting the oncoprotein Bcl2Like12 (Bcl2L12) in glioblastoma patients' brain, as they were able to cross the blood-brain-barrier, a difficult barrier for drug delivery, and reach the target tumor site in the

nervous system.¹⁹¹ The most clinically advanced NANP is an SNA being developed by the company Exicure to treat glioblastoma patients.¹⁹² SNAs were also functionalized with targeting antibodies to improve specificity of delivery towards HER2 overexpressing cancer cells.¹⁹³ SNAs were also applied to improve wound healing and immunomodulation (Figure 1. 30.).^{143,194}

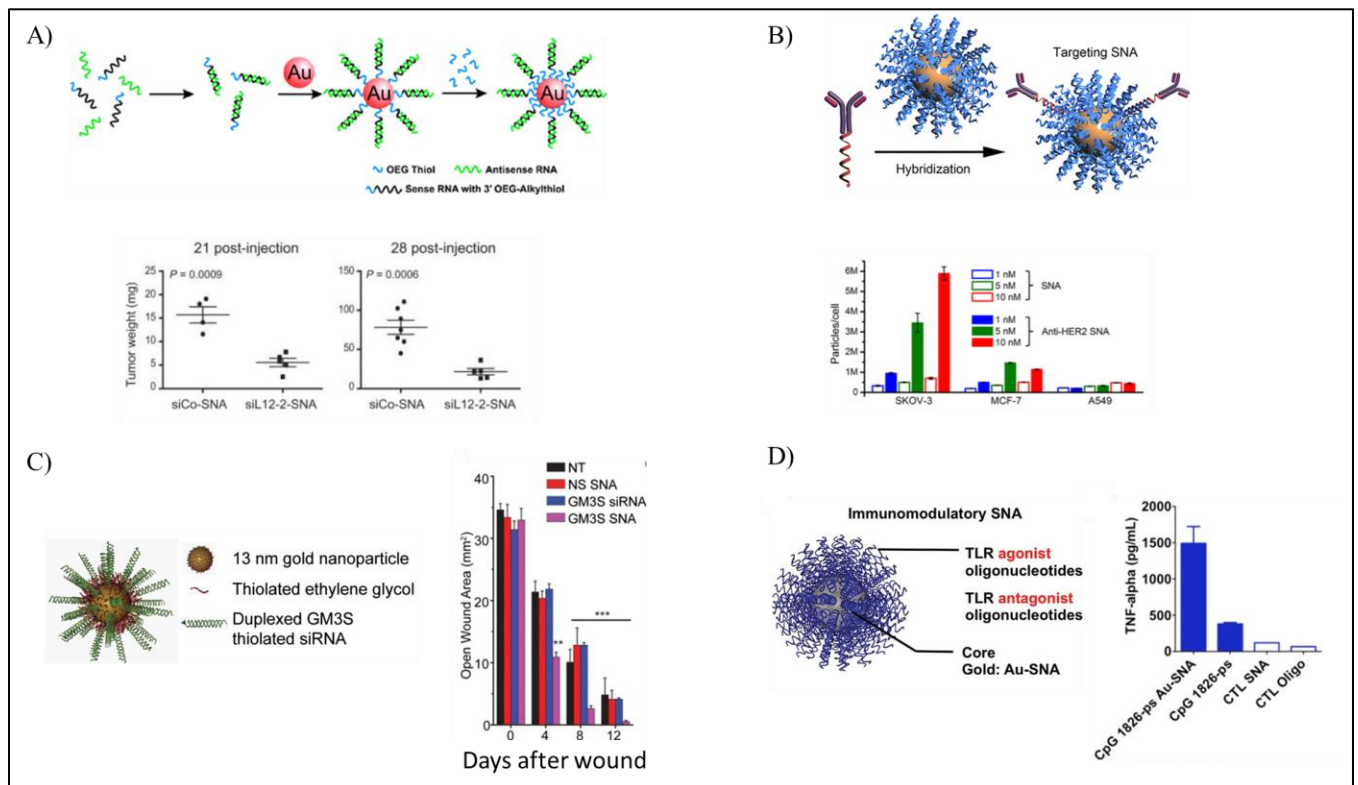


Figure 1. 30. Examples of SNAs used for the delivery of NATs. A) AuNP SNA that crosses the BBB and delivers siRNAs to treat glioblastoma (adapted from Ref.¹⁹¹). B) antibody functionalized SNAs for cell-selective delivery (adapted from Ref.¹⁹³). C) SNAs delivering siRNAs that can restore wound healing in mice (adapted from Ref.¹⁹⁴). D) immunomodulatory SNAs able to improve on delivery and immunostimulation resulting from CpG motifs (adapted from Ref.¹⁹⁵).

Aside from AuNPs, SNA's special structural features were generated using other materials in their cores, for example, polymers or lipids.¹⁷⁹ This class of SNAs became the focal point in recent years, mainly due to safety and toxicity/biocompatibility concerns on using metallic-based SNAs, Whereas many polymeric materials have been approved for

clinical use due to their robust safety.^{196,197} Hence, producing SNAs from such material avoids additional burden and concerns. Examples of SNAs from such material include lipid nanoparticles (LNPs) turned into SNAs by forming a DNA corona with cholesterol-DNA strands that anchor into the LNP surface. The SNA physical features on the LNP changed its biodistribution profile completely to the spleen, compared to liver biodistribution of the regular lipid nanoparticles (no DNA corona) (**Figure 1. 31 A**).¹⁹⁸ Many other DNA amphiphiles from DNA-polymer conjugates were designed to self-assemble into SNAs and are studied for delivery of NAT. Chemically modified DNA and RNA were conjugated to ring-opening polymerized poly(norbornene) polymer via an amide bond, and assembled into SNAs that improved transfection free uptake and activity of the NATs (**Figure 1. 31 B**).^{199,200} Also, SNAs were made from brush polycaprolactone polymers, where DNA was clicked via azide chemistry, and enhanced gene silencing and uptake was achieved (**Figure 1. 31. C**).²⁰¹

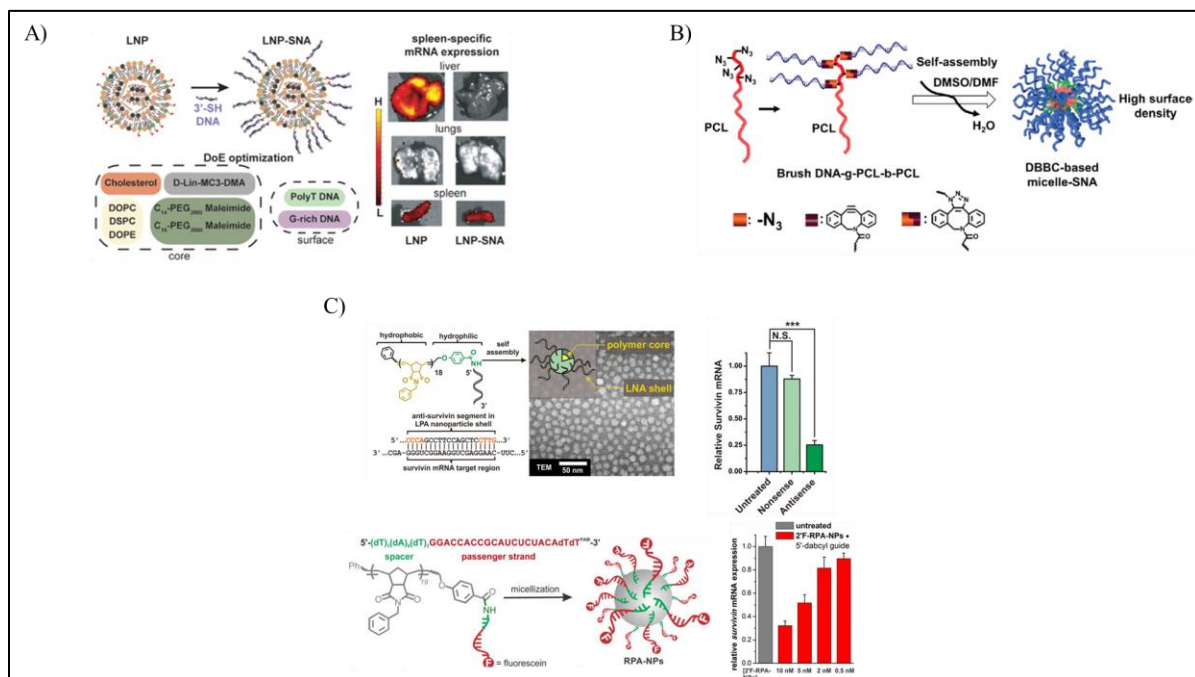


Figure 1. 31. Polymeric SNAs for the delivery of NATs. A) LNP based SNA changes the biodistribution profile and mRNA delivery locus (adapted from Ref.¹⁹⁸). B) Brush-like DNA amphiphiles assembling into dense SNAs with enhanced uptake and gene regulation (adapted from Ref.²⁰¹). C) poly(norbornyl) based SNAs, made from both ASOs and siRNAs (adapted from Ref.^{199,200}).

1.7.3. *Sequence-controlled SNAs (sc-SNAs)*

The first nucleic acid-polymer conjugates were made by conjugating functionalized DNA to pre-polymerized monomers. This method presented difficulties, such as size variation, difficulty in purification, and solubility issues between the hydrophobic polymer and the nucleic acid.²⁰² Nucleic acid-polymer conjugate synthesis tremendously improved when the conjugation to pre-formed polymers was carried on a solid support rather than in solution, where yields of conjugation increased, solubility and compatibility with solvents enhanced, and purification improved.^{179,202} Nonetheless, this improvement was not enough, as obtaining amphiphilic nucleic acids in decent yields remains a challenge due to 1) low yield coupling between water-soluble and insoluble entities, and 2) the need to pre-synthesize polymers before conjugating, yielding variations in molecular weight and dispersity in structures which is undesirable in biological applications (to avoid variation in results).^{7,38,104,179,202}

Sleiman and co-workers devised a new methodology that takes advantage of the high-yielding, stepwise solid phase synthesis of nucleic acids, to develop a class of sequence-controlled polymers.²⁰³ By utilizing the orthogonal chemistry of phosphoramidites and the iterative stepwise addition of monomers on an automated DNA synthesizer, a dendritic alkyl polymer was built from its monomers on a growing DNA strand.^{203,204} Then, the group expanded this notion to generate a variety of high-yield DNA amphiphiles, where monomers are added via phosphoramidite derivatives, which offers *full* control over length and sequence in a high yield (**Figure 1. 32. A**).²⁰⁴ In one instance, when 12 units of dodecane diol (or hexaethylene diol) are conjugated in a linear fashion to growing DNA strand, this amphiphile assembles into monodisperse and well-defined SNAs, with a hydrophobic micellar core and outer DNA corona (**Figure 1. 32. B**). Termed “sequence-controlled SNAs”, this class offers unique advantages over other methods to produce SNAs: they are produced in a fully automated fashion and in high yield, assemble from a single component, and have a hydrophobic core that can be utilized for encapsulation.⁴² Interestingly, the amphiphiles are water-soluble because the hydrophobic monomers are punctuated with phosphates.⁴² They assemble upon salt addition to overcome electrostatic repulsion between the phosphates. Early studies on these sc-SNAs

showed increased nucleic acid stability in biological conditions, increased cellular uptake and silencing activity when the NAT is part of the structure, and moderate loading capacity of the hydrophobic core with excellent and promising wide distribution profile in mice models (**Figure 1. 32. C, D**).^{42,205}

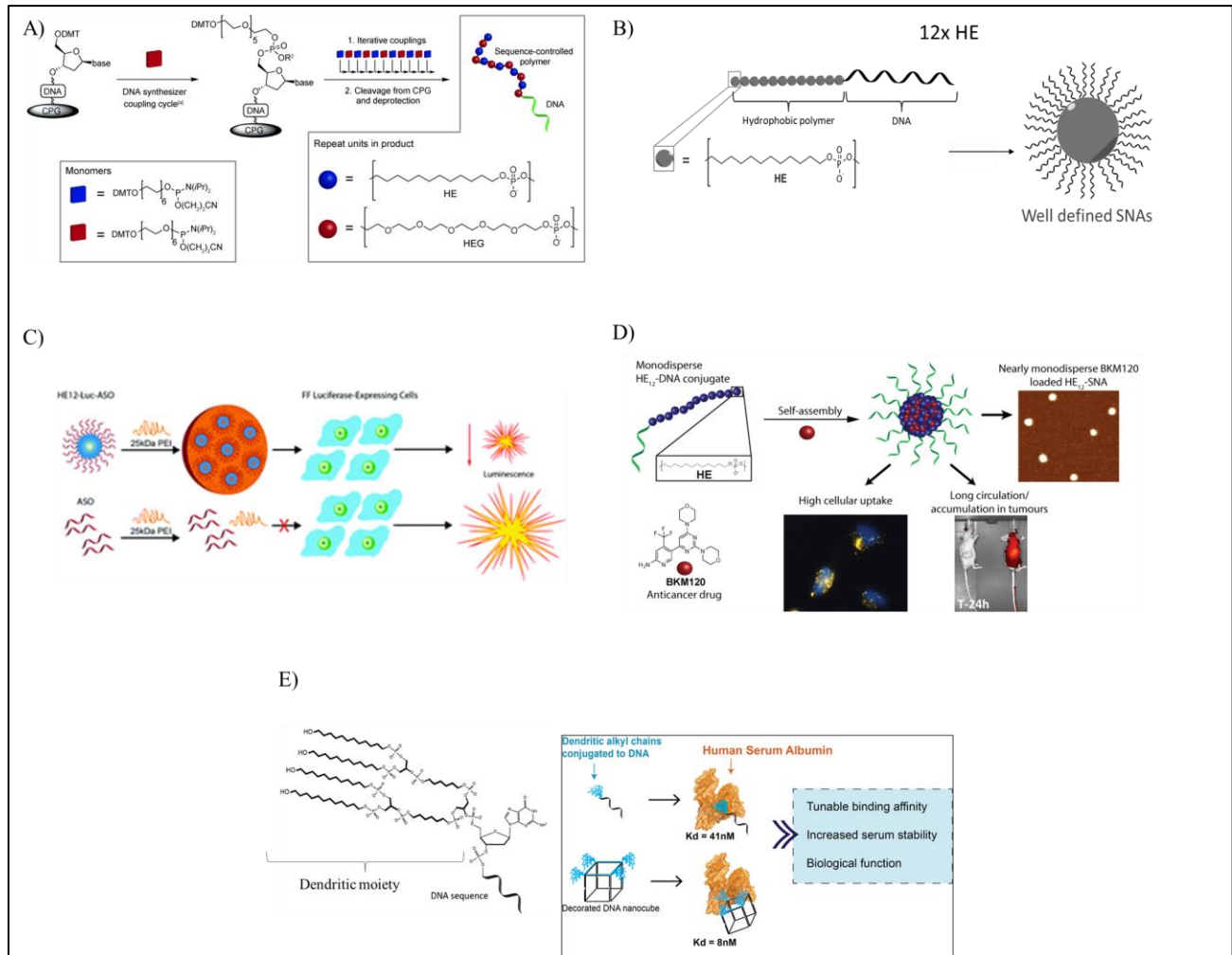


Figure 1. 32. Sequence controlled conjugates and SNAs produced on the DNA synthesizer and their promising applications. A) The stepwise manner of building a variety of polymers from their monomers in a high-yielding and efficient manner (adapted from Ref.²⁰³), B) 12 units of hexaethylene conjugated in a sequential manner produce well defined SNAs that show C) enhanced silencing activity when carrying an ASO (adapted from Ref.²⁰⁵), as well as D) promising biodistribution profile in mice models (adapted from Ref.⁴²).

As mentioned, polymers of branched design can also be produced by introducing branching units in between the monomers. A dendritic sc-DNA polymer amphiphile produced by similar methods did not self-assemble into an SNA; however, it displayed nanomolar binding affinity to albumin, which is of interest for the delivery of NATs and control of their protein corona *in vivo* (**Figure 1. 32. C**).^{206,207} Similarly, such a conjugate did not hinder the activity of the NAT conjugated to it and improved on its stability and decreased its uptake in macrophages.²⁰⁷ This dendritic moiety can also be used to functionalize other nanostructures such as DNA cubes, which further enhance the binding affinity and adds new functionality. Other structures were made as well, such as fibers from branched hexaethylene units, and dye-conjugated DNA amphiphiles.^{208,209}

The promising results from the first generation of sc-SNAs highlighted showcase the promising future for such DDS in enabling NATs to advance through the market. Being produced in a simple manner, possessing excellent biocompatibility, having high modularity and control over physical characteristics, these sc-SNAs amphiphiles have all it takes to cross the valley of death.

1.8. Scope and Context of This Thesis

The field of nucleic acid therapeutics is maturing and coming of age, where more products are being approved for clinical use. Using drug delivery systems will enable NATs to fulfill their biotechnological promise, by providing spatiotemporal control on their delivery. Nucleic acid nanoparticles, such as wireframe minimal assemblies and SNAs, are at the forefront of revolutionizing the drug delivery field and crossing the valley of death. Yet, the next generation of NANPs and SNAs should be tailored towards satisfying the vital considerations needed for NAT delivery: 1) increasing specificity and selectivity, 2) improving on stability and activity, 3) having a desired wide biodistribution profile, and 4) doing all of this while remaining a simply produced/manufactured vehicle.

The research covered in this thesis is focused on producing the next generation NANPs, sequence-controlled amphiphiles and spherical nucleic acids for the improved delivery of nucleic acid therapeutics both *in vitro* and *in vivo*. The work focuses on adding functionalities to these materials to inch them closer to clinical applications, via rational

design while keeping manufacturing hurdles in mind. We also start merging chemical advances that improve NATs to yield superior results, such as introducing chemical modifications to NANPs, and introducing conjugates that provide control over *in vivo* behavior. We examine the versatility of NANPs in biomedical applications by producing structures capable of delivering NATs, as well as enhance bio-sensing.

Chapter 2 describes the generation of SNAs with stimuli-responsive behaviour to increase their specificity for delivering NATs. The SNAs are made responsive to specific nucleic acid sequences via strand displacement. These nucleic acid sequences can be overexpressed biomarkers (miRNA,mRNA) in diseased cells, which tailors their specificity towards those cells. This relies on an intracellular intrinsic stimulus, rather than an external one. The design, synthesis, optimization of assembly, and selectivity are examined. The assembly of stimuli-responsive SNAs was characterized to confirm formation of the desired structure, as well as retaining the stimuli-responsive behavior via strand displacement. Then, the stability of these SNAs was tested in serum-containing cell culture media, to examine the improvement on nuclease degradation as part of a DDS. Lastly, the ability to suppress off-target effects and activate NAT delivery on demand was studied, to showcase that only in the presence of the correct cue the NAT is released and activated *in vitro*. The project resulted in DNA-minimal, stimuli-responsive, and robust SNA platform for conditional delivery of NATs.

Chapter 3 builds on Chapter 2, where chemical modifications were employed to improve the efficacy of SNAs for the delivery of NATs. SNAs reported in literature, as well as our own first generation SNAs did not utilize the large chemical toolbox of modifications available to improve stability and activity of NATs. Hence, we turn our focus onto fusing the two fields of SNAs and chemical modifications. Specifically, we use the 2'-Deoxy-2'-fluoro-D-arabinose sugar modification (FANA) to generate FANA-SNAs. The assembly of these SNAs and design requirements for maximum efficacy was studied. We found that having a cleavable linker was necessary to achieve the highest activity from SNAs. The modularity of these SNAs was also put to the test, where multiple targets in multiple cells were silenced successfully. Bridging the two fields also yielded transfection-free uptake into cells, where chemically modified SNAs had the highest efficacy in gene

regulation in comparison to unmodified SNAs or modified NATs, *in vitro*. This chapter yielded extremely stable, effective, and modular SNAs, and showcases the importance of employing chemical modifications into NANPs.

Chapter 4 takes a segue from self-assembled DDS and aims to study another amphiphilic conjugate generated by sequence-controlled automated synthesis. A dendritic conjugate (D) studied in our lab was previously demonstrated to have nanomolar affinity to albumin. This protein is the most abundant in circulation and has an attractive biodistribution profile that it can confer to NATs. This chapter focuses on building from the *in vitro* studies of this conjugate and investigating the *in vivo* behaviour of NATs conjugated to the dendritic moiety (D-ASOs and D-siRNAs). Biodistribution profile, efficacy following systemic and local injection in mouse models were investigated, showcasing selective albumin binding *in vivo* and promising enhanced activity in certain organs and cell types. The project highlights the versatility of sc-polymer conjugates and the effect of protein corona formation *in vivo*.

Appendix I and II focuses on wireframe, minimal DNA nanostructures, and their adaptability to deliver NATs as well as enhance fluorescence readout in biosensing. In Appendix I, carefully designed strands are synthesized to construct 2D-DNA polygons that are entirely composed of modified DNA as NAT carriers. The work was focused on studying synthesis, assembly, and preliminary effectiveness in improving circulation *in vivo* and efficacy *in vitro* by simply changing size and shape rather than conjugates. As for Appendix II, we used the same nanostructure design to produce a variety of 2D shapes and sizes, that are then studied to yield ultra-bright fluorescent structures for molecular sensing and diagnostics. The recyclability of the structures, and the ability to control the number of dyes functionalized to the structures, while being able to produce ultrabright units that are well-defined and small in size is attractive for employment in biosensing methods. This work was in collaboration with an industrial partner, Quantum Si Inc., where such structures were studied as fluorescent reporters in biosensors for next generation sequencing.

Together, these projects showcase the promising future of nucleic acid nanotechnology in biomedical applications, such as nucleic acid therapeutics delivery and biosensing.

1.9. References

- 1 Crick, F. Central Dogma of Molecular Biology. *Nature* **227**, 561-563, doi:10.1038/227561a0 (1970).
- 2 Clancy, S. B., W. Translation: DNA to mRNA to Protein. *Nature Education* **1**, 101 (2008).
- 3 Stranger, B. E. & Dermitzakis, E. T. From DNA to RNA to disease and back: the 'central dogma' of regulatory disease variation. *Hum Genomics* **2**, 383-390, doi:10.1186/1479-7364-2-6-383 (2006).
- 4 *Transcription and Translation*, <<https://www.cancer.gov/publications/dictionaries/cancer-terms/def/transcription>> (
- 5 Yu, A.-M., Jian, C., Yu, A. H. & Tu, M.-J. RNA therapy: Are we using the right molecules? *Pharmacol Ther* **196**, 91-104, doi:10.1016/j.pharmthera.2018.11.011 (2019).
- 6 Wu, S. Y., Lopez-Berestein, G., Calin, G. A. & Sood, A. K. RNAi therapies: drugging the undruggable. *Sci Transl Med* **6**, 240ps247, doi:10.1126/scitranslmed.3008362 (2014).
- 7 Roberts, T. C., Langer, R. & Wood, M. J. A. Advances in oligonucleotide drug delivery. *Nature Reviews Drug Discovery* **19**, 673-694, doi:10.1038/s41573-020-0075-7 (2020).
- 8 Dalbeth, N., Lauterio, T. J. & Wolfe, H. R. Mechanism of action of colchicine in the treatment of gout. *Clin Ther* **36**, 1465-1479, doi:10.1016/j.clinthera.2014.07.017 (2014).
- 9 Bharadwaj, R. & Yu, H. The spindle checkpoint, aneuploidy, and cancer. *Oncogene* **23**, 2016-2027, doi:10.1038/sj.onc.1207374 (2004).
- 10 Dimitrov, D. S. Therapeutic proteins. *Methods Mol Biol* **899**, 1-26, doi:10.1007/978-1-61779-921-1_1 (2012).
- 11 Le, X.-F., Pruefer, F. & Bast, R. C. HER2-targeting Antibodies Modulate the Cyclin-dependent Kinase Inhibitor p27Kip1 via Multiple Signaling Pathways. *Cell Cycle* **4**, 87-95, doi:10.4161/cc.4.1.1360 (2005).
- 12 Stockwell, B. Outsmarting Cancer. A biologist talks about what makes disease-causing proteins so difficult to target with drugs. *Sci Am* **305**, 20 (2011).
- 13 Esteller, M. Non-coding RNAs in human disease. *Nat Rev Genet* **12**, 861-874, doi:10.1038/nrg3074 (2011).
- 14 Mattick, J. S. RNA regulation: a new genetics? *Nat Rev Genet* **5**, 316-323, doi:10.1038/nrg1321 (2004).
- 15 Zamecnik, P. C. & Stephenson, M. L. Inhibition of Rous sarcoma virus replication and cell transformation by a specific oligodeoxynucleotide. *Proceedings of the National Academy of Sciences* **75**, 280-284, doi:10.1073/pnas.75.1.280 (1978).
- 16 Khvorova, A. & Watts, J. K. The chemical evolution of oligonucleotide therapies of clinical utility. *Nature Biotechnology* **35**, 238-248, doi:10.1038/nbt.3765 (2017).
- 17 Saiki, R. K. *et al.* Primer-directed enzymatic amplification of DNA with a thermostable DNA polymerase. *Science* **239**, 487-491, doi:10.1126/science.2448875 (1988).

- 18 Beaucage, S. L. & Caruthers, M. H. Deoxynucleoside phosphoramidites—A new class of key intermediates for deoxypolynucleotide synthesis. *Tetrahedron Letters* **22**, 1859-1862, doi:[https://doi.org/10.1016/S0040-4039\(01\)90461-7](https://doi.org/10.1016/S0040-4039(01)90461-7) (1981).
- 19 Merrifield, R. B. Solid Phase Peptide Synthesis. I. The Synthesis of a Tetrapeptide. *Journal of the American Chemical Society* **85**, 2149-2154, doi:10.1021/ja00897a025 (1963).
- 20 Horvath, S. J., Firca, J. R., Hunkapiller, T., Hunkapiller, M. W. & Hood, L. in *Methods in Enzymology* Vol. 154 314-326 (Academic Press, 1987).
- 21 Damha, M. J., Giannaris, P. A. & Zabarylo, S. V. An improved procedure for derivatization of controlled-pore glass beads for solid-phase oligonucleotide synthesis. *Nucleic Acids Research* **18**, 3813-3821, doi:10.1093/nar/18.13.3813 (1990).
- 22 Caruthers, M. H. The chemical synthesis of DNA/RNA: our gift to science. *J Biol Chem* **288**, 1420-1427, doi:10.1074/jbc.X112.442855 (2013).
- 23 Kosuri, S. & Church, G. M. Large-scale de novo DNA synthesis: technologies and applications. *Nat Methods* **11**, 499-507, doi:10.1038/nmeth.2918 (2014).
- 24 Kulkarni, J. A. *et al.* The current landscape of nucleic acid therapeutics. *Nature Nanotechnology* **16**, 630-643, doi:10.1038/s41565-021-00898-0 (2021).
- 25 Mathew V, W. A. Inotersen: new promise for the treatment of hereditary transthyretin amyloidosis. *Drug Des Devel Ther.* **13**, 1515-1525 (2019).
- 26 Weng, Y. *et al.* The challenge and prospect of mRNA therapeutics landscape. *Biotechnology Advances* **40**, 107534, doi:<https://doi.org/10.1016/j.biotechadv.2020.107534> (2020).
- 27 Sahin, U., Karikó, K. & Türeci, Ö. mRNA-based therapeutics — developing a new class of drugs. *Nature Reviews Drug Discovery* **13**, 759-780, doi:10.1038/nrd4278 (2014).
- 28 Cohen, J. ‘Base editors’ open new way to fix mutations. *Science* **358**, 432-433, doi:10.1126/science.358.6362.432 (2017).
- 29 Adli, M. The CRISPR tool kit for genome editing and beyond. *Nature Communications* **9**, 1911, doi:10.1038/s41467-018-04252-2 (2018).
- 30 Gillmore, J. D. *et al.* CRISPR-Cas9 In Vivo Gene Editing for Transthyretin Amyloidosis. *New England Journal of Medicine* **385**, 493-502, doi:10.1056/NEJMoa2107454 (2021).
- 31 Li, C. & Samulski, R. J. Engineering adeno-associated virus vectors for gene therapy. *Nature Reviews Genetics* **21**, 255-272, doi:10.1038/s41576-019-0205-4 (2020).
- 32 Broekhoff, T. F. *et al.* Early Cost-Effectiveness of Onasemnogene Apeparvovec-xioi (Zolgensma) and Nusinersen (Spinraza) Treatment for Spinal Muscular Atrophy I in The Netherlands With Relapse Scenarios. *Value in Health* **24**, 759-769, doi:<https://doi.org/10.1016/j.jval.2020.09.021> (2021).
- 33 Keefe, A. D., Pai, S. & Ellington, A. Aptamers as therapeutics. *Nature Reviews Drug Discovery* **9**, 537-550, doi:10.1038/nrd3141 (2010).
- 34 Lakhin, A. V., Tarantul, V. Z. & Gening, L. V. Aptamers: problems, solutions and prospects. *Acta Naturae* **5**, 34-43 (2013).

- 35 Kaur, H., Bruno, J. G., Kumar, A. & Sharma, T. K. Aptamers in the Therapeutics and Diagnostics Pipelines. *Theranostics* **8**, 4016-4032, doi:10.7150/thno.25958 (2018).
- 36 Macugen. http://www.ema.europa.eu/docs/en_GB/document_library/EPAR_-_Summary_for_the_public/human/000620/WC500026216.pdf.
- 37 Pan Qin, L. F., Liu Min, Zhang Xiao-Lian. Oligonucleotide aptamers: promising and powerful diagnostic and therapeutic tools for infectious diseases. *Journal of Infection* **77**, 83-98 (2018).
- 38 Weng, Y. *et al.* Improved Nucleic Acid Therapy with Advanced Nanoscale Biotechnology. *Molecular Therapy - Nucleic Acids* **19**, 581-601, doi:<https://doi.org/10.1016/j.omtn.2019.12.004> (2020).
- 39 Lostalé-Seijo, I. & Montenegro, J. Synthetic materials at the forefront of gene delivery. *Nature Reviews Chemistry* **2**, 258-277, doi:10.1038/s41570-018-0039-1 (2018).
- 40 Conway, J. W., McLaughlin, C. K., Castor, K. J. & Sleiman, H. DNA nanostructure serum stability: greater than the sum of its parts. *Chemical Communications* **49**, 1172-1174, doi:10.1039/C2CC37556G (2013).
- 41 Yin, H. *et al.* Non-viral vectors for gene-based therapy. *Nature Reviews Genetics* **15**, 541-555, doi:10.1038/nrg3763 (2014).
- 42 Bousmail, D. *et al.* Precision spherical nucleic acids for delivery of anticancer drugs. *Chemical Science* **8**, 6218-6229, doi:10.1039/C7SC01619K (2017).
- 43 Pastor, F. *et al.* An RNA toolbox for cancer immunotherapy. *Nature Reviews Drug Discovery* **17**, 751-767, doi:10.1038/nrd.2018.132 (2018).
- 44 Eder, P. S., DeVine, R. J., Dagle, J. M. & Walder, J. A. Substrate specificity and kinetics of degradation of antisense oligonucleotides by a 3' exonuclease in plasma. *Antisense Res Dev* **1**, 141-151, doi:10.1089/ard.1991.1.141 (1991).
- 45 Akinc, A. *et al.* The Onpatro story and the clinical translation of nanomedicines containing nucleic acid-based drugs. *Nature Nanotechnology* **14**, 1084-1087, doi:10.1038/s41565-019-0591-y (2019).
- 46 Geary, R. S., Norris, D., Yu, R. & Bennett, C. F. Pharmacokinetics, biodistribution and cell uptake of antisense oligonucleotides. *Adv Drug Deliv Rev* **87**, 46-51, doi:10.1016/j.addr.2015.01.008 (2015).
- 47 Tsui, N. B., Ng, E. K. & Lo, Y. M. Stability of endogenous and added RNA in blood specimens, serum, and plasma. *Clin Chem* **48**, 1647-1653 (2002).
- 48 Larson, S. D., Jackson, L. N., Chen, L. A., Rychahou, P. G. & Evers, B. M. Effectiveness of siRNA uptake in target tissues by various delivery methods. *Surgery* **142**, 262-269, doi:<https://doi.org/10.1016/j.surg.2007.03.011> (2007).
- 49 Andersson, S., Antonsson, M., Elebring, M., Jansson-Löfmark, R. & Weidolf, L. Drug metabolism and pharmacokinetic strategies for oligonucleotide- and mRNA-based drug development. *Drug Discovery Today* **23**, 1733-1745, doi:<https://doi.org/10.1016/j.drudis.2018.05.030> (2018).

- 50 Iversen, F. *et al.* Optimized siRNA-PEG Conjugates for Extended Blood Circulation and Reduced Urine Excretion in Mice. *Theranostics* **3**, 201-209, doi:10.7150/thno.5743 (2013).
- 51 White, P. J., Anastasopoulos, F., Pouton, C. W. & Boyd, B. J. Overcoming biological barriers to in vivo efficacy of antisense oligonucleotides. *Expert Reviews in Molecular Medicine* **11**, 19-e10, doi:<http://dx.doi.org/10.1017/S1462399409001021> (2009).
- 52 Geary, R. S. Antisense oligonucleotide pharmacokinetics and metabolism. *Expert Opinion on Drug Metabolism & Toxicology* **5**, 381-391, doi:10.1517/17425250902877680 (2009).
- 53 Wang, Z. & Malik, A. B. Nanoparticles squeezing across the blood-endothelial barrier via caveolae. *Ther Deliv* **4**, 131-133, doi:10.4155/tde.12.140 (2013).
- 54 Biscans, A. *et al.* Docosanoic acid conjugation to siRNA enables functional and safe delivery to skeletal and cardiac muscles. *Molecular Therapy* **29**, doi:10.1016/j.ymthe.2020.12.023 (2020).
- 55 Qin, L. & Crawford, J. M. in *Zakim and Boyer's Hepatology (Seventh Edition)* (eds Arun J. Sanyal, Thomas D. Boyer, Keith D. Lindor, & Norah A. Terrault) 2-19.e14 (Elsevier, 2018).
- 56 Doherty, G. J. & McMahon, H. T. Mechanisms of endocytosis. *Annu Rev Biochem* **78**, 857-902, doi:10.1146/annurev.biochem.78.081307.110540 (2009).
- 57 Juliano, R. L. The delivery of therapeutic oligonucleotides. *Nucleic Acids Research* **44**, 6518-6548, doi:10.1093/nar/gkw236 (2016).
- 58 Hillaireau, H. & Couvreur, P. Nanocarriers' entry into the cell: relevance to drug delivery. *Cellular and Molecular Life Sciences* **66**, 2873-2896, doi:10.1007/s00018-009-0053-z (2009).
- 59 Bost, J. P. *et al.* Delivery of Oligonucleotide Therapeutics: Chemical Modifications, Lipid Nanoparticles, and Extracellular Vesicles. *ACS Nano* **15**, 13993-14021, doi:10.1021/acsnano.1c05099 (2021).
- 60 Thierry, A. R. *et al.* Cellular uptake and intracellular fate of antisense oligonucleotides. *Curr Opin Mol Ther* **5**, 133-138 (2003).
- 61 Sharma, V. K. & Watts, J. K. Oligonucleotide therapeutics: chemistry, delivery and clinical progress. *Future Med Chem* **7**, 2221-2242, doi:10.4155/fmc.15.144 (2015).
- 62 Watts, J. K., Katolik, A., Viladoms, J. & Damha, M. J. Studies on the hydrolytic stability of 2'-fluoroarabinonucleic acid (2'F-ANA). *Organic & Biomolecular Chemistry* **7**, 1904-1910, doi:10.1039/B900443B (2009).
- 63 Dobrovolskaia, M. A. & McNeil, S. E. Immunological and hematological toxicities challenging clinical translation of nucleic acid-based therapeutics. *Expert Opin Biol Ther* **15**, 1023-1048, doi:10.1517/14712598.2015.1014794 (2015).
- 64 Matsukura, M. *et al.* Phosphorothioate analogs of oligodeoxynucleotides: inhibitors of replication and cytopathic effects of human immunodeficiency virus. *Proceedings of the National Academy of Sciences* **84**, 7706-7710, doi:10.1073/pnas.84.21.7706 (1987).
- 65 Phosphorothioates, Essential Components of Therapeutic Oligonucleotides. *Nucleic Acid Therapeutics* **24**, 374-387, doi:10.1089/nat.2014.0506 (2014).

- 66 Brown, D. A. *et al.* Effect of phosphorothioate modification of oligodeoxynucleotides on specific protein binding. *Journal of Biological Chemistry* **269**, 26801-26805, doi:[https://doi.org/10.1016/S0021-9258\(18\)47090-1](https://doi.org/10.1016/S0021-9258(18)47090-1) (1994).
- 67 Winkler, J., Stessl, M., Amartej, J. & Noe, C. R. Off-Target Effects Related to the Phosphorothioate Modification of Nucleic Acids. *ChemMedChem* **5**, 1344-1352, doi:<https://doi.org/10.1002/cmdc.201000156> (2010).
- 68 Damha, M. J. *et al.* Hybrids of RNA and Arabinonucleic Acids (ANA and 2'F-ANA) Are Substrates of Ribonuclease H. *J. Am. Chem. Soc.* 1998, 120, 12976–12977. *Journal of the American Chemical Society* **120**, 13545-13545, doi:10.1021/ja985535v (1998).
- 69 Noronha, A. M. *et al.* Synthesis and biophysical properties of arabinonucleic acids (ANA): circular dichroic spectra, melting temperatures, and ribonuclease H susceptibility of ANA:RNA hybrid duplexes. *Biochemistry* **39**, 7050-7062, doi:10.1021/bi000280v (2000).
- 70 Kalota, A. *et al.* 2'-Deoxy-2'-fluoro-β- d -arabinonucleic acid (2'F-ANA) modified oligonucleotides (ON) effect highly efficient, and persistent, gene silencing. *Nucleic Acids Research* **34**, 451-461, doi:10.1093/nar/gkj455 (2006).
- 71 Damha, M. J. *et al.* Hybrids of RNA and Arabinonucleic Acids (ANA and 2'F-ANA) Are Substrates of Ribonuclease H. *Journal of the American Chemical Society* **120**, 12976-12977, doi:10.1021/ja982325+ (1998).
- 72 Lok, C.-N. *et al.* Potent Gene-Specific Inhibitory Properties of Mixed-Backbone Antisense Oligonucleotides Comprised of 2'-Deoxy-2'-fluoro-d-arabinose and 2'-Deoxyribose Nucleotides. *Biochemistry* **41**, 3457-3467, doi:10.1021/bi0115075 (2002).
- 73 Lu, X. & Zhang, K. PEGylation of therapeutic oligonucleotides: From linear to highly branched PEG architectures. *Nano Research* **11**, 5519-5534, doi:10.1007/s12274-018-2131-8 (2018).
- 74 van Witteloostuijn, S. B., Pedersen, S. L. & Jensen, K. J. Half-Life Extension of Biopharmaceuticals using Chemical Methods: Alternatives to PEGylation. *ChemMedChem* **11**, 2474-2495, doi:10.1002/cmdc.201600374 (2016).
- 75 Shimizu, T. *et al.* A Cell Assay for Detecting Anti-PEG Immune Response against PEG-Modified Therapeutics. *Pharmaceutical Research* **35**, 223, doi:10.1007/s11095-018-2505-3 (2018).
- 76 Lorenz, C., Hadwiger, P., John, M., Vornlocher, H. P. & Unverzagt, C. Steroid and lipid conjugates of siRNAs to enhance cellular uptake and gene silencing in liver cells. *Bioorg Med Chem Lett* **14**, 4975-4977, doi:10.1016/j.bmcl.2004.07.018 (2004).
- 77 Soutschek, J. *et al.* Therapeutic silencing of an endogenous gene by systemic administration of modified siRNAs. *Nature* **432**, 173-178, doi:10.1038/nature03121 (2004).
- 78 Nishina, K. *et al.* Efficient in vivo delivery of siRNA to the liver by conjugation of alpha-tocopherol. *Mol Ther* **16**, 734-740, doi:10.1038/mt.2008.14 (2008).
- 79 Osborn, M. F. *et al.* Hydrophobicity drives the systemic distribution of lipid-conjugated siRNAs via lipid transport pathways. *Nucleic Acids Res* **47**, 1070-1081, doi:10.1093/nar/gky1232 (2019).

- 80 Hoogenboezem, E. N. & Duvall, C. L. Harnessing albumin as a carrier for cancer therapies. *Advanced Drug Delivery Reviews* **130**, 73-89, doi:<https://doi.org/10.1016/j.addr.2018.07.011> (2018).
- 81 Kuhlmann, M. *et al.* An Albumin-Oligonucleotide Assembly for Potential Combinatorial Drug Delivery and Half-Life Extension Applications. *Molecular Therapy - Nucleic Acids* **9**, 284-293, doi:<https://doi.org/10.1016/j.omtn.2017.10.004> (2017).
- 82 Andersen, J. T. & Sandlie, I. The versatile MHC class I-related FcRn protects IgG and albumin from degradation: implications for development of new diagnostics and therapeutics. *Drug metabolism and pharmacokinetics* **24**, 318-332 (2009).
- 83 Schnitzer, J. E. gp60 is an albumin-binding glycoprotein expressed by continuous endothelium involved in albumin transcytosis. *American Journal of Physiology-Heart and Circulatory Physiology* **262**, H246-H254, doi:10.1152/ajpheart.1992.262.1.H246 (1992).
- 84 Merlot, A. M., Kalinowski, D. S. & Richardson, D. R. Unraveling the mysteries of serum albumin-more than just a serum protein. *Front Physiol* **5**, 299-299, doi:10.3389/fphys.2014.00299 (2014).
- 85 Malhotra, A. & Mittal, B. R. siRNA gene therapy using albumin as a carrier. *Pharmacogenetics and Genomics* **24** (2014).
- 86 Zhou, J. & Rossi, J. J. The Therapeutic Potential of Cell-Internalizing Aptamers. *Current Topics in Medicinal Chemistry* **9**, 1144-1157, doi:10.2174/156802609789630893 (2009).
- 87 Tanaka, K., Okuda, T., Kasahara, Y. & Obika, S. Base-modified aptamers obtained by cell-internalization SELEX facilitate cellular uptake of an antisense oligonucleotide. *Molecular Therapy - Nucleic Acids* **23**, 440-449, doi:<https://doi.org/10.1016/j.omtn.2020.11.016> (2021).
- 88 Sievers, E. L. & Senter, P. D. Antibody-drug conjugates in cancer therapy. *Annu Rev Med* **64**, 15-29, doi:10.1146/annurev-med-050311-201823 (2013).
- 89 Yao, Y. D. *et al.* Targeted delivery of PLK1-siRNA by ScFv suppresses Her2+ breast cancer growth and metastasis. *Sci Transl Med* **4**, 130ra148, doi:10.1126/scitranslmed.3003601 (2012).
- 90 Sugo, T. *et al.* Development of antibody-siRNA conjugate targeted to cardiac and skeletal muscles. *J Control Release* **237**, 1-13, doi:10.1016/j.jconrel.2016.06.036 (2016).
- 91 Arnold, A. E. *et al.* Antibody-Antisense Oligonucleotide Conjugate Downregulates a Key Gene in Glioblastoma Stem Cells. *Mol Ther Nucleic Acids* **11**, 518-527, doi:10.1016/j.omtn.2018.04.004 (2018).
- 92 Jutten, B. *et al.* EGFR overexpressing cells and tumors are dependent on autophagy for growth and survival. *Radiother Oncol* **108**, 479-483, doi:10.1016/j.radonc.2013.06.033 (2013).
- 93 Tanowitz, M. *et al.* Asialoglycoprotein receptor 1 mediates productive uptake of N-acetylgalactosamine-conjugated and unconjugated phosphorothioate antisense oligonucleotides into liver hepatocytes. *Nucleic Acids Res* **45**, 12388-12400, doi:10.1093/nar/gkx960 (2017).

- 94 Prakash, T. P. *et al.* Targeted delivery of antisense oligonucleotides to hepatocytes using triantennary N-acetyl galactosamine improves potency 10-fold in mice. *Nucleic Acids Res* **42**, 8796-8807, doi:10.1093/nar/gku531 (2014).
- 95 Springer, A. D. & Dowdy, S. F. GalNAc-siRNA Conjugates: Leading the Way for Delivery of RNAi Therapeutics. *Nucleic Acid Ther* **28**, 109-118, doi:10.1089/nat.2018.0736 (2018).
- 96 Bissell, D. M. & Wang, B. Acute Hepatic Porphyria. *J Clin Transl Hepatol* **3**, 17-26, doi:10.14218/JCTH.2014.00039 (2015).
- 97 McClorey, G. & Banerjee, S. Cell-Penetrating Peptides to Enhance Delivery of Oligonucleotide-Based Therapeutics. *Biomedicines* **6**, doi:10.3390/biomedicines6020051 (2018).
- 98 McClorey, G. & Banerjee, S. Cell-Penetrating Peptides to Enhance Delivery of Oligonucleotide-Based Therapeutics. *Biomedicines* **6**, 51, doi:10.3390/biomedicines6020051 (2018).
- 99 Zhao, P. *et al.* Identification of a Met-Binding Peptide from a Phage Display Library. *Clinical Cancer Research* **13**, 6049-6055, doi:10.1158/1078-0432.Ccr-07-0035 (2007).
- 100 Liang, S. *et al.* Screening and identification of vascular-endothelial-cell-specific binding peptide in gastric cancer. *Journal of Molecular Medicine* **84**, 764-773, doi:10.1007/s00109-006-0064-2 (2006).
- 101 Moulton, H. M. & Moulton, J. D. Morpholinos and their peptide conjugates: therapeutic promise and challenge for Duchenne muscular dystrophy. *Biochim Biophys Acta* **1798**, 2296-2303, doi:10.1016/j.bbamem.2010.02.012 (2010).
- 102 Gait, M. J. *et al.* Cell-Penetrating Peptide Conjugates of Steric Blocking Oligonucleotides as Therapeutics for Neuromuscular Diseases from a Historical Perspective to Current Prospects of Treatment. *Nucleic Acid Ther* **29**, 1-12, doi:10.1089/nat.2018.0747 (2019).
- 103 Aartsma-Rus, A. & Corey, D. R. The 10th Oligonucleotide Therapy Approved: Golodirsen for Duchenne Muscular Dystrophy. *Nucleic Acid Therapeutics* **30**, 67-70, doi:10.1089/nat.2020.0845 (2020).
- 104 Mitchell, M. J. *et al.* Engineering precision nanoparticles for drug delivery. *Nature Reviews Drug Discovery* **20**, 101-124, doi:10.1038/s41573-020-0090-8 (2021).
- 105 Fraley, R., Subramani, S., Berg, P. & Papahadjopoulos, D. Introduction of liposome-encapsulated SV40 DNA into cells. *Journal of Biological Chemistry* **255**, 10431-10435, doi:[https://doi.org/10.1016/S0021-9258\(19\)70482-7](https://doi.org/10.1016/S0021-9258(19)70482-7) (1980).
- 106 Lee, M.-K. Liposomes for Enhanced Bioavailability of Water-Insoluble Drugs: In Vivo Evidence and Recent Approaches. *Pharmaceutics* **12**, 264 (2020).
- 107 Zhang, X., Goel, V. & Robbie, G. J. Pharmacokinetics of Patisiran, the First Approved RNA Interference Therapy in Patients With Hereditary Transthyretin-Mediated Amyloidosis. *The Journal of Clinical Pharmacology* **60**, 573-585, doi:<https://doi.org/10.1002/jcph.1553> (2020).

- 108 Zelphati, O. & Szoka, F. C., Jr. Mechanism of oligonucleotide release from cationic liposomes. *Proc Natl Acad Sci U S A* **93**, 11493-11498, doi:10.1073/pnas.93.21.11493 (1996).
- 109 Rungta, R. L. *et al.* Lipid Nanoparticle Delivery of siRNA to Silence Neuronal Gene Expression in the Brain. *Molecular therapy. Nucleic acids* **2**, e136-e136, doi:10.1038/mtna.2013.65 (2013).
- 110 Schlich, M. *et al.* Cytosolic delivery of nucleic acids: The case of ionizable lipid nanoparticles. *Bioengineering & Translational Medicine* **6**, e10213, doi:<https://doi.org/10.1002/btm2.10213> (2021).
- 111 Thi, T. T. H. *et al.* Lipid-Based Nanoparticles in the Clinic and Clinical Trials: From Cancer Nanomedicine to COVID-19 Vaccines. *Vaccines* **9**, 359 (2021).
- 112 Kowal, J., Tkach, M. & Théry, C. Biogenesis and secretion of exosomes. *Curr Opin Cell Biol* **29**, 116-125, doi:10.1016/j.ceb.2014.05.004 (2014).
- 113 Alvarez-Erviti, L. *et al.* Delivery of siRNA to the mouse brain by systemic injection of targeted exosomes. *Nature Biotechnology* **29**, 341-345, doi:10.1038/nbt.1807 (2011).
- 114 Ke, W. & Afonin, K. A. Exosomes as natural delivery carriers for programmable therapeutic nucleic acid nanoparticles (NANPs). *Advanced Drug Delivery Reviews*, 113835, doi:<https://doi.org/10.1016/j.addr.2021.113835> (2021).
- 115 Amreddy, N., Babu, A., Muralidharan, R., Munshi, A. & Ramesh, R. Polymeric Nanoparticle-Mediated Gene Delivery for Lung Cancer Treatment. *Topics in Current Chemistry* **375**, 35, doi:10.1007/s41061-017-0128-5 (2017).
- 116 Wong, K. H., Lu, A., Chen, X. & Yang, Z. Natural Ingredient-Based Polymeric Nanoparticles for Cancer Treatment. *Molecules* **25**, 3620 (2020).
- 117 Piotrowski-Daspit, A. S., Kauffman, A. C., Bracaglia, L. G. & Saltzman, W. M. Polymeric vehicles for nucleic acid delivery. *Advanced Drug Delivery Reviews* **156**, 119-132, doi:<https://doi.org/10.1016/j.addr.2020.06.014> (2020).
- 118 Jiang, D. *et al.* Multifunctionalized polyethyleneimine-based nanocarriers for gene and chemotherapeutic drug combination therapy through one-step assembly strategy. *Int J Nanomedicine* **12**, 8681-8698, doi:10.2147/ijn.S142966 (2017).
- 119 Patil, Y. & Panyam, J. Polymeric nanoparticles for siRNA delivery and gene silencing. *International Journal of Pharmaceutics* **367**, 195-203, doi:<https://doi.org/10.1016/j.ijpharm.2008.09.039> (2009).
- 120 Oerlemans, C. *et al.* Polymeric Micelles in Anticancer Therapy: Targeting, Imaging and Triggered Release. *Pharmaceutical Research* **27**, 2569-2589, doi:10.1007/s11095-010-0233-4 (2010).
- 121 Lombardo, D., Kiselev, M. A., Magazù, S. & Calandra, P. Amphiphiles Self-Assembly: Basic Concepts and Future Perspectives of Supramolecular Approaches. *Advances in Condensed Matter Physics* **2015**, 151683, doi:10.1155/2015/151683 (2015).

- 122 Kim, H. J., Kim, A., Miyata, K. & Kataoka, K. Recent progress in development of siRNA delivery vehicles for cancer therapy. *Advanced Drug Delivery Reviews* **104**, 61-77, doi:<https://doi.org/10.1016/j.addr.2016.06.011> (2016).
- 123 Jhaveri, A. M. & Torchilin, V. P. Multifunctional polymeric micelles for delivery of drugs and siRNA. *Frontiers in Pharmacology* **5**, doi:10.3389/fphar.2014.00077 (2014).
- 124 Amjad, M. W., Kesharwani, P., Mohd Amin, M. C. I. & Iyer, A. K. Recent advances in the design, development, and targeting mechanisms of polymeric micelles for delivery of siRNA in cancer therapy. *Progress in Polymer Science* **64**, 154-181, doi:<https://doi.org/10.1016/j.progpolymsci.2016.09.008> (2017).
- 125 Christie, R. J. *et al.* Targeted Polymeric Micelles for siRNA Treatment of Experimental Cancer by Intravenous Injection. *ACS Nano* **6**, 5174-5189, doi:10.1021/nn300942b (2012).
- 126 Sarisozen, C., Pan, J., Dutta, I. & Torchilin, V. P. Polymers in the co-delivery of siRNA and anticancer drugs to treat multidrug-resistant tumors. *Journal of Pharmaceutical Investigation* **47**, 37-49, doi:10.1007/s40005-016-0296-2 (2017).
- 127 Perche, F., Biswas, S., Wang, T., Zhu, L. & Torchilin, V. P. Hypoxia-Targeted siRNA Delivery. *Angewandte Chemie International Edition* **53**, 3362-3366, doi:<https://doi.org/10.1002/anie.201308368> (2014).
- 128 Biswas, S. & Torchilin, V. P. Dendrimers for siRNA Delivery. *Pharmaceuticals* **6**, 161-183 (2013).
- 129 Delong, R. *et al.* Characterization of complexes of oligonucleotides with polyamidoamine starburst dendrimers and effects on intracellular delivery. *J Pharm Sci* **86**, 762-764, doi:10.1021/js960409f (1997).
- 130 Sato, N. *et al.* Tumor targeting and imaging of intraperitoneal tumors by use of antisense oligo-DNA complexed with dendrimers and/or avidin in mice. *Clin Cancer Res* **7**, 3606-3612 (2001).
- 131 Palmerston Mendes, L., Pan, J. & Torchilin, V. P. Dendrimers as Nanocarriers for Nucleic Acid and Drug Delivery in Cancer Therapy. *Molecules* **22**, 1401 (2017).
- 132 Herma, R. *et al.* Carbosilane dendrimers with phosphonium terminal groups are low toxic non-viral transfection vectors for siRNA cell delivery. *International Journal of Pharmaceutics* **562**, 51-65, doi:<https://doi.org/10.1016/j.ijpharm.2019.03.018> (2019).
- 133 Dzitruk, V. *et al.* Dendrimers Show Promise for siRNA and microRNA Therapeutics. *Pharmaceutics* **10**, 126, doi:10.3390/pharmaceutics10030126 (2018).
- 134 Dong, Y., Siegwart, D. J. & Anderson, D. G. Strategies, design, and chemistry in siRNA delivery systems. *Advanced drug delivery reviews* **144**, 133-147, doi:10.1016/j.addr.2019.05.004 (2019).
- 135 Mishra, S., Heidel, J. D., Webster, P. & Davis, M. E. Imidazole groups on a linear, cyclodextrin-containing polycation produce enhanced gene delivery via multiple processes. *Journal of Controlled Release* **116**, 179-191, doi:<https://doi.org/10.1016/j.jconrel.2006.06.018> (2006).

- 136 Davis, M. E. The First Targeted Delivery of siRNA in Humans via a Self-Assembling, Cyclodextrin Polymer-Based Nanoparticle: From Concept to Clinic. *Molecular Pharmaceutics* **6**, 659-668, doi:10.1021/mp900015y (2009).
- 137 Yin, H. *et al.* Non-viral vectors for gene-based therapy. *Nat Rev Genet* **15**, 541-555, doi:10.1038/nrg3763 (2014).
- 138 Xiao, Y., Shi, K., Qu, Y., Chu, B. & Qian, Z. Engineering Nanoparticles for Targeted Delivery of Nucleic Acid Therapeutics in Tumor. *Mol Ther Methods Clin Dev* **12**, 1-18, doi:10.1016/j.omtm.2018.09.002 (2018).
- 139 Howard, K. A. *et al.* RNA interference in vitro and in vivo using a novel chitosan/siRNA nanoparticle system. *Mol Ther* **14**, 476-484, doi:10.1016/j.ymthe.2006.04.010 (2006).
- 140 Wang, Y. *et al.* Intravenous delivery of siRNA targeting CD47 effectively inhibits melanoma tumor growth and lung metastasis. *Mol Ther* **21**, 1919-1929, doi:10.1038/mt.2013.135 (2013).
- 141 Xiao, Y., Shi, K., Qu, Y., Chu, B. & Qian, Z. Engineering Nanoparticles for Targeted Delivery of Nucleic Acid Therapeutics in Tumor. *Molecular Therapy - Methods & Clinical Development* **12**, 1-18, doi:<https://doi.org/10.1016/j.omtm.2018.09.002> (2019).
- 142 Cutler, J. I., Auyeung, E. & Mirkin, C. A. Spherical Nucleic Acids. *Journal of the American Chemical Society* **134**, 1376-1391, doi:10.1021/ja209351u (2012).
- 143 Kapadia, C. H., Melamed, J. R. & Day, E. S. Spherical Nucleic Acid Nanoparticles: Therapeutic Potential. *BioDrugs* **32**, 297-309, doi:10.1007/s40259-018-0290-5 (2018).
- 144 Zhou, Q., Zhang, L. & Wu, H. Nanomaterials for cancer therapies. *Nanotechnology Reviews* **6**, 473-496, doi:doi:10.1515/ntrev-2016-0102 (2017).
- 145 Kim, M. W. *et al.* Cancer-targeted Nucleic Acid Delivery and Quantum Dot Imaging Using EGF Receptor Aptamer-conjugated Lipid Nanoparticles. *Scientific Reports* **7**, 9474, doi:10.1038/s41598-017-09555-w (2017).
- 146 Matea, C. T. *et al.* Quantum dots in imaging, drug delivery and sensor applications. *International journal of nanomedicine* **12**, 5421-5431, doi:10.2147/IJN.S138624 (2017).
- 147 Subramaniam, P. *et al.* Generation of a Library of Non-Toxic Quantum Dots for Cellular Imaging and siRNA Delivery. *Advanced Materials* **24**, 4014-4019, doi:<https://doi.org/10.1002/adma.201201019> (2012).
- 148 Levingstone, T. J., Herbaj, S., Redmond, J., McCarthy, H. O. & Dunne, N. J. Calcium Phosphate Nanoparticles-Based Systems for RNAi Delivery: Applications in Bone Tissue Regeneration. *Nanomaterials* **10**, 146 (2020).
- 149 Goldshtein, M., Forti, E., Ruvinov, E. & Cohen, S. Mechanisms of cellular uptake and endosomal escape of calcium-siRNA nanocomplexes. *International Journal of Pharmaceutics* **515**, 46-56, doi:<https://doi.org/10.1016/j.ijpharm.2016.10.009> (2016).
- 150 Bose, S. & Tarafder, S. Calcium phosphate ceramic systems in growth factor and drug delivery for bone tissue engineering: A review. *Acta Biomaterialia* **8**, 1401-1421, doi:<https://doi.org/10.1016/j.actbio.2011.11.017> (2012).

- 151 Maleki Dizaj, S. *et al.* An update on calcium carbonate nanoparticles as cancer drug/gene delivery system. *Expert Opin Drug Deliv* **16**, 331-345, doi:10.1080/17425247.2019.1587408 (2019).
- 152 Sun, T. *et al.* Engineered nanoparticles for drug delivery in cancer therapy. *Angew Chem Int Ed Engl* **53**, 12320-12364, doi:10.1002/anie.201403036 (2014).
- 153 Wilhelm, S. *et al.* Analysis of nanoparticle delivery to tumours. *Nature Reviews Materials* **1**, 16014, doi:10.1038/natrevmats.2016.14 (2016).
- 154 Di, J. *et al.* Size, shape, charge and “stealthy” surface: Carrier properties affect the drug circulation time in vivo. *Asian Journal of Pharmaceutical Sciences*, doi:<https://doi.org/10.1016/j.ajps.2020.07.005> (2020).
- 155 Seeman, N. C. & Sleiman, H. F. DNA nanotechnology. *Nature Reviews Materials* **3**, 17068, doi:10.1038/natrevmats.2017.68 (2017).
- 156 Seeman, N. C. Nucleic acid junctions and lattices. *Journal of Theoretical Biology* **99**, 237-247, doi:[https://doi.org/10.1016/0022-5193\(82\)90002-9](https://doi.org/10.1016/0022-5193(82)90002-9) (1982).
- 157 Roy, T., Szuttor, K., Smiatek, J., Holm, C. & Hardt, S. Conformation and Dynamics of Long-Chain End-Tethered Polymers in Microchannels. *Polymers* **11**, 488 (2019).
- 158 Wu, X.-r., Wu, C.-W. & Zhang, C. Discrete DNA three-dimensional nanostructures: the synthesis and applications. *Chinese Journal of Polymer Science* **35**, 1-24 (2016).
- 159 Tan, X., Jia, F., Wang, P. & Zhang, K. Nucleic acid-based drug delivery strategies. *Journal of Controlled Release* **323**, 240-252, doi:<https://doi.org/10.1016/j.jconrel.2020.03.040> (2020).
- 160 Lacroix, A. & Sleiman, H. F. DNA Nanostructures: Current Challenges and Opportunities for Cellular Delivery. *ACS Nano* **15**, 3631-3645, doi:10.1021/acsnano.0c06136 (2021).
- 161 Henry, S. J. W. & Stephanopoulos, N. Functionalizing DNA nanostructures for therapeutic applications. *WIREs Nanomedicine and Nanobiotechnology* **n/a**, e1729, doi:<https://doi.org/10.1002/wnan.1729>.
- 162 Walsh, A. S., Yin, H., Erben, C. M., Wood, M. J. & Turberfield, A. J. DNA cage delivery to mammalian cells. *ACS Nano* **5**, 5427-5432, doi:10.1021/nn2005574 (2011).
- 163 Qian, H. *et al.* Protecting microRNAs from RNase degradation with steric DNA nanostructures. *Chemical Science* **8**, 1062-1067, doi:10.1039/C6SC01829G (2017).
- 164 He, Y. *et al.* Hierarchical self-assembly of DNA into symmetric supramolecular polyhedra. *Nature* **452**, 198-201, doi:10.1038/nature06597 (2008).
- 165 Yurke, B., Turberfield, A. J., Mills, A. P., Simmel, F. C. & Neumann, J. L. A DNA-fuelled molecular machine made of DNA. *Nature* **406**, 605-608, doi:10.1038/35020524 (2000).
- 166 Yijun Guo, B. W., Shiyan Xiao, Dongbao Yao, Hui Li, Huaguo Xu, Tingjie Song, Xiang Li, Haojun Liang. Recent advances in molecular machines based on toehold-mediated strand displacement reaction. *Quant. Biol.* **5**, 25-41, doi:10.1007/s40484-017-0097-2 (2017).
- 167 Rothmund, P. W. K. Folding DNA to create nanoscale shapes and patterns. *Nature* **440**, 297-302, doi:10.1038/nature04586 (2006).

- 168 Wang, Z. *et al.* A Tubular DNA Nanodevice as a siRNA/Chemo-Drug Co-delivery Vehicle for Combined Cancer Therapy. *Angewandte Chemie International Edition* **60**, 2594-2598, doi:<https://doi.org/10.1002/anie.202009842> (2021).
- 169 Aldaye, F. A. & Sleiman, H. F. Modular Access to Structurally Switchable 3D Discrete DNA Assemblies. *Journal of the American Chemical Society* **129**, 13376-13377, doi:10.1021/ja075966q (2007).
- 170 Chen, J. H. & Seeman, N. C. Synthesis from DNA of a molecule with the connectivity of a cube. *Nature* **350**, 631-633, doi:10.1038/350631a0 (1991).
- 171 Lee, H. *et al.* Molecularly self-assembled nucleic acid nanoparticles for targeted in vivo siRNA delivery. *Nature Nanotechnology* **7**, 389-393, doi:10.1038/nnano.2012.73 (2012).
- 172 Fakhoury, J. J., McLaughlin, C. K., Edwardson, T. W., Conway, J. W. & Sleiman, H. F. Development and Characterization of Gene Silencing DNA Cages. *Biomacromolecules* **15**, 276-282, doi:10.1021/bm401532n (2014).
- 173 Bujold, K. E., Hsu, J. C. C. & Sleiman, H. F. Optimized DNA “Nanosuitcases” for Encapsulation and Conditional Release of siRNA. *Journal of the American Chemical Society* **138**, 14030-14038, doi:10.1021/jacs.6b08369 (2016).
- 174 Ren, K. *et al.* A DNA dual lock-and-key strategy for cell-subtype-specific siRNA delivery. *Nature Communications* **7**, 13580, doi:10.1038/ncomms13580 (2016).
- 175 Platnich, C. M., Rizzuto, F. J., Cosa, G. & Sleiman, H. F. Single-molecule methods in structural DNA nanotechnology. *Chemical Society Reviews* **49**, 4220-4233, doi:10.1039/C9CS00776H (2020).
- 176 Afonin, K. A., Dobrovolskaia, M. A., Church, G. & Bathe, M. Opportunities, Barriers, and a Strategy for Overcoming Translational Challenges to Therapeutic Nucleic Acid Nanotechnology. *ACS Nano* **14**, 9221-9227, doi:10.1021/acsnano.0c04753 (2020).
- 177 Kwak, M. & Herrmann, A. Nucleic acid amphiphiles: synthesis and self-assembled nanostructures. *Chemical Society Reviews* **40**, 5745-5755, doi:10.1039/C1CS15138J (2011).
- 178 Watson, K. J., Park, S.-J., Im, J.-H. & Mirkin, C. A. DNA–Block Copolymer Conjugates. *Journal of the American Chemical Society* **123**, 5592-5593, doi:10.1021/ja0156845 (2001).
- 179 Whitfield, C. J. *et al.* Functional DNA–Polymer Conjugates. *Chemical Reviews*, doi:10.1021/acs.chemrev.0c01074 (2021).
- 180 Alemdaroglu, F. E., Alemdaroglu, N. C., Langguth, P. & Herrmann, A. Cellular Uptake of DNA Block Copolymer Micelles with Different Shapes. *Macromolecular Rapid Communications* **29**, 326-329, doi:<https://doi.org/10.1002/marc.200700779> (2008).
- 181 Jeong, J. H., Kim, S. W. & Park, T. G. Novel Intracellular Delivery System of Antisense Oligonucleotide by Self-Assembled Hybrid Micelles Composed of DNA/PEG Conjugate and Cationic Fusogenic Peptide. *Bioconjugate Chemistry* **14**, 473-479, doi:10.1021/bc025632k (2003).

- 182 Kamps, A. C., Cativo, M. H. M., Chen, X.-J. & Park, S.-J. Self-Assembly of DNA-Coupled Semiconducting Block Copolymers. *Macromolecules* **47**, 3720-3726, doi:10.1021/ma500509u (2014).
- 183 Barnaby, S. N., Sita, T. L., Petrosko, S. H., Stegh, A. H. & Mirkin, C. A. in *Nanotechnology-Based Precision Tools for the Detection and Treatment of Cancer* (eds Chad A. Mirkin, Thomas J. Meade, Sarah Hurst Petrosko, & Alexander H. Stegh) 23-50 (Springer International Publishing, 2015).
- 184 Mirkin, C. A., Letsinger, R. L., Mucic, R. C. & Storhoff, J. J. A DNA-based method for rationally assembling nanoparticles into macroscopic materials. *Nature* **382**, 607-609, doi:10.1038/382607a0 (1996).
- 185 Rosi, N. L. *et al.* Oligonucleotide-modified gold nanoparticles for intracellular gene regulation. *Science* **312**, 1027-1030, doi:10.1126/science.1125559 (2006).
- 186 Prigodich, A. E. *et al.* Tailoring DNA Structure To Increase Target Hybridization Kinetics on Surfaces. *Journal of the American Chemical Society* **132**, 16296-16296, doi:10.1021/ja1087419 (2010).
- 187 Lytton-Jean, A. K. & Mirkin, C. A. A thermodynamic investigation into the binding properties of DNA functionalized gold nanoparticle probes and molecular fluorophore probes. *J Am Chem Soc* **127**, 12754-12755, doi:10.1021/ja052255o (2005).
- 188 Seferos, D. S., Prigodich, A. E., Giljohann, D. A., Patel, P. C. & Mirkin, C. A. Polyvalent DNA nanoparticle conjugates stabilize nucleic acids. *Nano Lett* **9**, 308-311, doi:10.1021/nl802958f (2009).
- 189 Cutler, J. I. *et al.* Polyvalent Nucleic Acid Nanostructures. *Journal of the American Chemical Society* **133**, 9254-9257, doi:10.1021/ja203375n (2011).
- 190 Giljohann, D. A., Seferos, D. S., Prigodich, A. E., Patel, P. C. & Mirkin, C. A. Gene Regulation with Polyvalent siRNA–Nanoparticle Conjugates. *Journal of the American Chemical Society* **131**, 2072-2073, doi:10.1021/ja808719p (2009).
- 191 Jensen, S. A. *et al.* Spherical nucleic acid nanoparticle conjugates as an RNAi-based therapy for glioblastoma. *Sci Transl Med* **5**, 209ra152, doi:10.1126/scitranslmed.3006839 (2013).
- 192 Kumthekar Priya, P. A first-in-human phase 0 clinical study of RNA interferencebased spherical nucleic acids in patients with recurrent glioblastoma. *Science Translational Medicine* **13**, 3945 (2021).
- 193 Zhang, K., Hao, L., Hurst, S. J. & Mirkin, C. A. Antibody-Linked Spherical Nucleic Acids for Cellular Targeting. *Journal of the American Chemical Society* **134**, 16488-16491, doi:10.1021/ja306854d (2012).
- 194 Randeria, P. S. *et al.* siRNA-based spherical nucleic acids reverse impaired wound healing in diabetic mice by ganglioside GM3 synthase knockdown. *Proc Natl Acad Sci U S A* **112**, 5573-5578, doi:10.1073/pnas.1505951112 (2015).
- 195 Radovic-Moreno, A. F. *et al.* Immunomodulatory spherical nucleic acids. *Proc Natl Acad Sci U S A* **112**, 3892-3897, doi:10.1073/pnas.1502850112 (2015).

- 196 Singh, P. *et al.* Gold Nanoparticles in Diagnostics and Therapeutics for Human Cancer. *Int J Mol Sci* **19**, 1979, doi:10.3390/ijms19071979 (2018).
- 197 Arvizo, R., Bhattacharya, R. & Mukherjee, P. Gold nanoparticles: opportunities and challenges in nanomedicine. *Expert Opin Drug Deliv* **7**, 753-763, doi:10.1517/17425241003777010 (2010).
- 198 Sinegra, A. J., Evangelopoulos, M., Park, J., Huang, Z. & Mirkin, C. A. Lipid Nanoparticle Spherical Nucleic Acids for Intracellular DNA and RNA Delivery. *Nano Lett* **21**, 6584-6591, doi:10.1021/acs.nanolett.1c01973 (2021).
- 199 Roloff, A., Nelles, D. A., Thompson, M. P., Yeo, G. W. & Gianneschi, N. C. Self-Transfecting Micellar RNA: Modulating Nanoparticle Cell Interactions via High Density Display of Small Molecule Ligands on Micelle Coronas. *Bioconjugate chemistry* **29**, 126-135, doi:10.1021/acs.bioconjchem.7b00657 (2018).
- 200 Rush, A. M. *et al.* Intracellular mRNA Regulation with Self-Assembled Locked Nucleic Acid Polymer Nanoparticles. *Journal of the American Chemical Society* **136**, 7615-7618, doi:10.1021/ja503598z (2014).
- 201 Zhang, C. *et al.* Biodegradable DNA-Brush Block Copolymer Spherical Nucleic Acids Enable Transfection Agent-Free Intracellular Gene Regulation. *Small (Weinheim an der Bergstrasse, Germany)* **11**, 5360-5368, doi:10.1002/sml.201501573 (2015).
- 202 Bousmail, D. *Sequence-Defined DNA Polymers: Applications in Drug Delivery and Supramolecular Assembly*, McGill University (Canada), (2019).
- 203 Edwardson, T. G., Carneiro, K. M., Serpell, C. J. & Sleiman, H. F. An efficient and modular route to sequence-defined polymers appended to DNA. *Angew Chem Int Ed Engl* **53**, 4567-4571, doi:10.1002/anie.201310937 (2014).
- 204 de Rochambeau, D., Sun, Y., Barlog, M., Bazzi, H. S. & Sleiman, H. F. Modular Strategy To Expand the Chemical Diversity of DNA and Sequence-Controlled Polymers. *The Journal of Organic Chemistry* **83**, 9774-9786, doi:10.1021/acs.joc.8b01184 (2018).
- 205 Fakhoury, J. J. *et al.* Antisense precision polymer micelles require less poly(ethylenimine) for efficient gene knockdown. *Nanoscale* **7**, 20625-20634, doi:10.1039/C5NR05157F (2015).
- 206 Lacroix, A., Edwardson, T. G. W., Hancock, M. A., Dore, M. D. & Sleiman, H. F. Development of DNA Nanostructures for High-Affinity Binding to Human Serum Albumin. *Journal of the American Chemical Society* **139**, 7355-7362, doi:10.1021/jacs.7b02917 (2017).
- 207 Lacroix, A., Fakih, H. H. & Sleiman, H. F. Detailed cellular assessment of albumin-bound oligonucleotides: Increased stability and lower non-specific cell uptake. *Journal of Controlled Release* **324**, 34-46, doi:<https://doi.org/10.1016/j.jconrel.2020.04.020> (2020).
- 208 Bousmail, D., Chidchob, P. & Sleiman, H. F. Cyanine-Mediated DNA Nanofiber Growth with Controlled Dimensionality. *Journal of the American Chemical Society* **140**, 9518-9530, doi:10.1021/jacs.8b04157 (2018).

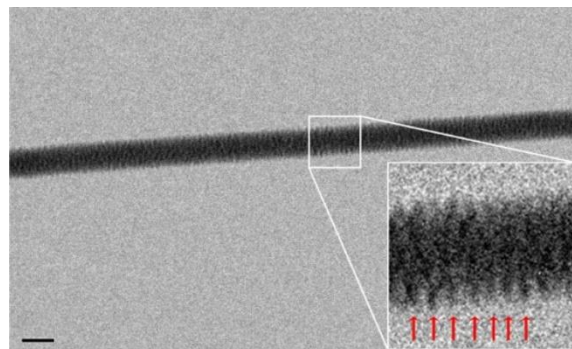
- 209 Dore, M. D. *et al.* Thermosetting supramolecular polymerization of compartmentalized DNA fibers with stereo sequence and length control. *Chem*, doi:<https://doi.org/10.1016/j.chempr.2021.05.022> (2021).

Preface 1

In Chapter 2, we describe the work to design a new generation of sequence-controlled spherical nucleic acids (SNAs), termed responsive-SNAs (RSNAs), for the delivery of therapeutics in a stimuli-responsive manner, via strand displacement. SNAs are produced in a simple automated manner, have excellent biocompatibility, are highly monodisperse, and can deliver functional nucleic acid therapeutics (NATs) *in vitro*. However, the first generation of SNAs lacked specificity and selectivity, as the NATs that they carry would be active in any cell that can take up the SNA.

Certain cells, such as cancer cells, can overexpress oligonucleotide biomarkers (miRNA, mRNA) that are essential for their survival. Designing the SNAs to be responsive to these intracellular cues and activating the therapeutic **only** in their presence, adds selectivity and specificity. The design of these RSNAs relies on partially hybridizing the NAT to the DNA corona. In the presence of the **fully** complementary trigger oligonucleotides, strand displacement will occur by their full binding to the DNA corona of the SNA and releasing the therapeutic. In the absence of the triggers the NAT will remain bound and is ineffective in gene silencing, hence adding specificity to the SNAs.

In this chapter, we characterize the assembly of the RSNAs with multiple techniques, to ensure that we still obtain monodisperse spherical structures. Then, we assess the specificity of our RSNAs by testing the release of the therapeutic cargo in the presence of triggers. Stability in biological media was examined showcasing enhanced protection of the cargo as part of the RSNA. Lastly, we showcase the specificity of the RSNAs *in vitro*, where their ASO cargo is only active in cells that carry the specific triggers to induce the release from the RSNA. These studies describe dynamic spherical nucleic acids for the selective and conditional delivery of nucleic acid therapies.

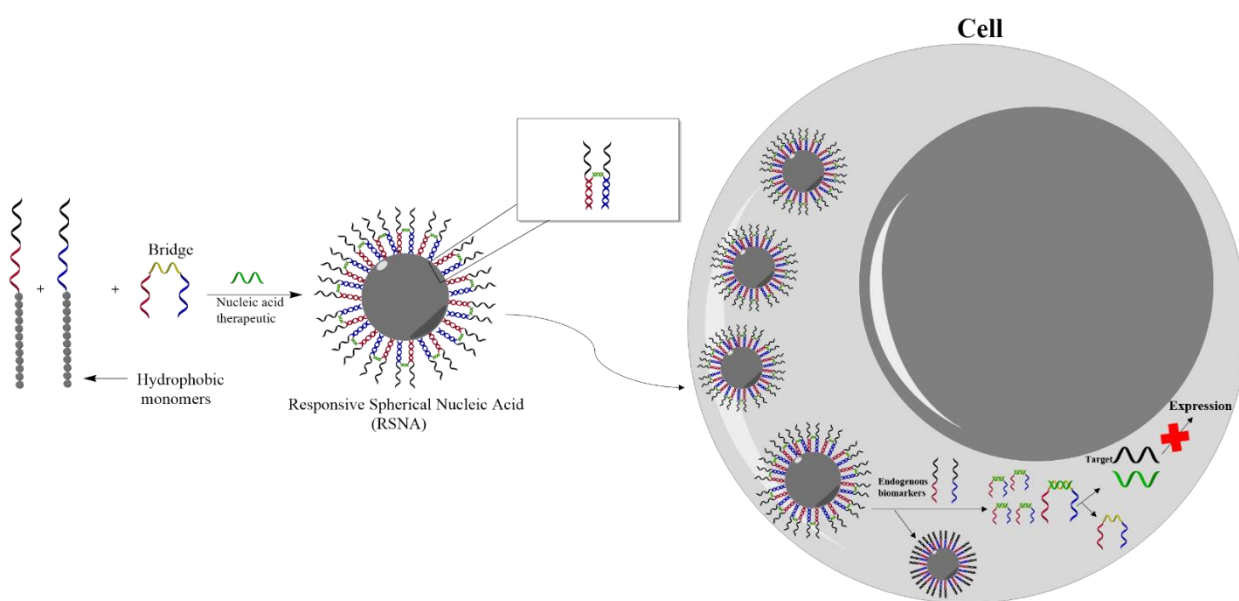


Direct electron photograph of DNA bundle by Enzo Di Fabrizio

“Simplicity is the ultimate sophistication”

Leonardo Da Vinci

2 | Minimalist Design of a Stimuli-Responsive Spherical Nucleic Acid for Conditional Delivery of Oligonucleotide Therapeutics



This chapter is adapted from the published manuscript titled “Minimalist Design of a Stimuli-Responsive Spherical Nucleic Acid for Conditional Delivery of Oligonucleotide Therapeutics” by Hassan H. Fakih, Johans J. Fakhoury, Danny Bousmail and Hanadi F. Sleiman. *ACS Applied Materials & Interfaces* 2019 11 (15), 13912-13920.

Contribution of authors

Hassan H. Fakih helped design the project and primarily contributed to production of experimental data from synthesis, purification, characterization, analysis, and *in vitro* experiments. **Johans J. Fakhoury** provided feedback, guidance and discussion about *in vitro* experiments and data. **Danny Bousmail** performed initial AFM imaging to prove spherical structure of SNAs. **Hanadi F. Sleiman** designed the project with **Hassan H. Fakih**, guided interpretation of data and discussion of experiments. **Hassan H. Fakih** and **Hanadi F. Sleiman** co-wrote the manuscript.

2.1. Abstract

In this work, we report a component-minimal Spherical Nucleic acid (SNA) from monodisperse DNA-polymer conjugates, that can load and release nucleic acid therapeutics in a stimuli-responsive manner. We show that this vehicle assembles from only 4 strands, and conditional release of its antisense therapeutic cargo can be induced upon recognition of specific oligonucleotide triggers via strand displacement. The latter (triggers) may be a microRNA which offers additional synergistic therapy, on top of the previously shown ability of the SNA to load hydrophobic drugs. The SNA is easy to prepare, has a dynamic character, releases its cargo only upon the presence of both triggers, and can survive biological conditions while protecting the cargo being delivered. The gene silencing potency of the cargo was tested in live cells and shown to be suppressed when loaded in the SNA, and its activity was restored only upon release. This vehicle has the essential characteristics of versatility, ease of synthesis, low cost, highly responsive behavior, and ability to support combination therapies, making it a promising candidate for cell-selective drug delivery and clinical transition.

2.2. Introduction

In this work, Nucleic acid therapeutics such as small interfering RNA (siRNA) and antisense oligonucleotides (AON) offer unique potential for gene therapy, due to their effectiveness and directed silencing of the targeted gene of interest. However, their minimal stability in biologically-relevant media, and poor pharmacokinetics have limited their applications.¹⁻⁵ Various vehicles to deliver these therapeutics are being explored, such as liposomes and polymeric nanoparticles.^{2,6,7} Unfortunately, these first-generation vehicles still face many challenges, slowing the translation of laboratory prototypes into clinical applications.⁴ In particular, most synthetic oligonucleotide carriers are a mixture of polydisperse molecules that are not precisely controlled in size, shape, and composition. Given that *in vivo* biodistribution is size and shape-dependent,^{4,8,9} their properties and toxicity can be heterogeneous.¹⁰ In addition, off-target effects are problematic, as they can end up harming healthy cells and organs. Hence, the need for new drug delivery modalities that provide targeting, as well as control over the size, shape, surface density and material used is paramount.^{2,4,11}

DNA nanotechnology, which utilizes DNA as a building block to self-assemble nanostructures through Watson-Crick base pairing, is an attractive approach for developing delivery vehicles.^{12,13} Not only are DNA-based structures biocompatible, but they also have well-defined shapes, sizes and monodispersity. They can be easily functionalized with different chemical moieties by exploiting standard phosphoramidite chemistry.¹² Importantly, DNA-based materials can release their cargo conditionally upon recognition of a chosen target, which allows them to discriminate between healthy and diseased cells, improving efficacy and decreasing off-target effects. Examples of stimuli-responsive DNA-based vehicles include origami nanorobots,^{14,15} pH-responsive DNA hydrogels¹⁶ and cages¹⁷, DNA cages with responsive aptamers,¹⁸⁻²⁰ a hairpin-based responsive DNA tetrahedron,²¹ and temperature-responsive cages.²² However, very few examples are based on cytoplasmic genetic markers as stimuli, which preserves the drug until target recognition inside the cell.^{23,24} We recently reported a “suitcase” DNA cage that can encapsulate and selectively release a siRNA strand in the presence of specific DNA or RNA sequences;²⁴ however, the design of this cage required the use of multiple modified DNA strands, its size (~ 9nm) was relatively small for favorable *in vivo* distribution, and it was only tested in fixed cells.^{25,26}

An especially powerful DNA functionalization is the attachment of hydrophobic polymers, which has led to the emergence of a new class of amphiphilic DNA block copolymers.²⁷⁻²⁹ We have developed precision spherical nucleic acids (SNA),³⁰⁻³⁴ based on a highly efficient solid-phase method to generate monodisperse and sequence-defined DNA-polymer conjugates.³¹ These spherical micellar particles are assembled in aqueous media, and they possess a hydrophobic core and a DNA-based corona. The SNAs have the capacity to load and deliver hydrophobic drugs, and were shown to have high monodispersity, stability in biological media, uptake into cells, and favorable biodistribution in mouse models.³⁰ More importantly, these SNAs, in comparison to other DNA nanostructures such as origami that requires hundreds of unique DNA strands, need only a single component for assembly.³⁵ Their DNA-minimal and simple structure is crucial in enabling large-scale production and translation to clinical applications.^{4 36}

In this work, we introduce a dynamic and responsive spherical nucleic acid (RSNA) that can deliver nucleic acid therapeutics in a precise, stimuli-responsive manner. We set out to design this new class of delivery vehicles with an important requirement, namely using the minimum number of components, compared to previously reported highly modified and multicomponent systems.^{27,37,38} Moreover, we show, for the first time, conditional gene silencing in live cells, in response to oligonucleotide triggers.

The approach relies on utilizing the DNA corona of our single-component SNAs to load and protect a nucleic acid cargo (**Figure 2. 1. A**). This cargo is incorporated via partial hybridization and is designed for release only in the presence of cytoplasmic genetic markers via strand displacement.³⁹ This is extremely important as vehicles responsive to endogenous stimuli are more suitable to clinical settings, and would not rely on external complicated apparatus for manipulation.⁴⁰ The design can be easily tailored to respond to the genetic markers of interest, as well as to deliver different nucleic acids by only redesigning the sequences of the DNA corona. Furthermore, the sequence recognition motif can itself also be a therapeutic if designed to act as an antisense oligonucleotide for a specific target (e.g., miRNA). Hence, this work develops a simple, stimuli-responsive, general multidrug delivery system. We study the loading of a nucleic acid antisense strand onto the SNA and characterize it via dynamic light scattering (DLS), atomic force microscopy (AFM), gel electrophoresis, and fluorescent studies. The specificity and dynamic character are also studied, as well as the stability in biological media and conditional gene silencing in live cells.

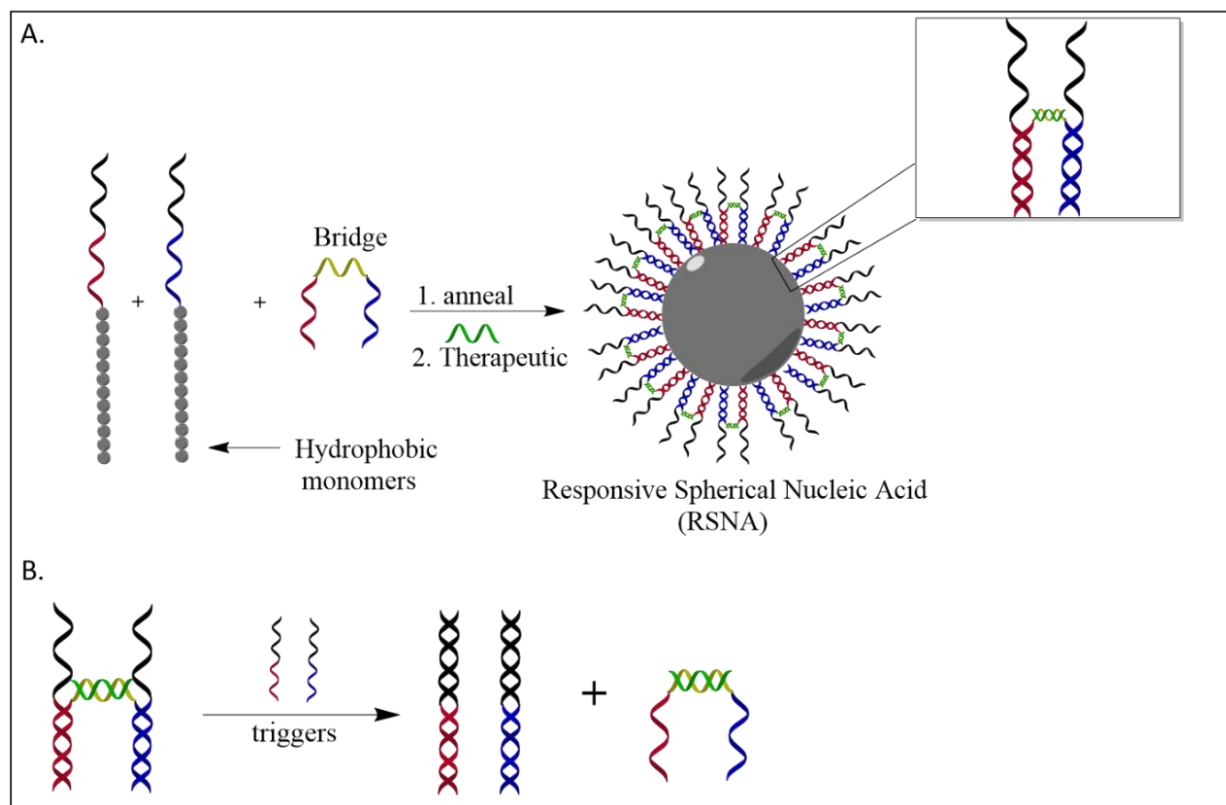


Figure 2. 1. Schematic representation of the responsive Spherical nucleic acid (RSNA). **A.** The components that assemble to form RSNA. Two ‘pillar’ amphiphilic strands assemble with a ‘bridge’ strand and the oligonucleotide therapeutic (Green) is hybridized to the horizontal portion of the bridge strand. **B.** Strand displacement by two cytoplasmic genetic markers (‘triggers’) releases the bridge strand and the therapeutic cargo, resulting in the responsiveness of the system (hydrophobic part not shown for simplicity)

2.3. Results and Discussion

2.3.1. *Design and assembly of RSNA*

Highly monodisperse spherical nucleic acids from DNA amphiphiles are typically assembled by annealing the amphiphilic strand in magnesium-containing aqueous buffer (under physiologically relevant conditions).^{30,31} In this work however, additional elements were used in the design of responsive SNA (RSNA, **Figure 2. 1. A**) for selective delivery. Two DNA-polymer strands (‘pillars’) are assembled together using a bridge strand in a partially-hybridized manner, which enables this bridge strand to be released in the presence of fully complementary strands (triggers) to the SNA pillars,

via strand displacement (**Figure 2. 1 B**) The therapeutic cargo strand (green) can be loaded by hybridization to the middle section of the bridge strand. The pillars of the SNA are 21mers, and the bridge strand has two arms, each a 14mer that is complementary to the pillars (red and blue, **Figure 2. 1. A, Supplementary Figure 2. 1.**). The SNA (RSNA) pillars can be designed to be responsive to endogenous biomarkers (**Figure 2. 1 B**) that are overexpressed in specific cancerous cells compared to normal ones. Such biomarkers can be miRNA which are 21-23 bases (same as the pillars) in length and many have been identified as a promising cancer targets.^{41,42} The binding will cause the burst release and activation of the nucleic acid therapeutic, as well as the possibility to elicit a miRNA antagomir effect. The advantage of such a design is that it is general in the sense that the SNA pillars can be redesigned to respond to any biomarker of interest, and the target can be readily changed by modifying the sequence of the nucleic acid therapeutic to a target of interest.

To assemble the RSNA, the pillars were annealed at 5 μ M concentration with 0.3 molar equivalents of the bridge strand, which we found to be the maximum loading capacity (**Supplementary Figure 2. 2.**). Then, the complementary strand is added to the bridge at room temperature (**Figure 2. 1.**). This avoids secondary structures or possible aggregation. The design was tested to fit a 50mer bridge strand that loads an 18mer antisense oligonucleotide. It was also tested to fit an siRNA cargo model²⁴ to show the versatility and universality of the system.¹¹

2.3.2. Characterization of the RSNA loaded with antisense or siRNA cargo

To test the proposed design, a 50mer long bridge strand was synthesized, and it consists of 3 regions: two 14mers complementary to the two pillars and a 22mer variable middle region that loads the cargo of choice. The 22mer loading region consists of an 18mer complementary region to an antisense oligonucleotide (nucleic acid therapeutic), and a 2-base spacer region on both ends (**Supplementary Figure 2. 1.**). To monitor the loading and the release, we used fluorescently labelled strands (**Figure 2. 2. A**). The assembly of the structure was first confirmed with dynamic light scattering (DLS), where the final fully loaded RSNA has a diameter of 31.6 nm (**Figure 2. 2. B**). The DLS data, representing the intensity vs radius, shows an increase in

diameter upon addition of each bridge strand and cargo strands, suggesting the successful hybridization of the corresponding strands to the SNA while still displaying high monodispersity (**Figure 2. 2. B**).

Fluorescence measurements were then carried out on the different states of the SNA using Forster resonance energy transfer (FRET) analysis with strategic placement of two dyes (**Figure 2. 2. A,C**). A Cy3 dye was placed on one of the DNA-polymer pillar strands, between the hydrophobic moiety and the DNA part. The bridge and cargo strands were loaded on the SNA and fluorescence was recorded. The trigger strands were then added to release the cargo (1:1 molar ratio with the cargo), where one of the trigger strands was end-labeled with Cy5, such that successful binding results in proximity of the two dyes (**Figure 2. 2. A**). Fluorescence data shows 99% FRET efficiency between Cy3 and Cy5 when the RSNA was incubated with the triggers (**Figure 2C**), where the Cy5 emission is significantly increased when exciting Cy3 (Excitation wavelength = 550 nm).

The samples were then loaded on a 2.5% native agarose gel. (**Figure 2. 2. C**) The fully assembled RSNA appeared as a single band, indicating its successful assembly and well-defined structure³¹ (**Figure 2. 2. C**, lane 1; left panel is fluorescence visualization, and right panel is DNA staining). Upon addition of the bridge and the cargo, a decrease in mobility of the RSNA structures was observed, as compared to the unloaded SNA (**Figure 2. 2. C**, lanes 2 and 3). When the trigger strands were added, release of the bridge+cargo strands were clearly observed as a faster moving band (**Figure 2C**, right panel, lane 4) along with a change in the fluorescence emission from Cy3 to Cy5 due to trigger binding and FRET between the two dyes (**Figure 2. 3. C**, left panel, lane 4). Typically, we incubate RSNA with 0.3 equivalents of the trigger strands, which results in around 50% release of cargo in 5-10 mins, and 100% in 2-3 hours (**Supplementary Figure 2. 3**). Hence the results show that we can assemble a minimalistic, stimuli-responsive SNA from just 3 components.

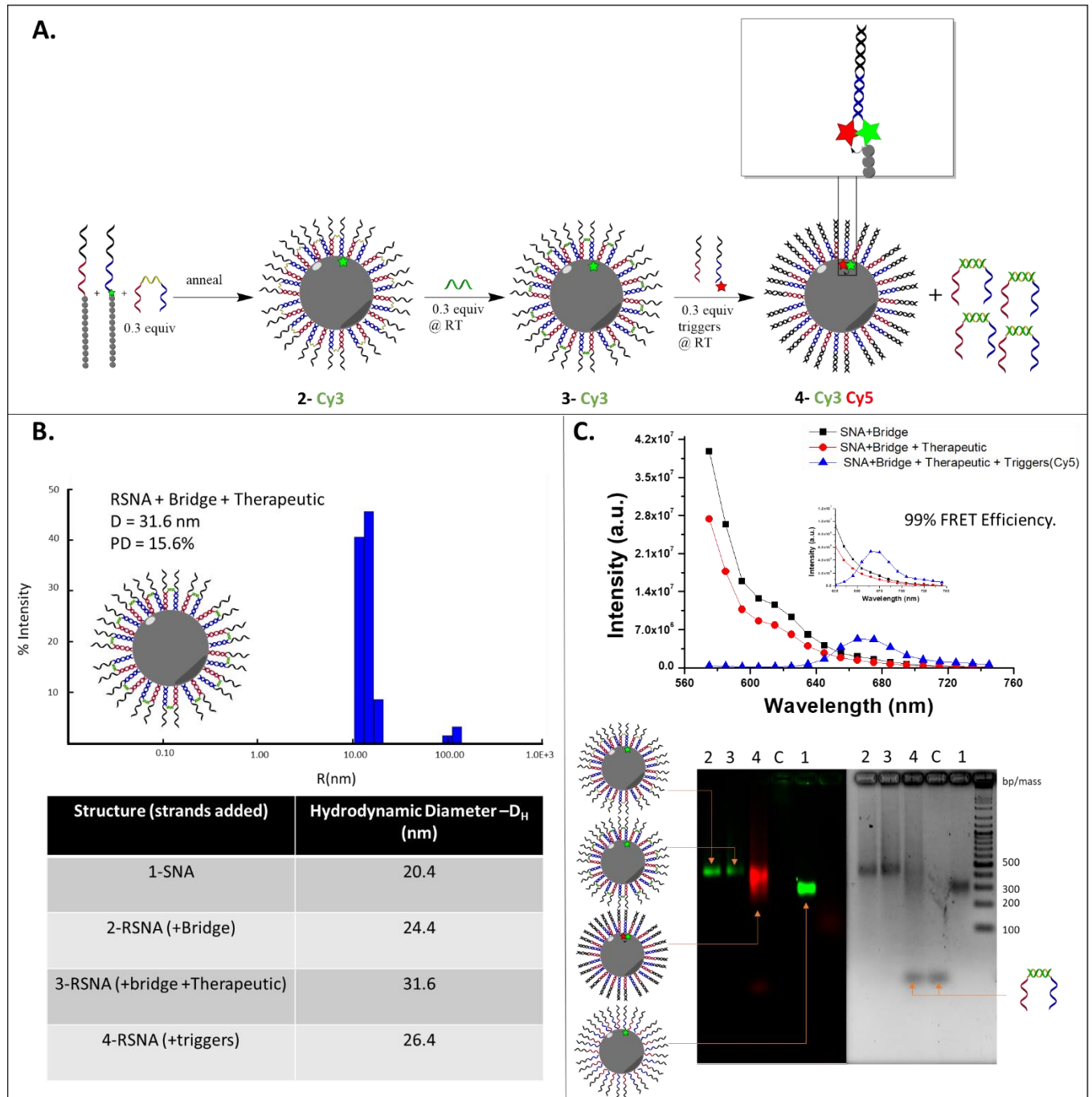


Figure 2. 2. A. Scheme of the different states of SNA loaded with Bridge and therapeutic. **B.** Characterization by DLS. **C.** fluorescence/FRET measurements along with agarose gel electrophoresis. Samples are prepared at 5 μ M concentration of SNA in 1xTAMg buffer. DNA ladder used is GeneRuler DNA Ladder Mix (100-10,000 bp/mass). Gel lanes: 1) SNA, 2) SNA loaded with bridge, 3) RSNA with both bridge and therapeutic, 4) released RSNA after addition of triggers (green star = Cy3, red star = Cy5, arrow indicates FRET).

2.3.3. *Two keys, one lock*

We were interested in testing whether the RSNA would release its cargo in the presence of one of the triggers, or whether it needs both triggers simultaneously. We thus incubated the RSNA with either trigger separately, or with both simultaneously. The results show that both triggers need to be added for cargo release, resulting in an AND gate for two stimuli (**Figure 2. 3**). Thus, the SNA can be designed to respond and release its therapeutic with the simultaneous presence of two biomarkers of a specific cell, with an additional level of selectivity, minimizing off-target effects on cells that share one of the biomarkers but not the other. If a single trigger needs to be used as target, then the bridge binding regions of the two pillar strands can be made identical in sequence.

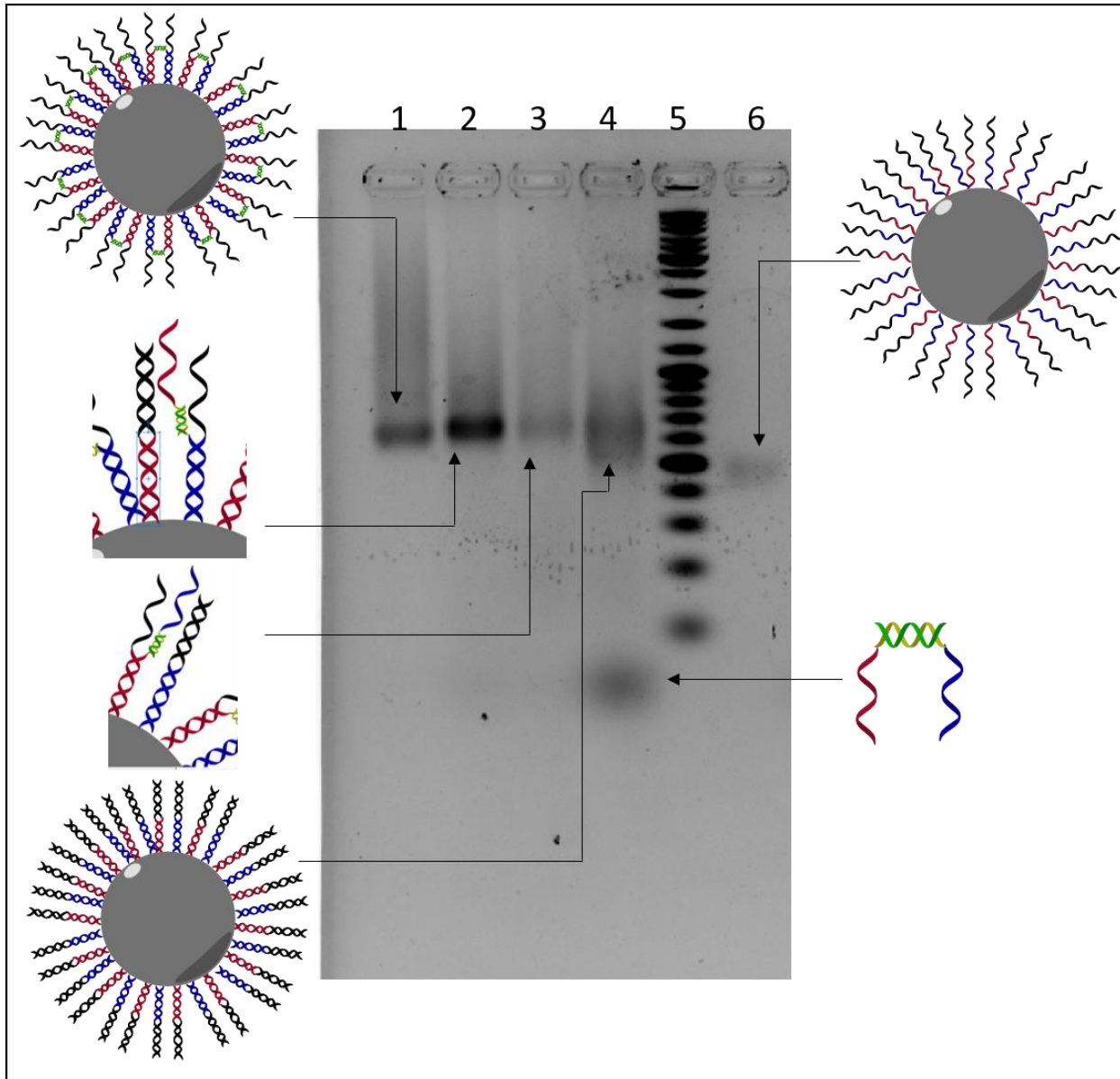


Figure 2. 3. Specificity of RNSA. Both triggers must be present simultaneously (lane 4) in order to release the cargo. Lane 1: RSNA; lane 2: RSNA with one trigger; lane 3: RSNA with second trigger. lane 4: RSNA with both triggers; lane 5: DNA ladder, GeneRuler DNA Ladder Mix (100-10,000 bp/mass); lane 6: RSNA without cargo. All SNA's were assembled at 5 μ M and loaded on agarose gel.

To simulate an siRNA cargo on the RSNA strands, we also tested a longer 57mer bridge strand (Bridge B). Bridge B has a 29-mer variable region that hybridizes to an 18mer model cargo strand (Bridge B.cargo) which simulates siRNA, with additional

arms for hybridization to the pillars. We were also successful in assembling this RSNA and show triggered cargo release with full characterization (**Supplementary Figure 2.4**), indicating the generality of the system.

To directly confirm the structure of the RSNA and any morphological changes upon loading the bridge and cargo strands, we performed atomic force microscopy (AFM) imaging in air (**Figure 2.4**). Results show a spherical morphology whose diameter increases from SNA to RSNA with bridge and cargo strands. The diameter (46.3 nm) is larger compared to DLS (31.6 nm), likely due to the drying effect of the sample which spreads the micelle on the mica surface, as previously reported.³⁰

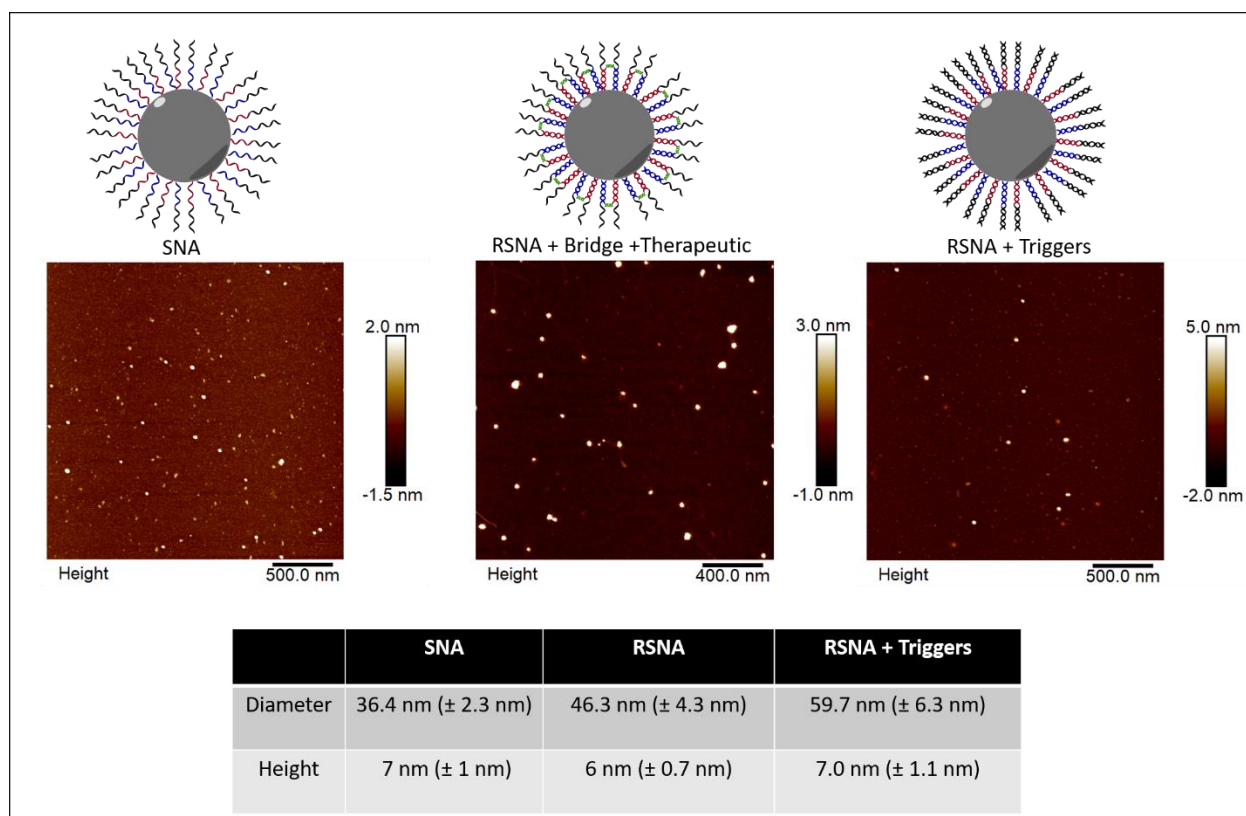


Figure 2.4. Atomic Force Microscopy characterization of SNA and RSNA. Samples prepared at 5 μ M SNA concentration in 1xTAMg buffer.

2.3.4. *Stability in biological conditions*

After confirmation of the assembly and full characterization of the dynamic properties of the RSNA, we proceeded to evaluate its stability and behavior in a biologically-relevant environment. We tested the stability of the structure by incubating it in cellular media, which is made of 10% fetal bovine serum in Dulbecco's modified Eagle medium (DMEM).^{43,44} Aliquots were taken at hourly timepoints and analyzed by denaturing polyacrylamide gel to assess whether the nanostructure can shield and stabilize the bridge strand which carries cargo. (**Figure 2. 5.**) The gel shows improved stability of the bridge strand when loaded within RSNA, which persists up to 6 hours and can still be detected at 12 hours, while the bridge strand on its own is mostly degraded between 1-2 hours. An exponential decay fit was used to estimate a half-life of 5 hours for the loaded bridge strand, a ca. 5-time fold increase compared to the strand on its own (0.9 hours). The degradation products of the bridge strand migrated similarly to the cargo strand, which prevented its quantification.

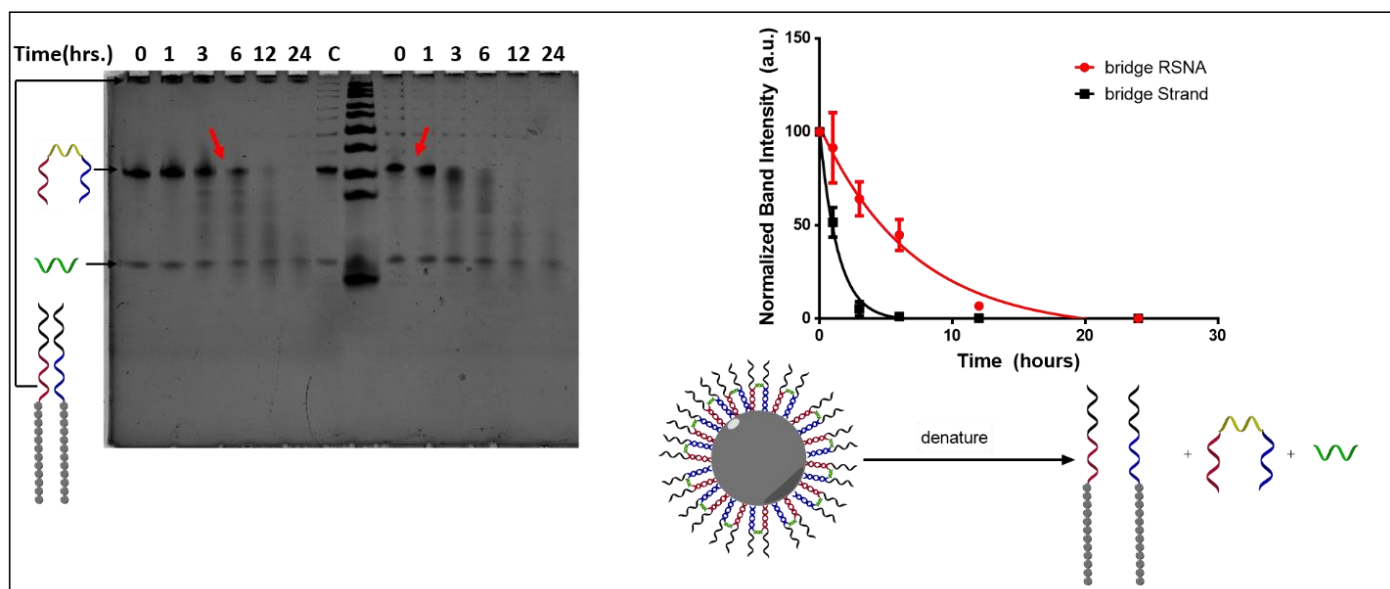


Figure 2. 5. Serum stability assessment of RSNA and its ability to improve the half-life of the cargo. Aliquots loaded on a 20% denaturing polyacrylamide gel electrophoresis (PAGE). First set of lanes are the denatures RSNA at different incubation times with serum, the second set is for the bridge+ therapeutic. Band intensities were normalized and then fitted with an exponential decay fit to estimate the half-life of the bridge strand. DNA ladder used is GeneRuler Ultra Low Range DNA Ladder (15-300 bp/mass).

2.3.5. *Unhindered silencing ability and activation on demand*

We were interested in testing whether the silencing ability of the nucleic acid therapeutics is hindered or improved when residing in our RSNA. Hence, we hybridized a phosphorothioated antisense nucleic acid (ASO) designed to downregulate Luciferase to the bridge strand. Transfection of the antisense RSNA was carried out in HeLa cells overnight.⁴⁵ The results (**Figure 2. 6. A**) show that sequestration of the ASO within the spherical nucleic acid significantly reduces its silencing ability. However, upon pre-transfection of the two trigger strands to the cells in a 2:1 ratio (with RSNA) followed by washing (**Supplementary Figure 2. 5.**), a significant improvement of the silencing ability was observed, suggesting cytoplasmic release of the cargo with the trigger strands. This shows that the silencing activity is initiated after the therapeutic is released from the RSNA, in the presence of the triggers. MTT cell viability assay was also performed and results show no significant toxicity to the cells (**Figure 2. 6. B**). The bridge+therapeutic had higher activity than the RSNA likely due to non-total release of the cargo after 24 hours. It is also higher than the therapeutic on its own due to the added protection provided by a double stranded nucleic acid compared to a single stranded one. To our knowledge, this is one of the first examples of conditional cytoplasmic release of nucleic acid cargo from a drug delivery vehicle in live cells and in the presence of triggers.^{15,46} A recent example showed the release of anti-microRNA in response to hybridization with an endogenous biomarker.⁴⁶ Many other systems were reported to deliver therapeutics based on exogenous stimuli (e.g., light⁴⁷, electric field etc.⁴⁰); also as mentioned earlier, extracellular conditional cargo release has also been reported.¹⁴⁻¹⁶

The specificity of the system in needing the fully complementary target as well as the right triggers was tested and showed no activation unless both are present (**Supplementary Figure 2. 7. and 2.8**).

Current efforts are directed at maximizing the intracellular release efficiency, while maintaining the specificity of this process.

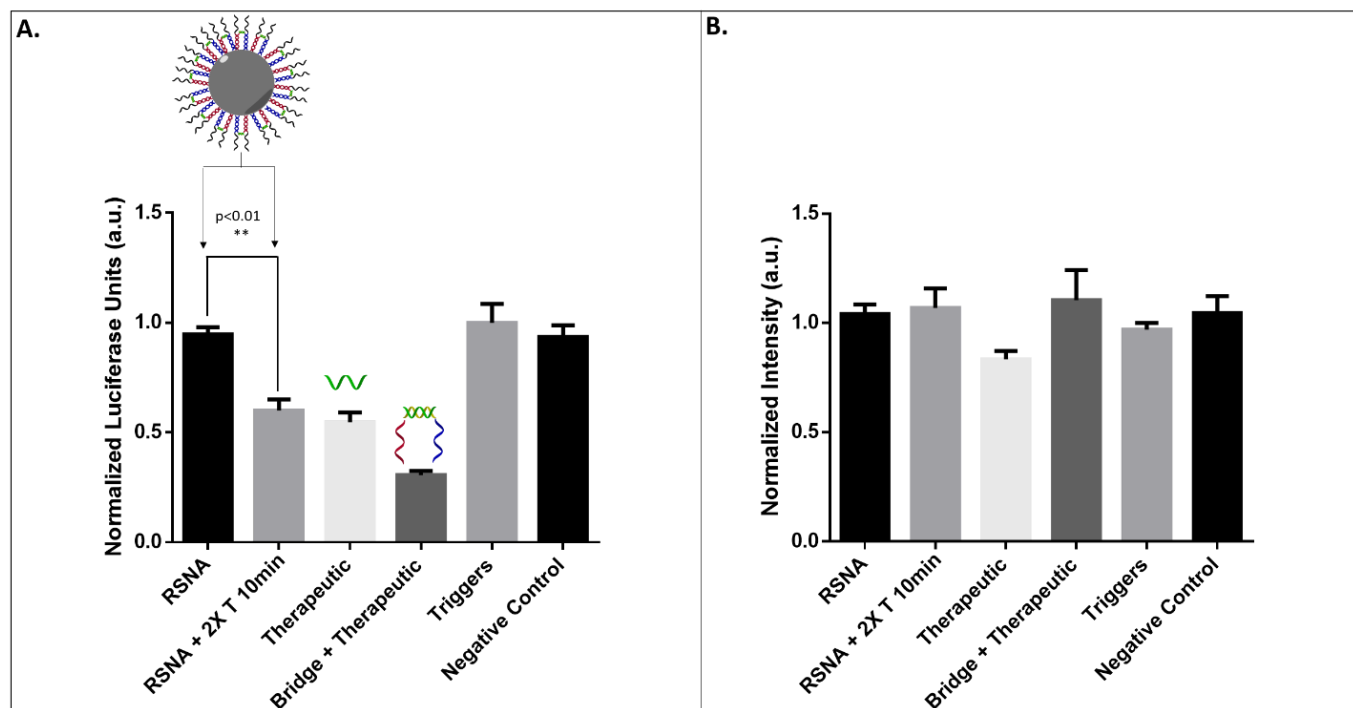


Figure 2. 6. A. Firefly Luciferase knockdown activity of different samples containing ASO. Firefly luciferase activity was measured after 24 hours incubation and normalized to MTT results and ASO-free control. **B.** MTT cell viability assay for cytotoxicity of samples, normalized to ASO-free control. Error bars are SD for triplets of each sample.

To highlight the importance of using the SNA, we performed the same experiment but on a control system that does not have the hydrophobic units and called it “monomeric SNA”. The results (**Figure 2. 7.**) show that there is no significant shielding of the activity of the ASO, indicating that the SNA’s geometric design allows for the improved shut-down of the activity of the cargo until released.

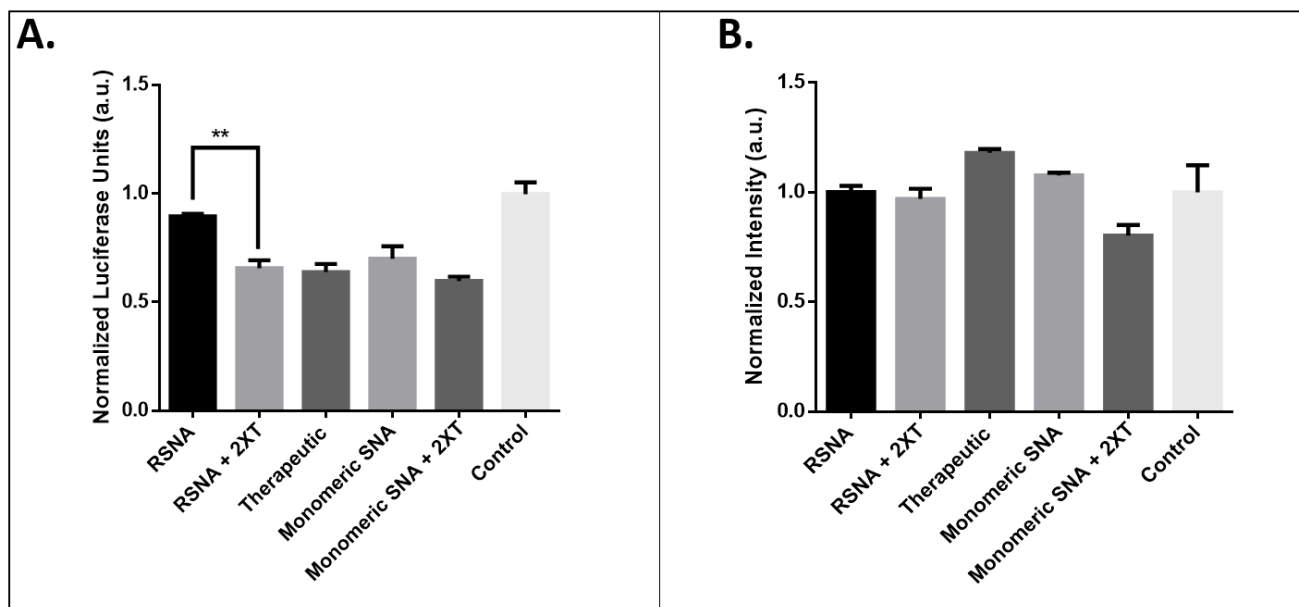


Figure 2. 7. Testing the importance of the SNA in shutting down the activity of the cargo until released compared to monomeric SNA. Monomeric SNA is the DNA portion of the fully loaded SNA but lacking the hydrophobic chains. A. shows the Firefly Luciferase knockdown and B. shows the MTT results.

2.4. Conclusion

We have shown the assembly of a stimuli-responsive spherical nucleic acid that conditionally and selectively delivers a nucleic acid therapeutic when a particular cytoplasmic genetic marker is present. The results showed that the RSNA-bound therapeutic was protected from nucleases in serum containing media. Moreover, its silencing activity was inhibited when bound and increased upon release. The release of the cargo requires two different triggering molecules and does not occur with a single stimulus, thus increasing the level of specificity in delivering therapeutics. The activity of the therapeutic was unhindered, as shown with an example of an antisense oligonucleotide against luciferase. Importantly, these complex functions were achieved from a simple, cost-effective three DNA strand design. This leads to a new class of responsive drug delivery vehicles that are stimuli-responsive, cheap, and have the power to co-deliver hydrophobic drugs and nucleic acid-based drugs. Future work on this project is testing the dual delivery

capabilities of the RSNA in vivo, as well as functionalizing the particle with targeting elements for a favored biodistribution.

An additional and important improvement to the system that we are currently working is to amplify the release of cargo from a recognition event. This is due to the relatively low abundance of miRNAs in target cells. Strategies involve using the hybridization chain reaction where one hybridization event can lead to multiple release events.⁴⁸ Other strategies include disassembly of the particle due to a specific stimulus.⁴⁹⁻

51

2.5. **Materials and methods**

Materials:

Detailed information on chemicals ordered and used are presented in the *Supporting Information*. Specific sequences of ssDNA were synthesized in-house using a Mermade MM6 synthesizer from Bioautomation (supporting information).

Assembly of SNA:

To assemble the SNA, strands were combined at 5 μM in Tris-Acetic acid - Magnesium_buffer (1xTAMg, SI) from 95 to 4 $^{\circ}\text{C}$ over 4 hours using Eppendorf Mastercycler 96-well thermocycler and Bio-Rad T100TM thermal cycler.

Dynamic Light Scattering (DLS):

SNAs size distribution was measured using a DynaProTM Instrument from Wyatt technology. Millipore water and 1xTAMg buffer were filtered using a 0.45 μm nylon syringe filter before use in DLS sample preparation. 15 μL of sample (concentration 5 μM) was used in each measurement. Measurements were performed at 25 $^{\circ}\text{C}$. Each measurement consisted of 20 acquisitions, with each acquisition lasting 10 seconds. Data was filtered to exclude acquisitions with a baseline above 1.01 and a SOS error above 150. A cumulants fit model was used to confirm the presence and determine the size the SNAs.

Fluorescence scans:

Samples were prepared at 5 μM and 25 μl and scanned in a 384-well plate. Cy3 was excited at 550 nm with a slit-width of 9 nm, and its emission was collected from 575 to 750 nm.

Gel Electrophoresis:

All agarose gels were 2.5% in 1xTAMg buffer. Samples were mixed with Glycerin and 1xTAMg buffer and then loaded in corresponding wells. Agarose gels were run at 95 V for 1 hour 45 mins, at 4 $^{\circ}\text{C}$, with typical sample loading is 20 pmoles with respect to DNA content, per lane (2 μL of 5 μM).

Atomic Force Microscopy:

Dry AFM was carried out using a MultiMode8™ SPM connected to a Nanoscope™ V controller (Bruker, Santa Barbara, CA). All images were obtained using ScanAsyst mode in air with AC160TS cantilevers (Nominal values: Tip radius – 9 nm, Resonant frequency – 300 kHz, Spring constant – 42 N/m) from Asylum Research. Samples were at 5 μM in TAMg buffer and 2.5-5 μL of this solution was deposited on a freshly cleaved mica surface (ca. 7 x 7 mm) and allowed to adsorb for 1-2 seconds. Then 50 μL of 0.22 μm filtered Millipore water was dropped on the surface and instantly removed with filter paper. The surface was then washed with a further 200 μL of water and the excess removed with a strong flow of nitrogen. Samples were dried under vacuum for at least 1 hour prior to imaging.

Serum Stability:

Samples (SNA or strands) were prepared in 1xTAMg buffer. SNA was prepared at 10 μM with 0.3 equivalents of bridge and therapeutic, and then diluted with cell culture media (DMEM, 10% FBS, 5% AB/AM) to a concentration of 2 μM . Samples were incubated at 37 $^{\circ}\text{C}$, and aliquots were taken at different timepoints and frozen until analysis. Aliquots were then loaded on a 15% denaturing gel to visualize the bridge and therapeutic strands for stability.

Cell Culture:

HeLa cells were maintained in 10% FBS and antibiotic/antimycotic (AB/AM) and cultured in 5% CO₂ at 37 °C. Typically, cells were split in 1 : 4 ratio every 3 days.

In vitro Silencing and Cytotoxicity Assays:

Luciferase knockdown assays were performed as described in Deleavey et al with a few modifications. Typically, HeLa cells were counted and seeded at a density of 10 000 cells per well in a 96-well plate. Cells were allowed to recover for 24 hours at 37 °C with 5% CO₂. Then, samples were added to the appropriate well in triplets where Lipofectamine reagent was used as transfection agent and control (Invitrogen). Cells were further incubated overnight (for a total of 24 hours post-DNA addition).

For luciferase assay, cells were washed with with PBS 1× and lysed with 25 µl Glo-lysis buffer (Promega) and 25 µl of Bright-Glo luciferase reagent (Promega, USA) was added to each well. Luminescence was measured using a Biotek Synergy HT plate reader. Data was acquired with the Gen5 software suite and data was manipulated and plotted using Graphpad Prism software suite.

For cytotoxicity and cell viability, the cells were incubated with the fluorescent reagent (CellTiter Blue) and further incubated for 1.5 h in 5% CO₂ at 37 °C. Subsequently, 96-well plates were allowed to equilibrate at room temperature and the fluorescence was measured at 590 nm (Ex. 530, Em. 590) using a BioTek Synergy HT micro-plate reader. All quantifications were done using GraphPad Prism 5 software.

Flow Cytometry:

HeLa cells were seeded at a density of 5×10^5 in a 6 well plate. After 24 hours, the cells were incubated with SNA at a final concentration of 1.5 µM. 1% of U2 strands were Cy3 labeled. After 4 hours of incubation, cells were detached, washed and resuspended in 1x PBS, followed by fixing with 4% paraformaldehyde. Samples were then processed using FACS FORTESSA. All measurements were performed in doublets.

Supporting Information. Additional experiments: design, materials, instrumentation details, and control experiments.

2.6. **Acknowledgement**

We thank the Natural Sciences and Engineering Research Council of Canada (NSERC), the Canadian Institutes for Health Research (CIHR), the Cancer Research Society, and the Canada Research Chairs Program for financial support. H.F.S. is a Cottrell Scholar of the Research Corporation. We would also like to thank Dr. Violeta Toader for help in the synthesis of the hydrophobic monomers.

2.7. **Supporting Information**

2.7.1. *General*

Tris(hydroxymethyl)aminomethane (Tris), ethylenediaminetetraacetate (EDTA), urea, 40% acrylamide/bis-acrylamide (19:1), ammonium persulfate (APS), N,N,N',N'-tetramethylethane-1,2 diamine (TEMED) and agarose were purchased from BioShop Canada Inc and used without further purification. Magnesium chloride hexahydrate and Nile Red were purchased from Sigma-Aldrich. Acetic acid, boric acid, ammonium hydroxide and 10x DPBS (with magnesium, calcium) were purchased from Fischer Scientific and used without further purification. GelRed™ nucleic acid stain was purchased from Biotium Inc. GeneRuler DNA Ladder Mix and DNA Gel Loading Dye (6X) were obtained from Thermo Scientific. 1 µmole 1000 Å universal synthesis CPG column, standard reagents used for automated DNA synthesis and Sephadex G25 (super fine DNA grade) were purchased from BioAutomation. DMT-1,12-dodecane-diol phosphoramidites were synthesized in the lab from 1,12-dodecane-diol (Alfa Aesar) and DMTCl (AK Scientific). 1x TBE buffer is composed of 90 mM Tris, 90 mM boric acid and 2 mM EDTA with a pH ~8.3. 1x TA buffer is composed of 45 mM Tris, 20 mM acetic acid and 7.6 mM Mg(Cl)₂, and its pH was adjusted to ~8.0 using glacial acetic acid. 1x DPBS (with magnesium and calcium) is composed of 8 mM

sodium phosphate dibasic, 138 mM of sodium chloride, 1.47mM of potassium phosphate monobasic, 2.6 mM potassium chloride, 0.5 mM magnesium chloride (anhydrous) and 0.9 mM calcium chloride (anhydrous).

Cyanine 3 (Cy3) phosphoramidite, Cyanine 5 (Cy5) phosphoramidite, 5'-fluorescein phosphoramidite, and Sulfurizing reagent II were purchased from GlenResearch.

Millipore water was used throughout any preparation of buffers.

Dulbecco's Modified Eagle Medium (DMEM) and phosphate-buffered saline (PBS) were purchased from Life Technologies. Lipofectamine reagent was purchased from Invitrogen. Fetal bovine serum (FBS), 0.05% Trypsin-EDTA and sodium pyruvate were obtained from Wisent Bioproducts. The Bright-Glo Luciferase Assay system was purchased from Promega. Cell-Titer Blue assay was also purchased from Promega. The HeLa X1/5 cells stably expressing luciferase are a generous gift from Dr. Pelletier (McGill).

2.7.2. *Instrumentation*

Standard oligonucleotide synthesis was performed on solid supports using a Mermade MM6 synthesizer from Bioautomation. UV absorbance DNA quantification measurements were performed with a NanoDrop Lite spectrophotometer from Thermo Scientific. For structure assembly, Eppendorf Mastercycler 96-well thermocycler and Bio-Rad T100TM thermal cycler were used to anneal all DNA nanoparticles. Polyacrylamide gel electrophoresis (PAGE) was performed using 20x20 cm vertical Hoefer 600 electrophoresis units, or a Bio-Rad Mini-PROTEAN® Tetra Vertical electrophoresis units. Agarose Gel Electrophoresis (AGE) were performed on Owl Mini and Owl EasyCast horizontal gel systems. Gels were imaged by BioRad ChemiDoc MP system.

Fluorescence data were measured by BioTek Synergy H4 Hybrid Multi-Mode Microplate Reader. Multimode 8 scanning probe microscope and Nanoscope V

controller (Bruker, Santa Barbara, CA) was used to acquire AFM images. Liquid Chromatography Electrospray Ionization Mass Spectrometry (LCESI-MS) was carried out using Dionex Ultimate 3000 coupled to a Bruker MaXis Impact™ QTOF. Dynamic light scattering (DLS) experiments were carried out using a DynaPro™ Instrument from Wyatt technology. Firefly Luciferase luminescence was measured using a Biotek Synergy HT plate reader. Cytotoxicity studies were performed using the CellTiter96 kit from Promega according to the manufacturer's instructions.

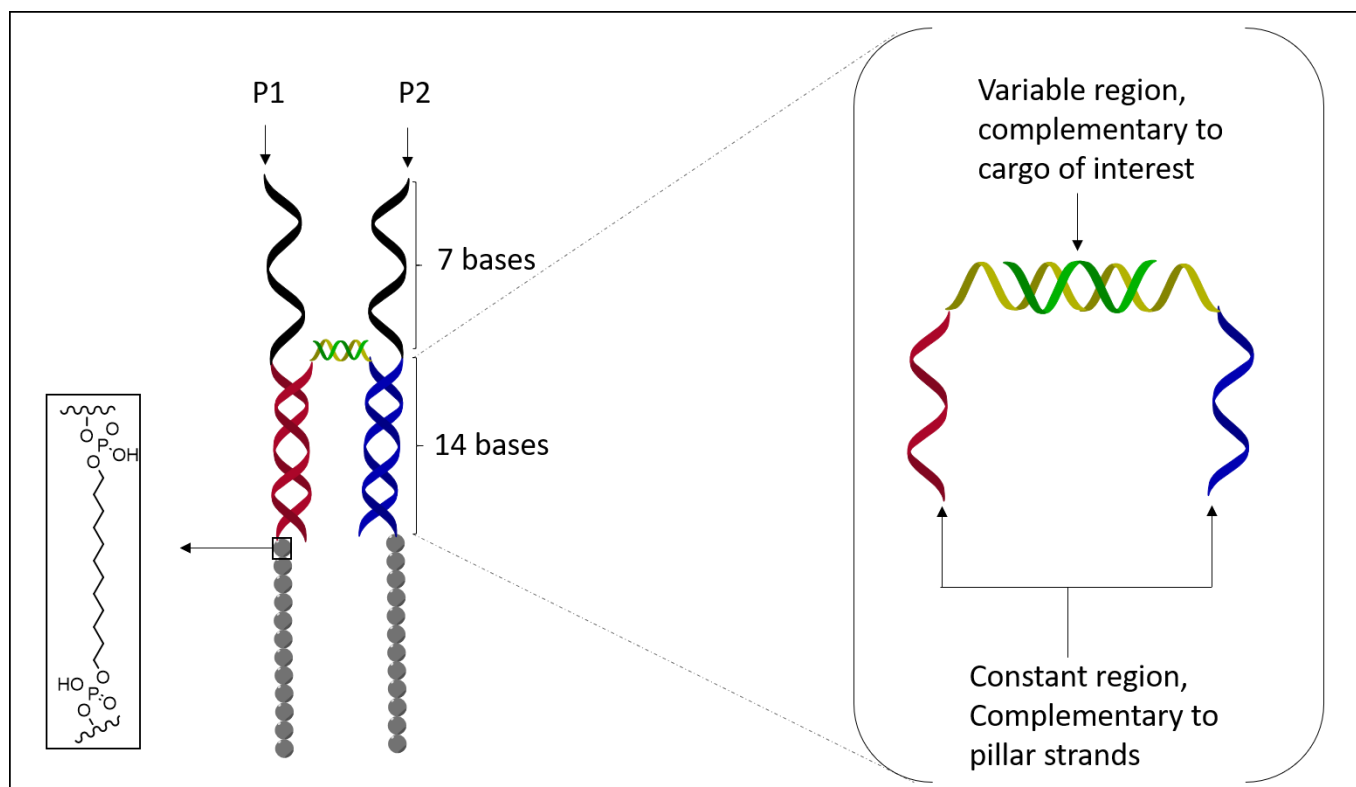
2.7.3. *Design and Synthesis*

Design:

A DNA-minimal and responsive spherical nucleic acid was designed to encapsulate nucleic acid therapeutics (NATs) (**Supplementary Figure 2. 1.**). The design comprises two main strands that are DNA amphiphiles. These strands are designated as the pillar strands, as they are the one responsible for the formation of the SNA. The hydrophobic part of the pillars is composed of twelve consecutive dodecane units, with phosphates between them. The DNA part was 21 bases long.

The NAT could be single or double stranded, just by removing or adding the cargo strand (yellow). The main component of the NAT is the bridge strand, where it has 2 sides that are complementary to the pillar strands (blue and red). This allows its placement on the SNA, via hybridization of 14 bases on each side. The rest of the bridge strand is variable, as it can be modified, extended, or shortened, to be complimentary to a cargo strand of interest. In this manuscript, the cargo strand was always 18 bases. The variable part of the bridge strand was tested at two different sizes: 22mer and 29mer long. The latter is to simulate the size of an siRNA as previously

reported by Bujold *et al.*²⁴, and the former is complementary to an 18mer antisense oligonucleotide with a 2T base spacer on each end.



Supplementary Figure 2. 1. design and sequencing of the RSNA. The bridge arms are complementary to the pillars with 14 bases (red and blue), leaving a 7-base toehold for strand displacement (black). The bridge strand's variable and constant regions are shown on the right.

Synthesis:

All solid-phase syntheses were performed on a 1 μ mol scale using universal 1000 Å LCAA-CPG solid-supports. Coupling efficiencies were monitored following removal of the dimethoxytrityl (DMT) 5'-OH protecting group. DBCO-dT-CE and DMT-dodecanediol phosphoramidites were dissolved in the appropriate solvents (anhydrous acetonitrile/dichloromethane 1:3 (v/v) and acetonitrile respectively) under a nitrogen atmosphere (<0.04 ppm for oxygen, and <0.5 ppm trace moisture) for a final concentration of 0.1M. The DMT-dodecane-diol was activated using 0.25M 5-

(ethylthio)tetrazole in anhydrous acetonitrile and an extended coupling time of 5 minutes was employed. 3% dichloroacetic acid in dichloromethane was used to remove the DMT protecting group on the DNA synthesizer. Sulfurization (including those containing DBCO) was executed prior to capping on the DNA synthesizer using Sulfurizing Reagent II (cat.# 40-4037, Glen Research). Following synthesis, strands were cleaved from the solid-support and deprotected using 28% aqueous ammonium hydroxide solution for 20 hours at 60°C. Strands were dried under vacuum at 60°C, resuspended in Millipore H₂O, then filtered with 0.22 μm centrifugal filters.

Strands were purified using polyacrylamide gel electrophoresis. Aqueous solution of oligomer was mixed with an equal volume of Urea prior to loading on gel in order to assist in denaturation. oligomers were run on either 18% or 15% polyacrylamide/8M urea gels in 1xTBE for 30 minutes at 250V, followed by 60 minutes at 500V. Following gel electrophoresis, bands were imaged using a handheld UV illuminator (254nm) and excised, crushed, and suspended in ~5-10 mL H₂O. This suspension was frozen by brief submersion in liquid nitrogen, before being incubated at 60°C for 16 hours. The supernatant was concentrated by evaporation, desalted using size exclusion

chromatography (Sephadex G-25), and quantified (OD260) using a NanoDrop Lite spectrophotometer from Thermo Scientific.

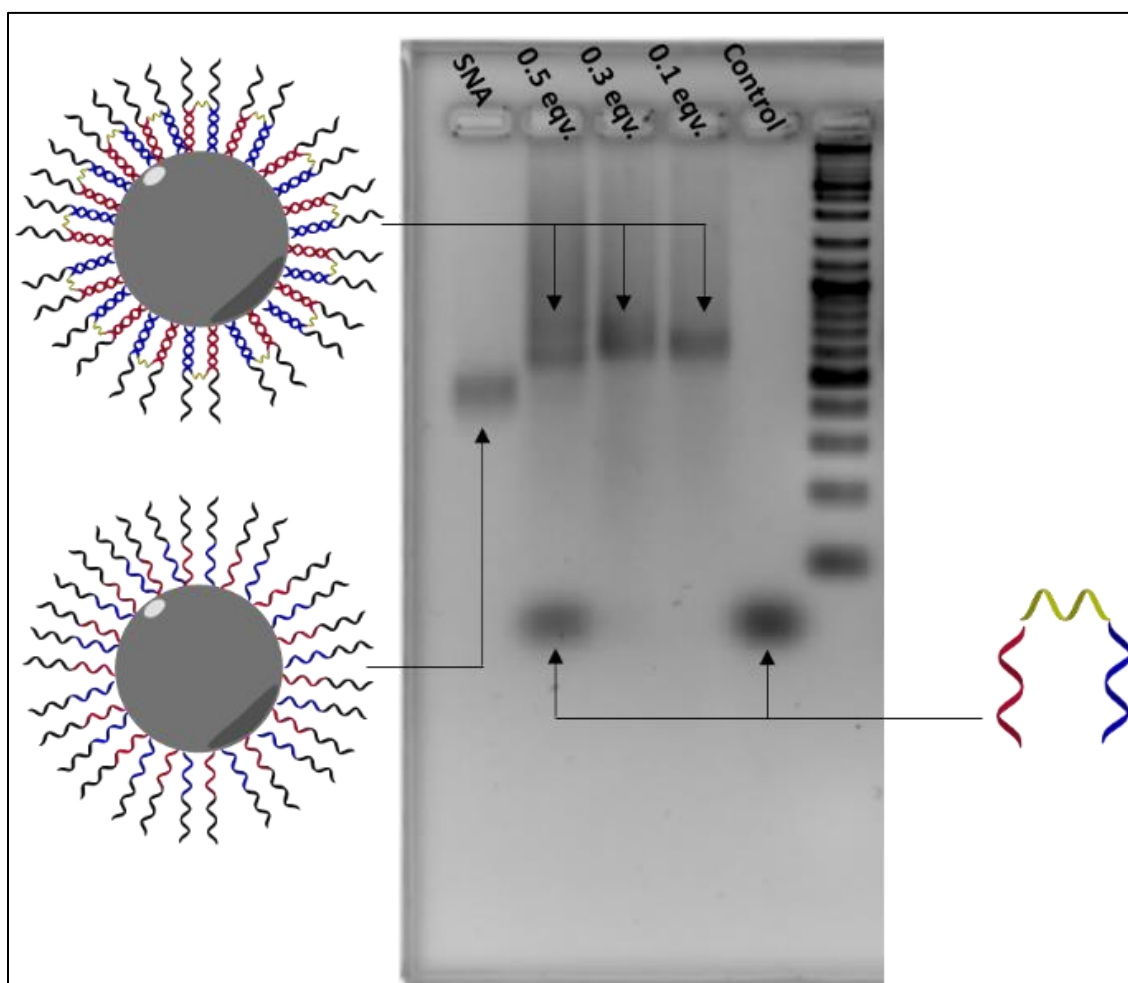
The below table contains all the strands synthesized along with their sequences.

Strand (n. of bases)	Sequence (5' to 3')	Description
U1 (21)	XXXXXXXXXXXXX TATGTTAAACCAAGACTACCG	Pillar 1
U2 (21)	TATCCACACCTATCCGTAATC XXXXXXXXXXXXX	Pillar 2
U2Cy3 (21)	TATCCACACCTATCCGTAATC -Cy3-XXXXXXXXXXXXX	Pillar 2 with Cy3
BridgeB (57)	GATTACGGATAGGTTAATGAATTGAAGAATTCAATTATTCTTGCTTGGTTTAACATA	Big bridge, which models an siRNA
bridgeB.cargo (18)	AATAATTGAATTCTCAA	complement to the big bridge that models an siRNA
Bridge (50)	GATTACGGATAGGTTTGGGATACGACAAGGATATTTCTTGGTTTAACATA	Bridge complementary to the NAT tested
NAT (18)	atatccttgcgatccc	Antisense oligonucleotide tested, against Luciferase
Trigger 1 (21)	CGGTAGTCTTGTTTAACATA	Trigger 1, complementary to P1
Trigger 2 (21)	GATTACGGATAGGTGTGGATA	Trigger 2, complementary to P2
Trigger 2 Cy5 (21)	Cy5-GATTACGGATAGGTGTGGATA	Trigger 2, complementary to P2
Negative control (18)	AATAATTGAATTCTCAA	Control strand in cell assays

Table 2. 1. Sequences of strands and polymers used, color-coded similarly to strands in figures. Complementary strands are of same color. (special amidites/nucleotides: X= dodecane-diol, lower case = phosphorothioated)

2.7.4. *SNA's loading capacity with bridge strand*

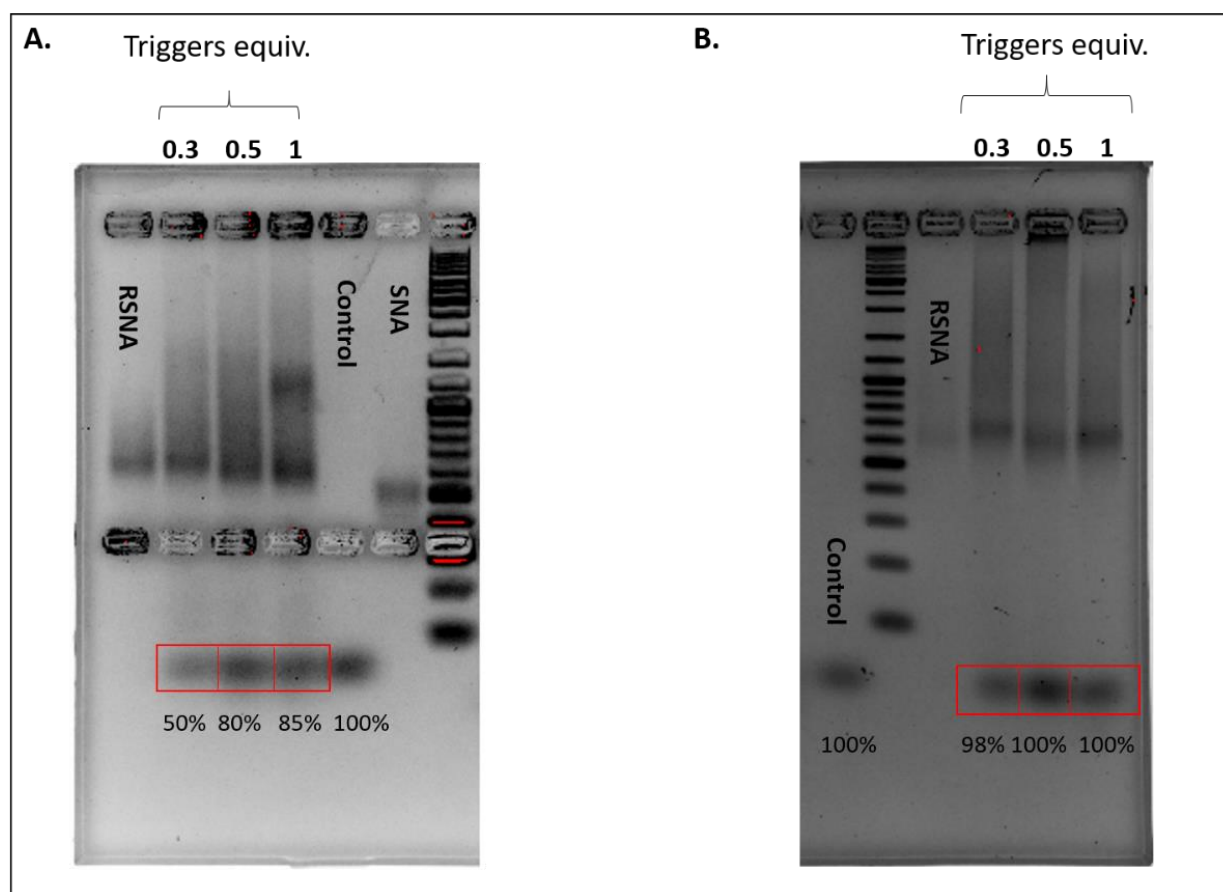
To test how much the SNA can load of the bridge strand on its corona, we titrated it with 3 molar equivalents: 0.5, 0.3, and 0.1 equivalence. We annealed the SNA with each equivalence from 95 to 4 °C for 4 hours and then loaded them on a 2.5% agarose gel (**Supplementary Figure 2. 2.**). The first showed a residual amount of the bridge strand not hybridized, indicating that we cannot load more than 0.5 molar equivalence. 0.3 didn't show any excess bridge strands, hence we decided to move forward with it in all the experiments.



Supplementary Figure 2. 2. Agarose gel showing mobility of SNA loaded with different equivalents of bridge strand. SNA assembled at 5 μ M. DNA ladder used is GeneRuler DNA Ladder Mix (100-10,000 bp/mass).

2.7.5. *SNA's loading capacity with bridge strand*

We wanted to quantify the amount of cargo released when we incubate with different equivalents of triggers, as well as the difference between few mins vs hours of incubation with triggers. So, we incubated RSNA loaded with 0.3 equivalents of bridge+cargo (NAT) with either 0.3, 0.5, or 1 equivalents of triggers. The equivalents are with respect to the pillar strands. Then, we either loaded them on a gel after a few mins of incubation, or after 1+ hours. The results (**Supplementary Figure 2. 3.**) show that within minutes, 0.3 equivalents were able to release approximately 50% of the encapsulated cargo. If left for longer, almost 100% is released. Quantification was done using the gel imager, by comparing the density of the bands with a control amount of cargo loaded on its own.



Supplementary Figure 2. 3. testing different equivalents of triggers at different timepoints. A. after 5-10 mins incubation. B. after 1-2 hours incubation. gels are 2.5% agarose. All SNAs were prepared at 5 μ M.. DNA ladder used is GeneRuler DNA Ladder Mix (100-10,000 bp/mass).

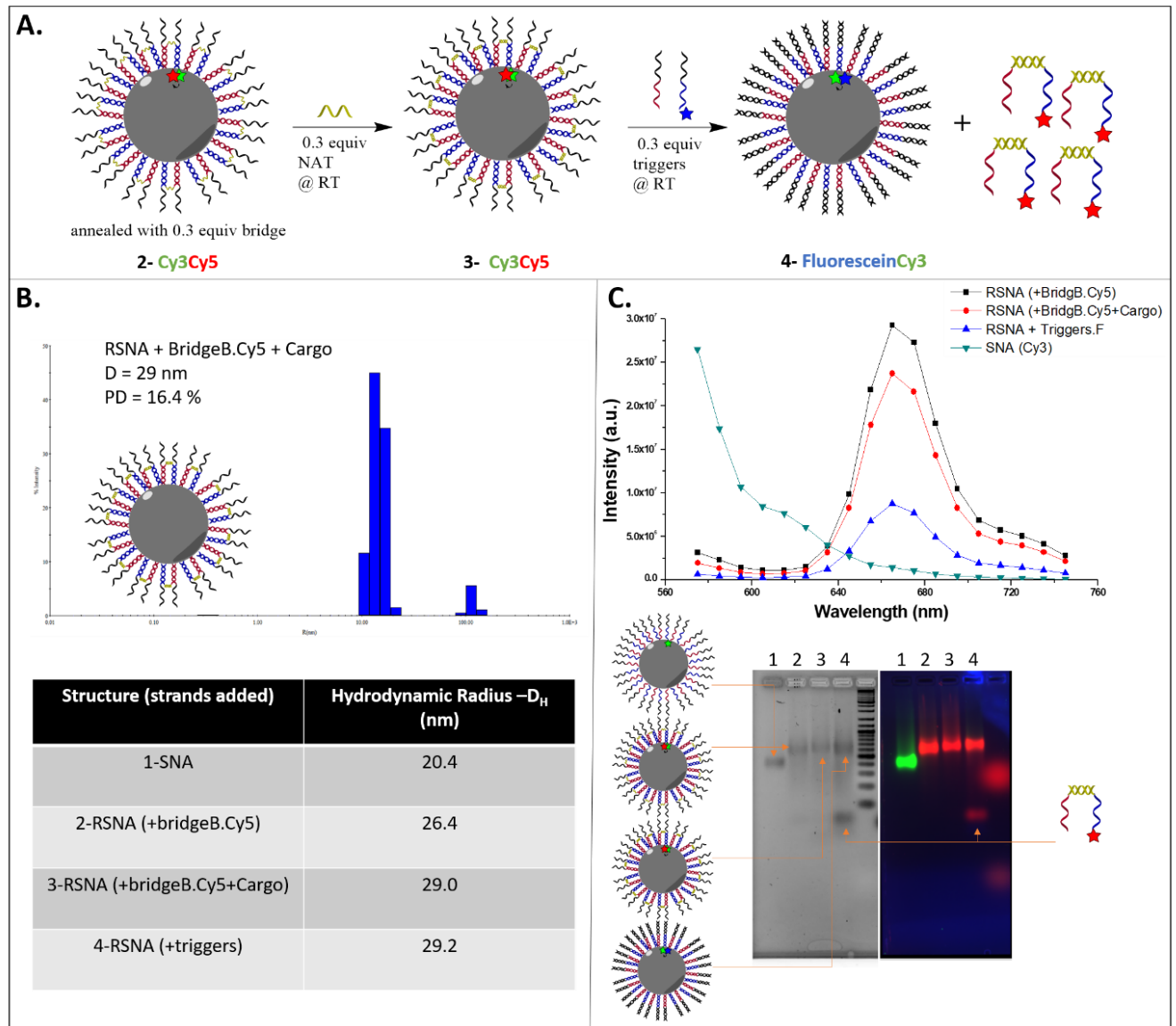
2.7.6. *Loading with a different-sized bridge*

To test that our design can fit a cargo as large as siRNA, we used a 57mer bridge strand (Bridge B). The top region is a 29mer that hybridizes to an 18mer model cargo strand, which simulates siRNA, with additional arms for loading on the pillars.²⁴ To monitor the loading and release, we used fluorescently labeled strands. The assembly of the structure was first confirmed with dynamic light scattering (DLS), where the final RSNA has a diameter of 29 nm (**Supplementary Figure 2. 4.**). The DLS data shows an increase in diameter upon addition of each of the bridge and cargo strands, suggesting hybridization of the corresponding strands to the SNA (**Supplementary Figure 2. 4.**).

Fluorescence measurements were then carried out on the different states of the SNA using Forster resonance energy transfer (FRET) analysis with strategic placement of two dyes. A Cy3 dye was placed on the interface between the hydrophobic moiety and the DNA part in one of the pillars. Then, the bridge strand was labeled with a Cy5 dye, such its hybridization brings the two dyes in close proximity and allows FRET to occur. One of the trigger strands was additionally labeled with fluorescein, to follow its successful binding. Fluorescence data shows that there is 92% FRET efficiency between Cy3 and Cy5 when the RSNA is assembled with the bridge and cargo strands (**Supplementary Figure 2. 4.**), where the Cy5 emission is significantly increased when exciting Cy3 (Excitation wavelength = 550 nm). After adding the triggers, a very large drop in Cy5 emission is observed, indicating the release of the Cy5-labeled Bridge and the disappearance of the FRET signal.

The samples were loaded on a 2.5% native agarose gel (**Supplementary Figure 2. 4.**), where the fully assembled RSNA appears as a single band. Upon addition of the bridge and the cargo, we can see a gradual decrease in mobility of the RSNA structures compared to the unloaded SNA, and a significant increase in Cy5 emission. When the trigger strands were added, release of the bridge+cargo strands were clearly observed as a faster moving band with Cy5 emission. The fluorescein signal on the triggers is not as visible, likely because of the smaller quantum yield of this dye, and only the

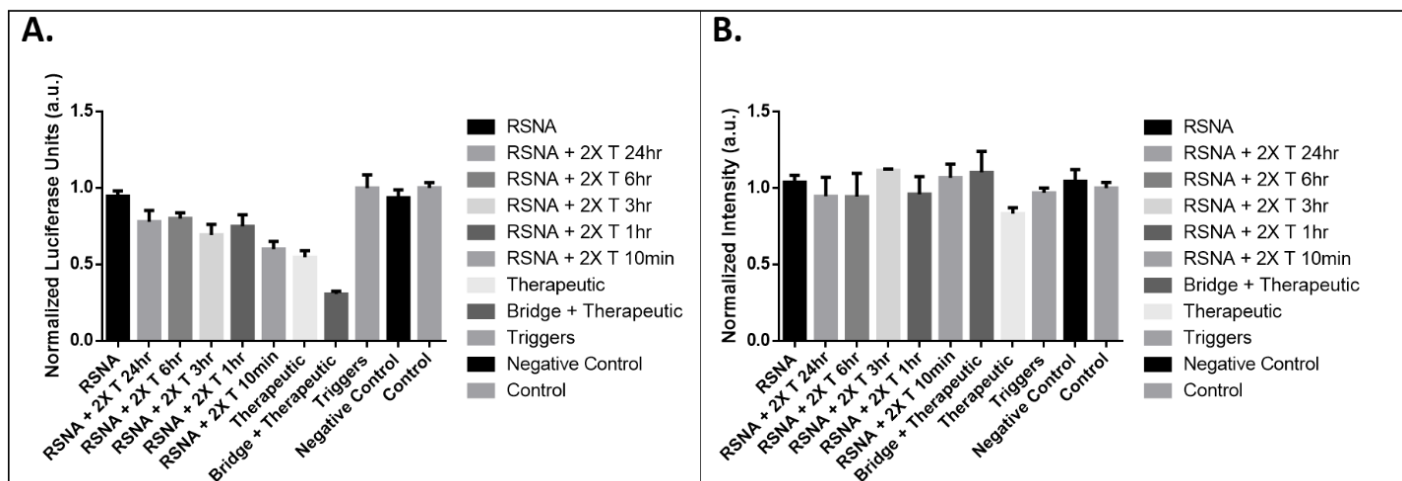
addition of 0.3 equivalence of the cargo and the erasers. The remaining Cy5 signal and minimal fluorescein signal is also likely due to partial cargo release and quenching of some of the fluorescein signal being quenched. The results show that we can for sure load different bridge sizes within the SNA, even one that simulates an siRNA cargo.



Supplementary Figure 2. 4. A. Scheme of the different states of SNA loaded with bridge **B.** Cy5 during characterization using DLS measurements, fluorescence/FRET measurements, and agarose gel electrophoresis. **C.** Samples prepared at 5 μ M SNA concentration, in 1xTA buffer. DNA ladder used is GeneRuler DNA Ladder Mix (100-10,000 bp/mass).

2.7.7. *Transfecting cells with trigger strands*

In order to release the cargo from the RSNA, we had to transfect the trigger strands into HeLa cells so they are available to react with the RSNA once it is inside the cell. We decided to transfect 2X the concentration of the micelle to make sure we have enough available for release. We tested different transfection times of the triggers before adding the RSNA to the cells. All cells were washed with PBS, and their media changed, after adding the triggers and before adding the RSNAs. The results below (**Supplementary Figure 2. 5.**) show that 10 min transfection time of the triggers gave the best silencing. This could be explained due to the stability of the triggers, as they are 21mer strands and unmodified. Leaving them longer makes them more susceptible to degradation.

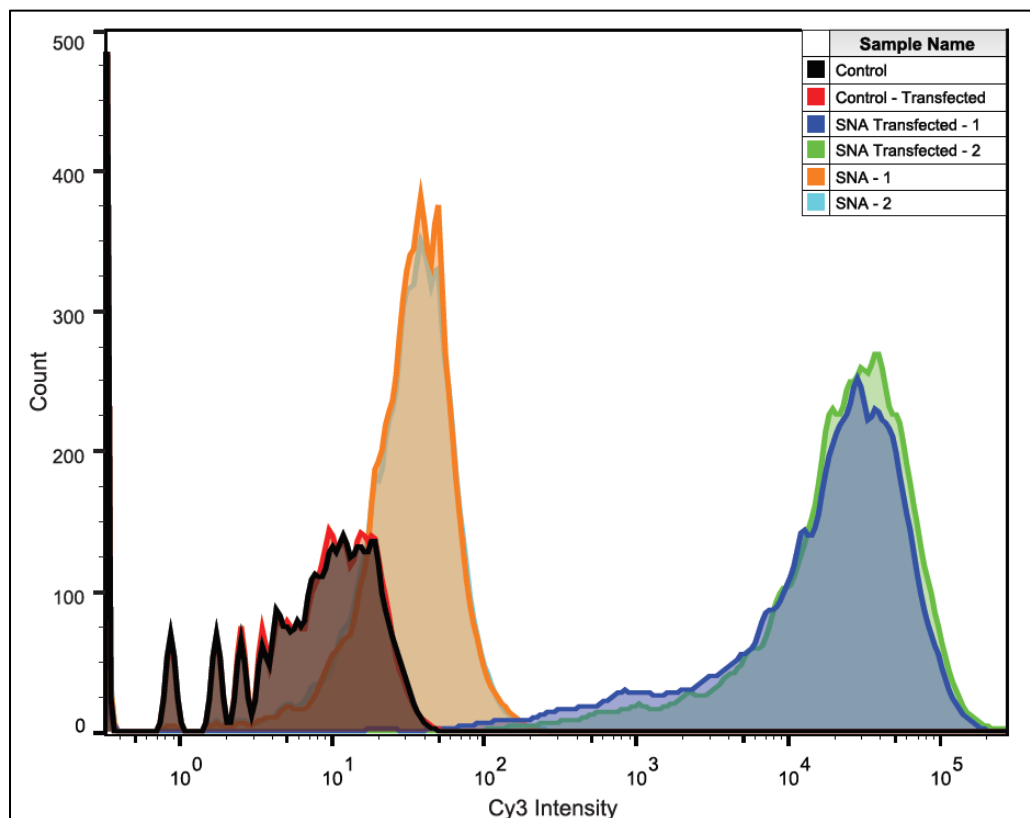


Supplementary Figure 2. 5. Testing the different transfection times of trigger strands (T) before adding the RSNA. **A.** Firefly Luciferase knockdown activity of different samples containing ASO. Firefly luciferase activity was measured after 24 hours incubation and normalized to **B.** MTT.

2.7.8. *Cellular uptake of SNA*

Based on our earlier results (flow cytometry and fluorescence microscopy), the SNAs can enter cells in their naked form and can deliver small molecule cargo without transfection.³⁰

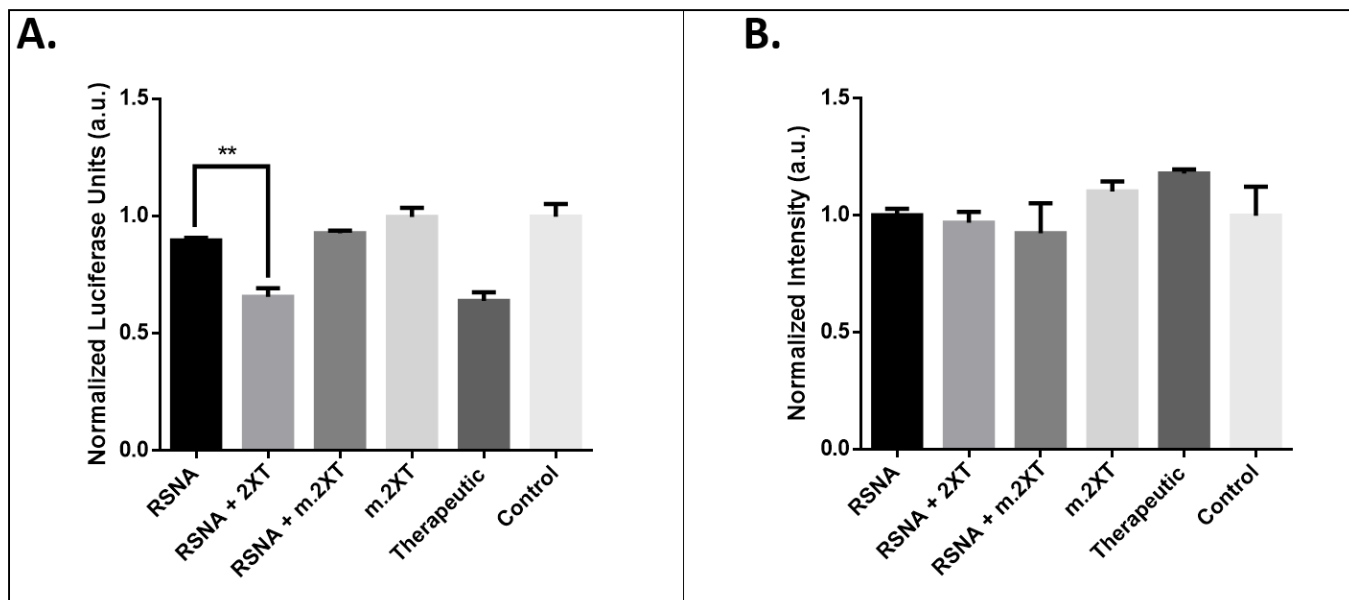
To reconfirm this, we conducted a new Flow Cytometry experiment (**Supplementary Figure 2. 6.**) to compare the cellular uptake of SNA with and without transfection. The experiment was conducted on HeLa cells after 4 hours of incubation, on Cy3-labelled SNA, where the Cy3-tag resides between the DNA and hydrophobic portion. In both cases, we saw cellular uptake, however it is significantly greater in the case of transfected SNA. Samples were done in duplicates.



Supplementary Figure 2. 6. Flow Cytometry histogram showing the uptake of naked vs transfected SNA in HeLa Cells after 4-hour incubation.

2.7.9. *Specificity of release and targeting*

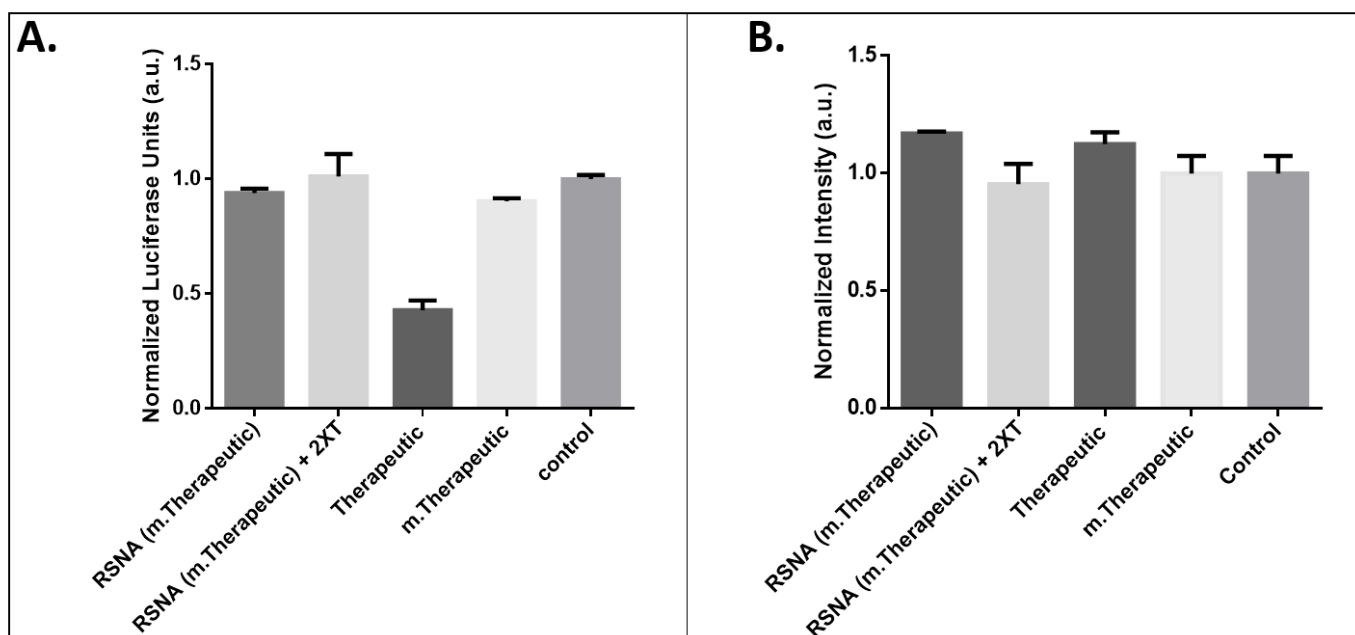
To test the specificity of the release, we pre-incubated the cells with two non-complementary triggers, and then added the SNA (**Supplementary Figure 2. 7.**). The result below show that these non-complementary triggers do not result in release and activation of the ASO strand, demonstrating the specificity of the system.



Supplementary Figure 2. 7. Testing the specificity of release of cargo from SNA in the presence of complementary (2XT) and noncomplementary (m 2XT) trigger strands using Firefly Luciferase knockdown assay. (A) Firefly luciferase activity was measured after 24 hours incubation and normalized to the MTT measurement (B).

Another specificity test that can be done is to use a non-complementary ASO to the target. We transfected an SNA carrying a scrambled 18mer (m.Therapeutic) as cargo

(**Supplementary Figure 2. 8.**). The results below show that indeed it has no silencing activity:



Supplementary Figure 2. 8. Testing the specificity of cargo using Firefly Luciferase knockdown assay. **A.** Firefly luciferase activity was measured after 24 hours incubation and normalized to the **B.** MTT measurement.

2.8. References

- 1 Opalinska, J. B. & Gewirtz, A. M. Nucleic-acid therapeutics: basic principles and recent applications. *Nat Rev Drug Discov* **1**, 503-514, doi:10.1038/nrd837 (2002).
- 2 Ganta, S., Devalapally, H., Shahiwala, A. & Amiji, M. A review of stimuli-responsive nanocarriers for drug and gene delivery. *Journal of Controlled Release* **126**, 187-204, doi:<https://doi.org/10.1016/j.jconrel.2007.12.017> (2008).
- 3 Tokatlian, T. & Segura, T. siRNA applications in nanomedicine. *Wiley Interdiscip Rev Nanomed Nanobiotechnol* **2**, 305-315, doi:10.1002/wnan.81 (2010).
- 4 Blanco, E., Shen, H. & Ferrari, M. Principles of nanoparticle design for overcoming biological barriers to drug delivery. *Nat Biotech* **33**, 941-951, doi:10.1038/nbt.3330 (2015).
- 5 Riley, M. & Vermerris, W. Recent Advances in Nanomaterials for Gene Delivery—A Review. *Nanomaterials* **7**, 94 (2017).
- 6 Tibbitt, M. W., Dahlman, J. E. & Langer, R. Emerging Frontiers in Drug Delivery. *Journal of the American Chemical Society* **138**, 704-717, doi:10.1021/jacs.5b09974 (2016).
- 7 Peer, D. *et al.* Nanocarriers as an emerging platform for cancer therapy. *Nat Nanotechnol* **2**, 751-760, doi:10.1038/nnano.2007.387 (2007).
- 8 Kumar, S., Anselmo, A. C., Banerjee, A., Zakrewsky, M. & Mitragotri, S. Shape and size-dependent immune response to antigen-carrying nanoparticles. *Journal of Controlled Release* **220, Part A**, 141-148, doi:<https://doi.org/10.1016/j.jconrel.2015.09.069> (2015).
- 9 Sun, W. & Gu, Z. Engineering DNA scaffolds for delivery of anticancer therapeutics. *Biomaterials Science* **3**, 1018-1024, doi:10.1039/C4BM00459K (2015).
- 10 Albanese, A., Tang, P. S. & Chan, W. C. The effect of nanoparticle size, shape, and surface chemistry on biological systems. *Annu Rev Biomed Eng* **14**, 1-16, doi:10.1146/annurev-bioeng-071811-150124 (2012).
- 11 Ediriwickrema, A. & Saltzman, W. M. Nanotherapy for Cancer: Targeting and Multifunctionality in the Future of Cancer Therapies. *ACS Biomaterials Science & Engineering* **1**, 64-78, doi:10.1021/ab500084g (2015).
- 12 Seeman, N. C. & Sleiman, H. F. DNA nanotechnology. *Nature Reviews Materials* **3**, 17068, doi:10.1038/natrevmats.2017.68 (2017).
- 13 Hu, Q., Li, H., Wang, L., Gu, H. & Fan, C. DNA Nanotechnology-Enabled Drug Delivery Systems. *Chemical Reviews*, doi:10.1021/acs.chemrev.7b00663 (2018).
- 14 Douglas, S. M., Bachelet, I. & Church, G. M. A logic-gated nanorobot for targeted transport of molecular payloads. *Science* **335**, 831-834, doi:10.1126/science.1214081 (2012).
- 15 Li, S. *et al.* A DNA nanorobot functions as a cancer therapeutic in response to a molecular trigger in vivo. *Nature Biotechnology* **36**, 258, doi:10.1038/nbt.4071

<https://www.nature.com/articles/nbt.4071#supplementary-information> (2018).

- 16 Li, J. *et al.* Self-assembly of DNA Nanohydrogels with Controllable Size and Stimuli-Responsive Property for Targeted Gene Regulation Therapy. *Journal of the American Chemical Society* **137**, 1412-1415, doi:10.1021/ja512293f (2015).
- 17 Kim, S. H. *et al.* Reversible Regulation of Enzyme Activity by pH-Responsive Encapsulation in DNA Nanocages. *ACS Nano* **11**, 9352-9359, doi:10.1021/acsnano.7b04766 (2017).
- 18 Chang, M., Yang, C. S. & Huang, D. M. Aptamer-conjugated DNA icosahedral nanoparticles as a carrier of doxorubicin for cancer therapy. *ACS Nano* **5**, 6156-6163, doi:10.1021/nn200693a (2011).
- 19 Zhu, G. *et al.* Self-assembled, aptamer-tethered DNA nanotrains for targeted transport of molecular drugs in cancer theranostics. *Proc Natl Acad Sci U S A* **110**, 7998-8003, doi:10.1073/pnas.1220817110 (2013).
- 20 Banerjee, A. *et al.* Controlled Release of Encapsulated Cargo from a DNA Icosahedron using a Chemical Trigger. **125**, 6992-6995, doi:doi:10.1002/ange.201302759 (2013).
- 21 Goodman, R. P. *et al.* Reconfigurable, braced, three-dimensional DNA nanostructures. *Nature Nanotechnology* **3**, 93, doi:10.1038/nnano.2008.3
<https://www.nature.com/articles/nnano.2008.3#supplementary-information> (2008).
- 22 Juul, S. *et al.* Temperature-controlled encapsulation and release of an active enzyme in the cavity of a self-assembled DNA nanocage. *ACS Nano* **7**, 9724-9734, doi:10.1021/nn4030543 (2013).
- 23 Bujold, K. E. *et al.* Sequence-responsive unzipping DNA cubes with tunable cellular uptake profiles. *Chemical Science* **5**, 2449-2455, doi:10.1039/C4SC00646A (2014).
- 24 Bujold, K. E., Hsu, J. C. C. & Sleiman, H. F. Optimized DNA “Nanosuitcases” for Encapsulation and Conditional Release of siRNA. *Journal of the American Chemical Society* **138**, 14030-14038, doi:10.1021/jacs.6b08369 (2016).
- 25 Kudgus, R. A. *et al.* Tuning Pharmacokinetics and Biodistribution of a Targeted Drug Delivery System Through Incorporation of a Passive Targeting Component. *Scientific Reports* **4**, 5669, doi:10.1038/srep05669 (2014).
- 26 Wang, J., Sui, M. & Fan, W. Nanoparticles for tumor targeted therapies and their pharmacokinetics. *Current drug metabolism* **11**, 129-141, doi:10.2174/138920010791110827 (2010).
- 27 Jhaveri, A. M. & Torchilin, V. P. Multifunctional polymeric micelles for delivery of drugs and siRNA. *Front Pharmacol* **5**, 77, doi:10.3389/fphar.2014.00077 (2014).
- 28 Zhao, Z., Du, T., Liang, F. & Liu, S. Amphiphilic DNA Organic Hybrids: Functional Materials in Nanoscience and Potential Application in Biomedicine. *International Journal of Molecular Sciences* **19**, 2283 (2018).
- 29 Li, H. *et al.* Molecular spherical nucleic acids. **115**, 4340-4344, doi:10.1073/pnas.1801836115 %J Proceedings of the National Academy of Sciences (2018).

- 30 Bousmail, D. *et al.* Precision spherical nucleic acids for delivery of anticancer drugs. *Chemical Science* **8**, 6218-6229, doi:10.1039/C7SC01619K (2017).
- 31 Edwardson, T. G. W., Carneiro, K. M. M., Serpell, C. J. & Sleiman, H. F. An Efficient and Modular Route to Sequence-Defined Polymers Appended to DNA. *Angewandte Chemie International Edition* **53**, 4567-4571, doi:10.1002/anie.201310937 (2014).
- 32 de Rochambeau, D. *et al.* “DNA–Teflon” sequence-controlled polymers. *Polymer Chemistry* **7**, 4998-5003, doi:10.1039/C6PY00532B (2016).
- 33 de Rochambeau, D., Sun, Y., Barlog, M., Bazzi, H. S. & Sleiman, H. F. Modular Strategy To Expand the Chemical Diversity of DNA and Sequence-Controlled Polymers. *The Journal of Organic Chemistry* **83**, 9774-9786, doi:10.1021/acs.joc.8b01184 (2018).
- 34 Dore, M. D., Fakhoury, J. J., Lacroix, A. & Sleiman, H. F. Templated synthesis of spherical RNA nanoparticles with gene silencing activity. *Chemical Communications*, doi:10.1039/C8CC06994H (2018).
- 35 Rothemund, P. W. Folding DNA to create nanoscale shapes and patterns. *Nature* **440**, 297-302, doi:10.1038/nature04586 (2006).
- 36 Shi, J., Kantoff, P. W., Wooster, R. & Farokhzad, O. C. Cancer nanomedicine: progress, challenges and opportunities. *Nat Rev Cancer* **17**, 20-37, doi:10.1038/nrc.2016.108 (2017).
- 37 Du, F.-S., Wang, Y., Zhang, R. & Li, Z.-C. Intelligent nucleic acid delivery systems based on stimuli-responsive polymers. *Soft Matter* **6**, 835-848, doi:10.1039/B915020J (2010).
- 38 Karimi, M. *et al.* Smart micro/nanoparticles in stimulus-responsive drug/gene delivery systems. *Chem Soc Rev* **45**, 1457-1501, doi:10.1039/c5cs00798d (2016).
- 39 Zhang, D. Y. & Seelig, G. Dynamic DNA nanotechnology using strand-displacement reactions. *Nature Chemistry* **3**, 103, doi:10.1038/nchem.957 (2011).
- 40 Mura, S., Nicolas, J. & Couvreur, P. Stimuli-responsive nanocarriers for drug delivery. *Nature materials* **12**, 991-1003, doi:10.1038/nmat3776 (2013).
- 41 Stenvang, J., Petri, A., Lindow, M., Obad, S. & Kauppinen, S. Inhibition of microRNA function by anti-miR oligonucleotides. *Silence* **3**, 1, doi:10.1186/1758-907x-3-1 (2012).
- 42 Li, Z. & Rana, T. M. Therapeutic targeting of microRNAs: current status and future challenges. *Nat Rev Drug Discov* **13**, 622-638, doi:10.1038/nrd4359 (2014).
- 43 Conway, J. W., McLaughlin, C. K., Castor, K. J. & Sleiman, H. DNA nanostructure serum stability: greater than the sum of its parts. *Chem Commun (Camb)* **49**, 1172-1174, doi:10.1039/c2cc37556g (2013).
- 44 Hahn, J., Wickham, S. F., Shih, W. M. & Perrault, S. D. Addressing the instability of DNA nanostructures in tissue culture. *ACS Nano* **8**, 8765-8775, doi:10.1021/nn503513p (2014).
- 45 Fakhoury, J. J. *et al.* Antisense precision polymer micelles require less poly(ethylenimine) for efficient gene knockdown. *Nanoscale* **7**, 20625-20634, doi:10.1039/C5NR05157F (2015).
- 46 Li, J. *et al.* Engineering a customized nanodrug delivery system at the cellular level for targeted cancer therapy. **61**, 497-504, doi:10.1007/s11426-017-9176-3 (2018).

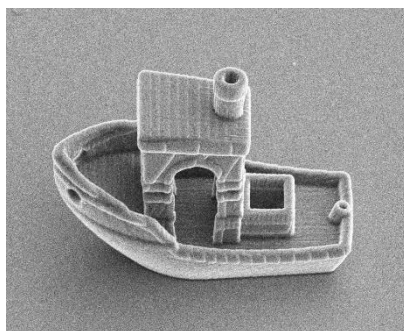
- 47 Chang, Y. T. *et al.* Near-infrared light-responsive intracellular drug and siRNA release using au nanoensembles with oligonucleotide-capped silica shell. *Advanced materials (Deerfield Beach, Fla.)* **24**, 3309-3314, doi:10.1002/adma.201200785 (2012).
- 48 Dong, J., Cui, X., Deng, Y. & Tang, Z. Amplified detection of nucleic acid by G-quadruplex based hybridization chain reaction. *Biosensors and Bioelectronics* **38**, 258-263, doi:<https://doi.org/10.1016/j.bios.2012.05.042> (2012).
- 49 Sigg, S. J., Postupalenko, V., Duskey, J. T., Palivan, C. G. & Meier, W. Stimuli-Responsive Codelivery of Oligonucleotides and Drugs by Self-Assembled Peptide Nanoparticles. *Biomacromolecules* **17**, 935-945, doi:10.1021/acs.biomac.5b01614 (2016).
- 50 Nagamine, K., Hase, T. & Notomi, T. Accelerated reaction by loop-mediated isothermal amplification using loop primers. *Molecular and Cellular Probes* **16**, 223-229, doi:<https://doi.org/10.1006/mcpr.2002.0415> (2002).
- 51 Notomi, T. *et al.* Loop-mediated isothermal amplification of DNA. *Nucleic Acids Research* **28**, e63-e63, doi:10.1093/nar/28.12.e63 (2000).

Preface 2

We demonstrated in chapter 2 the ability of SNAs to deliver nucleic acid therapeutics to cells efficiently with a stimuli-responsive behaviour. However, the stability of the unmodified SNAs was modest (6 hours in serum conditions), and the silencing activity of the phosphorothioate-modified therapeutic ASO was only 50%. In chapter 3, we focus on improving the stability of the SNAs and boosting the silencing efficacy of the therapeutic it carries. To do that, we aim at interfacing the chemical modifications strategy with drug delivery systems. Specifically, we develop and study chemically modified SNAs by incorporating 2'-Fluoroarabinose nucleotides (FANA) into the therapeutic ASO corona, termed FANA-SNAs.

SNAs and many other nucleic acid-based particles developed do not incorporate chemical modifications into their design and building blocks beyond the simple phosphorothioate backbone modification. Yet, the field is immensely developed and have yielded many modifications that improve on the efficacy of NATS. If these particles are to be utilized for the delivery of NATs, incorporating chemical modifications is crucial and advantageous. FANA modification is one attractive example, where FANA-modified NATs have been shown to have enhanced biological stability, increased binding affinity towards their target, and increased silencing efficacy due to its catalytic activity in breaking down its mRNA target by going through the RNase-H mechanism.

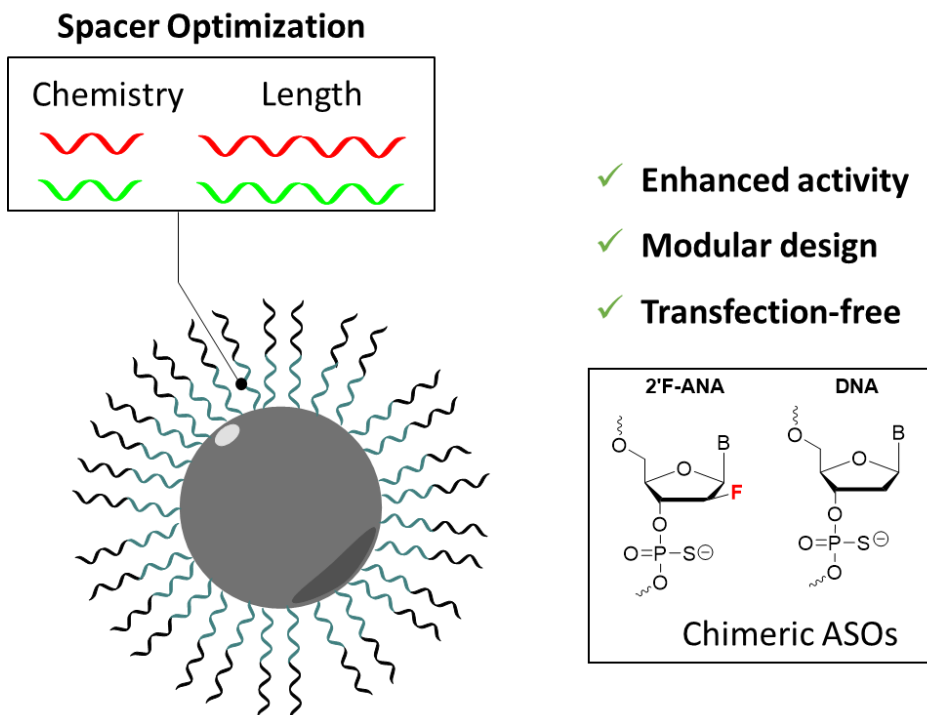
In this chapter, we characterize and explore the design parameters and therapeutic activity of FANA-SNAs. We show the importance of having a cleavable spacer for maximal activity, the modularity of SNAs by targeting various genes, and the enhanced activity of these particles without the use of transfection agents. This chapter highlights the advantage of bridging the two fields of drug delivery systems and chemical modifications in the context of SNAs, where better silencing, stability and delivery was achieved.



“Self-propelling, micrometer-sized boat” By R.P. Doherty et al./Soft Matter

“Strive not to be a success, but rather to be of value”

3 | Design and Enhanced Gene Silencing Activity of Spherical 2'-Fluoroarabinose Nucleic Acids (FANA-SNAs)



This chapter is adapted from the published manuscript titled “Design and Enhanced Gene Silencing Activity of Spherical 2'-Fluoroarabinose Nucleic Acids (FANA-SNAs)” by Hassan H. Fakh, Adam Katolik, Elise Malek-Adamian, Johans Fakhoury, Sepideh Kaviani, Masad J Damha and Hanadi F. Sleiman, *Chemical Science.*, 2021,12, 2993-3003.

Contribution of authors

Hassan H. Fakh helped design the project and primarily contributed to production of experimental data from synthesis, purification, characterization, analysis, and *in vitro* experiments. **Adam Katolik and Elise Malek-Adamian** synthesized the FANA-modified strands and provided them to **Hassan** who continued the synthesis. **Johans J. Fakhoury** provided feedback and co-initiated with **Hanadi F. Sleiman**, the collaboration with **Masad J. Damha**. **Sepideh Kaviani** helped with AFM imaging for revision of the manuscript following acceptance. **Hanadi F. Sleiman and Masad J. Damha** co-designed the project with **Hassan H. Fakh**, guided interpretation of data and discussion of experiments. **Hassan H. Fakh, Masad J. Damha and Hanadi F. Sleiman** co-wrote the manuscript.

3.1. Abstract

Drug delivery vectors for nucleic acid therapeutics (NATs) face significant barriers for translation into the clinic. Spherical nucleic acids (SNAs) - nanoparticles with an exterior shell made up of DNA strands and a hydrophobic interior- have recently shown great potential as vehicles to improve the biodistribution and efficacy of NATs. To date, SNA design has not taken advantage of the powerful chemical modifications available to NATs. Here, we modify SNAs with 2'-deoxy-2'-fluoro-D-arabinonucleic acid (FANA-SNA), and show increased stability, enhanced gene silencing potency and unaided uptake (gymnosis) as compared to free FANA. By varying the spacer region between the nucleic acid strand and the attached hydrophobic polymer, we show that a cleavable DNA based spacer is essential for maximum activity. This design feature will be important when implementing functionalized nucleic acids into nanostructures for gene silencing. The modularity of the FANA-SNA was demonstrated by silencing two different targets. Transfection-free delivery was superior for the modified SNA compared to the free FANA oligonucleotide

3.2. Introduction

Nucleic acid therapeutics (NATs), such as small interfering RNA (siRNA) and antisense oligonucleotides (ASOs) offer unique potential as therapeutics, because they can selectively and efficiently silence genes involved in disease¹⁻³. An essential strategy for translating NATs to the clinic has been the chemical modification of their natural DNA or RNA backbone. This improves their stability in biological media and augments their therapeutic efficacy^{4,5}. One salient sugar-modified DNA analogue is 2'-deoxy-2'-fluoro- β -D-arabinonucleic acid (FANA), which is compatible with both ASO and siRNA modalities⁴⁻⁹. The FANA modification increases hydrolytic and nuclease stability¹⁰ and decreases immune side-effects and toxicity^{5,9-11}. Importantly, it increases both binding affinity to the target mRNA and recruitment of RNase-H for its destruction, thereby improving the silencing mechanism^{4-6,8-11}. In addition, carrier-free cellular internalization (gymnosis) of FANA oligonucleotides permits the sequence-specific silencing of multiple

targets in many cell types, both at the protein and mRNA level, at concentrations in the low micromolar range¹²⁻¹⁶.

While chemical modifications of nucleic acid therapeutics have radically improved their stability and activity, there are still critical issues that need to be addressed, including biodistribution, pharmacokinetics and extra-hepatic delivery^{1-3,17,18}. NATs are rapidly cleared by the kidneys and those left in circulation accumulate in the liver^{4,19}. While this is useful for hepatic diseases, other diseases require biodistribution to critical organs such as brain, muscle, heart, tumour, etc. all of which still present significant challenges for nucleic acid therapies.

Nano-sized drug delivery systems have emerged as promising technologies to guide NATs to targets beyond the liver^{4,19-22}. Nanoparticles such as liposomes, gold nanoparticles, viral delivery systems and polymers^{17,23-25} can encapsulate various drugs including combination therapies, and incorporate targeting ligands that allow them to specifically bind to disease cells^{17,23,24}. Spherical nucleic acids (SNAs) are promising nanocarriers for nucleic acid therapeutics^{22,26}. They consist of a nanoparticle core, which can be liposomal, metallic, or polymeric, and a dense nucleic acid corona. This 3D structure has unique biological and physiological properties. SNAs have higher affinity to their nucleic acid target, are less susceptible to nucleases, can be taken up by many cell lines, and are less toxic and immunogenic^{22,26}. In some cases, they have favourable biodistribution beyond the liver in vivo (brain, skin, etc.)^{22,27,28}.

One of our laboratories has developed a new class of spherical nucleic acids assembled from monodisperse, sequence-controlled polymers. They are created by adapting DNA solid-phase automated synthesis whereby monomer units are attached in a sequence-controlled fashion to a growing oligonucleotide chain²⁹ via phosphoramidite chemistry. This modular control allows the synthesis of amphiphilic oligonucleotide polymers that self-assemble into a variety of nanostructures such as fibres and sheets³⁰, hydrophobic DNA cubes³¹⁻³³, and SNAs³⁴⁻³⁷. In particular, conjugating twelve units of dodecane (punctuated with phosphates) to DNA or RNA gives amphiphiles that spontaneously form monodisperse SNAs in aqueous media, with a hydrophobic core and a

nucleic acid corona³⁵⁻³⁷. These SNAs can encapsulate small molecule drugs and are stable in biological media. They are readily taken up into cells and have a favourable biodistribution profile in mouse models³⁵⁻³⁷. They also show higher activity (2-3-fold), requiring less transfection agents compared to linear nucleic acids³⁴, and they can be designed to release cargo in the presence of specific biomolecules³⁷. Furthermore, these SNAs are assembled from a single component in comparison to other nucleic acid based structures such as origami³⁸, making them DNA-minimal and favourable in terms of large-scale production and translation into clinical applications^{19,39}. In comparison to other SNAs, our sequence-controlled polymeric SNAs are made from biocompatible, biodegradable materials, can encapsulate small molecule drugs and allow for near infinite variation in polymer chemistry and sequence in an automated fashion⁴⁰. This gives them distinct advantages in biocompatibility and ease of synthesis, as well as control of size, shape, and function²⁹.

Despite these benefits, our SNAs and most other SNAs reported in literature lack chemical modifications to the nucleic acids beyond a simple phosphorothioate backbone^{27,28,41-48}. We reasoned that combining SNAs with the powerful nucleic acid chemical modifications that have enabled clinical applications will provide NATs with improved biodistribution and gene silencing activity. However, the design rules that ensure optimal activity while maintaining the SNA morphology are not clear.

In this work, we prepared FANA spherical nucleic acids (FANA-SNA) by covalent attachment a FANA ASO to twelve [dodecanediol phosphate] units (**Figure 3. 1**). The FANA ASO consists of 5-nt FANA “wings” flanking 8-nt DNA “gap” in the middle of the sequence. This architecture was shown to have low nanomolar silencing activity⁹. In aqueous media this construct spontaneously assembles into a SNA micelle. We found that a cleavable spacer between the FANA strand and the hydrophobic polymer modification is essential for reaching full activity of the SNA. Furthermore, carrier-free cellular internalization of FANA-SNAs resulted in superior gene silencing activity relative to the free (unconjugated) FANA ASO. The modularity of our FANA-SNAs was demonstrated by successfully silencing three different cellular targets. Thus, the combination of ASO modification and a cleavable linker are required for optimal activity. Combined with

SNA's stability, low polydispersity, ability to deliver small molecule drugs, improved biodistribution and design simplicity, we anticipate that FANA-SNAs will be powerful gene silencing tools with enhanced therapeutic potential.

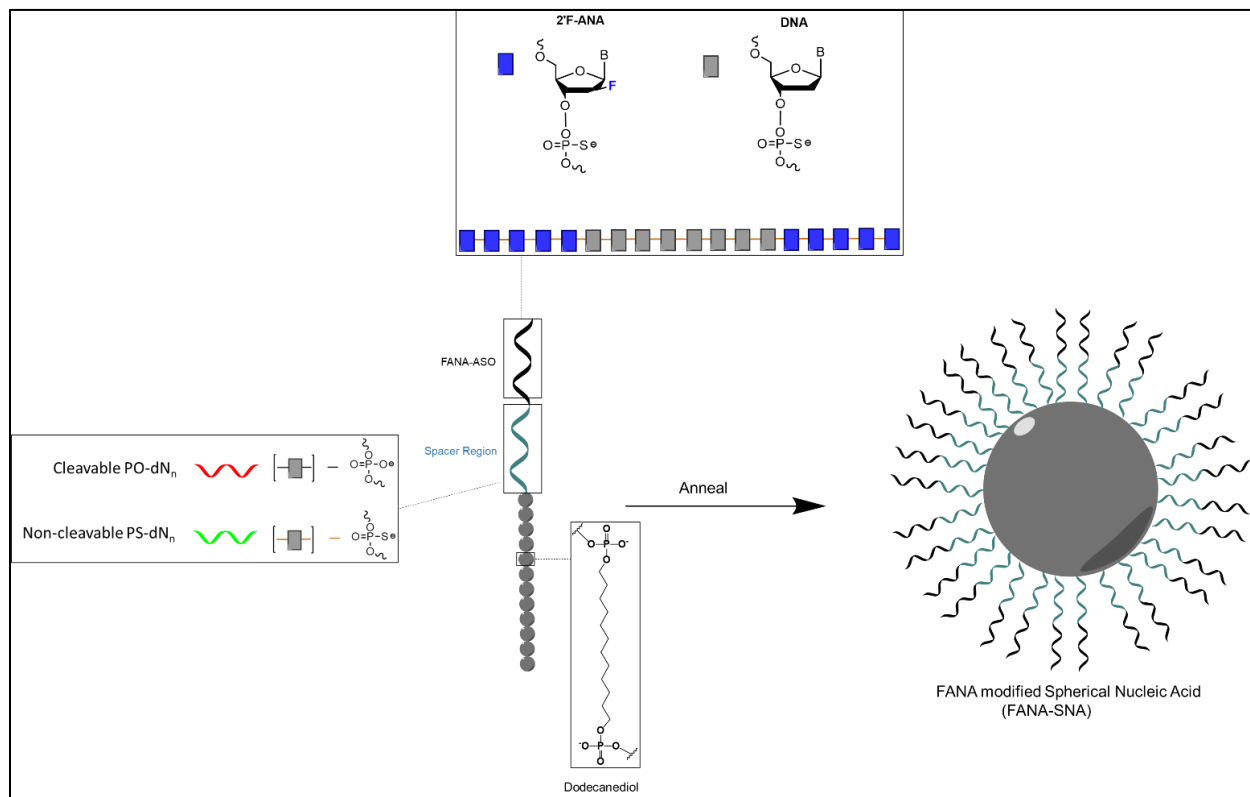


Figure 3. 1. Design and assembly of FANA SNA. Conjugating twelve dodecanediol units to FANA ASO gapmer 18 nt in length results in the formation of an SNA with low polydispersity and well-defined size and shape. The spacer region is modulated to optimize activity. N represents nucleotides, n represents the number of nucleotides. PO and PS represent phosphodiester and phosphorothioate backbone, respectively.

3.3. Results and Discussion

3.3.1. Antisense oligonucleotides (ASOs)

The table below shows all the strands and variations of ASO used throughout the manuscript (**Figure 3. 1.**). More information on the sequences used can be found in the methods section (**Table 3. 2.**).

Strand name	Base modification	Target	Spacer	Conjugate	Symbol
FANA-ASO	FANA	Luciferase	—	—	
FANA-SNA	FANA	Luciferase	—	(Dodecanediol) × 12	
FANA-(PO-dN ₄)-ASO	FANA	Luciferase	(PO-dN ₄)	—	
FANA-(PO-dN ₄)-SNA	FANA	Luciferase	(PO-dN ₄)	(Dodecanediol) × 12	
FANA-(PS-dN ₄)-ASO	FANA	Luciferase	(PS-dN ₄)	—	
FANA-(PS-dN ₄)-SNA	FANA	Luciferase	(PS-dN ₄)	(Dodecanediol) × 12	
FANA-(PO-dN ₈)-ASO	FANA	Luciferase	(PO-dN ₈)	—	
FANA-(PO-dN ₈)-SNA	FANA	Luciferase	(PO-dN ₈)	(Dodecanediol) × 12	
FANA-(PS-dN ₈)-ASO	FANA	Luciferase	(PS-dN ₈)	—	
FANA-(PS-dN ₈)-SNA	FANA	Luciferase	(PS-dN ₈)	(Dodecanediol) × 12	
FANA-survivin-(PO-dN ₄)-ASO	FANA	Survivin	(PO-dN ₄)	—	
FANA-survivin-(PO-dN ₄)-SNA	FANA	Survivin	(PO-dN ₄)	(Dodecanediol) × 12	
PS-DNA-ASO	—	Luciferase	—	—	
PS-survivin-ASO	—	Survivin	—	—	
PO-DNA-negativeASO(18)	—	—	—	—	
PS-DNA-mmASO	—	Mismatch to luciferase	—	—	
FANA-(PO-dN ₄)-mmASO	FANA	Mismatch to luciferase	(PO-dN ₄)	—	
FANA-(PO-dN ₄)-mmSNA	FANA	Mismatch to luciferase	(PO-dN ₄)	(Dodecanediol) × 12	
FANA-DNA-NegativeASO	FANA	—	—	—	
FANA-DNA-NegativeSNA	FANA	—	—	(Dodecanediol) × 12	
PS-(PO-dN ₄)-DNA-SNA	—	Luciferase	—	(Dodecanediol) × 12	
FANA-APOB-(PO-dN ₄)-ASO	FANA	APOB	(PO-dN ₄)	—	
FANA-APOB-(PO-dN ₄)-SNA	FANA	APOB	(PO-dN ₄)	(Dodecanediol) × 12	
Control	—	—	—	—	No strand was used

Table 3. 1. Variation of the ASO or SNA based on their base modification, target, spacer region and conjugation. FANA = 2'-Fluoroarabino nucleic acid with phosphothioate (PS) linkages. ASO = antisense oligonucleotide with PS linkages against firefly luciferase. SNA = strand with 12 units of dodecanediol that assembles into spherical nucleic acid. PO-dN₄/8 = 4 or 8 nucleotide spacer with phosphate linkages (PO). PS-dN₄/8 = 4 or 8 nucleotide spacer with PS linkages. Survivin = FANA antisense oligonucleotide with PS linkages against Survivin. NegativeASO = non-targeting sequence with PS linkages. mmASO = antisense oligonucleotide against firefly luciferase with 3

mismatches and PS linkages. APOB = FANA antisense oligonucleotide against APOB with PS linkages.

3.3.2. Synthesis and characterization of FANA-modified SNAs (FANA-SNAs)

We first verified that introducing a FANA-modified oligonucleotide in the SNA does not affect the self-assembly. We synthesized FANA-SNA with different spacer regions (no spacer or PO-dN₄ spacer) between the FANA portion and the hydrophobic polymer, and we assembled the nanoparticles in a magnesium containing buffer (1X TA)²⁹. Characterization was carried out using dynamic light scattering (DLS) and atomic force microscopy (AFM) (**Figure 3. 2.**). As seen in Figure 2, the ASO-conjugates form well-defined spherical structures with a comparable size to previously characterized SNAs^{49,50}. The addition of spacer led to a slight increase in size for the FANA-(PO-dN₄)-SNA. In both cases, the larger features observed by AFM are attributed to dimers or small aggregates resulting from the AFM conditions (dried sample on mica surface) and the palindromic nature of part of the sequence. We verified by agarose gel electrophoresis the monodisperse nature of the assembly (**Supplementary Figure 3. 7.**).

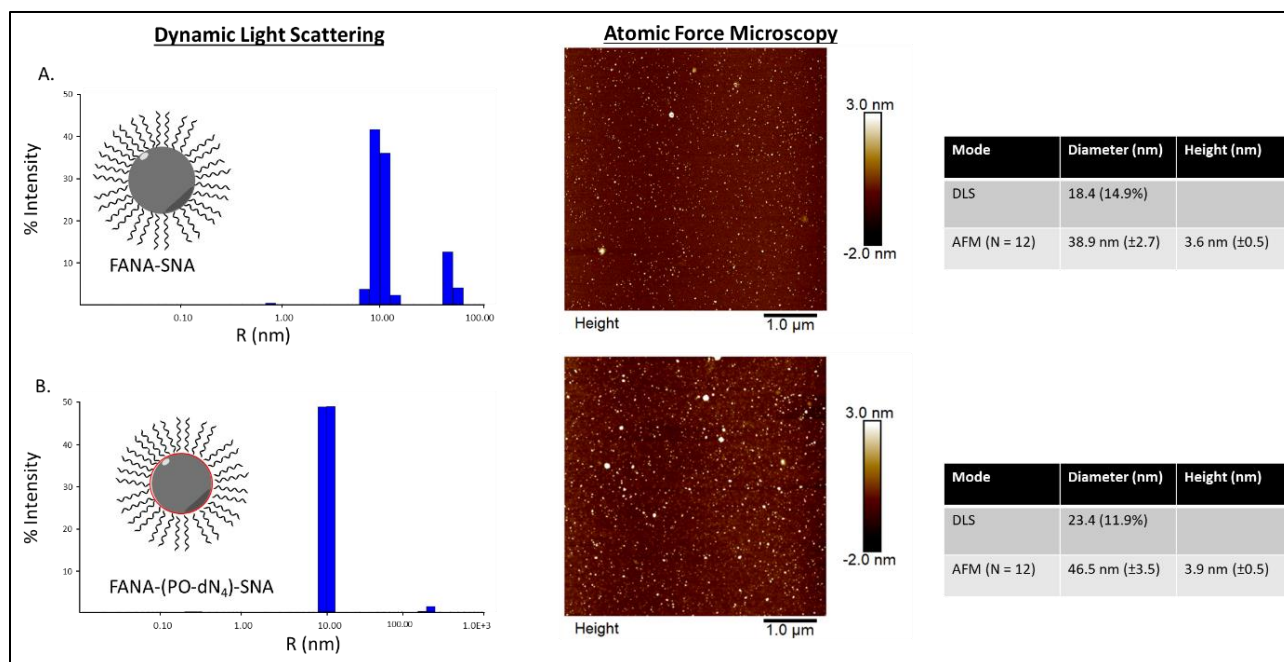


Figure 3. 2. Dynamic light scattering and atomic force microscopy characterization of A) FANA-SNA (no spacer) and B) FANA-(PO-dN₄)-SNA.

3.3.3. *Gene silencing activity of the SNAs*

After confirming the formation of the nanoparticles, we tested and compared the activity of FANA-SNA and FANA-ASO targeting luciferase mRNA. The ASOs and SNAs were transfected into luciferase expressing HeLa cells for 24 hours and assessed for their gene-silencing activity (luciferase activity, **Figure 3. 3. A**) and cell-death/cytotoxicity (CellTiter-Blue assay, **Figure 3. 3. B**). Results show that even though the FANA-SNA is active, its activity is significantly lower than its free FANA-ASO counterpart. However, when a 4-nt spacer with a phosphate backbone was introduced (FANA-(PO-dN₄)-SNA), the activity fully recovered; in fact it was superior to the activity seen for free FANA-ASO. None of the ASOs or the SNAs showed any significant toxicity to the cells, as the metabolic activity was equivalent across all samples.

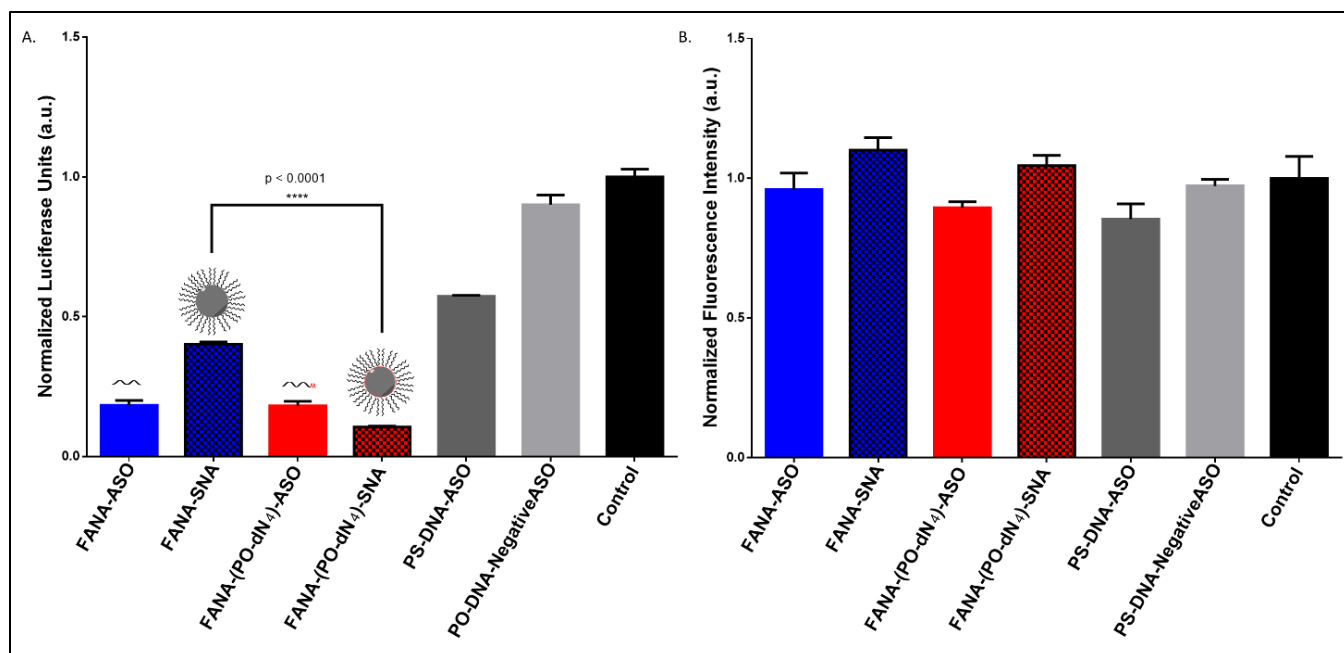


Figure 3. 3. Firefly luciferase knockdown activity comparison between various free FANA-ASO and FANA-SNA (see Table 3.1 for description of the different strands). **A.** Luciferase activity was measured after 24 h incubation and normalized to CellTiter-Blue and Control (no ASO). **B.** fluorescence measurement of CellTiter-Blue cytotoxicity results normalized to Control (no ASO). Error bars represent SD of triplicate experiments for each sample. ASO final concentration is 150 nM for all samples.

3.3.4. *Steric vs stability of spacer*

We reasoned that the superior activity FANA-SNAs with a (PO-dN₄) spacer was possibly due to a) the separation of the ASO portion from the hydrophobic core, thus increasing flexibility and reducing steric hindrance of the ASO strands, and/or b) the metabolically cleavable nature of the PO-DNA spacer, which would release off the free ASO strand from the SNA (**Figure 3. 4 A**). To assess these scenarios, we synthesized four new conjugates: (i) FANA-(PS-dN₄)-SNA, where the phosphate linkages that connect the dodecanediol units to the ASO are replaced by phosphorothioate (PS) linkages. Because of their superior resistance to nucleases, PS linkages are expected to increase spacer stability and significantly slow down the release of the FANA from the SNA. (ii) FANA-(PO-dN₈)-SNA and FANA-(PS-dN₈)-SNA, where the spacer length is increased, allowing us to test the effect of

increased separation and decreased steric hindrance (**Figure 3. 4 B**). The gene silencing experiment showed that the PO-dN_{4/8} spacers are superior (more activity seen) than the more stable PS-dN_{4/8} spacers (**Figure 3. 4 C**). The longer spacers (PO or PS) were less active than shorter ones, likely due to increased off-target interactions. (iii) Next, we tested a FANA-SNA containing a non-cleavable hexaethylene glycol (HEG) spacer, which also showed lower activity compared to FANA-(PO-dN₄)-SNA (**Supplementary Figure 3. 2.**). These results support the notion that the more metabolically cleavable PO-DNA spacer is required for the increased activity of FANA-SNA.

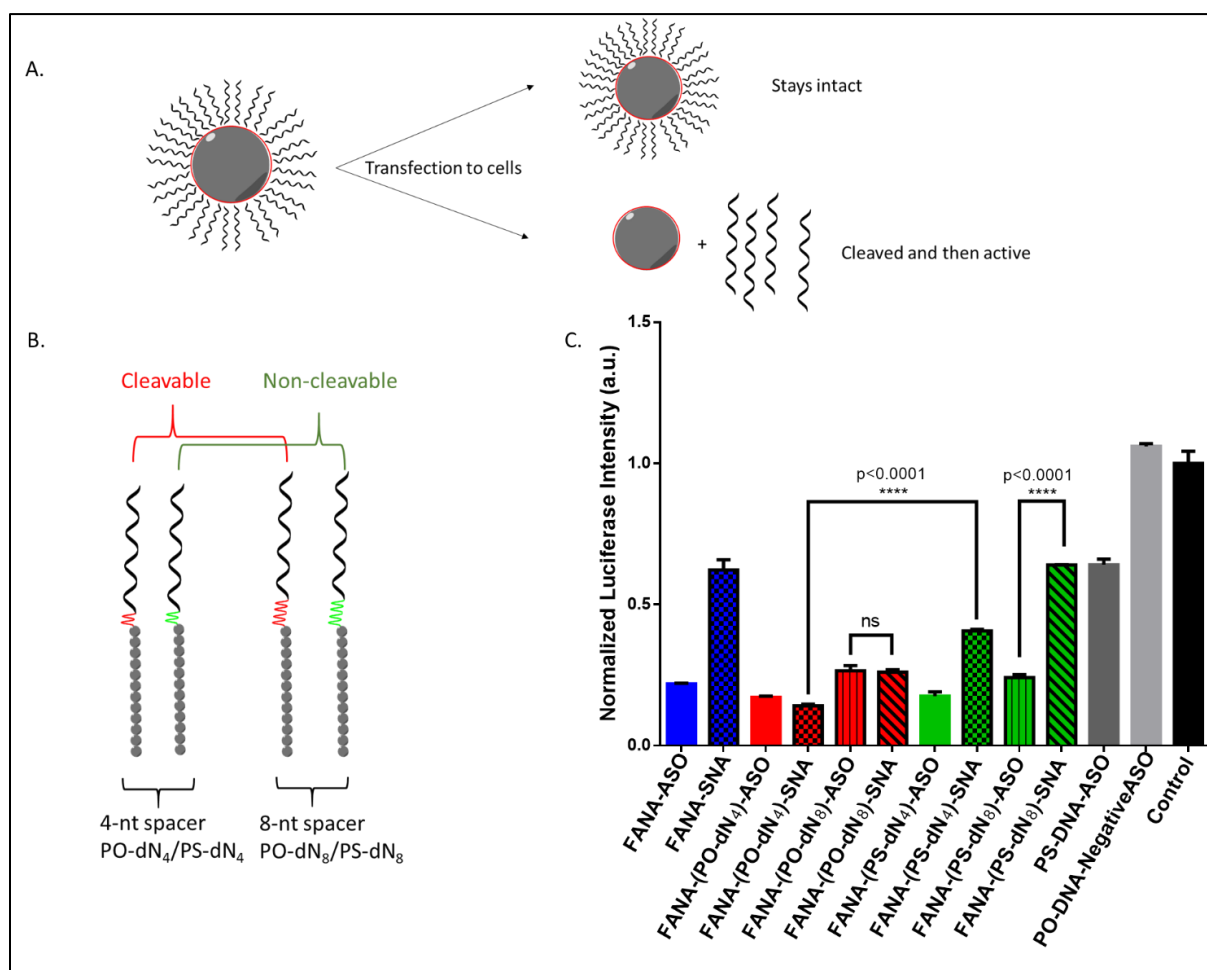


Figure 3. 4. A. Assessing steric versus cleavability of SNAs. The improved activity of mod-(PO-dN₄)-SNA could be due to having increased flexibility away from the hydrophobic core, or due to its cleavability and release once in the cytoplasm. **B.** The new designs with variable spacers. **C.** Luciferase activity was measured after 24 h incubation and normalized to CellTiter-Blue and

Control (no ASO). Error bars represent SD for triplets of each sample. ASO final concentration is 150 nM (in strands) for all samples.

3.3.5. *Assessing the cellular uptake of SNAs with varying spacer structure*

To examine if the superior activity of the FANA-(PO-dN4)-SNAs was due to enhanced cellular uptake relative to the FANA-(PS-dN4)-SNAs, cellular uptake was assessed via flow cytometry in 3 different cell lines. The SNAs were modified with a Cy3 dye on the interface between the ASO and conjugate to avoid any influence on uptake from the dye itself.

The data shown in **Figure 3. 5.** shows that both SNAs (cleavable and non-cleavable spacer) have similar uptake in all 3 cell lines, suggesting that the higher activity imparted by the (PO-dN4) spacer likely results from the release of the ASO from the SNA and endosomes, and not from increase in uptake. It is important to note that the higher uptake signal seen for the free ASOs is due to having an exposed Cy3 dye, which is known to cleave over time and increase intracellular fluorescence as studied in our previous work ^{51,52}. Additional data analysis and plots are included in Supplementary information (**Supplementary Figure 3. 3.**).

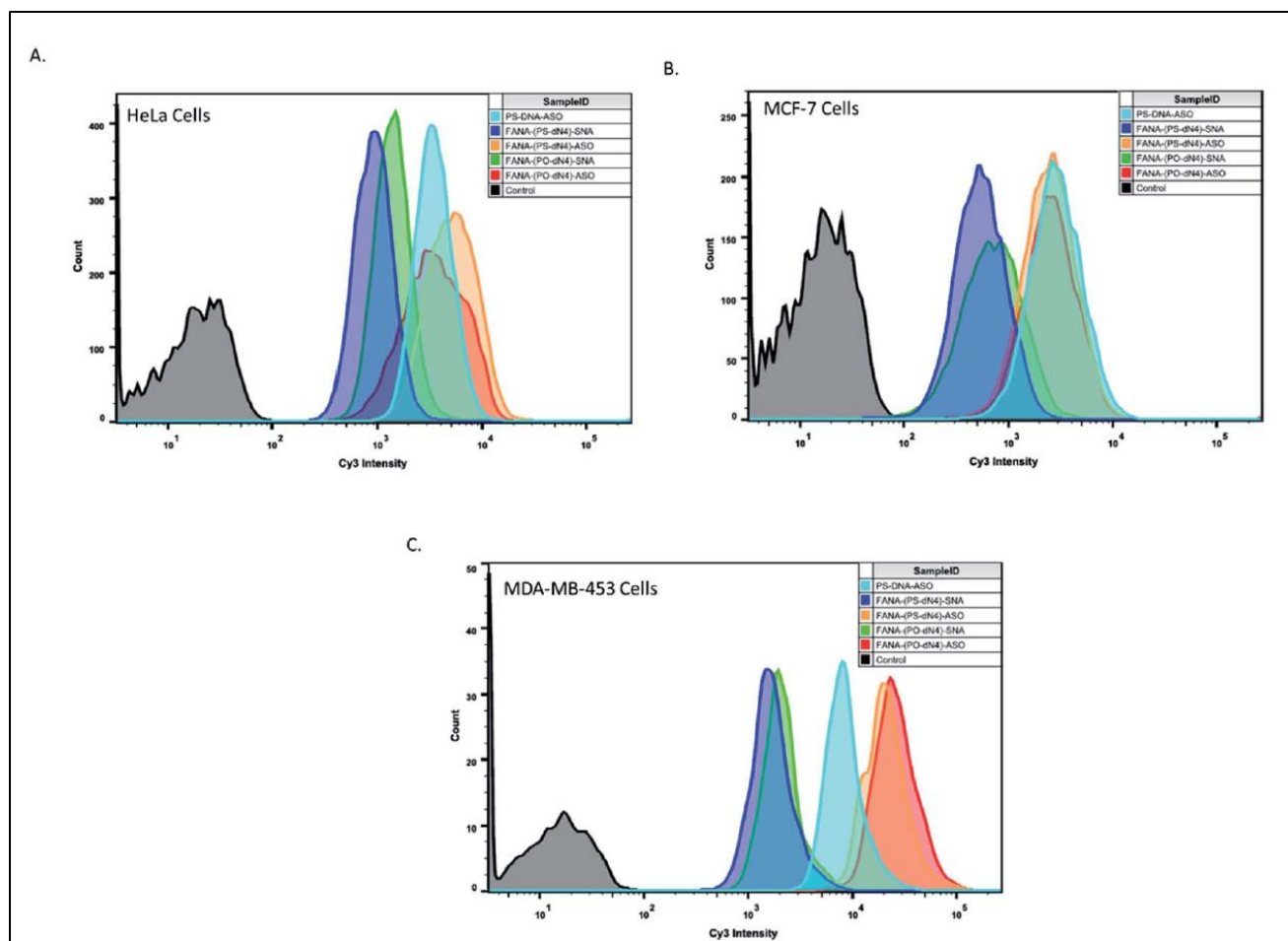


Figure 3. 5. Flow cytometry experiment to assess the uptake of various samples in different cell lines. Cells were incubated at 0.5 μM final concentration of sample (in strands) for 24 hours, followed by detachment and assessment. Samples were made in duplicates. 10,000 cells count was collected for all samples in HeLa and MCF-7 cells, and 1,000 cells count was collected in MDA-453 cells. one duplicate is shown for simplicity.

3.3.6. *Duration of effect*

Next, we compared the activities of the various FANA-SNAs over an extended period of time (**Figure 3. 6**). The results of the silencing experiment show that FANA-(PO-dN₄)-SNA remains the most active, and that its activity increased over the 72 hr period; in contrast, the activity of FANA-(PS-dN₄)-SNA plateaued at 48 h, with no significant change after 72 h (**Figure 3. 6**).

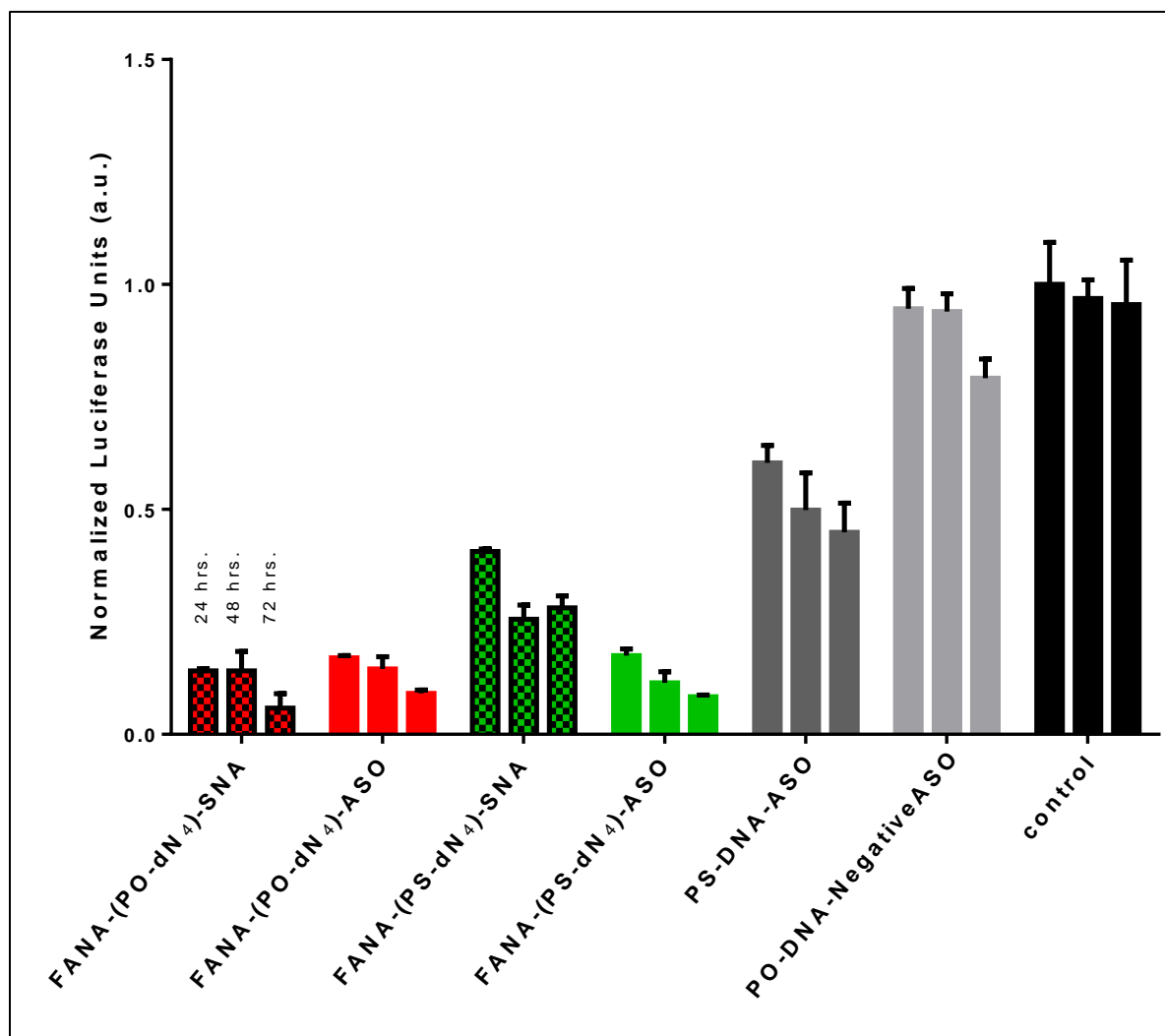


Figure 3. 6. Duration of effect: Luciferase activity after 24, 48, or 72 h incubation, and normalized to CellTiter-Blue and Control (no ASO). Error bars represent SD for triplets of each sample. ASO final concentration is 150 nM strands for all samples.

3.3.7. *FANA SNA exhibits greater activity compared to free FANA ASO*

We measured the activity of FANA-(PO-dN₄)-SNA and FANA-(PO-dN₄)-ASO at 150, 100, 50 and 10 nM after 24 hours of incubation (**Figure 3. 7.**). The free ASO showed the expected gradual loss of activity as its concentration was decreased from 150 to 10 nM. The SNA shows superior silencing activity over FANA-(PO-dN₄)-ASO at most of the concentrations tested (e.g., 50-100 nM; **Figure 3. 7. B.**)

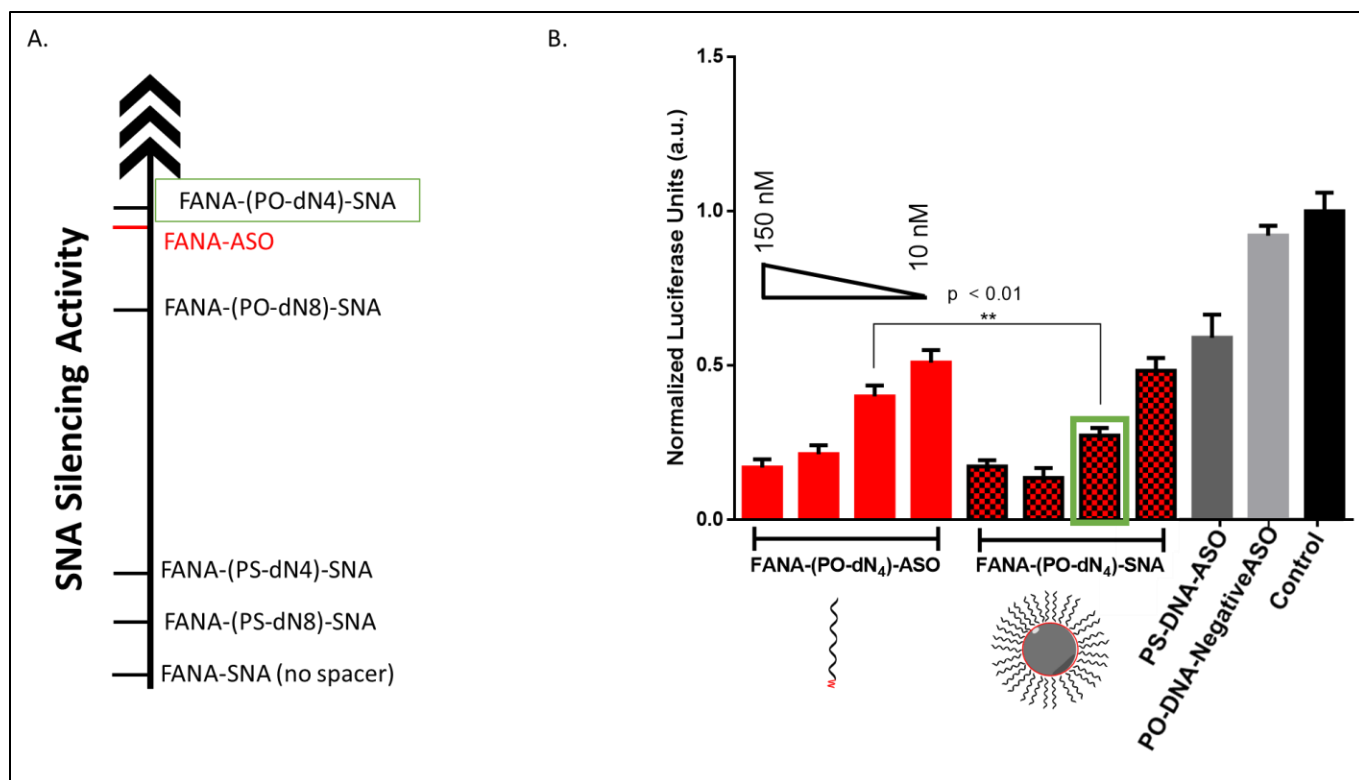


Figure 3. 7. A. Relative gene silencing activity of SNAs and free ASOs at 150 nM (in strands). **B.** Firefly luciferase knockdown assay for a titration of different concentrations of FANA-(PO-dN₄)-SNA compared to FANA-(PO-dN₄)-ASO, where at 50 nM (in strands) the SNA performs better. Luciferase activity was measured after 24 h incubation and normalized to CellTiter-Blue and Control (no ASO). Error bars represent SD for triplets of each sample. Concentrations tested are: 150, 100, 50 and 10 nM (in strands).

3.3.8. *Serum stability*

FANA-SNAs were incubated in cell media containing Fetal Bovine Serum (10%) and collected aliquots at different timepoints were assessed on a denaturing polyacrylamide gel (PAGE). As seen in Figure 8, little degradation is observed for SNAs with the PS-dN₄ spacer over 48 hours. However, the SNA with a PO-dN₄ spacer undergoes more extensive cleavage (around 20%) relative to the SNA with a PS-dN₄ spacer, consistent with the notion that the PO linker releasing the ASO more readily (**Figure 3. 8.**). This cleavage is expected to be more extensive intracellularly,

considering the acidity of the endosomal-lysosomal compartments and the presence of additional nucleases in this environment. No significant differences were observed between the FANA-SNAs and the corresponding free FANA demonstrating the excellent nuclease stability of the FANA modification under these conditions.

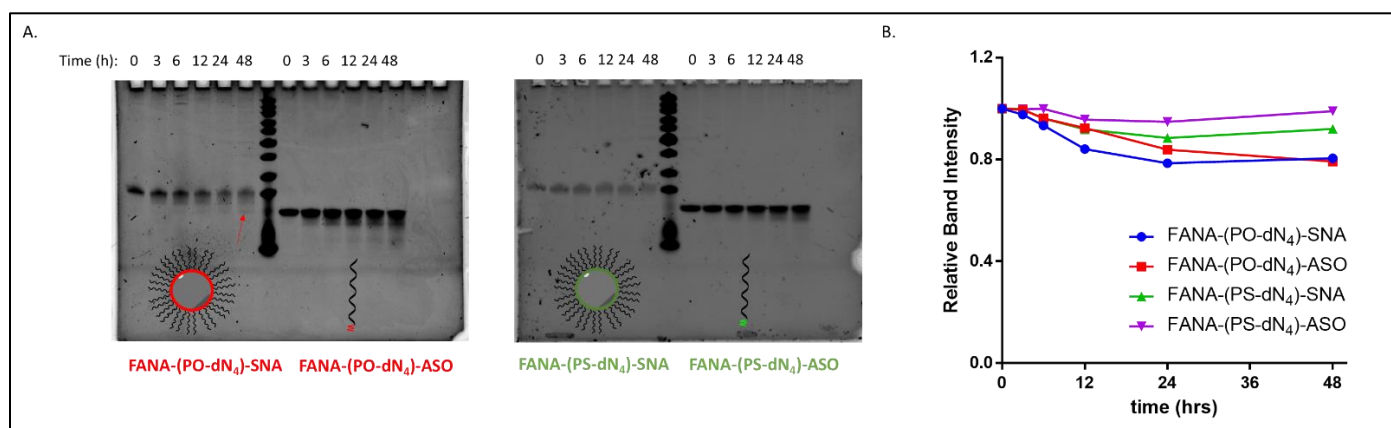


Figure 3. 8. Serum stability of cleavable vs non-cleavable SNAs over time. Aliquots at different timepoints were treated with Proteinase K and loaded on a A) 20% denaturing polyacrylamide gel electrophoresis (PAGE). Arrows points to fragment moving similarly to the free ASO. B) Plot of relative band intensity for each sample over time. Each sample was normalized to the initial intensity at time 0 h).

3.3.9. *Testing against different mRNA targets*

The SNAs' design is versatile and modular, as they can theoretically silence any target of interest by changing their oligonucleotide sequence. To show this, we changed the sequence to target survivin, an overexpressed oncogene in numerous tumour cells responsible for cell proliferation and inhibition of apoptosis, allowing them to build resistance to therapy^{42,53,54}. If silenced, the cancer cells will stop proliferating, which can be measured via their metabolic activity using the CellTiter-Blue assay. We opted for the design with the PO-dN₄ cleavable spacer that shows the highest activity. The results show that the SNAs are indeed effective against an endogenous target (**Figure 3. 9. A.**). In fact, the SNA has significantly higher activity compared to the free ASO counterpart. Titration of various concentrations was also performed, showing that the SNA retains higher activity at decreasing concentrations (**Supplementary Figure 3. 4.**).

In order to provide evidence of gene knockdown at the RNA level, we targeted the APOB gene in HepG2 cells³⁶. We quantified the relative silencing by measuring mRNA degradation with RT-qPCR. The data (**Figure 3. 9. B.**) shows the successful decrease of RNA level using FANA-APOB-(PO-dN₄)-ASO/SNA to a greater extent than the non-targeting controls (we used the mismatched FANA-(PO-dN₄)-ASO/SNA of the luciferase target).

Hence the SNAs display modularity by showing effective silencing against two other targets, both at the protein and RNA level.

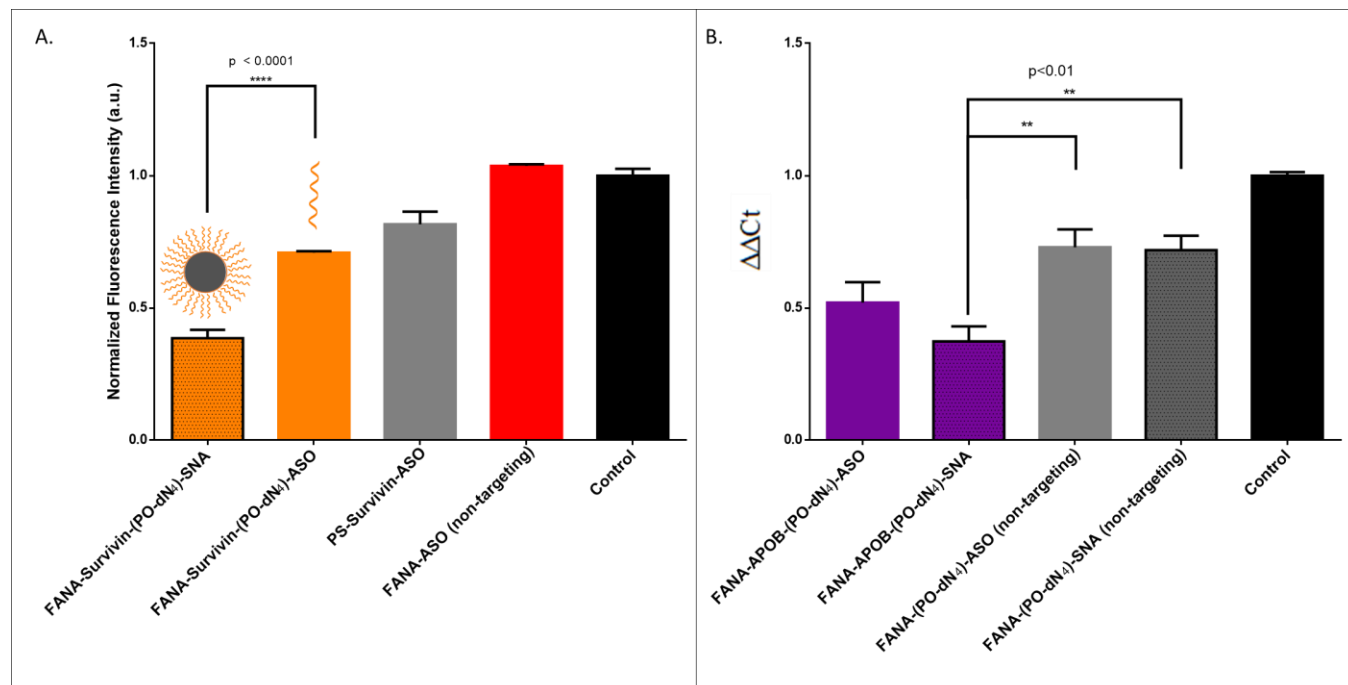


Figure 3. 9. A. CellTiter-Blue cytotoxicity assay comparison between free FANA-ASO and FANA-SNA targeting Survivin. Metabolic activity was measured after 24 h incubation and normalized to Control (no ASO). ASO final concentration is 500 nM (of strands) for all samples
B. qRT-PCR Gene-silencing comparison between free FANA-ASO and FANA-SNA targeting APOB mRNA in HepG2 cells. Knockdown was measured by qRT-PCR after 24 h incubation and normalized to Control (no ASO) and to GAPDH as reference mRNA. Error bars represent SD for triplets of each sample. ASO final concentration is 150nM (of strands) for all samples. FANA-ASO/SNA targeting luciferase was used as a non-targeting control here in both experiments as indicated.

3.3.10. *SNA improves transfection-free delivery (gymnosis)*

FANA ASOs are known to penetrate cells without transfection (gymnosis) ¹²⁻¹⁶. Furthermore, we have previously shown that DNA-SNAs are taken up by cells to a greater extent than free DNA in absence of transfection agents, and that they are able to efficiently deliver small molecule drugs in cells. However, our previous ASO-SNAs did not show silencing activity without transfection agents ⁵⁰. We tested the ability of FANA-SNAs for gymnotic silencing of luciferase mRNA in HeLa cells. In this experiment (**Figure 3. 10.**), the ASO and SNAs were incubated at 1 μ M (strand concentration) for 3 days, following a previously reported protocol ¹². Figure 10 shows that gymnotic delivery of FANA-(PO-dN₄)-SNA and FANA-ASO downregulated luciferase expression compared to control untreated cells; however, silencing was more significant for the SNA. In contrast, a targeting PS-DNA with no FANA modifications and a mismatch control (PS-DNA) did not produce silencing under similar conditions.

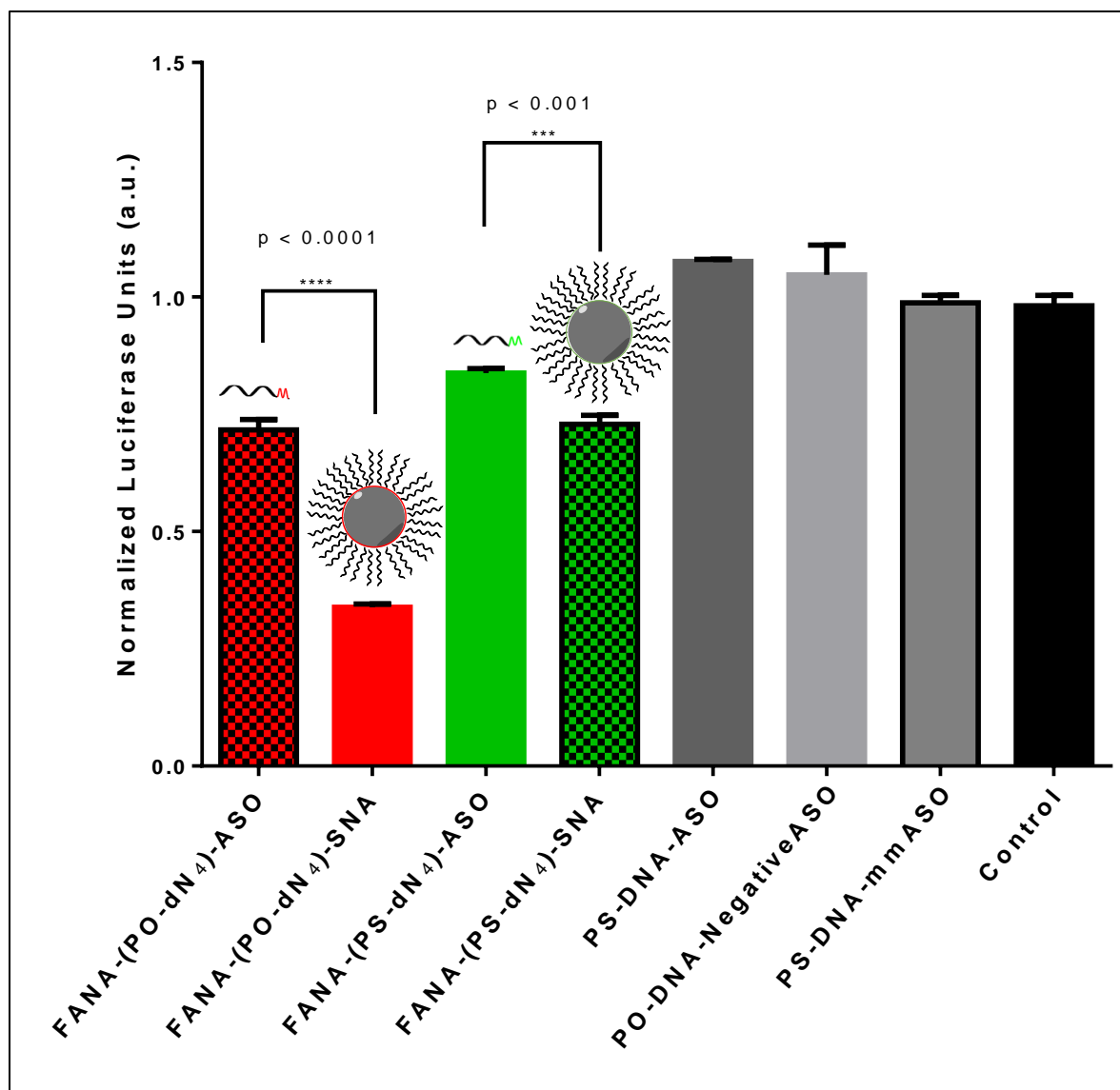


Figure 3. 10. Gymnotic gene silencing of FANA-SNA, FANA and DNA ASO. Luciferase activity of various samples at 72 h incubation, normalized to CellTiter-Blue and Control (no ASO). Error bars represent SD for triplets of each sample. ASO final concentration is 1 μ M (in strands) for all samples.

3.3.11. *Discussion*

To our knowledge, only one reported example has previously shown incorporation of FANA modifications into the *corona* rather than the interior of a nanoparticle delivery system, which was a poly(D,L-lactide-*co*-glycolide) particle⁵⁵. The inhibitory effect of FANA ASOs is attributed to RNase H1 activation or steric hindrance depending on the mRNA target site and ASO design^{9,16}. The current work investigates for the first time the behaviour and silencing activity of a FANA modified ASO as part of a spherical nucleic acid (SNA) previously developed in our group^{29,50}. This system arises from sequentially synthesizing an ASO conjugated to twelve dodecanediol artificial “nucleotide” units in sequence-defined and automated manner. This allows it to assemble into an exceptionally stable monodisperse particle of tuneable properties (size, shape, functionality, biodistribution) for delivery^{49,50,56}. FANA has the benefit of increasing gene silencing efficacy, nuclease resistance and reduced immune-stimulatory side-effects^{4-9,16}.

We first verified that such a modification did not impact the assembly of the SNA (**Figure 3. 2.**). We then showed that, while still capable of gene silencing, the activity of the FANA-SNA particle was significantly reduced compared to free ASO (Figure 3). However, when a PO-DNA tetranucleotide spacer was introduced between the ASO and the SNA (i.e., FANA-(PO-dN₄)-SNA), the activity fully recovered and, in fact, was superior to the activity of the free FANA-ASO. The spacer design between the oligonucleotide and the core is therefore crucial in many aspects to the SNA’s overall activity performance, as it can modulate the crowding and loading capacity on its surface^{22,46,57,58}. This work suggests that release of the ASO from our SNA is another important factor. In support of this, we observed greater silencing activity with FANA-SNAs containing a PO-DNA spacer relative to a more stable PS-DNA (**Figure 3. 3.**). By changing the length (4- vs. 8-nucleotide) and the stability (PO vs. PS) of the spacer, we showed that a less stable and shorter phosphate linker is better than a longer spacer for activity (**Figure 3. 4.**). A hexaethylene glycol spacer was also detrimental for our SNAs, similar to what is reported in literature^{43,45,46 59}.

The increased activity for the SNA with PO spacer is not due to increased uptake into cells, as both PO-dN₄ and PS-dN₄ have similar uptake levels across three different cell lines (**Figure 3. 5.**). This indicates that the cleavability of the spacer plays a major role after the uptake of SNAs into cells. The activity of the FANA-(PO-dN₄)-SNA was consistent and improved up to 72 hours of incubation with cells (**Figure 3. 6.**).

The cleavability of siRNA conjugates has recently been touched upon briefly by Prakash *et al.*⁶⁰ and Biscans *et al.*⁶¹, in an investigation of siRNA-hydrophobic conjugates extra-hepatic delivery. They also noticed that a cleavable portion between the ASO and the conjugate gave the most active version, with no impact on biodistribution. Wada *et al.*⁶² have also recently investigated the effect of linker stability in a cholesterol-ASO conjugate, and found that the release of the conjugate from the ASO was essential for enhanced activity. A recent study by Wang *et al.*⁶³ discusses that lipid conjugated ASOs have higher uptake into cells than their unconjugated counterpart, but they traffic through the same pathway of late endosomes. However, they found that ASO-conjugates, in comparison to free ASOs, tend to remain more associated with plasma and endosomal membranes rather than getting digested by the endosomes themselves. This causes their increased activity and release from endosomes to find their target RNA. This faster release from endosomes is critical to reach full activity, and in the case of our SNA, we hypothesize that having a metabolically cleavable spacer allows for the ASO to be cleaved and released, while the hydrophobic dodecanediol-based core may remain bound to the endosomal membrane and to proteins⁶³. It is important to note that the SNA did not significantly shed its ASO corona up to the measured 48 hours of incubation in serum containing cell culture (**Figure 3. 8.**), suggesting that the ASO on the SNA circulates as a nanoparticle and acts as an ASO once cleaved and released in the cytosol.

Furthermore, the FANA-(PO-dN₄)-SNA shows increased activity at lower concentration compared to its free ASO counterpart (**Figure 3. 7.**). This is another advantage for using a nanoparticle, where the dose of the oligonucleotide drug can

be decreased without compromising its effect⁶³. The SNA is modular in its design, and it can be adapted to target other endogenous targets inside cells, such as Survivin and APOB (**Figure 3. 9.**).

Oligonucleotides typically require targeting ligands or transfection agents to aid their uptake into cells^{12,22,39,64}. Here, we demonstrate that our FANA-SNAs exhibit more potent gymnotic gene silencing relatively to the free FANA-ASO (**Figure 3. 10.**). In comparison to the previously reported gymnotic silencing with FANA-ASOs, we obtained slightly better activity (70% silencing) compared to 60% at 1 μM ¹². We anticipate that changing the chemistry of the sequence-controlled polymer in the SNA core has the potential to further increase this activity.

In conclusion, we have demonstrated that carefully designed FANA modified SNAs are highly efficient particles for gene silencing. They combine the efficacy of modified oligonucleotides with the enhanced stability and uptake of spherical nucleic acids, and they show higher activity at lower concentrations, modularity in targeting different mRNAs, as well as unaided uptake into cells. Additionally, taking advantage of the hydrophobic core and FANA shell, surface modifications such as targeting ligands, and small encapsulated molecules that enhance endosomal release could readily be implemented. We envisage this system to see applications in delivery and therapy of oligonucleotide therapeutics.

3.4. Acknowledgement

We would like to acknowledge the help of Dr. Violeta Toader on the synthesis of the dodecanediol phosphoramidite conjugate. We are grateful to Henrietta Lacks, now deceased, and to her surviving family members for their contributions to biomedical research. We thank the Natural Sciences and Engineering Research Council of Canada (Discovery and NSERC CREATE Training grant to H.F.S. and M.J.D.), FRQNT, and the Canada Research Chairs program.

3.5. Supporting Information

3.5.1. General

Tris(hydroxymethyl)aminomethane (Tris), ethylenediaminetetraacetate (EDTA), urea, 40% acrylamide/bis-acrylamide (19:1), ammonium persulfate (APS), N,N,N',N'-tetramethylethane-1,2 diamine (TEMED) and agarose were purchased from BioShop Canada Inc and used without further purification. Magnesium chloride hexahydrate and Nile Red were purchased from Sigma-Aldrich. Acetic acid, boric acid, ammonium hydroxide and 10x DPBS (with magnesium, calcium) were purchased from Fischer Scientific and used without further purification. GelRed™ nucleic acid stain was purchased from Biotium Inc. GeneRuler DNA Ladder Mix and DNA Gel Loading Dye (6X) were obtained from Thermo Scientific. 1 μmole 1000 Å universal synthesis CPG column, standard reagents used for automated DNA synthesis and Sephadex G25 (super fine DNA grade) were purchased from BioAutomation. DMT-1,12-dodecane-diol phosphoramidites were synthesized in the lab from 1,12-dodecane-diol (Alfa Aesar) and DMTCI (AK Scientific). 1x TBE buffer is composed of 90 mM Tris, 90 mM boric acid and 2 mM EDTA with a pH ~8.3. 1x TA buffer is composed of 45 mM Tris, 20 mM acetic acid and 7.6 mM Mg(Cl)₂, and its pH was adjusted to ~8.0 using glacial acetic acid. 1x DPBS (with magnesium and calcium) is composed of 8 mM sodium phosphate dibasic, 138 mM of sodium chloride, 1.47mM of potassium phosphate monobasic, 2.6 mM potassium chloride, 0.5 mM magnesium chloride (anhydrous) and 0.9 mM calcium chloride (anhydrous).

Cyanine 3 (Cy3) phosphoramidite, Cyanine 5 (Cy5) phosphoramidite, 5'-fluorescein phosphoramidite, and Sulfurizing reagent II were purchased from GlenResearch.

Millipore water was used throughout any preparation of buffers.

Dulbecco's Modified Eagle Medium (DMEM) and phosphate-buffered saline (PBS) were purchased from Life Technologies. Lipofectamine reagent was purchased from Invitrogen. Fetal bovine serum (FBS), 0.05% Trypsin-EDTA and sodium pyruvate were obtained from Wisent Bioproducts. The Bright-Glo Luciferase Assay

system was purchased from Promega. Cell-Titer Blue assay was also purchased from Promega. The HeLa X1/5 cells stably expressing luciferase are a generous gift from Dr. Pelletier (McGill).

3.5.2. *Instrumentation*

Standard oligonucleotide synthesis was performed on solid supports using a Mermade MM6 synthesizer from Bioautomation. UV absorbance DNA quantification measurements were performed with a NanoDrop Lite spectrophotometer from Thermo Scientific. For structure assembly, Eppendorf Mastercycler 96-well thermocycler and Bio-Rad T100™ thermal cycler were used to anneal all DNA nanoparticles. Polyacrylamide gel electrophoresis (PAGE) was performed using 20x20 cm vertical Hoefer 600 electrophoresis units, or a Bio-Rad Mini-PROTEAN® Tetra Vertical electrophoresis units. Agarose Gel Electrophoresis (AGE) were performed on Owl Mini and Owl EasyCast horizontal gel systems. Gels were imaged by BioRad ChemiDoc MP system.

Fluorescence data were measured by BioTek Synergy H4 Hybrid Multi-Mode Microplate Reader. Multimode 8 scanning probe microscope and Nanoscope V controller (Bruker, Santa Barbara, CA) was used to acquire AFM images. Liquid Chromatography Electrospray Ionization Mass Spectrometry (LCESI-MS) was carried out using Dionex Ultimate 3000 coupled to a Bruker MaXis Impact™ QTOF. Dynamic light scattering (DLS) experiments were carried out using a DynaPro™ Instrument from Wyatt technology. Firefly Luciferase luminescence was measured using a Biotek Synergy HT plate reader. Cytotoxicity studies were performed using the CellTiter96 kit from Promega according to the manufacturer's instructions.

3.5.3. *Synthesis and purification*

Synthesis:

All solid-phase syntheses were performed on a 1 μ mol scale using universal 1000 Å LCAA-CPG solid-supports. Coupling efficiencies were monitored following removal of the dimethoxytrityl (DMT) 5'-OH protecting group. DBCO-dT-CE and DMT-dodecanediol phosphoramidites were dissolved in the appropriate solvents (anhydrous acetonitrile/dichloromethane 1:3 (v/v) and acetonitrile respectively) under a nitrogen atmosphere (<0.04 ppm for oxygen, and <0.5 ppm trace moisture) for a final concentration of 0.1M. The DMT-dodecane-diol was activated using 0.25M 5-(ethylthio)tetrazole in anhydrous acetonitrile and an extended coupling time of 5 minutes was employed. 3% dichloroacetic acid in dichloromethane was used to remove the DMT protecting group on the DNA synthesizer. Sulfurization was executed prior to capping on the DNA synthesizer using Sulfurizing Reagent II (cat.# 40-4037, Glen Research). Following synthesis, strands were cleaved from the solid-support and deprotected using 28% aqueous ammonium hydroxide solution for 20 hours at 60°C. Strands were dried under vacuum at 60°C, resuspended in Millipore H₂O, then filtered with 0.22 μ m centrifugal filters.

Strands were purified using polyacrylamide gel electrophoresis (PAGE) or high-performance liquid chromatography (HPLC).

PAGE Purification:

Aqueous solution of oligomer was mixed with an equal volume of Urea prior to loading on gel in order to assist in denaturation. oligomers were run on either 18% or 15% polyacrylamide/8M urea gels in 1xTBE for 30 minutes at 250V, followed by 60 minutes at 500V. Following gel electrophoresis, bands were imaged using a handheld UV illuminator (254nm) and excised, crushed, and suspended in ~5-10 mL H₂O. This suspension was frozen by brief submersion in liquid nitrogen, before being incubated at 60°C for 16 hours. The supernatant was concentrated by evaporation, desalted using size exclusion chromatography (Sephadex G-25), and

quantified (OD260) using a NanoDrop Lite spectrophotometer from Thermo Scientific.

HPLC Purification:

0.5 OD of sample in 20-50 μ L of Millipore water were injected into a Hamilton PRP-1 5 μ m 2.1x150mm column at 60°C. The mobile phases were TEAA and HPLC grade acetonitrile, with an elution gradient of 3-70% acetonitrile over 30 minutes. Strands were detected using a diode array detector monitoring absorbance at 260nm. The below table contains all the strands synthesized along with their sequences.

3.5.4. *Table of oligonucleotide sequences*

Bold nucleotides are FANA modified bases. D represents dodecane-units. Underline is phosphorothioate linkages, while non-underlined are regular phosphate linkages.

Strand (# of bases)	Sequence (5' to 3')		Description
FANA-ASO (18)	AUAUCCTTGTGCGTAUCC		FANA modified ASO against luciferase mRNA
FANA-SNA (18)	DDDDDDDDDD- AUAUCCTTGTGCGTAUCC		FANA modified ASO against luciferase mRNA with 12 units of dodecane to form SNA.
FANA-(PO-dN ₄)-ASO (22)	(ATAT)- AUAUCCTTGTGCGTAUCC		Same as FANA-ASO but includes a 4-nt PO spacer. Used to compare spacer vs no spacer activity.
FANA-(PO-dN ₄)-SNA (22)	DDDDDDDDDD-(ATAT)- AUAUCCTTGTGCGTAUCC		Same as FANA-SNA but includes a 4-nt PO spacer. Used to compare spacer vs no spacer activity.
FANA-(PS-dN ₄)-ASO (22)	(ATAT)- AUAUCCTTGTGCGTAUCC		Same as FANA-ASO but includes a 4-nt PS spacer. Used to compare to its PO counterpart.
FANA-(PS-dN ₄)-SNA (22)	DDDDDDDDDD-(ATAT)- AUAUCCTTGTGCGTAUCC		Same as FANA-SNA but includes a 4-nt PS spacer. Used to compare to its PO counterpart.
FANA-(PO-dN ₆)-ASO (26)	(ATATTTT)- AUAUCCTTGTGCGTAUCC		Longer spacer version of the cleavable modality.
FANA-(PO-dN ₆)-SNA (26)	DDDDDDDDDD-(ATATTTT)- AUAUCCTTGTGCGTAUCC		Longer spacer version of the cleavable modality with 12 units of dodecane to form SNA.
FANA-(PS-dN ₆)-ASO (26)	(ATATTTT)- AUAUCCTTGTGCGTAUCC		Longer spacer version of the non-cleavable modality.
FANA-(PS-dN ₆)-SNA (26)	DDDDDDDDDD-(ATATTTT)- AUAUCCTTGTGCGTAUCC		Longer spacer version of the non-cleavable modality with 12 units of dodecane to form SNA.
FANA-Survivin-(PO-dN ₄)-ASO (25)	(ATAT)- UGACAGAUAGGAACCGCUU		FANA modified ASO against surviving mRNA with a 4-nt PO spacer
FANA-Survivin-(PO-dN ₄)-SNA (25)	DDDDDDDDDD-(ATAT)- UGACAGAUAGGAACCGCUU		FANA modified ASO against surviving mRNA with a 4-nt PO spacer with 12 units of dodecane to form SNA.
PS-DNA-ASO (18)	<u>ATATCCTTGTGCGTATCCC</u>		Unmodified ASO against luciferase as control. All PS
PS-Survivin-ASO (21)	<u>TGACAGATAAGGAACCTGCTT</u>		Unmodified ASO against Survivin as control. All PS
PO-DNA-NegativeASO(18)	AATAATTGAATTCTTCAA		Negative non targeting control with all PO backbone, used in cell assays.
PS-DNA-mmASO(18)	<u>ATATCCTAGTTGAATCCC</u>		Multiple mismatch version of PS-ASO against luciferase.
FANA-(PO-dN ₄)-mmASO (22)	(ATAT)- AUAUCCTAGTTGAAUCC		FANA modified multiple mismatch version of ASO against luciferase.
FANA-(PO-dN ₄)-mmSNA (22)	DDDDDDDDDD-(ATAT)- ATATCCTAGTTGAATCCC		FANA modified multiple mismatch version of ASO against luciferase with 12 units of dodecane to form SNA.
FANA-DNA-NegativeASO(18)	AAUAATTGAATTCTUCAA		FANA modified negative scramble control to FANA-ASO against luciferase.
FANA-DNA-NegativeSNA(18)	DDDDDDDDDD- AAUAATTGAATTCTUCAA		FANA modified negative scramble control to FANA-ASO against luciferase with 12 units of dodecane to form SNA.
PS-(PO-dN ₄)-DNA-SNA (22)	DDDDDDDDDD-(ATAT)- <u>ATATCCTTGTGCGTATCCC</u>		PS modified ASO against luciferase with cleavable spacer, with 12 units of dodecane to form SNA.
FANA-APOB-(PO-dN ₄)-ASO (24)	(ATAT)- GCCUCAGTCTGCTTCGCACC		FANA modified ASO against APOB mRNA with a cleavable spacer
FANA-APOB-(PO-dN ₄)-SNA (24)	DDDDDDDDDD-(ATAT)- GCCUCAGTCTGCTTCGCACC		FANA modified SNA against APOB mRNA with a cleavable spacer

Table 3. 2. sequence ID table of all oligonucleotides used in this manuscript. Bold nucleotides are FANA modified bases. D represents dodecane-units. Underline is phosphorothioate linkages, while non-underlined are regular phosphate linkages.

3.5.5. *Methods*

Assembly of SNAs:

To assemble the SNA, an ASO-polymer conjugate strand was annealed at the corresponding concentration (usually 10 μM in DNA strands, 30 μL) in Tris-Acetic acid -Magnesium_buffer (1xTA, 7.6mM, Supporting information) from 95 to 4 $^{\circ}\text{C}$ over 4 hours using Eppendorf Mastercycler 96-well thermocycler and Bio-Rad T100TM thermal cycler. All concentrations referred to in the manuscript are with respect to the DNA strand concentration. For example, 150nM concentration of SNA corresponds to 150nM of the strands that constitutes the SNA, which is an ASO-polymer conjugate.

Dynamic Light Scattering (DLS):

SNAs size distribution was measured using a DynaProTM Instrument from Wyatt technology. Millipore water and 1xTAMg buffer were filtered using a 0.45 μm nylon syringe filter before use in DLS sample preparation. A 15 μL sample (concentration 5 μM) was used in each measurement. Measurements were performed at 25 $^{\circ}\text{C}$. Each measurement consisted of 20 acquisitions, with each acquisition lasting 10 seconds. Data was filtered to exclude acquisitions with a baseline above 1.01 and a SOS error above 150. A cumulants fit model was used to confirm the presence and determine the size the SNAs.

Atomic Force Microscopy:

Dry AFM was carried out using a MultiMode8TM SPM connected to a NanoscopeTM V controller (Bruker, Santa Barbara, CA). All images were obtained using ScanAsyst mode in air with AC160TS cantilevers (Nominal values: Tip radius – 9 nm, Resonant frequency – 300 kHz, Spring constant – 42 N/m) from Asylum Research. Samples were at 5 μM in TA buffer and 2.5-5 μL of this solution was deposited on a freshly cleaved mica surface (ca. 7 x 7 mm) and allowed to adsorb for 1-2 seconds. Then 50 μL of 0.22 μm filtered Millipore water was dropped on the surface and instantly

removed with filter paper. The surface was then washed with a further 200 μ L of water and the excess removed with a strong flow of nitrogen. Samples were dried under vacuum for at least 1 hour prior to imaging.

In vitro Silencing and Viability Assays:

HeLa cells were maintained in 10% FBS and antibiotic/antimycotic (AB/AM) and cultured in 5% CO₂ at 37 °C. Typically, cells were split in 1:4 ratio every 3 days. Luciferase knockdown assays were performed as described by Deleavey et al. (7) with minor modifications. Typically, HeLa cells were counted and seeded at a density of 10 000 cells per well in a 96-well plate. Cells were allowed to recover for 24 hours at 37 °C with 5% CO₂. Then, samples were added to the appropriate well in triplets where Lipofectamine reagent was used as transfection agent and control (Invitrogen) following the vendor's procedure (using Optimem as transfection media mix). Cells were further incubated overnight (for a total of 24-72 hours post-DNA addition). All samples were added in equimolar amounts of ASO strands.

For luciferase assay, cells were washed with PBS 1 \times and lysed with 25 μ l Glo-lysis buffer (Promega) and 25 μ l of Bright-Glo luciferase reagent (Promega, USA) was added to each well. Luminescence was measured using a Biotek Synergy HT plate reader. Data was acquired with the Gen5 software suite and was analyzed and plotted using Graphpad Prism software suite.

For cytotoxicity and cell viability, the cells were incubated with a fluorescent reagent (CellTiter Blue) for 1.5 h in 5% CO₂ at 37 °C. Subsequently, 96-well plates were allowed to equilibrate at room temperature and the fluorescence was measured at 590 nm (Ex. 530, Em. 590) using a BioTek Synergy HT micro-plate reader. All quantifications were done using GraphPad Prism 5 software.

Quantitative polymerase chain reaction (qPCR):

Reverse transcription and subsequent amplification were run in one pot using iTaqTM Universal SYBR Green Supermix. Each reaction used 20ng of RNA, 150nM

of each primer, and had a total volume of 15µL. The relative amount of ApoB mRNA was quantified against the amount of the endogenous control mRNA of GAPDH. The primers used for ApoB and GAPDH and shown in Table 2. The thermal cycling conditions were as follows: 30 sec at 95°C, followed by 40 cycles of 15 s at 95°C, 30 s at 60°C. A negative control (distilled water), and RT-negative controls (no reverse transcriptase) were included in each run. Three independent qPCR reactions (PCR triplicates) were performed. The $\Delta\Delta C_t$ method was used for relative quantification

Gene	Forward	Reverse
ApoB	5'-TTTGCCCTCAACCTACCAAC-3'	5'-TGCGATCTTGTTGGCTACTG-3'
GAPDH	5'-GGAGCGAGATCCCTCCAAAAT-3'	5'-GGCTGTTGTCATACTTCTCATGG-3'

Table 3. 3. primers used RT-qPCR experiment for the APOB in HepG2 cells.

Flow Cytometry:

HeLa cells were seeded at a density of 5×10^5 in a 6-well plate. After 24 hours, the cells were incubated (without transfection) with the corresponding samples at a final concentration of 1 µM for 24 hours as well. Then, cells were detached, washed and resuspended in 1x PBS and processed using FACS FORTESSA. All measurements were performed in doublets.

Serum Stability:

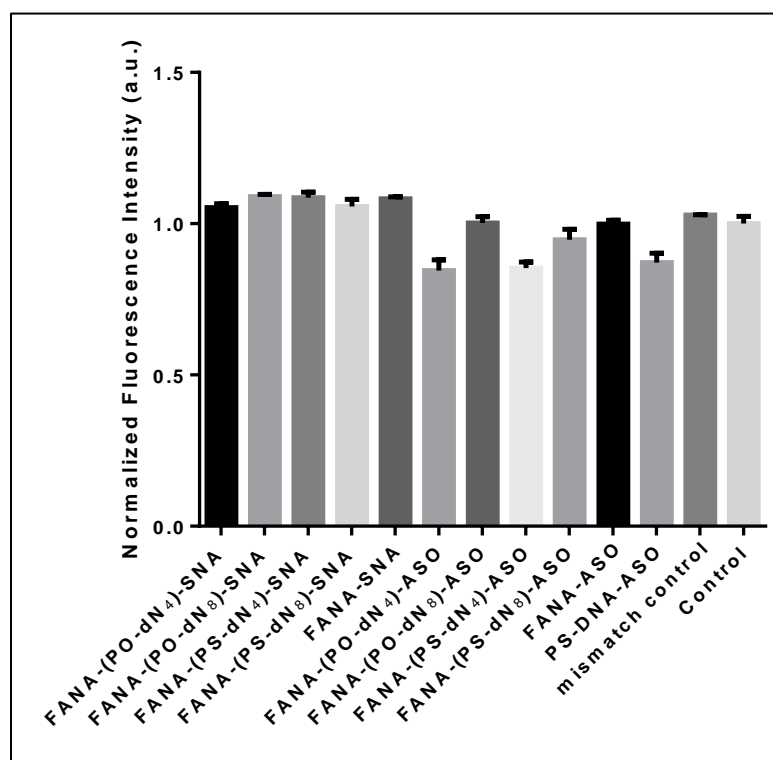
Samples (SNA or strands) were prepared in 1xTAMg buffer. SNA was prepared at 10 µM (in strands) and then diluted with cell culture media (DMEM, 10% FBS, 5%

AB/AM) to a concentration of 2 μM . Samples were incubated at 37 $^{\circ}\text{C}$, and aliquots were taken at different timepoints and frozen until analysis. Aliquots were then treated with proteinase K and resolved on a 15% denaturing (UREA Polyacrylamide) gel to visualize for stability over time. The intensity of the bands was then plotted to visualize the decay over time (x). The equation followed for the plots is:

$$\text{Relative Band intensity}_x = \text{intensity}_x / \text{intensity}_0$$

3.5.6. *Viability assay*

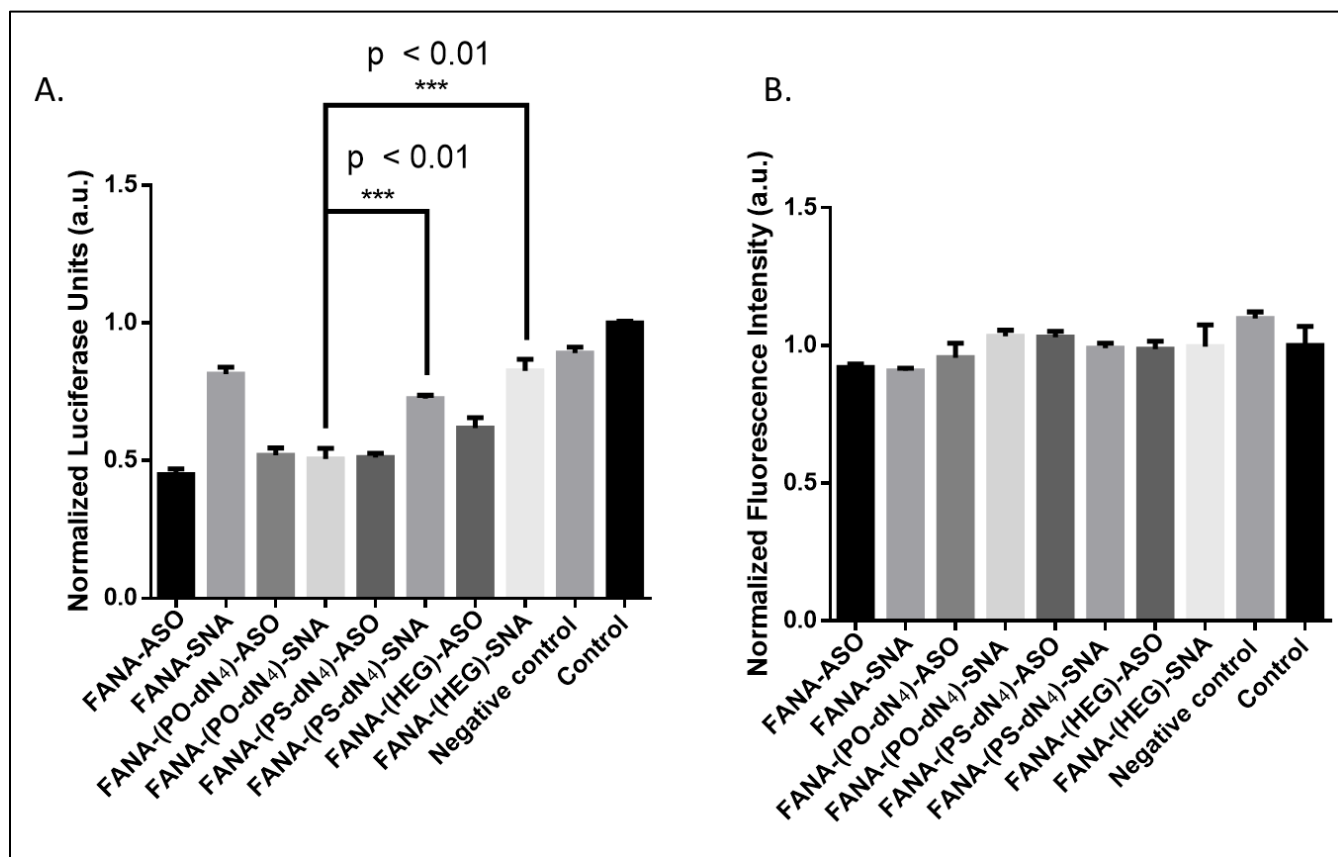
CellTiter-Blue cytotoxicity assay to assess the toxicity of the oligonucleotides used by comparing the metabolic activities of the corresponding cells was done. Results showed no significant toxicity supporting the compatibility and low toxicity of such SNAs and oligos for cell assays. All oligonucleotides were incubated for 24 hours in HeLa cells at a concentration of 150 nM, followed by 1.5-hour incubation with MTT reagent (CellTiter-Blue from Promega).



Supplementary Figure 3. 1. Viability assay data for multiple samples in HeLa cells.

3.5.7. *Testing Hexaethylene glycol as a spacer*

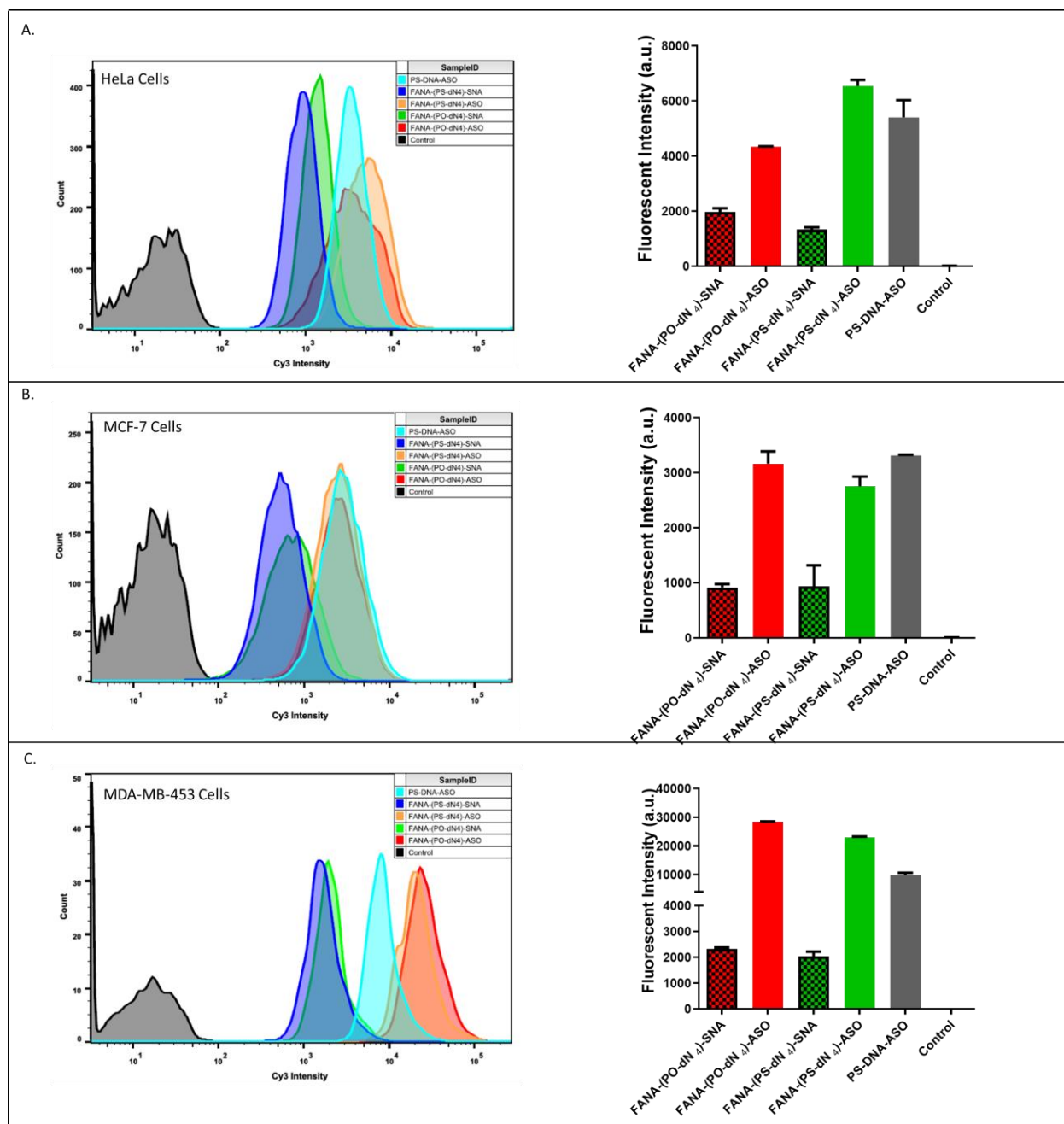
Hexaethylene glycol spacer was used instead of a 4-nucleotide spacer, as another comparison of metabolically non-cleavable linkers. Same experimental conditions were carried out, and the results showed that HEG-spacer SNAs have the same reduced activity compared to mod- (PO-N₄)-SNA.



Supplementary Figure 3. 2. A. Firefly luciferase knockdown activity comparison between various samples normalized to **B.** MTT results and AON-free control. Error bars represent SD for triplets for each sample.

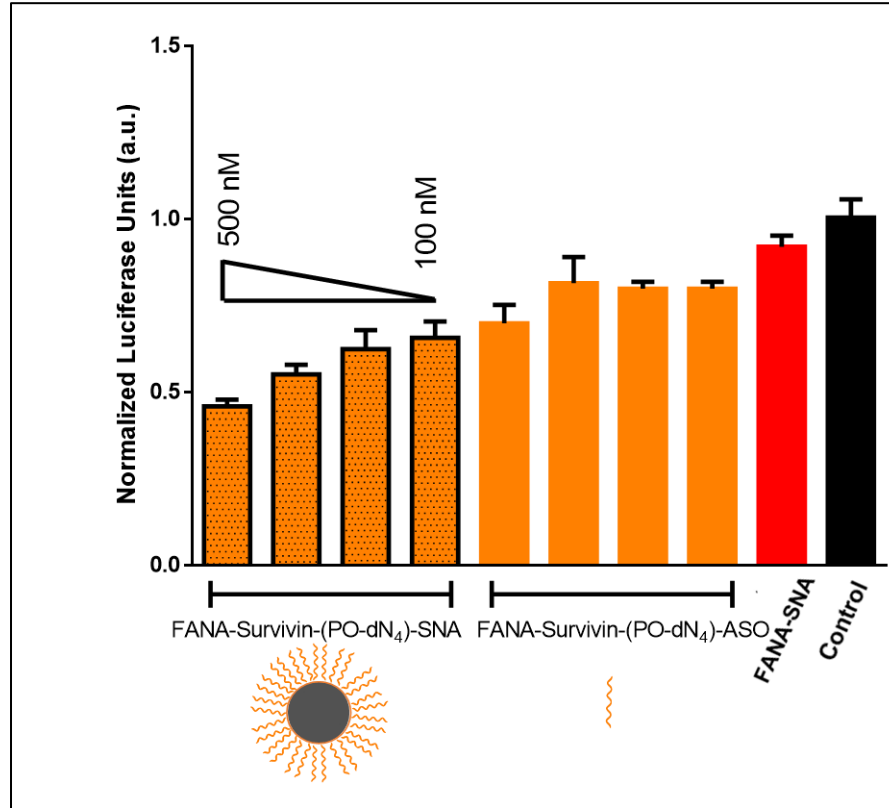
3.5.8. *Flow cytometry uptake assessment of SNAs with different spacers*

To assess if the increased activity of FANA-(PO-dN₄)-SNA is coming from its cleavability or from higher uptake into cells compared to FANA-(PS-dN₄)-SNA, we incubated synthesized both versions with a Cy3 dye (Between the linker and the hydrophobic conjugate) to assess via flow cytometry. Samples were incubated at 0.5 μ M for 24 hours, followed by live flow cytometry assessment for uptake. The experiment was done in three different cell lines: Hela X1/5, MCF-7 and MDA-453 to showcase the uptake of the SNAs in a variety of cell lines. The results show that they both go into cells to the same extent, further supporting the notion that the higher activity is not coming from increased uptake, but rather from its metabolically cleavable nature that aids its release from endosomes.



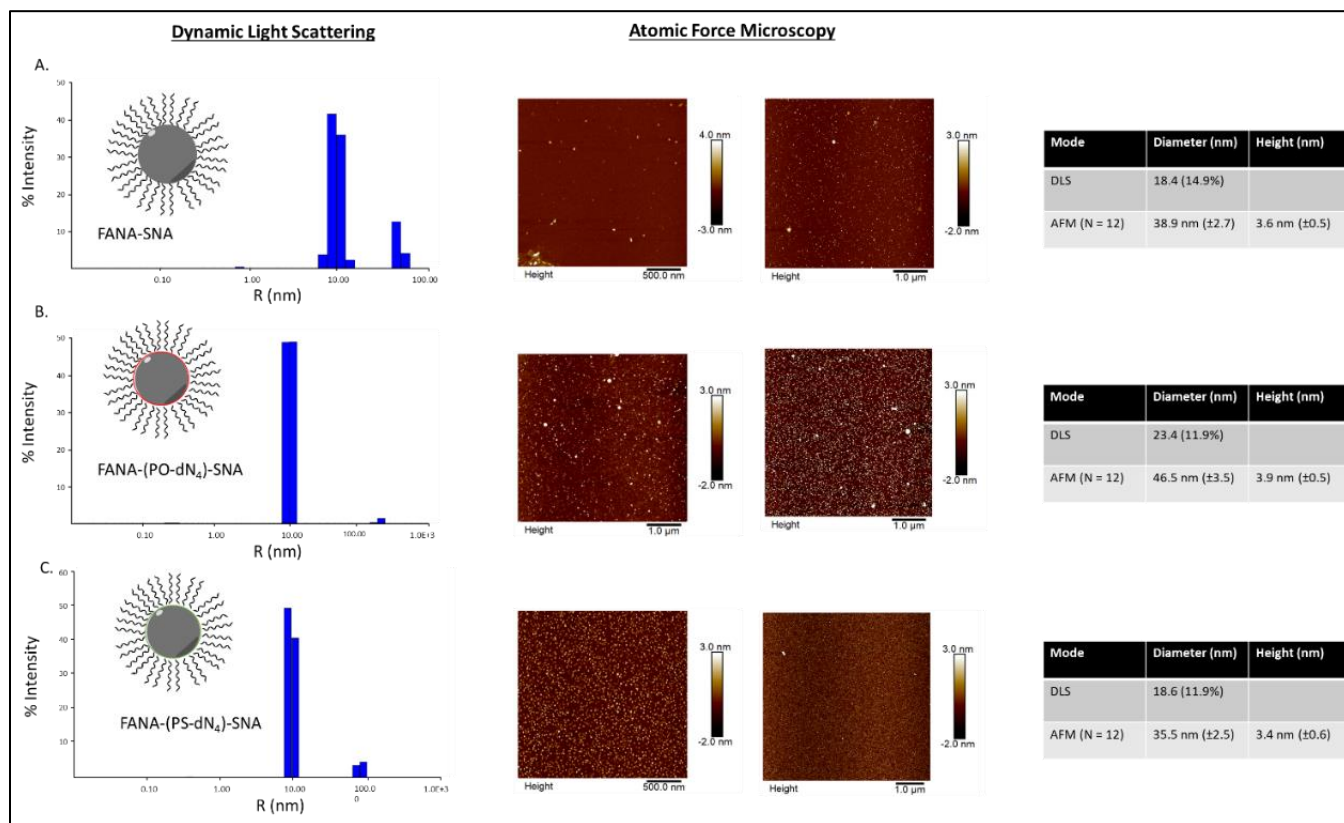
Supplementary Figure 3.3. Flow cytometry experiment to assess the uptake of various samples in different cell lines. Cells were incubated at 0.5 μ M final concentration of sample for 24 hours, followed by detachment and assessment. Samples were made in duplicates. 10,000 cells count was collected for all samples in HeLa and MCF-7 cells, and 1,000 cells count was collected in MDA-453 cells.

3.5.9. *Titration with various concentration of modSurvivin-SNA*



Supplementary Figure 3. 4. CellTiter-Blue cytotoxicity assay at various concentrations of NAT. metabolic activity was measured after 24 h incubation and normalized to AON-free control. Error bars represent SD for triplets for each sample.

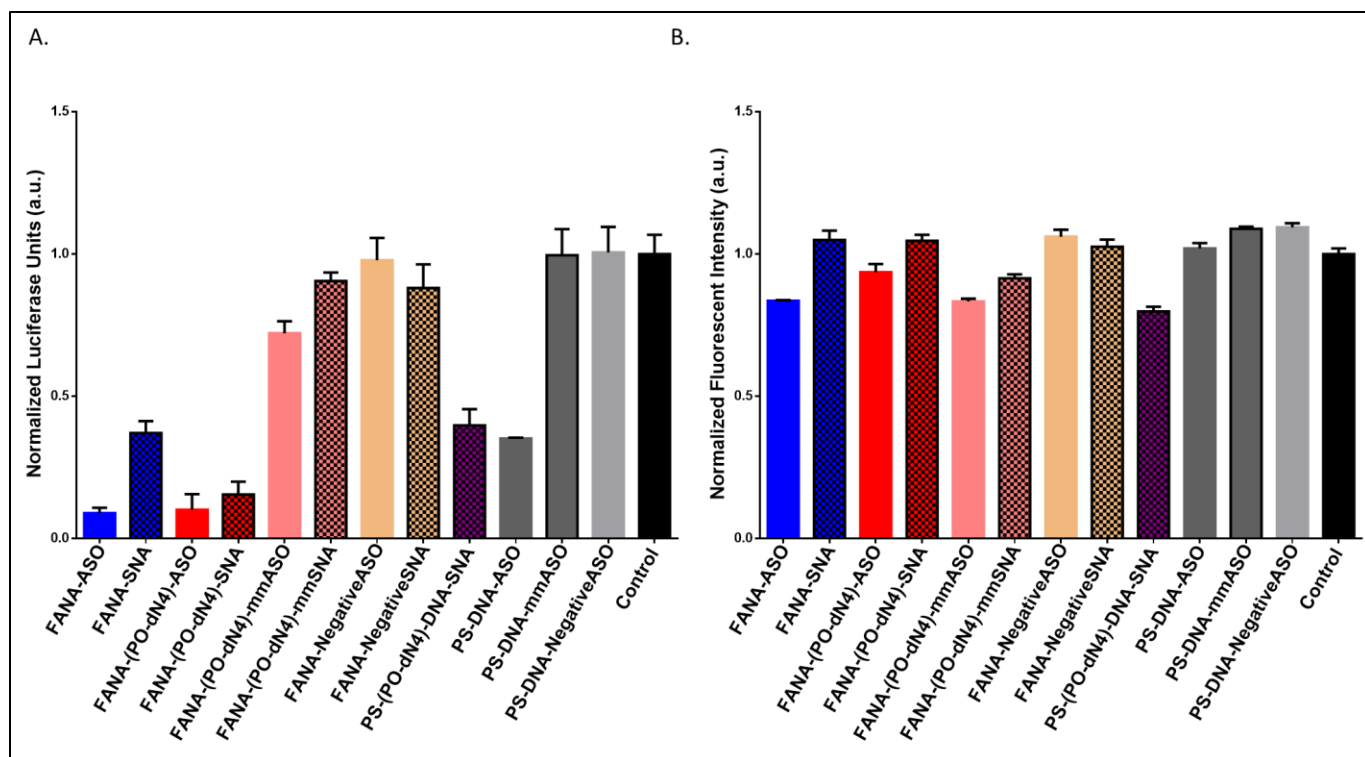
3.5.10. *Characterization of FANA-(PS-dN4)-SNA*



Supplementary Figure 3. 5. Dynamic light scattering and additional atomic force microscopy characterization of A) FANA-SNA (no spacer), B) FANA-(PO-dN₄)-SNA and C) FANA-(PS-dN₄)-SNA.

3.5.11. *Silencing controls*

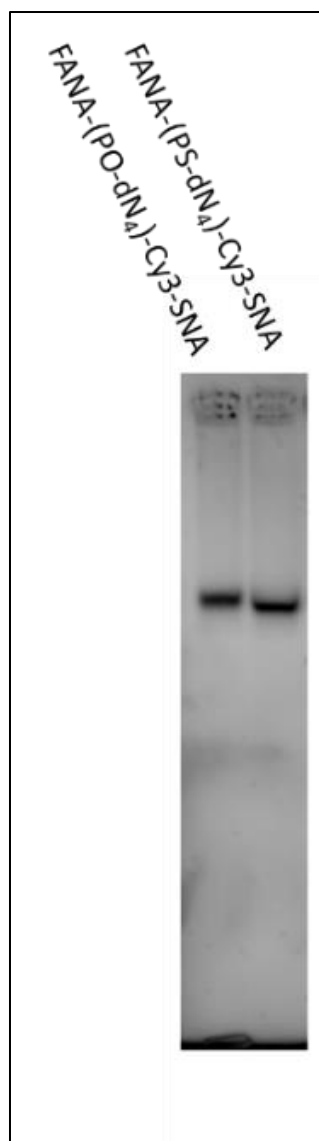
In order to confirm that the silencing activity we are seeing is not due to any cell death or off targeting, we performed a series of controls either as mismatch strands having few mismatched bases, or negative control that has a non-targeting sequence. In both cases, the controls were single stranded ASOs and SNAs, and had FANA modifications. The sequences of each control tested is provided in **Table 3. 1**.



Supplementary Figure 3. 6. Firefly luciferase knockdown activity comparison between various free FANA-ASO and FANA-SNA. **A.** Luciferase activity was measured after 24 h incubation and normalized to CellTiter-Blue and Control (no ASO). **B.** fluorescence measurement of CellTiter-Blue cytotoxicity results normalized to Control (no ASO). Error bars represent SD of triplicate experiments for each sample. ASO final concentration is 150 nM for all samples.

3.5.12. *Agarose gel of SNA assembly*

the below 2.5% agarose gel shows the assembly and mobility of Cy3 modified FANA-(PO-dN₄)-SNA and FANA-(PS-dN₄)-SNA into a tight band with no leftover strands or unconjugated ASO strands.



Supplementary Figure 3. 7. 2.5% agarose gel showing the assembly and mobility of Cy3 modified FANA-(PO-dN4)-SNA and FANA-(PS-dN4)-SNA under cy3 emission. Gel was run at 100V for 1hr45mins in 1xTAMg buffer at 4oC.

3.6. References

- 1 Opalinska, J. B. & Gewirtz, A. M. Nucleic-acid therapeutics: basic principles and recent applications. *Nat Rev Drug Discov* **1**, 503-514, doi:10.1038/nrd837 (2002).
- 2 Blanco, E., Shen, H. & Ferrari, M. Principles of nanoparticle design for overcoming biological barriers to drug delivery. *Nat Biotech* **33**, 941-951, doi:10.1038/nbt.3330 (2015).
- 3 Riley, M. & Vermerris, W. Recent Advances in Nanomaterials for Gene Delivery—A Review. *Nanomaterials* **7**, 94 (2017).
- 4 Deleavey, Glen F. & Damha, Masad J. Designing Chemically Modified Oligonucleotides for Targeted Gene Silencing. *Chemistry & Biology* **19**, 937-954, doi:<https://doi.org/10.1016/j.chembiol.2012.07.011> (2012).
- 5 Kalota, A. *et al.* 2'-Deoxy-2'-fluoro-β- d -arabinonucleic acid (2'F-ANA) modified oligonucleotides (ON) effect highly efficient, and persistent, gene silencing. *Nucleic Acids Research* **34**, 451-461, doi:10.1093/nar/gkj455 (2006).
- 6 Dowler, T. *et al.* Improvements in siRNA properties mediated by 2'-deoxy-2'-fluoro-β- d -arabinonucleic acid (FANA). *Nucleic Acids Research* **34**, 1669-1675, doi:10.1093/nar/gkl033 (2006).
- 7 Deleavey, G. F. *et al.* Synergistic effects between analogs of DNA and RNA improve the potency of siRNA-mediated gene silencing. *Nucleic Acids Research* **38**, 4547-4557, doi:10.1093/nar/gkq181 (2010).
- 8 Min, K.-L., Viazovkina, E., Galarneau, A., Parniak, M. A. & Damha, M. J. Oligonucleotides comprised of alternating 2'-Deoxy-2'-fluoro-β-d-arabinonucleosides and d-2'-deoxyribonucleosides (2'F-ANA/DNA 'Altimers') induce efficient RNA cleavage mediated by RNase H. *Bioorganic & Medicinal Chemistry Letters* **12**, 2651-2654, doi:[https://doi.org/10.1016/S0960-894X\(02\)00439-0](https://doi.org/10.1016/S0960-894X(02)00439-0) (2002).
- 9 Lok, C.-N. *et al.* Potent Gene-Specific Inhibitory Properties of Mixed-Backbone Antisense Oligonucleotides Comprised of 2'-Deoxy-2'-fluoro-d-arabinose and 2'-Deoxyribose Nucleotides. *Biochemistry* **41**, 3457-3467, doi:10.1021/bi0115075 (2002).
- 10 Watts, J. K., Katolik, A., Viladoms, J. & Damha, M. J. Studies on the hydrolytic stability of 2'-fluoroarabinonucleic acid (2'F-ANA). *Organic & Biomolecular Chemistry* **7**, 1904-1910, doi:10.1039/B900443B (2009).
- 11 Takahashi, M. *et al.* Dual Mechanisms of Action of Self-Delivering, Anti-HIV-1 FANA Oligonucleotides as a Potential New Approach to HIV Therapy. *Molecular Therapy - Nucleic Acids* **17**, 615-625, doi:10.1016/j.omtn.2019.07.001 (2019).
- 12 Souleimanian, N. *et al.* Antisense 2'-Deoxy, 2'-Fluoroarabino Nucleic Acids (2'F-ANAs) Oligonucleotides: In Vitro Gymnotic Silencers of Gene Expression Whose Potency Is Enhanced by Fatty Acids. *Mol Ther Nucleic Acids* **1**, e43-e43, doi:10.1038/mtna.2012.35 (2012).
- 13 Schmidt, K. *et al.* Targeting the Oncogenic Long Non-coding RNA *SLNCR1* by Blocking Its Sequence-Specific Binding to the Androgen Receptor. *Cell Reports* **30**, 541-554.e545, doi:10.1016/j.celrep.2019.12.011 (2020).

- 14 Della Valle, F. *et al.* Transdifferentiation of Mouse Embryonic Fibroblasts into Dopaminergic Neurons Reactivates LINE-1 Repetitive Elements. *Stem Cell Reports* **14**, 60-74, doi:10.1016/j.stemcr.2019.12.002 (2020).
- 15 Smaldone, G. *et al.* KCTD15 is overexpressed in human childhood B-cell acute lymphoid leukemia. *Scientific Reports* **9**, 20108, doi:10.1038/s41598-019-56701-7 (2019).
- 16 Takahashi, M. *et al.* Dual Mechanisms of Action of Self-Delivering, Anti-HIV-1 FANA Oligonucleotides as a Potential New Approach to HIV Therapy. *Mol Ther Nucleic Acids* **17**, 615-625, doi:10.1016/j.omtn.2019.07.001 (2019).
- 17 Ganta, S., Devalapally, H., Shahiwala, A. & Amiji, M. A review of stimuli-responsive nanocarriers for drug and gene delivery. *Journal of Controlled Release* **126**, 187-204, doi:<https://doi.org/10.1016/j.jconrel.2007.12.017> (2008).
- 18 Tokatlian, T. & Segura, T. siRNA applications in nanomedicine. *Wiley Interdiscip Rev Nanomed Nanobiotechnol* **2**, 305-315, doi:10.1002/wnan.81 (2010).
- 19 Blanco, E., Shen, H. & Ferrari, M. Principles of nanoparticle design for overcoming biological barriers to drug delivery. *Nat Biotechnol* **33**, 941-951, doi:10.1038/nbt.3330 (2015).
- 20 Weng, Y. *et al.* Improved Nucleic Acid Therapy with Advanced Nanoscale Biotechnology. *Mol Ther Nucleic Acids* **19**, 581-601, doi:10.1016/j.omtn.2019.12.004 (2020).
- 21 GalNAC-siRNA Conjugates: Leading the Way for Delivery of RNAi Therapeutics. *Nucleic Acid Therapeutics* **28**, 109-118, doi:10.1089/nat.2018.0736 (2018).
- 22 Kapadia, C. H., Melamed, J. R. & Day, E. S. Spherical Nucleic Acid Nanoparticles: Therapeutic Potential. *BioDrugs* **32**, 297-309, doi:10.1007/s40259-018-0290-5 (2018).
- 23 Tibbitt, M. W., Dahlman, J. E. & Langer, R. Emerging Frontiers in Drug Delivery. *Journal of the American Chemical Society* **138**, 704-717, doi:10.1021/jacs.5b09974 (2016).
- 24 Peer, D. *et al.* Nanocarriers as an emerging platform for cancer therapy. *Nat Nanotechnol* **2**, 751-760, doi:10.1038/nnano.2007.387 (2007).
- 25 Juliano, R., Alam, M. R., Dixit, V. & Kang, H. Mechanisms and strategies for effective delivery of antisense and siRNA oligonucleotides. *Nucleic Acids Research* **36**, 4158-4171, doi:10.1093/nar/gkn342 (2008).
- 26 Gudipati, S., Zhang, K. & Rouge, J. L. Towards Self-Transfecting Nucleic Acid Nanostructures for Gene Regulation. *Trends in Biotechnology* **37**, 983-994, doi:10.1016/j.tibtech.2019.01.008 (2019).
- 27 Jensen, S. A. *et al.* Spherical nucleic acid nanoparticle conjugates as an RNAi-based therapy for glioblastoma. *Sci Transl Med* **5**, 209ra152, doi:10.1126/scitranslmed.3006839 (2013).
- 28 Lewandowski, K. T. *et al.* Topically Delivered Tumor Necrosis Factor- α -Targeted Gene Regulation for Psoriasis. *J Invest Dermatol* **137**, 2027-2030, doi:10.1016/j.jid.2017.04.027 (2017).

- 29 Edwardson, T. G., Carneiro, K. M., Serpell, C. J. & Sleiman, H. F. An efficient and modular route to sequence-defined polymers appended to DNA. *Angew Chem Int Ed Engl* **53**, 4567-4571, doi:10.1002/anie.201310937 (2014).
- 30 Bousmail, D., Chidchob, P. & Sleiman, H. F. Cyanine-Mediated DNA Nanofiber Growth with Controlled Dimensionality. *Journal of the American Chemical Society* **140**, 9518-9530, doi:10.1021/jacs.8b04157 (2018).
- 31 Edwardson, T. G., Carneiro, K. M., McLaughlin, C. K., Serpell, C. J. & Sleiman, H. F. Site-specific positioning of dendritic alkyl chains on DNA cages enables their geometry-dependent self-assembly. *Nat Chem* **5**, 868-875, doi:10.1038/nchem.1745 (2013).
- 32 Serpell, C. J., Edwardson, T. G. W., Chidchob, P., Carneiro, K. M. M. & Sleiman, H. F. Precision Polymers and 3D DNA Nanostructures: Emergent Assemblies from New Parameter Space. *Journal of the American Chemical Society* **136**, 15767-15774, doi:10.1021/ja509192n (2014).
- 33 Chidchob, P., Edwardson, T. G. W., Serpell, C. J. & Sleiman, H. F. Synergy of Two Assembly Languages in DNA Nanostructures: Self-Assembly of Sequence-Defined Polymers on DNA Cages. *Journal of the American Chemical Society* **138**, 4416-4425, doi:10.1021/jacs.5b12953 (2016).
- 34 Fakhoury, J. J. *et al.* Antisense precision polymer micelles require less poly(ethylenimine) for efficient gene knockdown. *Nanoscale* **7**, 20625-20634, doi:10.1039/C5NR05157F (2015).
- 35 Bousmail, D. *et al.* Precision spherical nucleic acids for delivery of anticancer drugs. *Chemical Science* **8**, 6218-6229, doi:10.1039/C7SC01619K (2017).
- 36 Dore, M. D., Fakhoury, J. J., Lacroix, A. & Sleiman, H. F. Templated synthesis of spherical RNA nanoparticles with gene silencing activity. *Chemical Communications* **54**, 11296-11299, doi:10.1039/C8CC06994H (2018).
- 37 Fakhoury, J. J., Bousmail, D. & Sleiman, H. F. Minimalist Design of a Stimuli-Responsive Spherical Nucleic Acid for Conditional Delivery of Oligonucleotide Therapeutics. *ACS Applied Materials & Interfaces* **11**, 13912-13920, doi:10.1021/acsami.8b18790 (2019).
- 38 Rothmund, P. W. K. Folding DNA to create nanoscale shapes and patterns. *Nature* **440**, 297-302, doi:10.1038/nature04586 (2006).
- 39 Shi, J., Kantoff, P. W., Wooster, R. & Farokhzad, O. C. Cancer nanomedicine: progress, challenges and opportunities. *Nat Rev Cancer* **17**, 20-37, doi:10.1038/nrc.2016.108 (2017).
- 40 de Rochambeau, D., Sun, Y., Barlog, M., Bazzi, H. S. & Sleiman, H. F. Modular Strategy To Expand the Chemical Diversity of DNA and Sequence-Controlled Polymers. *The Journal of Organic Chemistry* **83**, 9774-9786, doi:10.1021/acs.joc.8b01184 (2018).
- 41 Banga, R. J., Chernyak, N., Narayan, S. P., Nguyen, S. T. & Mirkin, C. A. Liposomal Spherical Nucleic Acids. *Journal of the American Chemical Society* **136**, 9866-9869, doi:10.1021/ja504845f (2014).

- 42 Yan, R. *et al.* A NanoFlare-Based Strategy for In Situ Tumor Margin Demarcation and Neoadjuvant Gene/Photothermal Therapy. *Small* **14**, 1802745, doi:10.1002/sml.201802745 (2018).
- 43 Guan, C. *et al.* RNA-Based Immunostimulatory Liposomal Spherical Nucleic Acids as Potent TLR7/8 Modulators. *Small* **14**, e1803284-e1803284, doi:10.1002/sml.201803284 (2018).
- 44 Ferrer, J. R., Wertheim, J. A. & Mirkin, C. A. Dual Toll-Like Receptor Targeting Liposomal Spherical Nucleic Acids. *Bioconjug Chem* **30**, 944-951, doi:10.1021/acs.bioconjchem.9b00047 (2019).
- 45 Wang, S. *et al.* Rational vaccinology with spherical nucleic acids. *Proceedings of the National Academy of Sciences* **116**, 10473-10481, doi:10.1073/pnas.1902805116 (2019).
- 46 Barnaby, S. N. *et al.* Design Considerations for RNA Spherical Nucleic Acids (SNAs). *Bioconjug Chem* **27**, 2124-2131, doi:10.1021/acs.bioconjchem.6b00350 (2016).
- 47 Choi, C. H. J., Hao, L., Narayan, S. P., Auyeung, E. & Mirkin, C. A. Mechanism for the endocytosis of spherical nucleic acid nanoparticle conjugates. *Proceedings of the National Academy of Sciences* **110**, 7625-7630, doi:10.1073/pnas.1305804110 (2013).
- 48 Nemati, H. *et al.* Using siRNA-based spherical nucleic acid nanoparticle conjugates for gene regulation in psoriasis. *Journal of Controlled Release* **268**, 259-268, doi:<https://doi.org/10.1016/j.jconrel.2017.10.034> (2017).
- 49 Fakhri, H. H., Fakhoury, J. J., Bousmail, D. & Sleiman, H. F. Minimalist Design of a Stimuli-Responsive Spherical Nucleic Acid for Conditional Delivery of Oligonucleotide Therapeutics. *ACS Appl Mater Interfaces* **11**, 13912-13920, doi:10.1021/acsami.8b18790 (2019).
- 50 Bousmail, D. *et al.* Precision spherical nucleic acids for delivery of anticancer drugs. *Chem Sci* **8**, 6218-6229, doi:10.1039/c7sc01619k (2017).
- 51 Lacroix, A., Vengut-Climent, E., de Rochambeau, D. & Sleiman, H. F. Uptake and Fate of Fluorescently Labeled DNA Nanostructures in Cellular Environments: A Cautionary Tale. *ACS Central Science* **5**, 882-891, doi:10.1021/acscentsci.9b00174 (2019).
- 52 Lacroix, A., Fakhri, H. H. & Sleiman, H. F. Detailed cellular assessment of albumin-bound oligonucleotides: Increased stability and lower non-specific cell uptake. *Journal of Controlled Release* **324**, 34-46, doi:<https://doi.org/10.1016/j.jconrel.2020.04.020> (2020).
- 53 Olie, R. A. *et al.* A Novel Antisense Oligonucleotide Targeting Survivin Expression Induces Apoptosis and Sensitizes Lung Cancer Cells to Chemotherapy. *Cancer Research* **60**, 2805-2809 (2000).
- 54 Pennati, M., Folini, M. & Zaffaroni, N. Targeting survivin in cancer therapy. *Expert Opinion on Therapeutic Targets* **12**, 463-476, doi:10.1517/14728222.12.4.463 (2008).
- 55 Chan, D. P. Y., Deleavey, G. F., Owen, S. C., Damha, M. J. & Shoichet, M. S. Click conjugated polymeric immuno-nanoparticles for targeted siRNA and antisense oligonucleotide delivery. *Biomaterials* **34**, 8408-8415, doi:<https://doi.org/10.1016/j.biomaterials.2013.07.019> (2013).

- 56 Fakhoury, J. J. *et al.* Antisense precision polymer micelles require less poly(ethylenimine) for efficient gene knockdown. *Nanoscale* **7**, 20625-20634, doi:10.1039/c5nr05157f (2015).
- 57 Rosi, N. L. *et al.* Oligonucleotide-Modified Gold Nanoparticles for Intracellular Gene Regulation. *Science* **312**, 1027-1030, doi:10.1126/science.1125559 (2006).
- 58 Cutler, J. I., Auyeung, E. & Mirkin, C. A. Spherical Nucleic Acids. *Journal of the American Chemical Society* **134**, 1376-1391, doi:10.1021/ja209351u (2012).
- 59 Kusmierz, C. D., Bujold, K. E., Callmann, C. E. & Mirkin, C. A. Defining the Design Parameters for in Vivo Enzyme Delivery Through Protein Spherical Nucleic Acids. *ACS Cent Sci* **6**, 815-822, doi:10.1021/acscentsci.0c00313 (2020).
- 60 Prakash, T. P. *et al.* Fatty acid conjugation enhances potency of antisense oligonucleotides in muscle. *Nucleic Acids Research* **47**, 6029-6044, doi:10.1093/nar/gkz354 (2019).
- 61 Biscans, A. *et al.* The chemical structure and phosphorothioate content of hydrophobically modified siRNAs impact extrahepatic distribution and efficacy. *Nucleic Acids Research*, doi:10.1093/nar/gkaa595 (2020).
- 62 Wada, S. *et al.* Evaluation of the effects of chemically different linkers on hepatic accumulations, cell tropism and gene silencing ability of cholesterol-conjugated antisense oligonucleotides. *Journal of Controlled Release* **226**, 57-65, doi:<https://doi.org/10.1016/j.jconrel.2016.02.007> (2016).
- 63 Lipid Conjugates Enhance Endosomal Release of Antisense Oligonucleotides Into Cells. *Nucleic Acid Therapeutics* **29**, 245-255, doi:10.1089/nat.2019.0794 (2019).
- 64 Xiao, Y., Shi, K., Qu, Y., Chu, B. & Qian, Z. Engineering Nanoparticles for Targeted Delivery of Nucleic Acid Therapeutics in Tumor. *Molecular Therapy - Methods & Clinical Development* **12**, 1-18, doi:<https://doi.org/10.1016/j.omtm.2018.09.002> (2019).

Preface 3

In Chapter 4, we transition from self-assembling DNA conjugates into a new DNA amphiphilic conjugate, produced by the same automated DNA synthesis methods but displaying different properties. The dendritic conjugate (D) has four lipophilic arms and had been previously shown to bind strongly to albumin (nanomolar affinity). This strong, specific, and reversible binding is of interest for NATs, as the protein corona forming around them can influence *in vivo* behavior. Previous cellular studies conducted on the conjugate showed enhanced stability to nucleases and decreased non-specific cellular uptake, as well as lower macrophage sequestration. However, the *in vivo* properties were yet to be investigated, which is pursued in this Chapter. First, systemic biodistribution and gene silencing activity of albumin binding D-siRNA was studied in comparison to a well-studied, non-albumin binding docosanoic (DCA) DCA-siRNA. Activity of the siRNA was not hindered when conjugated to the dendritic conjugate and was comparable to DCA-siRNA in several organs, especially the local injection site (dorsal skin). We followed up by conducting a local injection efficacy study on the D-siRNA, where lung-injected D-siRNA showed enhanced activity in specific cell types in comparison to DCA-siRNA (leukocytes and epithelial cells). This study was carried out at the RNA Therapeutics Institute in MA, USA, as part of a collaboration with Prof. Anastasia Khvorova.

This chapter highlights the potential of producing conjugates using the sequence-controlled method, with high level of control and yield. These conjugates can be designed to have various functionalities, such as assembly in the case of SNAs, or specific protein binding such as the D conjugate. Both approaches can be used to increase the functionality of NATs and improve their properties, inching them closer to clinical application.

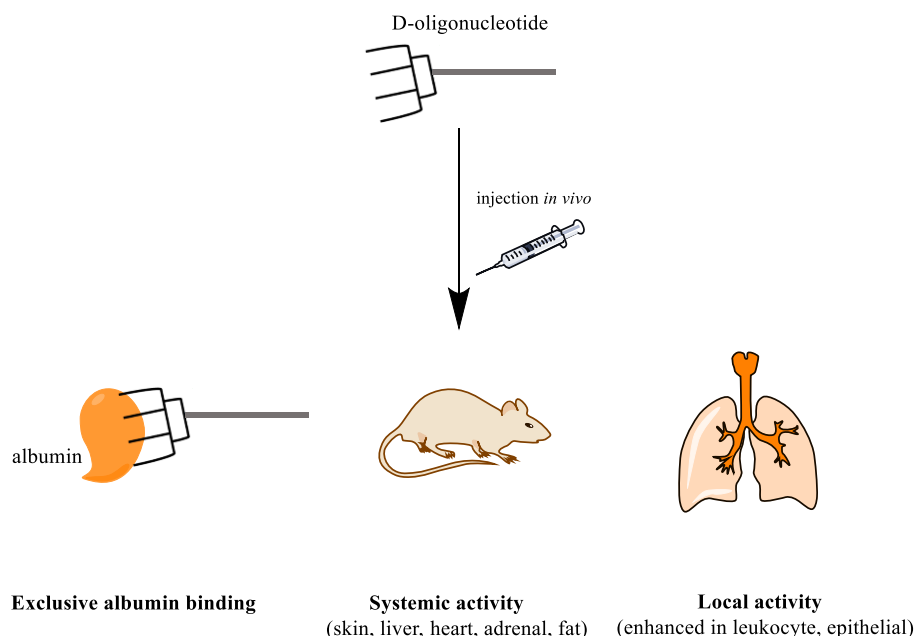


“A tribute to RNA Therapeutics Institute, a home away from home”

*“Science knows no country, because knowledge belongs to humanity,
and is the torch which illuminates the world”*

Louis Pasteur

4 | The *In Vivo* Properties of Albumin-Binding, Dendritic-Lipid Conjugated siRNA



This chapter is a manuscript in preparation titled “Investigating The In Vivo Behavior of Albumin-Binding Dendritic-Nucleic Acids” by Hassan H. Fakih, Qi Tang, Minwook Shin, Dimas Echeverria Aurèlie Lacroix, Jonathan Watts, Anastasia Khvorova and Hanadi F. Sleiman. *Manuscript in preparation*

Contribution of authors

Hassan H. Fakih helped design the project and primarily contributed to production of experimental data from synthesis, purification, characterization, analysis and helped with animal handling (injection, tissue collection, silencing activity and biodistribution). **Qi Tang** did injections in mice, performed microscopy imaging, and supervised/helped in all animal handling and data acquisition and analysis. **Minwook Shin** performed local lung injection experiment and acquired the data using flow cytometry, under the supervision of **Jonathan Watts**, **Hassan** and **Minwook** analyzed the data together. **Dimas Echeverria** and **Aurèlie Lacroix** helped in synthesis and purification of oligonucleotides, as well as discussions about synthesis and results. **Anastasia Khvorova** and **Hanadi F. Sleiman** designed the project, guided interpretation of data and discussion of experiments. **Hassan H. Fakih** and **Hanadi F. Sleiman** co-wrote the manuscript.

4.1. Abstract

The interaction of nucleic acid therapeutics with circulating proteins *in vivo* impacts their pharmacokinetics and pharmacodynamics. Albumin is the most abundant protein in circulation and has been used as a component of numerous drug delivery systems. Binding therapeutics to albumin increase their stability, improves pharmacokinetics, and aids accumulation in tumors due to transcytosis characteristics. Nonetheless, albumin targeting ligands usually suffer from mediocre affinity, difficult synthesis, or aggregation leading to heterogeneity in results as minor design variations have drastic effects. We previously reported the development of a dendritic conjugate (D) that is synthesized and conjugated to oligonucleotides in an automated fashion and has nanomolar affinity towards albumin. The conjugate was able to significantly improve stability to nucleases, decrease macrophage uptake of the therapeutic attached to it, and maintain efficacy *in vitro*. In this work, we study the impact of the dendritic moiety on circulation and efficacy *in vivo*, via systemic and local injections. The D-oligonucleotides eliminated kidney clearance of oligonucleotides, were able to bind albumin exclusively when in circulation, silenced their target in a number of organs when injected systemically, and improved silencing in specific cell types when injected locally. The dendritic conjugate had no apparent toxicity in both modes of injection, further demonstrating the promise of using this conjugate for nucleic acid therapeutics to mimic albumin circulatory properties.

4.2. Introduction

The interaction of therapeutic oligonucleotides with proteins in body fluids has a major influence on their pharmacokinetic and pharmacodynamic properties.^{1,2} This is due to the proteins adhering to the surface of oligonucleotides, which in turn alters the physical properties (charge, size, shape, surface chemistry) that govern biodistribution and behaviour *in vivo*.^{3,4} This has been observed for simple chemical modifications to the sequence of oligonucleotides, such as phosphorothioate (PS) backbone modifications, as well as conjugates and nanoparticles carrying these therapeutics.^{1,3,5} However, the interactions of oligonucleotides with the serum proteins are not specific, which limits our understanding of each protein's role and influence.

Albumin, which accounts to 60% of total protein content in blood and interstitial tissues, is an attractive protein to study, as it has been shown to increase the half-life of therapeutics, improve pharmacokinetics, and aid in the accumulation in solid tumors due to transcytosis properties.⁶ This has led to the use of albumin for various applications, including nucleic acid therapeutics for tumor delivery, vaccine adjuvants as well as improving extravasation to organs.⁷⁻⁹ Binding albumin improves on the biodistribution of the nucleic acid therapeutics, as albumin dictates a longer circulation *in vivo*, improve distribution to organs where albumin resides (interstitial tissues, liver, lung, lymph nodes, tumors), and offers a non-degradative cellular uptake mechanism.¹⁰⁻¹⁴ These are a result of the extended half-life of albumin (around 20 days) which is due to its non-degradative cellular uptake pathway via neonatal Fc receptor (FcRn) that rescues it from degradation in the lysosome and shuttles it back into circulation.^{13,15,16} Albumin has also been used for improve tumor delivery, such as the FDA approved drug Abraxane that is an albumin bound paclitaxel particle with improved delivery and efficacy in tumors in comparison to paclitaxel by itself.¹⁷ This is due to the natural affinity of albumin towards tumors as an energy source, that has been hypothesized to be either via direct digestion of albumin as a source of energy, or provide nutrients via micropinocytosis enhanced by albumin^{13,18,19}. Localization in tumors is also attributed to the transcytosis-based transport of albumin based on its receptor (gp60) and increased secretion of SPARC by tumors, a protein with high affinity to albumin. However, careful design of albumin-binding ligands should be carried, as binding affinity and structure plays an important role in cellular uptake and efficacy as shown in studies done *in vitro*.^{20,21} These studies showed that minor changes in hydrophobic content and albumin-binding affinity via design alterations, can lead to drastic effects on therapeutic efficacy.²⁰ Hence, a strong, selective and carefully designed albumin-binding moieties are attractive modalities to append to nucleic acid therapeutics.

We have previously developed a conjugate, Dendrimer-1 (D), that can be easily synthesized and appended to oligonucleotides in an automated fashion, and binds albumin exclusively with nanomolar affinity ($K_d = 41 \text{ nM}$) (**Error! Reference source not found.**).²² Such specificity in binding to albumin allows us to explore the protein's influence on oligonucleotide's pharmacokinetics/dynamics, and reduces dynamic

exchange between free serum proteins that can alter the desired outcome.²³ We recently also performed a detailed cellular assessment on the impact of D-oligonucleotides, showing that the albumin-binding moiety significantly increases stability of oligonucleotides, decreases non-specific cellular uptake and macrophage sequestering, and does not impact the silencing activity of the therapeutic it carries in cells (both ASO and siRNA).^{22,24} To study the potential of albumin-binding D-oligonucleotides, *in vivo* experiments are vital, as they allow us to assess the native interactions of such constructs with body fluids and proteins in circulation, in a more advanced model than 2D cell culture systems.

In this chapter, we investigate the properties of the high-affinity albumin-binding Dendritic-nucleic acids *in vivo*. We first assess the protein binding profile via size exclusion chromatography using a modified siRNA conjugated to the dendritic moiety once injected into circulation *in vivo*, in comparison to an unconjugated siRNA and a non-albumin binding docosanoic acid (DCA) siRNA compound that has been studied previously.^{25,26} The data showed exclusive binding of D-siRNA to albumin, even after 2 hours post-injection. Then, we studied the distribution and silencing ability of D-siRNAs compared to DCA-siRNA, showing promising efficacy in some organs (namely liver, heart, fat, injections site/back skin). The efficacy in the local injection site (dorsal skin) was particularly enhanced, so we decided further to investigate this via cell-specific assessment. We performed a CD47 silencing study in the lung via intratracheal injection and followed the decrease of production of the protein in various cell-types present in the lung. Surprisingly, the albumin-binding D-siRNAs were tolerated at a high dose of 20 mg/kg whereas mice injected with DCA-siRNA did not survive. Lowering the dose to 5 mg/kg and following the protein expression over 1 and 2 weeks showed enhanced silencing overall using the D-siRNA, as well as in specific cell types (leukocytes, epithelial cells). An initial toxicity screen via blood chemistry and complete blood count also showed no significant alterations, suggesting no noticeable toxicity and promising downstream use of the dendritic conjugate as a therapeutic modality for systemic administration, and in particular local administration as well as cell-type specific diseases.

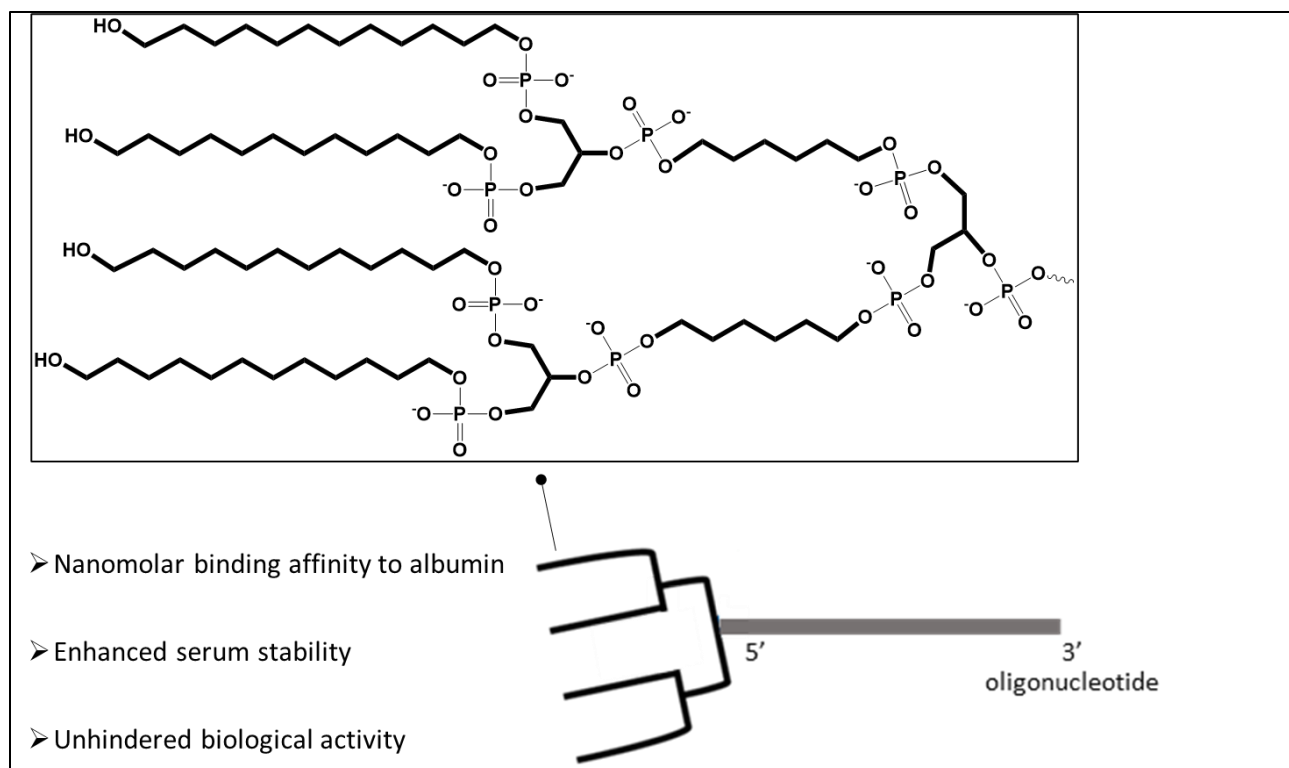


Figure 4. 1. Structure of the dendritic moiety studied, termed "D" for short.

4.3. Materials and methods

4.3.1. Oligonucleotide synthesis

Oligonucleotides were synthesized on a MerMade 6/12 synthesizer (Bioautomation) and AKTA Oligopilot 100 (GE Healthcare Life Sciences) following standard protocols. In brief, conjugated sense strands were synthesized at 5-20 μ mol scales on custom-synthesized lipid-functionalized controlled pore glass (CPG) supports for DCA conjugate.¹⁶⁻¹⁸ For the dendritic sense strand, synthesis was on a CPG functionalized with Unylinker (ChemGenes, Wilmington, MA, USA) and commercially available amidites (Cy3, C6, C12, Hexaethylene glycol and symmetrical branching from Chemgenes and Glen research) were used to build the dendritic moiety as previously described.^{13,15} Antisense strands were synthesized on CPG functionalized with UnyLinker (ChemGenes, Wilmington, MA, USA). They

were first deprotected with a solution of bromotrimethylsilane/pyridine (3:2, v/v) in dichloromethane for the (*E*)-vinylphosphonate deprotection, then cleaved and deprotected with 28% aqueous ammonium hydroxide solution for 20 hours at 60°C. All strands were cleaved and deprotected using 28% aqueous ammonium hydroxide solution for 20 hours at 60°C, followed by drying under vacuum at 60°C, and resuspended in Millipore H₂O. Oligonucleotides were purified using an Agilent Prostar System (Agilent, Santa Clara, CA, USA) over a C18 column for lipid-conjugated sense strands and over an ion-exchange column for antisense strands. Purified oligonucleotides were desalted by size-exclusion chromatography and characterized by liquid chromatography-mass spectrometry (LC/MS) analysis on an Agilent 6530 accurate-mass quadrupole time-of-flight (Q-TOF) LC/MS (Agilent Technologies).

Sequences of the compounds and their modifications are in the table below (#: PS backbone, m: 2'-o-methyl, f: 2'-fluoro, C12: hexaethylene spacer, C6: triethylene spacer, SB: symmetrical branching, V: (*E*)-vinylphosphonate)

Strands	Sequence (5' to 3')
D-sense (HTT targeting)	(C12)(SB)(C6)(SB)(dT)(dT)(mC)#(mA)#(mG)(mU)(fA)(fA)(fA)(mG)(fA)(mG)(mA)(mU)(mU)#(mA)#(mA)
DCA-sense (HTT targeting)	(mC)#(mA)#(mG)(mU)(fA)(fA)(fA)(mG)(fA)(mG)(mA)(mU)(mU)#(mA)#(mA)(dT)(dT)-DCA
Antisense (HTT targeting)	V(mU)#(fU)#(mA)(mA)(mU)(fC)(mU)(mC)(mU)(mU)(mU)(mA)(mC)#(fU)#(mG)#(fA)#(mU)#(mA)#(mU)#(fA)
DCA-NTC-sense (HTT experiment)	(mU)#(mG)#(mA)(mC)(fA)(fA)(fA)(mU)(fA)(mC)(mG)(mA)(mU)#(mU)#(mA)(dT)(dT)-DCA
NTC-antisense (HTT experiment)	V(mU)#(fA)#(mA)(mU)(mC)(fG)(mU)(mA)(mU)(mU)(mU)(mG)(mU)#(fC)#(mA)#(fA)#(mU)#(mC)#(mA)#(fU)
D-sense (CD47 targeting)	(C12)(SB)(C6)(S)(dT)(dT)(mU)#(mC)#(mA)(fC)(mA)(fU)(mA)(fA)(mA)(fU)(mG)(mA)(mU)(fU)#(mA)#(mA)
DCA-sense (CD47 targeting)	(mU)#(mC)#(mA)(fC)(mA)(fU)(mA)(fA)(mA)(fU)(mG)(mA)(mU)(fU)#(mA)#(mA) (dT)(dT)-DCA
Antisense (CD47 targeting)	V(mU)#(fU)#(mA)(fA)(fU)(fC)(mA)(fU)(mU)(fU)(mA)(fU)(mG)(fU)#(mG)#(fA)#(mC)#(mU)#(mU)#(fU)#(mU)
D-NTC-sense (CD47 experiment)	(C12)(SB)(C6)(S)(dT)(dT)(mA)#(mU)#(mU)(fG)(mA)(fC)(mA)(fA)(mA)(fU)(mA)(mC)(mG)(fA)#(mU)#(mA)
NTC-antisense (CD47 experiment)	V(mU)#(fU)#(mA)(fA)(fU)(fC)(mA)(fU)(mU)(fU)(mA)(fU)(mG)(fU)#(mG)#(fA)#(mC)#(mU)#(mU)#(fU)#(mU)
D-sense (protein binding experiment)	(C12)(SB)(C6)(S)-(dT)(dT)(Cy3)#(mU)#(mA)#(mG)(mC)(fU)(fA)(fA)(mU)(fA)(mC)(mU)(mA)(mA)#(mC)#(mA)
DCA-sense (protein binding experiment)	(Cy3)#(mU)#(mA)#(mG)(mC)(fU)(fA)(fA)(mU)(fA)(mC)(mU)(mA)(mA)#(mC)#(mA)(dT)(dT)-DCA
Sense (protein binding experiment)	(Cy3)#(mU)#(mA)#(mG)(mC)(fU)(fA)(fA)(mU)(fA)(mC)(mU)(mA)(mA)#(mC)#(mA)(dT)(dT)
Antisense (protein binding experiment)	V(mU)#(fG)#(mU)(mU)(mA)(fG)(mU)(mA)(mU)(mU)(mA)(mG)(mC)#(fU)#(mA)#(fA)#(mU)#(mG)#(mU)#(fA)

Table 4. 1. Oligonucleotide sequences synthesized and used

4.3.2. Injection of lipid-conjugated siRNAs into mice

Animal experiments of siRNA conjugates were performed in accordance with animal care ethics approval and guidelines of University of Massachusetts Medical School Institutional Animal Care and Use Committee (IACUC; Protocol #202000010) at the RNA therapeutics institute. In all experiments, 7 to 8-week-old female FVB/NJ mice (The Jackson Laboratory) were used and were injected s.c. or i.v. with either non-targeting control siRNA (Ntc), or lipid-conjugated siRNA (n = 5-6 per group) at a concentration of 20mg/kg unless specified.

For distribution studies, 3 mice per sample were injected. For the efficacy studies, 5-8 to mice per sample, per gene were studied. For the toxicity studies, three mice per sample were injected.

4.3.3. In vivo mRNA silencing experiments

At 1-week post-injection, mice were euthanized and perfused with PBS. Tissues were collected and stored in RNAlater (Sigma) at 4°C overnight. mRNA was quantified using the QuantiGene 2.0 Assay (Affymetrix). The 1.5-mm punches (three punches per tissue) were placed in QIAGEN Collection Microtubes holding 3-mm tungsten beads and lysed in 300 µl Homogenizing Buffer (Affymetrix) containing 0.2 mg/ml proteinase K (Invitrogen) using a QIAGEN TissueLyser II. Samples were then centrifuged at 1000 × g for 10 min and incubated for 1 h at 55° to 60°C. Lysates and diluted probe sets (mouse Htt, mouse Ppib or mouse Hprt) were added to the bDNA capture plate and signal was amplified and detected as described previously.¹⁹ Luminescence was detected on a Tecan M1000 (Tecan, Morrisville, NC, USA).

4.3.4. Peptide nucleic acid (PNA) hybridization assay

Tissue concentrations of antisense strands were determined using a peptide nucleic acid (PNA) hybridization assay.²⁷ Tissues punches were placed in QIAGEN Collection Microtubes holding 3-mm tungsten beads and lysed in 300 µl MasterPure tissue lysis solution (EpiCentre) containing 0.2 mg/ml proteinase K (Invitrogen) using a QIAGEN TissueLyser II. Lysates were then centrifuged at 1000 × g for 10

min and incubated for 1 h at 55° to 60°C. Sodium dodecyl sulphate (SDS) was precipitated from lysates by adding 20 µl 3 M potassium chloride and pelleted centrifugation at 5000 × g for 15 min. Conjugated siRNAs in cleared supernatant were hybridized to a Cy3-labeled PNA probe fully complementary to the antisense strand (PNABio, Thousand Oaks, CA, USA). Samples were analyzed by HPLC (Agilent, Santa Clara, CA, USA) over a DNAPac PA100 anion-exchange column (Thermo Fisher Scientific), in a gradient of sodium perchlorate, as follows: Buffer A: 50% water; 50% acetonitrile; 25 mM Tris-HCl, pH 8.5; 1 mM ethylenediaminetetraacetate. Buffer B: 800 mM sodium perchlorate in buffer A. Gradient conditions: 10% buffer B within 4 min, 50% buffer B for 1 min and 50% to 100% buffer B within 5 min. Cy3 fluorescence was monitored and peaks integrated. Final concentrations were ascertained using calibration curves generated by spiking known quantities of lipid-conjugated siRNA into tissue lysates from an untreated animal. Spiked samples for calibration and experimental samples were processed and analyzed under the same laboratory conditions.

4.3.5. *Fluorescence microscopy*

Organs were collected from euthanized mice, washed with PBS, molded with OCT embedding medium and frozen. Frozen sections were cut using Leica Cryostat CM1950 at 5µm thickness, and slides are left to air dry overnight. Then, the slides are hydrated with PBS buffer for 5 mins twice at room temperature, followed by mounting the coverslip on the slides using ProLong™ Gold Antifade Mountant with DAPI staining for nuclei.

4.3.6. *Lipoprotein size exclusion chromatography*

For lipoprotein profiling, we followed the same protocol previously described by Osborne et al.¹⁸ Briefly, mice were injected intravenously with 20 mg/kg of Cy3-labeled oligonucleotides. After 15 minutes, whole mouse blood (~500 µl) was collected in a sterile EDTA-coated tube following cheek incision with a lancet. Samples were spun at 10,000 RPM for 10 minutes at 4°C. 50 µl of plasma was directly injected on Superose 6 Increase 10/300 size exclusion column (GE

Healthcare). Oligonucleotide migration was monitored by Cy3 fluorescence at 570 nm, and lipoprotein protein content was monitored by absorbance at 280 nm.

4.3.7. CD47 protein expression assessment in specific cell-types in the lung via flow cytometry

An enzymatic dissociation solution was prepared with 100 µl of Enzyme D, 15 µl of Enzyme A, 62.5 µl of Enzyme P (Skeletal Muscle Dissociation Kit, Miltenyi Biotec, Bergisch Gladbach, Germany), 250 U/ml Collagenase IV (Worthington, Lakewood, NJ, USA), and 2.3 ml of Dulbecco's Modified Eagle Medium (DMEM, Sigma). Collected mouse lung was dissociated to single-cell suspension using gentleMACS™ C Tubes (Miltenyi Biotec) and a gentleMACS™ Octo Dissociator (Miltenyi Biotec) with the enzymatic dissociation solution. Dissociated cells were filtered through a 70-µm strainer and centrifuged (500 x g, 10 min, 4°C). After discarding the supernatant, red blood cells were lysed using ACK lysis buffer (155 mM NH₄Cl, 12 mM NaHCO₃, 0.1 mM EDTA in DW), followed by washing with DMEM (500 x g, 10 min, 4°C). Next, the cell pellet was suspended with a flow cytometry buffer (0.5% BSA, 2 mM EDTA in DMEM) for flow cytometry analysis. Cells were stained with VioGreen-conjugated CD45 antibody (clone REA737, Miltenyi Biotec), APC-conjugated CD31 antibody (clone REA784, Miltenyi Biotec), FITC-conjugated CD326 antibody (clone REA977, Miltenyi Biotec), PE-Vio770-conjugated CD140a antibody (clone REA637, Miltenyi Biotec), and PE-conjugated CD47 antibody (clone REA170, Miltenyi Biotec) for 30 min at 4°C. Cells were then washed twice with 700 µl of flow cytometry buffer and resuspended in flow cytometry buffer containing 1 µM SYTOX™ Blue (Thermo Fisher Scientific). Stained cells were analyzed using a MACSQuant® VYB Flow Cytometer (Miltenyi Biotec) and data were analyzed using FlowJo software (v10.6, BD Biosciences, Ashland, OR, USA).

4.3.8. Reverse Phase HPLC analysis of D-siRNA vs DCA-siRNA

The LC data of oligonucleotides was performed on an Agilent 6530 accurate mass Q-TOF using the following conditions: buffer A: 100 mM 1,1,1,3,3,3-

hexafluoroisopropanol (HFIP) and 9 mM triethylamine (TEA) in LC–MS grade water; buffer B:100 mM HFIP and 9 mM TEA in LC–MS grade methanol; column, Agilent AdvanceBio oligonucleotides C18; 50-100% B 8min; temperature, 60°C; flow rate, 0.5 ml/min. LC peaks were monitored at 260nm.

4.4. Results

4.4.1. Protein binding profile of dendritic-modified oligonucleotides

We want investigate the serum protein binding properties of D-siRNA by performing a lipoprotein binding profile study via size exclusion chromatography as previously developed by Osborne *et al*²⁸. It was found that the binding profile of a conjugate depends on its hydrophobicity, the more hydrophobic conjugates (such as docosanoic acid, DCA) were found to be bound to low-density and high-density lipoproteins in plasma (LDL and HDL respectively) and not with albumin.²⁸ Even if our dendritic moiety is bigger and has more aliphatic material (69 carbons) compared to DCA (28 carbons), it was found to be less hydrophobic than DCA via reverse-phase HPLC (**Supplementary figure 4. 1.**). This is a result of having multiple phosphates punctuating the structure of the conjugate, which increases its solubility and prevents it from aggregation.

Following the hydrophobicity comparison, we looked at the serum protein binding profile of each conjugate post-injection in mice. Animals were injected intravenously with Cy3-labeled D-siRNA or DCA-siRNA at a dose of 10mg/kg, and plasma was collected 15 mins post-injection. Then, we monitor the retention time of the compounds at 570 nm to associate it with that of the various proteins in the plasma as previously developed.²⁶ Consequently, D-siRNA following injection into mice has a retention time of 66 mins, which is in the range of albumin, compared to DCA-siRNA having a retention time of 57 mins associated with LDL/HDL binding(**Error! Reference source not found.**). Furthermore, collecting plasma samples for 2 hours post injection, still showed albumin association of the remaining D-siRNAs with the

same retention time (66 mins). This shows that even after a few hours in circulation, the dendritic conjugate is still bound to albumin *in vivo* and hasn't gone any protein exchange (other than albumin), indicating its high affinity to albumin that is hypothesized to dictate its behavior *in vivo* as it did *in vitro*. (Chromatograms are included in **Supplementary figure 4. 2.**)

Sample	Peak Retention Time (mins)
Plasma	VLDL = 30-32
	LDL = 48-55
	HDL = 59-62
	Albumin = 64-68
siRNA (in buffer)	72
D-siRNA (in buffer)	70
siRNA (in plasma)	NA
D-siRNA (in plasma, 15 and 120 mins post injection)	66
DCA-siRNA (in plasma)	57

Figure 4. 2. Tabulated retention times of various samples following injection on size exclusion chromatography (SEC). Plasma proteins were monitored at 280 nm and Cy3 labeled oligonucleotides were monitored at 570nm. Plasma samples are collected from mice (n=2) 15 mins after IV injection. Retention times of the various proteins in plasma are assigned as previously demonstrated.²⁸

4.4.2. Assessment of biodistribution and efficacy of D-oligonucleotides

To study the *in vivo* biodistribution and gene silencing efficacy of D-siRNA we performed an extensive study on the localization of D-oligonucleotides and their efficacy in a variety of organs. For that, we conjugated the dendritic moiety to fully chemically modified siRNAs targeting the ubiquitous target Huntingtin (Htt).²⁹

We subcutaneously (dorsal skin) injected female mice with a single dose of 20 mg/kg of either non-targeting NTC-DCA-siRNA, targeting positive control Htt-DCA-siRNA, or albumin binding Htt-D-siRNA. All compounds had a cleavable

(dT)₂ linker between the siRNA and the conjugate for maximum silencing efficacy as previously reported (**Figure 4. 3. A**).^{30,31} Then, mRNA levels of Htt and Hprt (hypoxanthine-guanine phosphoribosyl transferase, a housekeeping gene) were measured 1 week post-injection in a variety of organs (**Figure 4. 3. B**). The data shows significant silencing (compared to NTC) of the albumin-binding siRNA in liver, dorsal skin (injection site, i.s), heart, adrenal glands, and fat.

Interestingly, we performed PNA hybridization assay to quantify the Htt-sense strand from the same experiment to compare the silencing to biodistribution (**Figure 4. 3. C**).³² We found that D-siRNA distributed similarly to all organs as DCA-siRNA, but to higher extent in liver, kidney, and slightly in the lung. This did not fully correlate with silencing data in some organs, for example D-siRNA was more active in the skin but accumulated to the same extent as DCA, whereas comparable silencing is present in the liver where D-siRNA is more localized than DCA-siRNA.

Localization of D-siRNA in the tissues mentioned could be explained by the biosynthesis of albumin in the liver, and its increased circulation in interstitial tissues/spaces of the skin, muscle, lung, heart, kidneys, and spleen.^{10,17,33} apart from the liver, these organs have a continuous endothelium that express gp60 abundantly, which is an albumin-binding glycoprotein that could also explain the localization observed.¹⁶ albumin is also an ample component of lung lining fluids (concentration of about 10% of that found in serum)^{11,14}. This opens up the potential to harness the ability to hijack albumin's biodistribution, to target these organs and environments.

A closer look at the liver distribution, the production site of albumin, was done via fluorescent microscopy imaging of liver tissue, and it showed a more even distribution and hepatocyte uptake of D-siRNAs compared to DCA-siRNAs (**Supplementary figure 4. 3.**). This could be due to the more hydrophobic nature of DCA that leads to its aggregation, as well as the albumin-binding influence on D-siRNA driving its hepatocytic uptake and distribution.^{17,22,24,34}

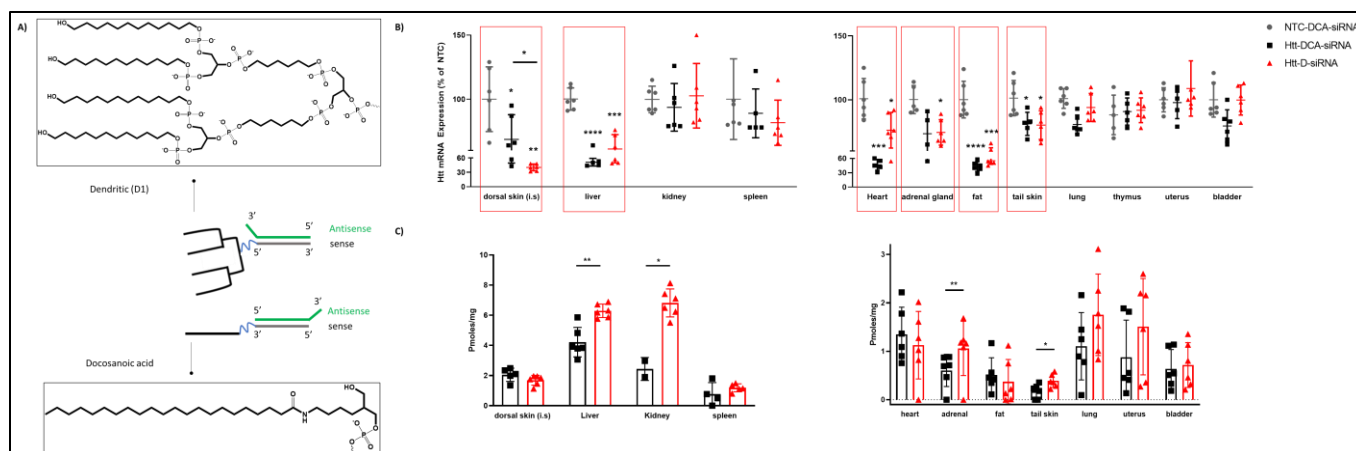


Figure 4. 3. Comparing in vivo silencing activity of the dendritic conjugate to the standard DCA conjugate targeting Htt mRNA in mice. **A.** structure and chemical modification of the compared samples, **B.** measurement of mRNA levels of Huntigton gene in various organs using QuantiGene® (Affymetrix), normalized to a housekeeping gene, Hprt (Hypoxanthine-guanine phosphoribosyl transferase) and presented as percent of NTC control (mean \pm SD) **C.** Bar graph showing accumulation of conjugate siRNA from part B. mRNA levels and siRNA accumulation were from the same experiment, where female mice (20 mg/kg; n = 5–6 mice per group \pm SD) were injected a single subcutaneous injection of each compound and analyzed following 1 week. Data analysis: multiple comparisons = one-way ANOVA, Dunnett test (****p < 0.0001, ***p < 0.001, **p < 0.01, *p < 0.05). n.s., non-significant.

4.4.3. Increase in cell-specific uptake of D-siRNA in local injection site

The D-siRNAs showed a relatively enhanced silencing in the local injection site compared to DCA-siRNA (dorsal skin, **Figure 4. 3. B**), but that does not correlate with the biodistribution as they both localized to the same extent (**Figure 4. 3. C**). We hypothesized that D-siRNAs have increased cellular uptake in local injection site, which is responsible for the enhanced activity. To test this, we designed an experiment where we administered CD47 targeting siRNAs in the lung via intratracheal (IT) injection, followed by antibody-based fluorescent labeling of the various cell types present (leukocytes, endothelial cells, epithelial cells, and fibroblasts).¹ Targeting CD47 via IT injection would serve as a model to study any

¹ Manuscript in preparation Shin, Watts, et. al.

interesting properties of conjugates in local injections, as we are able to do cell-type specific labeling as well as protein silencing measurement.

We first compare the efficacy of CD47 targeting D-siRNAs and DCA-siRNAs at varying doses, 1 week post intratracheal injection: a similar dose to that of systemic administration of 20 mg/kg and a lower dose of 5 mg/kg (**Figure 4. 4.**) Remarkably, mice that were injected with 20 mg/kg DCA-siRNA did not survive whereas those injected with D-siRNA survived and did not demonstrate any signs of distress. Hence, no silencing data was recorded for DCA-siRNA at 20mg/kg dose. For D-siRNA, significant silencing was evident in all cell types, especially in endothelial, epithelial and fibroblasts. At 5 mg/kg dose, both DCA and D-siRNA injected mice were healthy. At that dose over 1 week, D-siRNA had better efficacy than DCA-siRNA in all cell types as well. This indicates that the dendritic conjugate is safer than DCA for lung local injections.

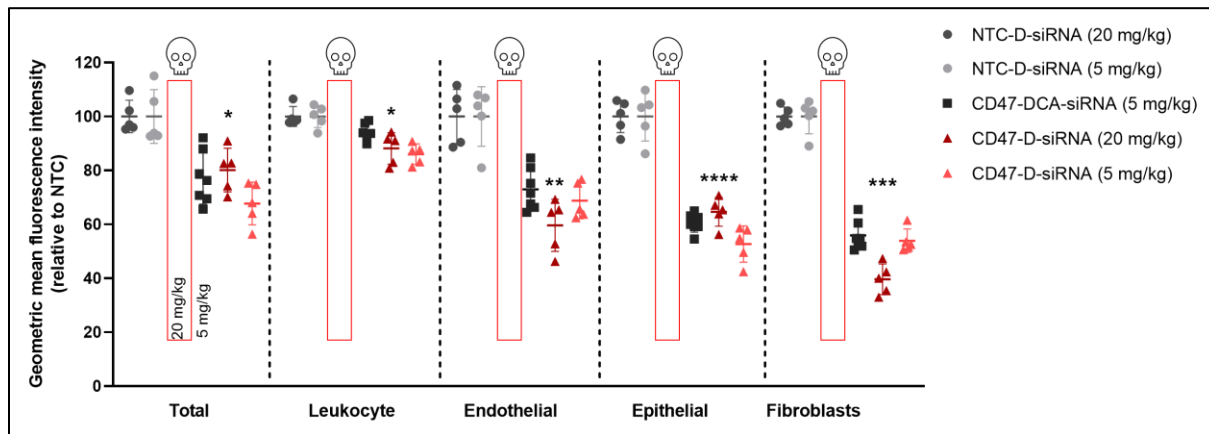


Figure 4. 4. Comparing in vivo silencing activity in local injection site of the dendritic conjugate to the DCA conjugate at 20 and 5 mg/kg doses 1 week post injection. CD47 protein levels in lungs of mice were measured using Flow Cytometry following fluorescent antibody staining. Measurement of CD47 protein levels via fluorescent labeling, normalized to a housekeeping gene, Hprt (Hypoxanthine-guanine phosphoribosyl transferase) and presented as percent of NTC control (mean \pm SD). Female mice (n = 4-8 mice per group \pm SD) were injected a single intratracheal injection of each compound and analyzed. Various cell types were separated by fluorescent antibody tagging and gating. 20 mg/kg DCA-siRNA injected mice did not survive, and no data points are available. Data analysis: multiple comparisons = one-way ANOVA, Dunnett test (****p < 0.0001, ***p < 0.001, **p < 0.01, *p < 0.05). n.s., non-significant. Only 20mg/kg D-siRNA statistical significance from 20mg/kg NTC-D-siRNA is shown (5mg/kg statistics is shown in the next figure).

We then monitored the silencing efficacy of D-siRNA at 5 mg/kg at a longer period of 2-weeks post injection (**Figure 4. 5.**). D-siRNA efficacy significantly improved, with noticeable around 35% silencing in leukocytes, 60% silencing in endothelial cells and 80% silencing in fibroblasts. Interestingly, although we achieve around 55% silencing in epithelial cells, it does not improve at 2-weeks.

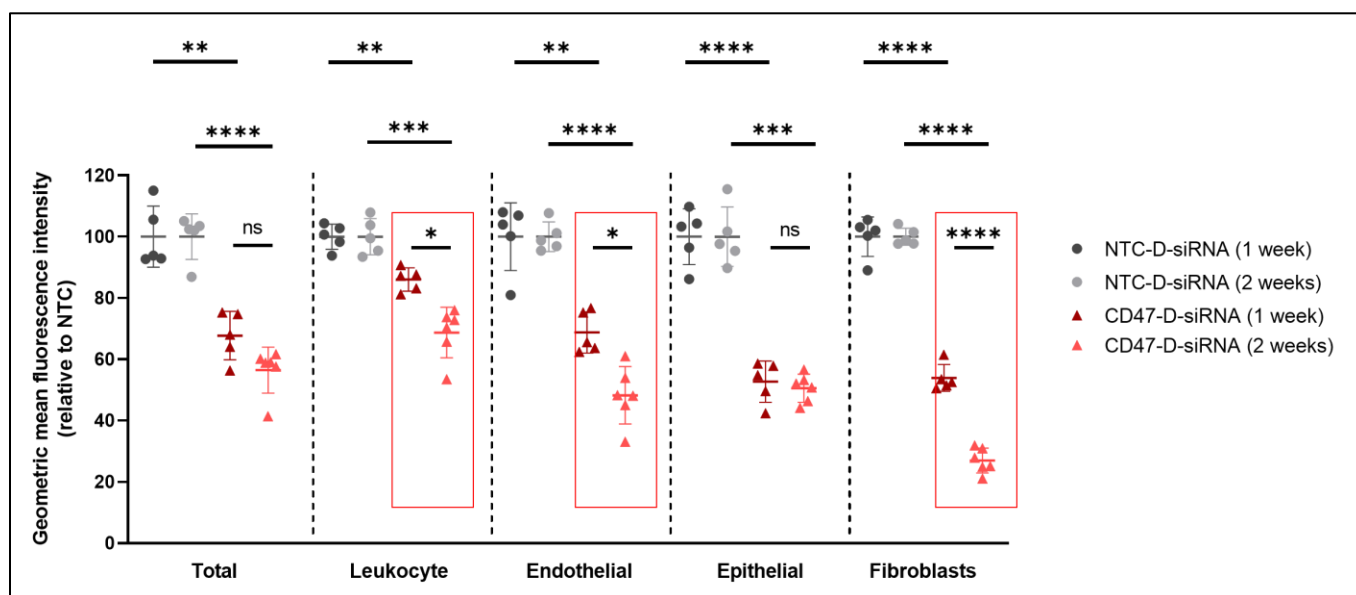


Figure 4. 5. Comparing in vivo silencing activity in local injection site of the dendritic conjugate at various time points post injection (1 week vs 2 weeks). CD47 protein levels in lungs of mice were measured using Flow Cytometry following fluorescent antibody staining. Measurement of CD47 protein levels via fluorescent labeling, normalized to a housekeeping gene, Hprt (Hypoxanthine-guanine phosphoribosyl transferase) and presented as percent of NTC control (mean \pm SD). Female mice (5 mg/kg i; n = 5-8 mice per group \pm SD) were injected a single intratracheal injection of each compound and analyzed following A) 1 week and B) 2 weeks. Various cell types were separated by fluorescent antibody tagging and gating. Data analysis: multiple comparisons = one-way ANOVA, Dunnett test (****p < 0.0001, ***p < 0.001, **p < 0.01, *p < 0.05). n.s., non-significant.

This data could explain the increased local activity we saw earlier in the dorsal skin, where D-siRNAs are able to be up-taken and transcytoses to various cell types as they bind albumin and mimic its biodistribution properties.¹⁰¹⁷ Binding albumin allows the siRNAs to shuttle between tissues and enter cells via non-degradative pathway, that is not otherwise possible with naked siRNAs or other non-albumin specific conjugates.^{16,17,35} the data also showcases the safety of this relatively

hydrophobic dendritic moiety in comparison to the more hydrophobic DCA. Although hydrophobicity can improve biodistribution and activity of therapeutics, tuning such property can lead to various effects. As DCA-siRNAs can aggregate due to their increased hydrophobicity, this could be a reason to their toxicity in sensitive tissues such as the lung.^{26,29}

4.5. Discussion

Harnessing the properties of albumin, such as long circulation half-life and transcytosis, is a promising strategy for nucleic acid therapeutics.^{3,7,17} We have previously developed the dendritic conjugate (D) and showed that it binds albumin in nanomolar affinity *in vitro*, as well as full activity of D-conjugated therapeutics (ASO and siRNA).^{22,24}

We started by confirming that the dendritic conjugate is binding albumin exclusively once injected *in vivo* via the protein binding SEC experiment (**Figure 4. 2.**). This indicates that D-siRNA is expected to bind tightly to albumin and circulate with it in the blood until extravasation into organs and tissues. Our initial data shows that it is still be bound to albumin up to 2 hours. The hydrophobic DCA conjugate was used as a reference to demonstrate that our conjugate is more hydrophilic and avoids binding LDL in plasma. This is due to the phosphates and hydroxyl groups present in D-conjugate that increase its water solubility, even if it is larger in size and has more aliphatic components than DCA. The engineering of hydrophobicity is an interesting direction to improve efficacy, distribution, and safety, which is demonstrated in this work and in our ongoing studies.

We then moved to assessing the silencing activity of D-conjugated oligonucleotides by appending it to fully chemically modified siRNAs that target huntingtin mRNA, to assess its body-wide activity. We compared the silencing activity of D-siRNAs to DCA-siRNAs, a pre-established conjugate in one of our labs that binds to HDL and LDL and has a wide range of silencing in organs. In both instances, D-siRNAs showed comparable

activity to DCA-siRNA, especially in the liver, dorsal skin, adrenal glands, and fat (**Figure 4. 3**). This is the first *in vivo* silencing efficacy we report on the strongly albumin-bound dendritic conjugate, showcasing that indeed it does not hinder *in vivo* silencing ability of oligonucleotides and RISC loading, and is comparable to the state-of-the-art conjugate DCA, which does not bind albumin.^{28,29} It is worth noting that the dendritic conjugate is placed on the 5' end of the sense strand as it is grown via phosphoramidites in sequential and automated fashion, and that the DCA conjugate is placed on the 3' end of the sense strand. This could have role in varying the activity of the siRNA by impacting the loading into RISC, but we believe its impact is minor. This will be something that we will explore in future studies. Nonetheless, our goal in this manuscript of demonstrating that the dendritic conjugate does not hinder efficacious delivery of siRNA was demonstrated, with comparable activity to DCA-siRNA.

PNA hybridization assay to examine the biodistribution of the Htt-siRNA showed interesting results, where D-siRNA was more present in the liver and kidney than DCA but has similar activity (**Figure 4. 3. C**). Interestingly, it also showed similar distribution in the local injection site (dorsal skin) but significantly higher activity for D-siRNA. This indicates that tissue accumulation and silencing efficacy do not always correlate, as has been previously reported.^{29,36} Increased silencing in dorsal skin or liver could be explained by increased cellular uptake into various cell types while having similar total organ accumulation. In other words, organ accumulation itself is not enough to produce activity, as non-degradative cellular uptake is still required. Albumin is known for its transcytosis uptake via gp60 receptor, and endosomal/lysosomal escape following uptake via the neonatal FcRn receptor that rescues it from that environment.^{12,13}

A closer look at the cellular uptake in the liver shows a more evenly distributed uptake of D-siRNAs, compared to a more aggregated distribution of DCA-siRNAs. albumin binding D-siRNAs also show an increased hepatocyte uptake as apparent in the signal associated with tetraploid hepatocytic cells (**Supplementary figure 4. 3**).²⁶

Targeting CD47 protein expression allows us to study if D-siRNAs' increased activity in the local injection site is due to improved and effective cellular uptake in various cell-types present in a specific organ, by performing intratracheal injection in the lung followed by cell-type specific fluorescent labeling and assessment of CD47 protein expression directly. The dendritic conjugate is a much safer conjugate for such lung injections, where at a high dose of 20 mg/kg no distress was observed for D-siRNA injected mice compared to no-survival of those injected with DCA-siRNA (Figure 4). At such dose and a lower dose (5 mg/kg) D-siRNA was able to induce effective gene silencing activity in multiple cell types at 1-week post injection. Monitoring the efficacy of D-siRNA at 5 mg/kg at a longer timepoint (2 weeks) showed significant improvement in efficacy in the leukocytes, endothelial cells and fibroblasts. 55% silencing was also achieved in epithelial cells, a rather challenging target population for NATs.

Silencing in leukocytes, fibroblasts and epithelial cells opens possibilities of using this conjugate for diseases associated with these cell types such as inflammatory diseases, cancer, and chronic obstructive pulmonary disease (**Figure 4. 5**).³⁷⁻⁴¹ The increased uptake into these cells is likely due to the expression of the FcRn receptor that binds albumin in these cells (lung epithelial cells, leukocytes, endothelial cells). It has been shown that the FcRn expression is relatively high and consistent in interstitial macrophages, alveolar macrophages, and endothelial cells, where the receptor is likely responsible for enhancing the efficacious uptake of the albumin-binding dendritic conjugate along with the siRNA attached to it.⁴²⁻⁴⁴

This work gives promise to using D-siRNAs at higher doses for more pronounced silencing over prolonged timepoints in the lung.

4.6. Conclusion

In conclusion, we have tested for the first time the impact of conjugating therapeutics to the strongly albumin-binding dendritic moiety *in vivo*. The data confirms the *in vitro* studies, where the conjugate almost exclusively binds albumin following injection into circulation. The biodistribution profile and activity of D-siRNA was assessed, showing a relatively broad distribution profile when injected systemically with significant gene silencing activity compared to the non-targeting control. Its activity was comparable to the previously studied DCA-siRNA compound, with a better performance in some organs (adrenal, local injection site). Building on the slightly enhanced activity in local injection site but not increased distribution, we investigated the hypothesis that D-siRNAs enter cells to higher extent by performing a cell type-specific silencing following a local injection in the lung. After distinguishing the various cell types in the lung by fluorescent labelling, D-siRNAs improved on the efficacy of the therapeutic 2-weeks post injection, in leukocytes and epithelial cells. The exclusive binding to albumin and enhanced silencing in specific cell types are attractive avenues for the field of therapeutic oligonucleotides, where applications for these properties are currently being pursued. Careful design and engineering of hydrophobic conjugates is an avenue worth exploring to control protein binding and further improve on efficacious delivery and safety.

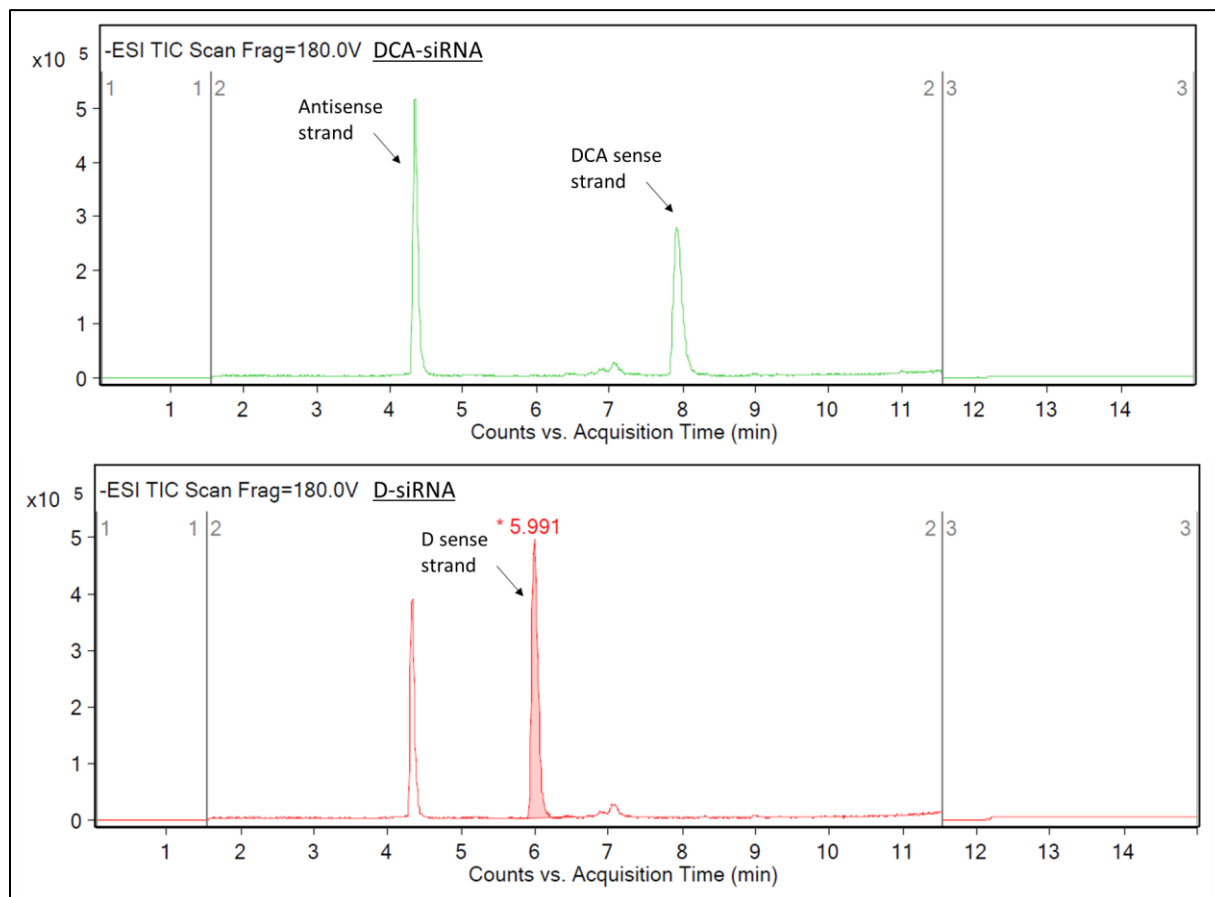
4.7. Acknowledgment

We would like to thank the NSERC CREATE PROMOTE program and QCAM FRQNT international scholarship program, for funding HHF for the exchange visit at UMass Medical School. We also would like to thank Nicholas McHugh and David Cooper for assisting on multiple oligonucleotide synthesis and purification. We thank Mathew Hassler and MaryBeth Dziewietin for facilitating the internship visit. We thank the Natural Sciences and Engineering Research Council of Canada (Discovery and NSERC CREATE Training grant to H. H. F., H. F. S.) and the Canada Research Chairs program.

4.8. Supporting information

4.8.1. *Hydrophobicity difference between D-siRNA and DCA-siRNA*

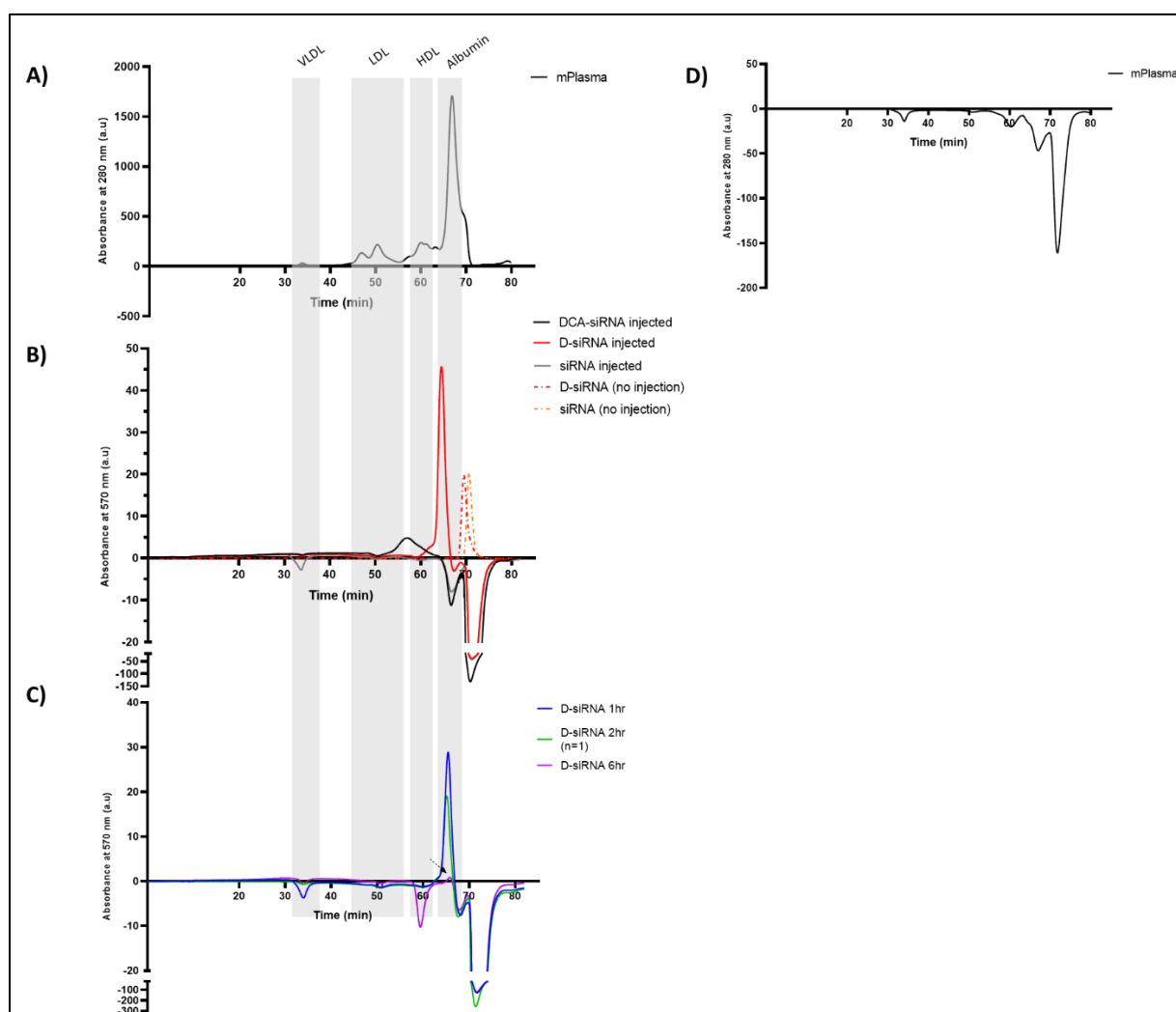
Although D-siRNA has 4 lipid moieties attached to it compared to only one for DCA, the presence of the phosphates mediates this hydrophobicity and makes the dendritic entity water soluble and less hydrophobic/ less susceptible to aggregation than DCA. This is seen here following the injection of two siRNA compounds containing either D or DCA, where D sense strand eluted faster than DCA sense strand.



Supplementary figure 4. 1. Reverse phase HPLC trace following the injection of D-siRNA or DCA-siRNA, showcasing the difference in hydrophobicity between them.

4.8.2. *SEC on mice plasma following injection with conjugated oligonucleotides*

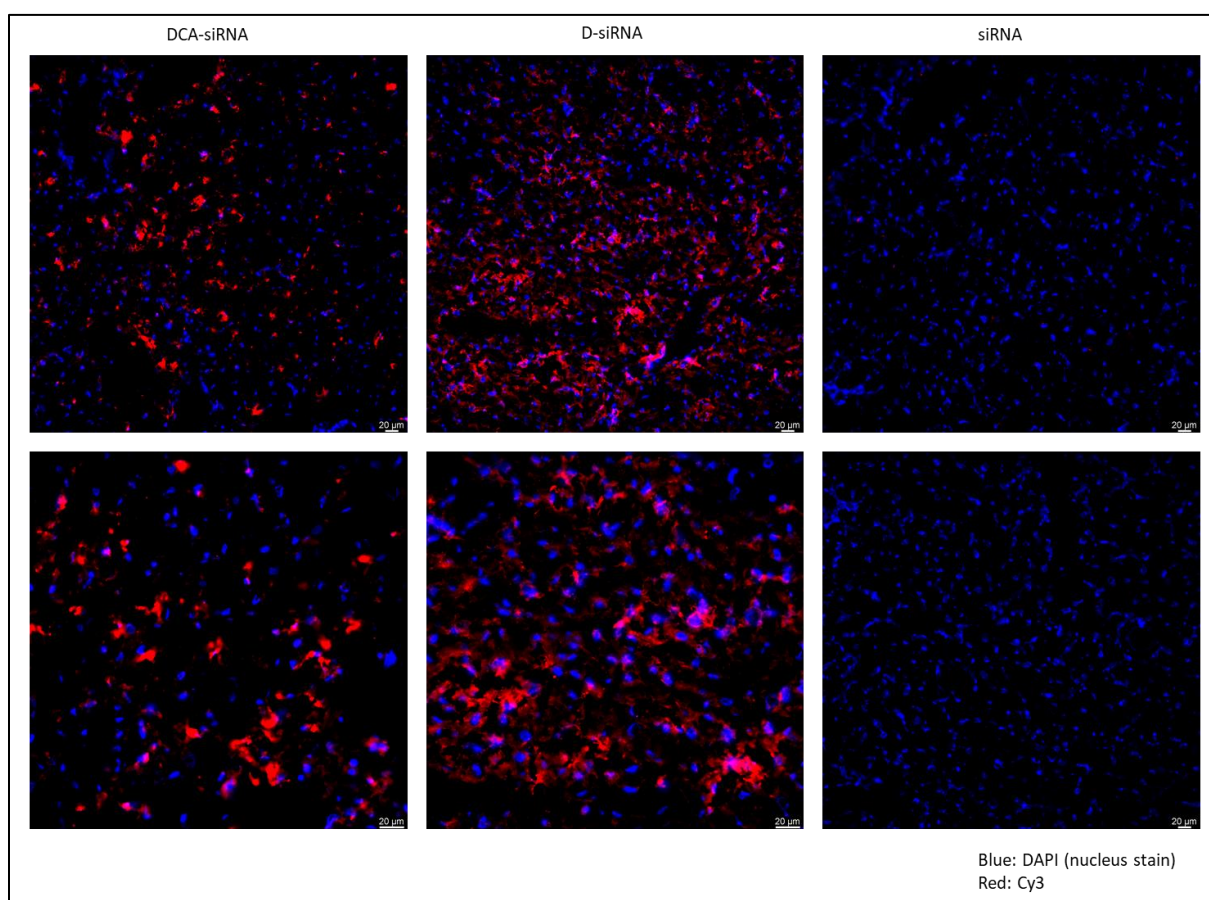
Negative peaks seen on the chromatograms are visible only following the injection of plasma containing samples (not visible for buffer injected samples). This could be due to instrumental error or components that absorb at 570 nm wavelength. Repetition of this experiment is being *planned* where we monitor fluorescence instead of absorbance. Nonetheless, the negative peaks are at the end of each run, and they are coming from samples that contain plasma, where plasma absorbance at 570 shows the negative peaks.



Supplementary figure 4. 2. Chromatograms from size exclusion chromatography of plasma from mice that were injected with various conjugates (n = 2, 15 mins post i.v. injection) where proteins were monitored at 280 nm and Cy3-oligonucleotides at 570 nm.

4.8.3. *Liver tissue imaging of DCA-siRNA and D-siRNA*

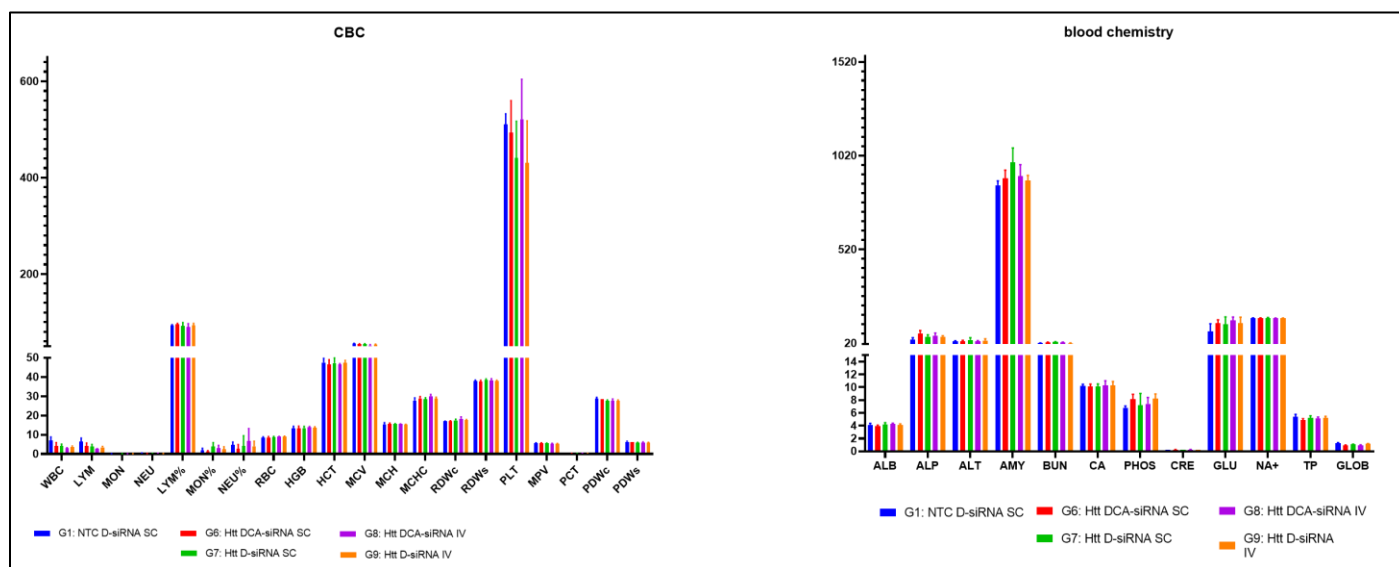
Female mice were subcutaneously injected with a 10mg/kg single dose of either Cy3-labeled DCA, D, or no conjugate siRNA. After 48 hours, mice livers were collected, and tissues of the liver were imaged under a brightfield microscope following nucleus DAPI staining. The images and their close-up (bottom row) show a more evenly distributed uptake for D-siRNA, with evident uptake in tetraploid hepatocytes (large nuclei) in comparison to DCA-siRNA that showed a less even distribution and no signal for non-conjugated siRNA.



Supplementary figure 4. 3. Microscopy images of Liver tissue to get a closer look at the liver delivery differences between DCA-siRNA and D-siRNA. Female mice (10 mg/kg; n = 2 mice per group) were injected with a single subcutaneous injection of each Cy3 labeled compound, and livers were collected after 48 hours. Bottom row is a zoom in image of the upper row. Blue = DAPI nucleus staining, Red = Cy3 fluorescence signal. A more even distribution and cellular uptake is seen for D-siRNA, with evident uptake in hepatocytes (tetrapod large nuclei by DAPI staining)

4.8.4. *Preliminary toxicity screening of D-siRNA*

A preliminary toxicity screening of the D-siRNA conjugate in comparison to the previously assessed DCA-siRNA via CBC and blood chemistry assessment was performed following 1-week post-injection subcutaneously and intravenously at a 20mg/kg dose^{29,41}. The data show no significant changes to any of the parameters tested, indicating similar safety to that of the DCA conjugate.



Supplementary figure 4. 4. Initial toxicity screening of D-siRNA via CBC and blood chemistry counts, showing no significant changes in any reading in comparison to DCA-siRNA. Female mice (n=3) were injected with one dose of siRNA (20mg/kg) and blood was collected after 1 week for analysis. Units of the data plotted is included in the table below, as it varies with each parameter measured.

WBC	LYM	MON	NEU	LYM%	MON%	NEU%	RBC	HGB	HCT	MCV	MCH	MCHC	RDWc	RDWs	PLT	MPV	PCT	PDWc	PDWs
10 ⁹ /l	10 ⁹ /l	10 ⁹ /l	10 ⁹ /l	%	%	%	10 ¹² /l	g/dl	%	fl	pg	g/dl	%	fl	10 ⁹ /l	fl	%	%	fl
ALB	ALP	ALT	AMY	TBIL	BUN	CA	PHOS	CRE	GLU	NA+	K+	TP	GLOB						
g/dL	U/L	U/L	U/L	mg/dL	mg/dL	mg/dL	mg/dL	mg/dL	mg/dL	mmol/dL	mmol/dL	g/dL	g/dL						

4.9. References

- 1 Nguyen, V. H. & Lee, B.-J. Protein corona: a new approach for nanomedicine design. *Int J Nanomedicine* **12**, 3137-3151, doi:10.2147/IJN.S129300 (2017).
- 2 Banker, M. J. & Clark, T. H. Plasma/serum protein binding determinations. *Curr Drug Metab* **9**, 854-859, doi:10.2174/138920008786485065 (2008).
- 3 Zhao, Z., Ukidve, A., Krishnan, V. & Mitragotri, S. Effect of physicochemical and surface properties on in vivo fate of drug nanocarriers. *Advanced Drug Delivery Reviews* **143**, 3-21, doi:<https://doi.org/10.1016/j.addr.2019.01.002> (2019).
- 4 Albanese, A., Tang, P. S. & Chan, W. C. W. The Effect of Nanoparticle Size, Shape, and Surface Chemistry on Biological Systems. *Annual Review of Biomedical Engineering* **14**, 1-16, doi:10.1146/annurev-bioeng-071811-150124 (2012).
- 5 Eckstein, F. Phosphorothioates, essential components of therapeutic oligonucleotides. *Nucleic Acid Ther* **24**, 374-387, doi:10.1089/nat.2014.0506 (2014).
- 6 Kratz, F. Albumin as a drug carrier: design of prodrugs, drug conjugates and nanoparticles. *J Control Release* **132**, 171-183, doi:10.1016/j.jconrel.2008.05.010 (2008).
- 7 Sarett, S. M. *et al.* Lipophilic siRNA targets albumin in situ and promotes bioavailability, tumor penetration, and carrier-free gene silencing. *Proceedings of the National Academy of Sciences* **114**, E6490-E6497, doi:10.1073/pnas.1621240114 (2017).
- 8 Liu, H. *et al.* Structure-based programming of lymph-node targeting in molecular vaccines. *Nature* **507**, 519-522, doi:10.1038/nature12978 (2014).
- 9 Lau, S. *et al.* Enhanced Extravasation, Stability and in Vivo Cardiac Gene Silencing via in Situ siRNA–Albumin Conjugation. *Molecular Pharmaceutics* **9**, 71-80, doi:10.1021/mp2002522 (2012).
- 10 Lomis, N. *et al.* Albumin Nanoparticle Formulation for Heart-Targeted Drug Delivery: In Vivo Assessment of Congestive Heart Failure. *Pharmaceuticals (Basel)* **14**, doi:10.3390/ph14070697 (2021).
- 11 Woods, A. *et al.* In vivo biocompatibility, clearance, and biodistribution of albumin vehicles for pulmonary drug delivery. *Journal of controlled release : official journal of the Controlled Release Society* **210**, 1-9, doi:10.1016/j.jconrel.2015.05.269 (2015).
- 12 Malhotra, A. & Mittal, B. R. SiRNA gene therapy using albumin as a carrier. *Pharmacogenetics and Genomics* **24** (2014).
- 13 Merlot, A. M., Kalinowski, D. S. & Richardson, D. R. Unraveling the mysteries of serum albumin-more than just a serum protein. *Front Physiol* **5**, 299-299, doi:10.3389/fphys.2014.00299 (2014).
- 14 John, T. A. *et al.* Evidence for the role of alveolar epithelial gp60 in active transalveolar albumin transport in the rat lung. *The Journal of Physiology* **533**, 547-559 (2001).
- 15 Andersen, J. T. & Sandlie, I. The versatile MHC class I-related FcRn protects IgG and albumin from degradation: implications for development of new diagnostics and therapeutics. *Drug metabolism and pharmacokinetics* **24**, 318-332 (2009).

- 16 Schnitzer, J. E. gp60 is an albumin-binding glycoprotein expressed by continuous endothelium involved in albumin transcytosis. *American Journal of Physiology-Heart and Circulatory Physiology* **262**, H246-H254, doi:10.1152/ajpheart.1992.262.1.H246 (1992).
- 17 Hoogenboezem, E. N. & Duvall, C. L. Harnessing albumin as a carrier for cancer therapies. *Advanced Drug Delivery Reviews* **130**, 73-89, doi:<https://doi.org/10.1016/j.addr.2018.07.011> (2018).
- 18 Commisso, C. *et al.* Macropinocytosis of protein is an amino acid supply route in Ras-transformed cells. *Nature* **497**, 633-637, doi:10.1038/nature12138 (2013).
- 19 Stehle, G. *et al.* Plasma protein (albumin) catabolism by the tumor itself--implications for tumor metabolism and the genesis of cachexia. *Crit Rev Oncol Hematol* **26**, 77-100, doi:10.1016/s1040-8428(97)00015-2 (1997).
- 20 Purdie, L., Alexander, C., Spain, S. G. & Magnusson, J. P. Alkyl-Modified Oligonucleotides as Intercalating Vehicles for Doxorubicin Uptake via Albumin Binding. *Molecular Pharmaceutics* **15**, 437-446, doi:10.1021/acs.molpharmaceut.7b00805 (2018).
- 21 Felber, A. E. *et al.* The interactions of amphiphilic antisense oligonucleotides with serum proteins and their effects on in vitro silencing activity. *Biomaterials* **33**, 5955-5965, doi:<https://doi.org/10.1016/j.biomaterials.2012.05.019> (2012).
- 22 Lacroix, A., Edwardson, T. G. W., Hancock, M. A., Dore, M. D. & Sleiman, H. F. Development of DNA Nanostructures for High-Affinity Binding to Human Serum Albumin. *Journal of the American Chemical Society* **139**, 7355-7362, doi:10.1021/jacs.7b02917 (2017).
- 23 Monopoli, M. P., Åberg, C., Salvati, A. & Dawson, K. A. Biomolecular coronas provide the biological identity of nanosized materials. *Nature Nanotechnology* **7**, 779-786, doi:10.1038/nnano.2012.207 (2012).
- 24 Lacroix, A., Fakih, H. H. & Sleiman, H. F. Detailed cellular assessment of albumin-bound oligonucleotides: Increased stability and lower non-specific cell uptake. *Journal of Controlled Release* **324**, 34-46, doi:<https://doi.org/10.1016/j.jconrel.2020.04.020> (2020).
- 25 Biscans, A. *et al.* Docosanoic acid conjugation to siRNA enables functional and safe delivery to skeletal and cardiac muscles. *Molecular Therapy* **29**, doi:10.1016/j.ymthe.2020.12.023 (2020).
- 26 Osborn, M. F. *et al.* Hydrophobicity drives the systemic distribution of lipid-conjugated siRNAs via lipid transport pathways. *Nucleic Acids Res* **47**, 1070-1081, doi:10.1093/nar/gky1232 (2019).
- 27 Godinho, B. M. D. C. *et al.* Pharmacokinetic Profiling of Conjugated Therapeutic Oligonucleotides: A High-Throughput Method Based Upon Serial Blood Microsampling Coupled to Peptide Nucleic Acid Hybridization Assay. *Nucleic Acid Therapeutics* **27**, doi:10.1089/nat.2017.0690 (2017).
- 28 Osborn, M. F. *et al.* Hydrophobicity drives the systemic distribution of lipid-conjugated siRNAs via lipid transport pathways. *Nucleic Acids Research* **47**, 1070-1081, doi:10.1093/nar/gky1232 (2018).

- 29 Biscans, A. *et al.* Diverse lipid conjugates for functional extra-hepatic siRNA delivery in vivo. *Nucleic Acids Research* **47**, 1082-1096, doi:10.1093/nar/gky1239 (2018).
- 30 Biscans, A. *et al.* The chemical structure and phosphorothioate content of hydrophobically modified siRNAs impact extrahepatic distribution and efficacy. *Nucleic Acids Research* **48**, 7665-7680, doi:10.1093/nar/gkaa595 (2020).
- 31 Fakih, H. H. *et al.* Design and enhanced gene silencing activity of spherical 2'-fluoroarabinose nucleic acids (FANA-SNAs). *Chemical Science* **12**, 2993-3003, doi:10.1039/D0SC06645A (2021).
- 32 Pharmacokinetic Profiling of Conjugated Therapeutic Oligonucleotides: A High-Throughput Method Based Upon Serial Blood Microsampling Coupled to Peptide Nucleic Acid Hybridization Assay. *Nucleic Acid Therapeutics* **27**, 323-334, doi:10.1089/nat.2017.0690 (2017).
- 33 Sand, K. M. K. *et al.* Unraveling the Interaction between FcRn and Albumin: Opportunities for Design of Albumin-Based Therapeutics. *Frontiers in Immunology* **5**, doi:10.3389/fimmu.2014.00682 (2015).
- 34 Tayyab, S. & Feroz, S. R. in *Advances in Protein Chemistry and Structural Biology* Vol. 123 (ed Rossen Donev) 193-218 (Academic Press, 2021).
- 35 Kuhlmann, M. *et al.* An Albumin-Oligonucleotide Assembly for Potential Combinatorial Drug Delivery and Half-Life Extension Applications. *Molecular Therapy - Nucleic Acids* **9**, 284-293, doi:<https://doi.org/10.1016/j.omtn.2017.10.004> (2017).
- 36 Ly, S., Echeverria, D., Sousa, J. & Khvorova, A. Single-Stranded Phosphorothioated Regions Enhance Cellular Uptake of Cholesterol-Conjugated siRNA but Not Silencing Efficacy. *Molecular Therapy - Nucleic Acids* **21**, 991-1005, doi:<https://doi.org/10.1016/j.omtn.2020.07.029> (2020).
- 37 Kelly, C. *et al.* Therapeutic Aerosol Bioengineering of siRNA for the Treatment of Inflammatory Lung Disease by TNF α Gene Silencing in Macrophages. *Molecular Pharmaceutics* **11**, 4270-4279, doi:10.1021/mp500473d (2014).
- 38 Dua, K. *et al.* The potential of siRNA based drug delivery in respiratory disorders: Recent advances and progress. *Drug Development Research* **80**, 714-730, doi:<https://doi.org/10.1002/ddr.21571> (2019).
- 39 Mei, D., Tan, W. S. D., Tay, Y., Mukhopadhyay, A. & Wong, W. S. F. Therapeutic RNA Strategies for Chronic Obstructive Pulmonary Disease. *Trends in Pharmacological Sciences* **41**, 475-486, doi:<https://doi.org/10.1016/j.tips.2020.04.007> (2020).
- 40 Spella, M., Lilis, I. & Stathopoulos, G. T. Shared epithelial pathways to lung repair and disease. *European Respiratory Review* **26**, 170048, doi:10.1183/16000617.0048-2017 (2017).
- 41 Biscans, A. *et al.* Docosanoic acid conjugation to siRNA enables functional and safe delivery to skeletal and cardiac muscles. *Molecular Therapy* **29**, 1382-1394, doi:<https://doi.org/10.1016/j.ymthe.2020.12.023> (2021).

- 42 Bequignon, E. *et al.* FcRn-Dependent Transcytosis of Monoclonal Antibody in Human Nasal Epithelial Cells In Vitro: A Prerequisite for a New Delivery Route for Therapy? *Int J Mol Sci* **20**, doi:10.3390/ijms20061379 (2019).
- 43 Latvala, S., Jacobsen, B., Otteneder, M. B., Herrmann, A. & Kronenberg, S. Distribution of FcRn Across Species and Tissues. *J Histochem Cytochem* **65**, 321-333, doi:10.1369/0022155417705095 (2017).
- 44 Bern, M., Sand, K. M. K., Nilsen, J., Sandlie, I. & Andersen, J. T. The role of albumin receptors in regulation of albumin homeostasis: Implications for drug delivery. *Journal of Controlled Release* **211**, 144-162, doi:<https://doi.org/10.1016/j.jconrel.2015.06.006> (2015).

5 | Discussion and Conclusions

5.1. Discussion, conclusion, and contributions to knowledge

The work presented in this thesis aims at generating and optimizing nucleic-acid bases nanoparticles for biomedical applications, specifically as drug nanocarriers. Specifically, the work is focused on optimizing nucleic acid nanoparticles (NANPs) for the delivery of nucleic acid therapeutics. Particles built from DNA have high programmability and versatility, but these particles need to be optimized by equipping them with properties that are essential for applicability. These particles should aim at enhancing the specificity of the therapeutic they carry, improve on its stability and efficacy, and be cost-effective in its production.

Attaching hydrophobic polymers to DNA led to the emergence of a new class of amphiphilic DNA block copolymers. Our lab has developed a highly efficient solid-phase method to generate monodisperse and sequence-defined DNA-polymer conjugates, that can produce a variety of conjugates with an array of properties. Since this method is automated, scalable, controllable, and made from biocompatible and biodegradable materials, we aimed at designing a range of molecules and vehicles that can aid the delivery of nucleic acid therapeutics. This includes spherical nucleic acids (SNAs) that assemble from monodisperse linearly conjugated amphiphiles, and dendritic conjugates. Both amphiphiles' prototypes showed promising properties for applicability in the delivery of therapeutics, such as enhanced biostability, favoured biodistribution, and controlling protein binding.

In Chapter 2, we focused on optimizing the SNAs design by adding stimuli-responsiveness to enhance selectivity. By designing the SNAs to carry the therapeutic in a dormant form and release it in its active form in the presence of specific stimuli, we are improving on the selectivity of action of the therapeutic. Hence this chapter focuses on carrier optimization. We showed that responsive behaviour can be implemented by relying

on the strand displacement mechanism.^{1,2} We partially hybridized the therapeutic to the SNA, which is released in the presence of the fully complementary trigger strands that in our design can be genetic biomarkers (miRNA, mRNA) of specific cells.^{2,3} The work in chapter 2 showed that these particles improve on stability of the therapeutic, are modular by simply switching the nucleic acid therapeutic (NAT) sequence to the desired target, and most importantly have selective activity of the therapeutics only in the presence of the stimulus.⁴ Such particles are attractive as they rely on an cell-specific stimulus instead of an external one, eliminating the need for equipment to stimulate the therapeutic release and achieving conditional release with disease biomarkers.^{1,5-7} Additionally, the design was shown to respond two, not just one, of the triggers (akin to an AND gate) which further increases the specificity. This can be applied to discriminate the activation of therapeutics for example in specific cancer cells that overexpress two microRNAs compared to healthy cells that do not overexpress any or only 1 microRNA.^{8,9} This work presents a promising, simple, and effective method to control the efficacy of therapeutics that are part a of well-established drug delivery vehicle such as the SNA.¹⁰ Previous DNA nanostructures that selectively release cargo needed a large number of component strands (DNA origami) or highly modified strands (DNA wireframe cages); our nanoparticles can be made from a minimal number of strands (4) with easy to introduce modifications.^{3,11-13}

In chapter 3, we turned our focus to optimizing the therapeutic index of SNAs. The SNAs in chapter 2 possess optimized selectivity, but the efficacy of the therapeutics used (50% gene silencing) and stability (half-life= 6 hours in serum) are modest. To our surprise, both fields of chemical modifications to NATs and DNA nanotechnology are well-advanced, yet do not crosstalk as much as they should. Indeed, most SNAs and NANPs in the field (when this project was published) at most have used only the phosphorothioate backbone or mirror image DNA as a modification. Hence, we aimed at bridging the fields together by developing a chemically modified SNA with improved activity and stability. We implemented one of the most promising modifications, 2'fluoroarabino (FANA), and incorporate it on the DNA portion of the SNA-forming amphiphile, which are termed FANA-SNAs.¹⁴ What makes FANA advantageous over other modifications is that it increases stability in biological conditions, enhances the binding affinity towards the target

mRNA, reduces immunogenicity, and it is one of the few modifications that does not hinder the RNase H catalytic activity when implemented into ASOs.¹⁵⁻¹⁸ The therapeutic in this design was the FANA-modified DNA portion of the amphiphile, which will assemble to have the therapeutic ASO in a corona around the core; thus the entire structure is assembled from a single DNA strand type. In this work, we demonstrated that such modifications can be implemented into SNAs where assembly properties were not affected, and stability was boosted. Importantly, we found that implementation of a cleavable linker in between the therapeutic and its conjugate was critical for retaining the enhanced efficacy from these FANA-SNAs. We also demonstrated the modularity of these NANPs by targeting multiple genes by simple changing the sequence of the therapeutic, highlighting the simplicity and compatibility of such SNAs for the delivery of NATs. This marriage between the two fields also resulted in enhanced free uptake and activity *in vitro*, where having both an SNA with FANA modifications yielded the highest silencing yield without the need for transfection agents. This chapter highlights the positive outcome of combining various advancements in the field of nucleic acid therapeutics, and reports on the importance of design parameters to achieve enhanced efficacy and outcome (such as cleavable linker).^{2,15,19,20} The next generation SNAs for the delivery of nucleic acid therapeutics will benefit from such studies that showcase the advantages of adding chemical modifications and fine-tuning designs.²⁰

In chapter 2 and 3, we showcased how we can optimize the linear amphiphile-assembling SNAs as drug delivery vehicles of NATs by adding selectivity properties and boosting the efficacy and stability of the therapeutic. In chapter 4, we focus on studying another amphiphile that has other interesting properties. The dendritic moiety (D) is synthesized in the same automated fashion from biodegradable material but has its hydrophobic chains in a branched design rather than in a linear form.²¹ Our previous work on this conjugate showed that it can bind albumin in nanomolar affinity, while still being able to effectively deliver NATs *in vitro*.^{22,23} Binding to some serum proteins, particularly albumin, can positively influence distribution and efficacy of therapeutics.^{15,20} We hypothesized that if we can control the binding of proteins to NAT *in vivo*, by selective binding to albumin, we can improve on the pharmacokinetics and pharmacodynamics. Albumin is specifically an interesting protein to bind to as it is very abundant in circulation,

but also has non-degradative cellular uptake pathways, which is what NATs usually suffer from.^{18,24,25} In this chapter we investigated the albumin-binding ability of dendritic-conjugated siRNAs (D-siRNA) in mouse models, where we demonstrate that upon systemic injection, the D-siRNAs are indeed binding albumin selectively and are able to induce gene silencing in multiple organs such as liver, heart, kidney, adrenal and fat. We also investigated the increased activity in local injection site, where we administer the D-siRNAs locally in the lung. The data showed that the dendritic moiety is tolerated at high doses, whereas more hydrophobic state-of-the-art conjugates are not. In addition, albumin-binding D-siRNAs showed silencing in leukocytes which to our knowledge has not been reported before. The enhanced silencing activity in fibroblasts (80%) and in epithelial cells (50%) is also promising and under further investigation. The ability to induce gene silencing activity in such cell types with D-siRNAs is potentially due to the ability to bind albumin, which provides a non-degradative uptake pathway for the siRNAs and possible endosomal escape mechanisms to be effective. Further investigation is underway, especially for applications to diseases that involve these cells, such as infections and pulmonary diseases.²⁵⁻²⁷

Lastly, in appendices I and II, we take advantage of the ability to control size and shape of DNA minimal wireframe nanostructures, to investigate the effect of such parameters in delivery and biosensing.^{2,6,20,28-31} In appendix I, we focus on developing varied structures and sizes (triangle and square) to multivalently load NATs and investigate their pharmacokinetics. To do that, we first aimed at synthesizing fully chemically modified NANPs, which to our knowledge has not been reported. We were able to assemble these structures in good yield, and able to load them with multiple copies of siRNAs that target the same gene (or potentially, various genes). We then showcase that these NANPs have an acceptable preliminary toxicity *in vivo* and induce gene silencing *in vitro*. We will next investigate how the size change between triangle and square assembly plays a role in the pharmacokinetics of the siRNAs they carry. Early studies demonstrated that the triangle indeed distributes differently than the component strand to organs. As for appendix II, we switch the application of these modular structures to instead carry multiple copies of fluorescently-labelled probe strands.²⁸ This was a collaborative work with a

sequencing company, Quantum Si., where we aim to take advantage of the multivalency of such structures to multiply the probe signal readout, while maintaining compactness and compatibility.²⁸ We demonstrated the ability to 3 and 4 probe strands, in triangle and square respectively. Both structures were compatible with the microarray system used for sequencing at the company.

In conclusion, this thesis demonstrates that the applications of nucleic acid-based material in the biomedical field, whether sensing or drug delivery, are highly promising. The future of nucleic acid nanotechnology, especially if chemical engineering of the properties of these materials is carried out, such as optimizing hydrophobicity, size, shape, assembly, and chemical modifications. The studies and conclusions outlined in this thesis can be applied to many other types of nucleic acid materials other than SNAs and DNA minimal structures, and to numerous disease targets.

5.2. **Suggestions for future work**

In this section, we outline some future work ideas and suggestions that can build on the work presented in this thesis.

Spherical Nucleic Acids:

The work presented in chapters 2 and 3 on sequence-controlled spherical nucleic acids has promising potential to be used as drug delivery vehicles. Considering the results of enhanced silencing activity from chemical modifications (chapter 3) and responsive selectivity (chapter 2), the natural next step is to combine both properties in the same entity. Hence, the next step is to apply FANA and other modifications to stimuli responsive SNAs. This will hopefully yield a selective release of a more potent and chemically modified therapeutic from promising drug delivery system.^{10,15,19,30,32}

We also would like to design the responsive SNAs against an endogenous overexpressed trigger, as mentioned in chapter 2. This will allow us to test the applicability of this design in a disease cell model. For example, we can target the overexpressed

miRNAs miR-21 and miR-6 associated with breast cancer cells to be the inducers for the release of our therapeutic oligonucleotide specifically in these cells.³³

Another important future direction for these SNAs is their *targeting*. These SNAs have been shown to have a wide biodistribution profile *in vivo* which is promising.³⁴ However, specific diseases require improved distribution to specific organs.^{15,19,20} Therefore, functionalizing SNAs with targeting ligands, such as aptamers and antibodies, is hypothesized to improve their selective accumulation in target organs which increases their therapeutic efficacy.^{6,19} Complementing targeted biodistribution with selective cellular uptake and activation of therapeutic will greatly mitigate off-target effects, improve efficacy, and decrease the need for high doses.

Additionally, we also believe that utilizing the core of the SNAs to *co-deliver small molecule drugs* in combination with NATs to enhance effects in certain diseases (e.g., cancer) is of interest to the field.³⁴ For example, one can target genes that are involved with chemoresistance with siRNAs to inhibit them and co-deliver chemotherapeutic drugs to those silenced cells. We believe this will yield enhanced efficacy as has been recently reported.³⁵ Hence, we need to assess the biodistribution and gene silencing of these structures next.

New conjugate designs:

In chapter 4, we saw how redesigning the polymeric conjugate entity yielded new and interesting properties such as protein binding. We believe the space of chemically engineering the conjugate for various properties is of extreme importance and will yield many interesting outcomes for NATs delivery.^{30,36-40} One direction could be increasing the dendritic arms of the conjugate seen in chapter 4 and study the impact on albumin binding. Also, we can start introducing other functional entities, such as positively charged or ionizable molecules instead of hydroxyl groups, which can aid in uptake and lysosomal escape.^{6,15,41,42}

The enhanced activity in the lung in specific cell types such as leukocytes and endothelial/epithelial cells is novel and utilizing the albumin-binding dendritic conjugate for diseases associated with these cells is of particular interest. For example, chronic obstructive pulmonary disease is the 3rd leading cause of death worldwide.⁴³ Nucleic acid therapeutics for COPD are being developed and work best if administered directly to the lung.⁴³ miR-206 from lung tissues of patients have been found to be upregulated in pulmonary endothelial cells and negatively correlated with the progression of the disease.⁴⁴ Targeting the endothelial cells of patients with Dendritic-conjugated siRNAs targeting miR-206 expression could have therapeutic benefit. Other targets include miR-195 that is upregulated in leukocytes of the lung.⁴³⁻⁴⁵

Additionally, these conjugates can be placed on nanoparticles like SNAs or liposomes to control their protein corona and ultimately impact their pharmacokinetic/pharmacodynamics.¹⁹ If we can engineer the corona of these nanoparticles to bind selective proteins that will dictate their biodistribution, we can then enhance the therapeutic efficacy of such particles.

Other future directions could be the design of conjugates that yield different assemblies than spherical shapes, such as rods and sheets. If we are able to control the assembly of such shapes from similar material, we can then study how they behave as drug delivery vehicles such as cellular uptake efficiency, stability, and circulation behavior/pattern.⁶

Multivalent structures for various applications:

As seen in appendix I and II, DNA minimal structures are extremely useful and can be tailored for multiple applications. For drug delivery, we envision the ability to control organ distribution and multidrug delivery with NANPs as interesting future work to pursue and continue working on. The preliminary data showed that these fully modified particles can alter biodistribution profile solely by size and shape, without the use of any conjugates. They also were able to induce gene silencing when the therapeutic is part of the structure, but not as efficiently as a stand-alone therapeutic. Redesigning these structures to optimize

their therapeutic index, as well to produce other shapes and sizes is of interest. These nanostructures can also be functionalized with targeting ligands and conjugates as previously mentioned, where they can be targeted to specific organs. One example is to pursue the structures that are preferentially localizing in the heart to study and treat stroke incidents using nucleic acid therapeutics.

After studying the effect of size and molecular weight, it is interesting to investigate any effect that results from 2D vs 3D designs. This could be done by engineering particles having similar overall weight and size but arranged differently in space.^{2,6,19,46}

5.3. Publications' List

1. **Hassan H. Fakh**, Adam Katolik, Elise Malek-Adamian, Johans Fakhoury, Masad J Damha and Hanadi F. Sleiman. "Design and Enhanced Gene Silencing Activity of Spherical 2'-Fluoroarabinose Nucleic Acids (FANA-SNAs)" In **Chemical Science, Advance Article 2021**, 12, 2993-3003.
2. Aurelie Lacroix, Hassan H. Fakh and Hanadi F. Sleiman "Detailed cellular assessment of albumin-bound oligonucleotides: Increased stability and lower non-specific cell uptake" In **Journal of Controlled Release. 2020**, 324, 34-46.
3. Maryam Habibian, S. Harikrishna, Johans J. Fakhoury, Maria Barton, Eman A. Ageely, Regina Cencic, **Hassan H. Fakh**, Adam Katolik, Mayumi Takahashi, John Rossi, Jerry Pelletier, Keith T Gagnon, P I Pradeepkumar, Masad J Damha. "Effect of 2'-5'/3'-5' phosphodiester linkage heterogeneity on RNA interference" **Nucleic Acid Research, 2020**.
4. Katherine E. Bujold, **Hassan H. Fakh** and Hanadi F. Sleiman "Design Strategy to Access siRNA-Encapsulating DNA "Nanosuitcases" That Can Conditionally Release Their Cargo". In **RNA Interference and Cancer Therapy: Methods and Protocols. 2019**, 69-81.
5. **Hassan H. Fakh**, Johans J. Fakhoury, Danny Bousmail, Hanadi F. Sleiman. "Minimalist Design of a Stimuli-Responsive Spherical Nucleic Acid for Conditional Delivery of Oligonucleotide Therapeutics". **ACS Applied Materials and Interfaces, 2019**, 11, 15, 13912-13920.

5.4. References

- 1 Mura, S., Nicolas, J. & Couvreur, P. Stimuli-responsive nanocarriers for drug delivery. *Nat Mater* **12**, 991-1003, doi:10.1038/nmat3776 (2013).
- 2 Tan, X., Jia, F., Wang, P. & Zhang, K. Nucleic acid-based drug delivery strategies. *Journal of Controlled Release* **323**, 240-252, doi:<https://doi.org/10.1016/j.jconrel.2020.03.040> (2020).
- 3 Bujold, K. E., Hsu, J. C. C. & Sleiman, H. F. Optimized DNA “Nanosuitcases” for Encapsulation and Conditional Release of siRNA. *Journal of the American Chemical Society* **138**, 14030-14038, doi:10.1021/jacs.6b08369 (2016).
- 4 Fakhir, H. H., Fakhoury, J. J., Bousmail, D. & Sleiman, H. F. Minimalist Design of a Stimuli-Responsive Spherical Nucleic Acid for Conditional Delivery of Oligonucleotide Therapeutics. *ACS Applied Materials & Interfaces* **11**, 13912-13920, doi:10.1021/acsami.8b18790 (2019).
- 5 Li, S. *et al.* A DNA nanorobot functions as a cancer therapeutic in response to a molecular trigger in vivo. *Nat Biotechnol* **36**, 258-264, doi:10.1038/nbt.4071 (2018).
- 6 Mitchell, M. J. *et al.* Engineering precision nanoparticles for drug delivery. *Nature Reviews Drug Discovery* **20**, 101-124, doi:10.1038/s41573-020-0090-8 (2021).
- 7 Sarisozen, C., Joshi, U., Mendes, L. P. & Torchilin, V. P. in *Stimuli Responsive Polymeric Nanocarriers for Drug Delivery Applications* (eds Abdel Salam Hamdy Makhlouf & Nedal Y. Abu-Thabit) 269-304 (Woodhead Publishing, 2019).
- 8 Li, Z. & Rana, T. M. Therapeutic targeting of microRNAs: current status and future challenges. *Nat Rev Drug Discov* **13**, 622-638, doi:10.1038/nrd4359 (2014).
- 9 Stenvang, J., Petri, A., Lindow, M., Obad, S. & Kauppinen, S. Inhibition of microRNA function by anti-miR oligonucleotides. *Silence* **3**, 1-1, doi:10.1186/1758-907X-3-1 (2012).
- 10 Kapadia, C. H., Melamed, J. R. & Day, E. S. Spherical Nucleic Acid Nanoparticles: Therapeutic Potential. *BioDrugs* **32**, 297-309, doi:10.1007/s40259-018-0290-5 (2018).
- 11 Ren, K. *et al.* A DNA dual lock-and-key strategy for cell-subtype-specific siRNA delivery. *Nature Communications* **7**, 13580, doi:10.1038/ncomms13580 (2016).
- 12 Yijun Guo, B. W., Shiyun Xiao, Dongbao Yao, Hui Li, Huaguo Xu, Tingjie Song, Xiang Li, Haojun Liang. Recent advances in molecular machines based on toehold-mediated strand displacement reaction. *Quant. Biol.* **5**, 25-41, doi:10.1007/s40484-017-0097-2 (2017).
- 13 Wang, H., Luo, D., Wang, H., Wang, F. & Liu, X. Construction of Smart Stimuli-Responsive DNA Nanostructures for Biomedical Applications. *Chemistry – A European Journal* **27**, 3929-3943, doi:<https://doi.org/10.1002/chem.202003145> (2021).
- 14 Fakhir, H. H. *et al.* Design and enhanced gene silencing activity of spherical 2'-fluoroarabinose nucleic acids (FANA-SNAs). *Chemical Science* **12**, 2993-3003, doi:10.1039/D0SC06645A (2021).

- 15 Bost, J. P. *et al.* Delivery of Oligonucleotide Therapeutics: Chemical Modifications, Lipid Nanoparticles, and Extracellular Vesicles. *ACS Nano* **15**, 13993-14021, doi:10.1021/acsnano.1c05099 (2021).
- 16 Watts, J. K., Katolik, A., Viladoms, J. & Damha, M. J. Studies on the hydrolytic stability of 2'-fluoroarabinonucleic acid (2'F-ANA). *Organic & Biomolecular Chemistry* **7**, 1904-1910, doi:10.1039/B900443B (2009).
- 17 Kalota, A. *et al.* 2'-Deoxy-2'-fluoro- β -D-arabinonucleic acid (2'F-ANA) modified oligonucleotides (ON) effect highly efficient, and persistent, gene silencing. *Nucleic Acids Research* **34**, 451-461, doi:10.1093/nar/gkj455 (2006).
- 18 Sharma, V. K. & Watts, J. K. Oligonucleotide therapeutics: chemistry, delivery and clinical progress. *Future Med Chem* **7**, 2221-2242, doi:10.4155/fmc.15.144 (2015).
- 19 Weng, Y. *et al.* Improved Nucleic Acid Therapy with Advanced Nanoscale Biotechnology. *Molecular Therapy - Nucleic Acids* **19**, 581-601, doi:<https://doi.org/10.1016/j.omtn.2019.12.004> (2020).
- 20 Roberts, T. C., Langer, R. & Wood, M. J. A. Advances in oligonucleotide drug delivery. *Nature Reviews Drug Discovery* **19**, 673-694, doi:10.1038/s41573-020-0075-7 (2020).
- 21 Edwardson, T. G., Carneiro, K. M., Serpell, C. J. & Sleiman, H. F. An efficient and modular route to sequence-defined polymers appended to DNA. *Angew Chem Int Ed Engl* **53**, 4567-4571, doi:10.1002/anie.201310937 (2014).
- 22 Lacroix, A., Fakih, H. H. & Sleiman, H. F. Detailed cellular assessment of albumin-bound oligonucleotides: Increased stability and lower non-specific cell uptake. *Journal of Controlled Release* **324**, 34-46, doi:<https://doi.org/10.1016/j.jconrel.2020.04.020> (2020).
- 23 Lacroix, A., Edwardson, T. G. W., Hancock, M. A., Dore, M. D. & Sleiman, H. F. Development of DNA Nanostructures for High-Affinity Binding to Human Serum Albumin. *Journal of the American Chemical Society* **139**, 7355-7362, doi:10.1021/jacs.7b02917 (2017).
- 24 Geary, R. S., Norris, D., Yu, R. & Bennett, C. F. Pharmacokinetics, biodistribution and cell uptake of antisense oligonucleotides. *Adv Drug Deliv Rev* **87**, 46-51, doi:10.1016/j.addr.2015.01.008 (2015).
- 25 Hoogenboezem, E. N. & Duvall, C. L. Harnessing albumin as a carrier for cancer therapies. *Advanced Drug Delivery Reviews* **130**, 73-89, doi:<https://doi.org/10.1016/j.addr.2018.07.011> (2018).
- 26 Bequignon, E. *et al.* FcRn-Dependent Transcytosis of Monoclonal Antibody in Human Nasal Epithelial Cells In Vitro: A Prerequisite for a New Delivery Route for Therapy? *Int J Mol Sci* **20**, doi:10.3390/ijms20061379 (2019).
- 27 Bern, M., Sand, K. M. K., Nilsen, J., Sandlie, I. & Andersen, J. T. The role of albumin receptors in regulation of albumin homeostasis: Implications for drug delivery. *Journal of Controlled Release* **211**, 144-162, doi:<https://doi.org/10.1016/j.jconrel.2015.06.006> (2015).

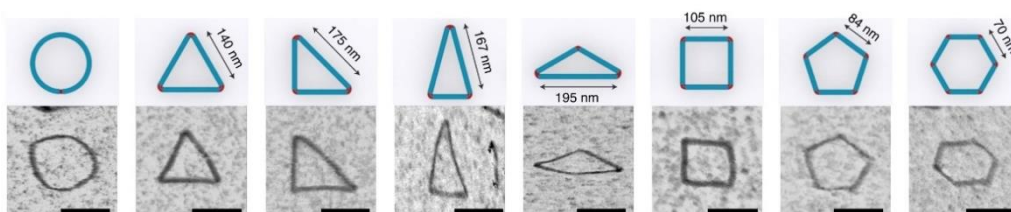
- 28 Fu, S. *et al.* DNA nanotechnology enhanced single-molecule biosensing and imaging. *TrAC Trends in Analytical Chemistry* **140**, 116267, doi:<https://doi.org/10.1016/j.trac.2021.116267> (2021).
- 29 Kong, G. *et al.* DNA nanostructure-based fluorescent probes for cellular sensing. *Analytical Methods* **12**, 1415-1429, doi:10.1039/D0AY00105H (2020).
- 30 Dong, Y., Siegwart, D. J. & Anderson, D. G. Strategies, design, and chemistry in siRNA delivery systems. *Advanced drug delivery reviews* **144**, 133-147, doi:10.1016/j.addr.2019.05.004 (2019).
- 31 Lim, X. The architecture of structured DNA. *Nature* **546**, 687-689 (2017).
- 32 Amjad, M. W., Kesharwani, P., Mohd Amin, M. C. I. & Iyer, A. K. Recent advances in the design, development, and targeting mechanisms of polymeric micelles for delivery of siRNA in cancer therapy. *Progress in Polymer Science* **64**, 154-181, doi:<https://doi.org/10.1016/j.progpolymsci.2016.09.008> (2017).
- 33 Khordadmehr, M. *et al.* Key microRNAs in the biology of breast cancer; emerging evidence in the last decade. *Journal of Cellular Physiology* **234**, 8316-8326, doi:<https://doi.org/10.1002/jcp.27716> (2019).
- 34 Bousmail, D. *et al.* Precision spherical nucleic acids for delivery of anticancer drugs. *Chemical Science* **8**, 6218-6229, doi:10.1039/C7SC01619K (2017).
- 35 Jang, M., Han, H. D. & Ahn, H. J. A RNA nanotechnology platform for a simultaneous two-in-one siRNA delivery and its application in synergistic RNAi therapy. *Scientific Reports* **6**, 32363, doi:10.1038/srep32363 (2016).
- 36 Bousmail, D. *Sequence-Defined DNA Polymers: Applications in Drug Delivery and Supramolecular Assembly*, McGill University (Canada), (2019).
- 37 de Rochambeau, D., Sun, Y., Barlog, M., Bazzi, H. S. & Sleiman, H. F. Modular Strategy To Expand the Chemical Diversity of DNA and Sequence-Controlled Polymers. *The Journal of Organic Chemistry* **83**, 9774-9786, doi:10.1021/acs.joc.8b01184 (2018).
- 38 Biscans, A. *et al.* Diverse lipid conjugates for functional extra-hepatic siRNA delivery in vivo. *Nucleic Acids Research* **47**, 1082-1096, doi:10.1093/nar/gky1239 (2018).
- 39 Khvorova, A. & Watts, J. K. The chemical evolution of oligonucleotide therapies of clinical utility. *Nature Biotechnology* **35**, 238-248, doi:10.1038/nbt.3765 (2017).
- 40 Osborn, M. F. *et al.* Hydrophobicity drives the systemic distribution of lipid-conjugated siRNAs via lipid transport pathways. *Nucleic Acids Res* **47**, 1070-1081, doi:10.1093/nar/gky1232 (2019).
- 41 Schlich, M. *et al.* Cytosolic delivery of nucleic acids: The case of ionizable lipid nanoparticles. *Bioengineering & Translational Medicine* **6**, e10213, doi:<https://doi.org/10.1002/btm2.10213> (2021).
- 42 Zhang, X., Goel, V. & Robbie, G. J. Pharmacokinetics of Patisiran, the First Approved RNA Interference Therapy in Patients With Hereditary Transthyretin-Mediated Amyloidosis. *The Journal of Clinical Pharmacology* **60**, 573-585, doi:<https://doi.org/10.1002/jcph.1553> (2020).

- 43 Mei, D., Tan, W. S. D., Tay, Y., Mukhopadhyay, A. & Wong, W. S. F. Therapeutic RNA Strategies for Chronic Obstructive Pulmonary Disease. *Trends in Pharmacological Sciences* **41**, 475-486, doi:<https://doi.org/10.1016/j.tips.2020.04.007> (2020).
- 44 Kelly, C. *et al.* Therapeutic aerosol bioengineering of siRNA for the treatment of inflammatory lung disease by TNF α gene silencing in macrophages. *Mol Pharm* **11**, 4270-4279, doi:10.1021/mp500473d (2014).
- 45 Gu, W. *et al.* Role of miR-195 in cigarette smoke-induced chronic obstructive pulmonary disease. *International immunopharmacology* **55**, 49-54 (2018).
- 46 Lacroix, A. & Sleiman, H. F. DNA Nanostructures: Current Challenges and Opportunities for Cellular Delivery. *ACS Nano* **15**, 3631-3645, doi:10.1021/acsnano.0c06136 (2021).

Preface 4

In Appendix I and II we exploit the unique ability to precisely control size and shape of nucleic acid nanoparticles (NANPs), to study the influence of these structural properties in two different applications. The first appendix focuses on our initial effort to produce nucleic acid minimal NANPs with varying sizes, capable of delivering a variety of NATs, and study the impact of this size variation on pharmacokinetics of the drug. It is well known these properties can alter clearance rates, organ biodistribution and cell uptake, and we were interested in studying these effects on NANPs. A key component in producing these particles is that they are assembled from fully modified nucleic acids such as those used in the clinic, instead of the traditional unmodified NANPs or NANPs with phosphorothioate or mirror-image DNA backbone modification. To our knowledge, this is the first reported fully chemically modified NANPs. The work is a collaboration with the lab of Prof. Anastasia Khvorova at the RNA Therapeutics Institute of UMass Medical School. The work was part of the CREATE PROMOTE exchange program, where I visited the collaborator's work in the USA.

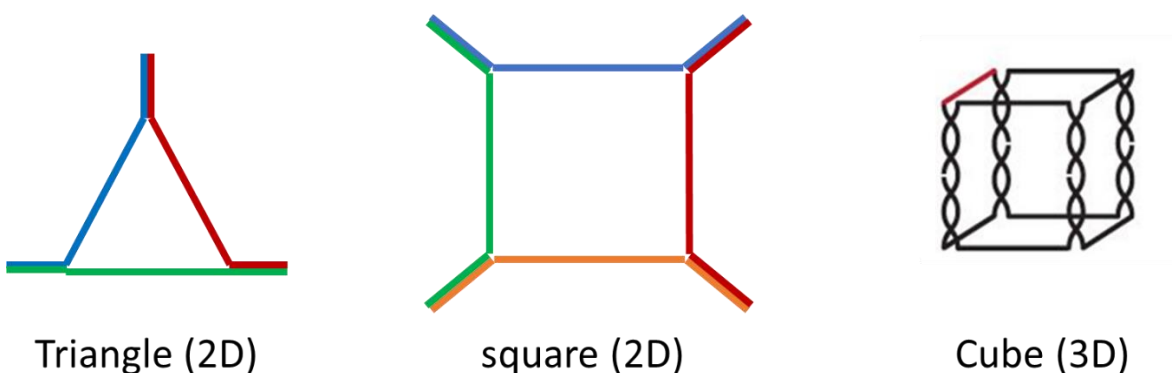
The second appendix is focused on applications in biosensing, where we produce fluorescently labelled size-controlled NANPs using the same design. Having highly fluorescent structures is desired in many biosensing applications such as next-generation sequencing, where a signal readout needs to be strong and bright. However, preciseness and compactness are another vital property in such applications to ensure compatibility with the system. Since NANPs design can be controlled to produce compact but highly functionalized structures, we aim to optimize the production of such particles that are highly fluorescent by multivalent functionalization. This work was in collaboration with Quantum Si. Inc, a start-up company that provides revolutionary next generation sequencing services, based in Guilford, USA.



Adapted from Yao, G., Zhang, F., Wang, F. *et al.* Meta-DNA structures. *Nat. Chem* 2020

“If I have seen further, it is by standing on the shoulders of giants”

Appendix I | Size-controlled, fully modified minimal-NANPs for therapeutics delivery



Contribution of authors

Hassan H. Fakh helped design the project and primarily contributed to production of experimental data from synthesis, purification, characterization, assembly, analysis and helped with samples preparation for *in vitro* studies. **Dimas Echeverria** helped with synthesis of cube strands by assisting in machine setup and input on optimizing yield. **Jillian Caiazza** performed the *in vitro* silencing experiments. **Qi Tang and Hassan H. Fakh** performed the biodistribution and pharmacokinetics experiment in mice, analyzed the data together for the biodistribution whereas the pharmacokinetics data is yet to be analyzed. **Anastasia Khvorova** and **Hanadi F. Sleiman** designed the project and guided interpretation of data and discussion of experiments.

AI.1. Abstract

Nucleic acid Nanoparticles (NANPs) provide unprecedented precise control over their structural parameters, thanks to the specific Watson-Crick base pairing governing the self-assembly of these nanomaterials. This control, along with ease of manufacturing is attractive for various applications, such as drug delivery and biosensing. For drug delivery, the ability to produce particles with various physical properties (size, shape) allows us to further understand the influence of such characteristics on in vivo behaviour, and control pharmacokinetics of the drug delivery system and the drug it is carrying. Ultimately, we are interested in designs that result in delivery of nucleic acids beyond the liver or kidneys. In this work, we design and develop a set of wireframe minimal nucleic acid nanoparticles that can form a variety of sizes and shapes in 2D and 3D. These particles can be easily functionalized to carry multiple nucleic acid therapeutics (NATs) targeting the same gene, or multiple NATs against various genes. We assess the assembly of fully modified NANPs, report preliminary results on how various size/molecular weight can alter biodistribution and showcase that such structures are still active in silencing. This work is ongoing.

AI.2. Introduction

The ability to control the structural properties of nanomaterials (size, shape etc.) with precision and ease is of great interest in the field of nanofabrication. These parameters greatly influence drug delivery systems and their pharmacokinetics/pharmacodynamics in circulation.^{1,2} They can dictate stability, clearance, biodistribution, and even activity following uptake; Hence the careful design of such carriers is of extreme importance. Oligonucleotide therapeutics (antisense oligonucleotides ASOs, small interfering RNAs siRNAs) in general suffer from small size (hence rapid clearance) and negatively charged surface (hence decreased cellular uptake) which impedes their biological function.³ Nucleic acid nanoparticles (NANPs), which are 2D and 3D nanostructures built from nucleic acids are excellent materials to develop programmable and precise particles with total control over size and shape, thanks to the specific Watson-Crick base pairing that governs their self-assembly.⁴ They have demonstrated increased cellular uptake and stability compared to their individual building blocks.⁴⁻⁷ In addition, we can theoretically build a large library of sizes, shapes and models of structures and carriers from DNA nanotechnology, due to the

ease of their design, predictable assembly, and ease of manufacturing.^{8,9} Finally, we can simply adapt the structures to carry the desired sequence by simply adjusting the sequences on the structures to carry it intrinsically.⁴ The carrier is now also the therapeutic.

Importantly as well, NANPs are multivalent vehicles that can carry multiple copies of therapeutic cargo that are aimed towards the same target, or various targets. For example, trigonal prisms made from nucleic acids were able to deliver multiple copies of therapeutics to cells, that enhance their activity as well as control the amount of delivered drug, all on one particle.^{10,11} One can imagine delivering therapeutics that are aimed at multiple targets in a single entity. Unfortunately, most of these NANPs are either non-chemically modified, thus unable to survive *in vivo* conditions, or only slightly modified by phosphorohioate backbones, thus resulting in limited gene silencing ability. In addition, studies on how the size or shape of such particles purely influence circulation, pharmacokinetics and *in vivo* gene silencing are still lacking.

In this work, we aim to develop multivalent DNA-minimal wireframe polygons with varying sizes and shapes and explore their effects on drug delivery. Triangles, squares, and cubes that are fully chemically modified, were generated to carry multiple copies of similar or distinct siRNAs. The assembly of these structures was characterized, and their variation in size was studied *in vivo* where they had different biodistribution profiles, indicating the importance of such physical properties and their impact on biodistribution. *In vitro silencing* was also validated for these structures, showing that they do not hinder the activity of the cargo to a significant extent. The work presented is an ongoing project and reports on preliminary promising results of using such structures to alter distribution and targeting purely from physical parameters.

AI.3. Results and Discussion

AI.3.1. Design

To produce triangles and squares from modular strands, we adopted a design developed by our lab, where therapeutic strands are imagined as sides/arms to the polygons (**Figure AI. 1 A**).¹² Briefly, these strands have 5' and 3' regions that are 15bp long and clip onto other strands with complementary sequences on their extremities. The middle part of these strands is encoded with the sequence of the antisense strand of a specific siRNA. 3 arms coming together would yield a triangle and 4 arms coming together yields a square (**Figure AI. 1 A**). To produce a 3D cube, we adopted a design also developed by our lab where 4 96bp clip strands come together via hybridization to form the cube as shown (**Figure AI. 1 B**). The top and bottom of the cube are single stranded regions that can be further hybridized to other strands such as siRNAs.

For the triangle, we designed the arms to carry 3 different siRNAs against the following genes: sFLT1, HTT, and PPIB. For the square, it was designed to carry siRNAs like the triangle, with an extra siRNA against HTT (2HTT, 1 sFLT1, 1 PPIB). These sequences were validated and provided by the Khvorova lab in previous work.^{13,14} For the cube, we encoded the blue colored siRNA to be against ApoE, and the green against HTT. The sequences of the strand synthesized, with their chemical modifications and mass spectroscopy confirming the successful synthesis of these fully chemically modified strands are included in the experimental section (**Error! Reference source not found.**).

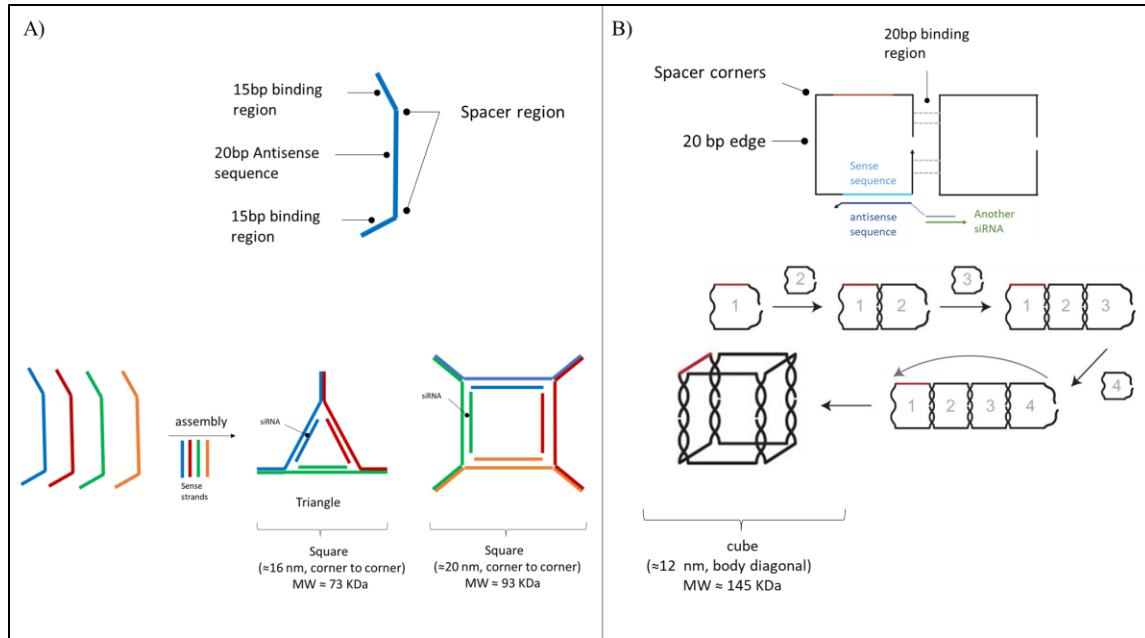


Figure AI. 1. Design, assembly, and parameters of A) triangle, square, and B) cube.

AI.3.2. Assembly test

To test the assembly of the structures, we performed a sequential ladder assembly where we added one strand after the other to form the structure with annealing. Then, these samples were run on a native polyacrylamide gel in 1xTAMg buffer to monitor the change in mobility of each step of the assembly (**Figure AI. 1.**). The data shows that the assembly was not very clean, but the major product is indeed the triangle (lane 3), square (lane 4) and the cube (lane 9), where all of them had the slowest mobility compared to their intermediates, confirming their assembly.

This was a significant result to us as using fully chemically modified strands have alterations to their structural parameters (length, packing, twist, binding affinity etc.) in comparison to unmodified DNA that is usually used in the assembly of such material. The

assembly yields for the triangle and square were good, with the cube showing some higher-order side-products

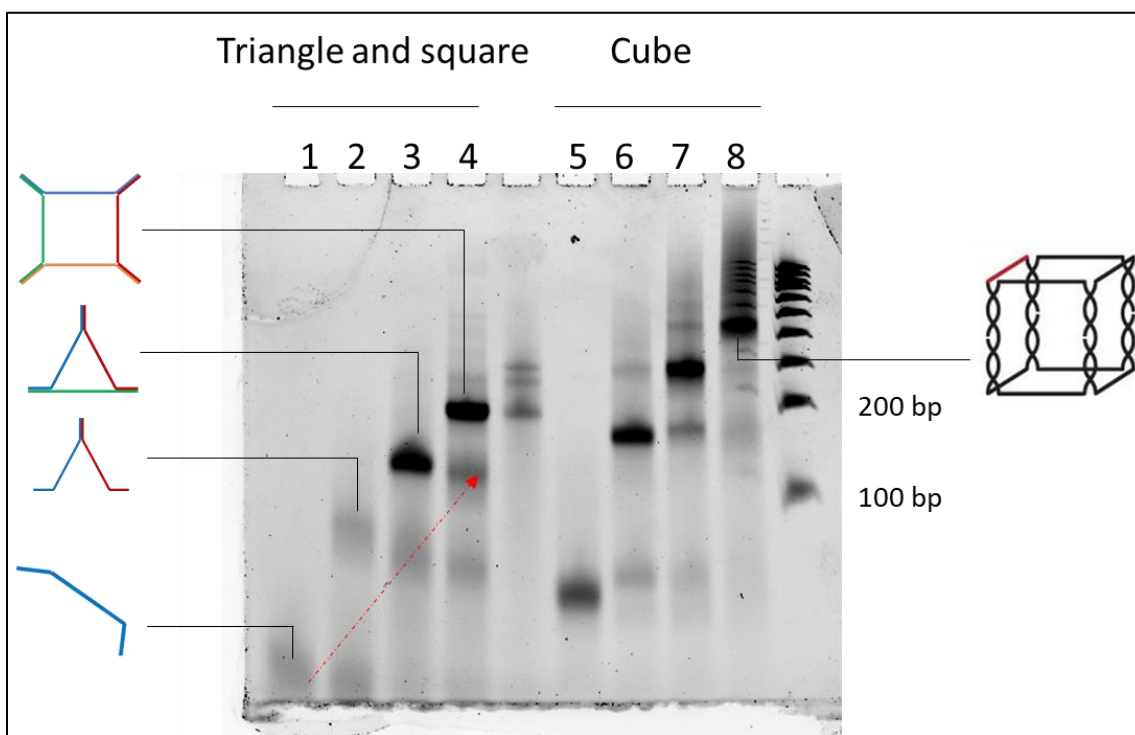


Figure AI. 2. 8% Polyacrylamide native gel showing the sequential assembly of triangle, square and cube at 1 μ M. samples were Run for 1.5 hr at 130V in 1xTAMg. Lane 1: A1, Lane2: A1+A3, Lane 3: A1+A3+A5, lane 4: A1+A3+A6+A7, lane 5: C1, lane 6: C1+C2, lane 3: C1+C2+C3, lane 4: C1+C2+C3+C4.

AI.3.3. Assembly at higher concentration and cleanup:

After the initial assembly test indicating that structures are forming, we needed to tackle the issue of leftover strands or incomplete structures visible on the previous gel. In addition, we were interested in testing the assembly at higher concentration to assess if this is tolerated, as DNA nanostructures may aggregate if assembled at increased concentration.

In the gel below, we assemble various triangles and squares by interchanging some of the sequences that target various genes, and the cube, at either 1 or 5 μ M (**Figure AI. 3.**). Then, we spin down the assemblies each in a microcon to attempt to get rid of the malformed or incomplete structures. For the triangle (58 KDa) and square (77 KDa), we

used a cut-off filter of 50 KDa, and for the cube (126 KDa) we used the 100 KDa cut-off filter. We did the size-exclusion filtration centrifugation (Microcon) either for 1 round or 3 rounds, using the assembly buffer for washing.

The data shows that triangles and squares, regardless of which sequence we use, assemble well at both concentrations (**Figure AI. 3.**). Following the size-exclusion cleanup procedure, both the one- or three-times wash were somewhat able to get rid of the malformed structures and left-over strands (indicated by the arrows). For the square, there is still a slightly visible band which most likely corresponds to a 3-arm structure that weighs more than 50 KDa, the cut-off size of the filter. The cube at lower concentration seems to fall apart or the band disappears after 3 rounds of wash (could be an experimental error as we do not even see component strands), however it is maintained at higher concentration. Size-exclusion treatment with 3 wash cycles was used for all further assemblies and tests.

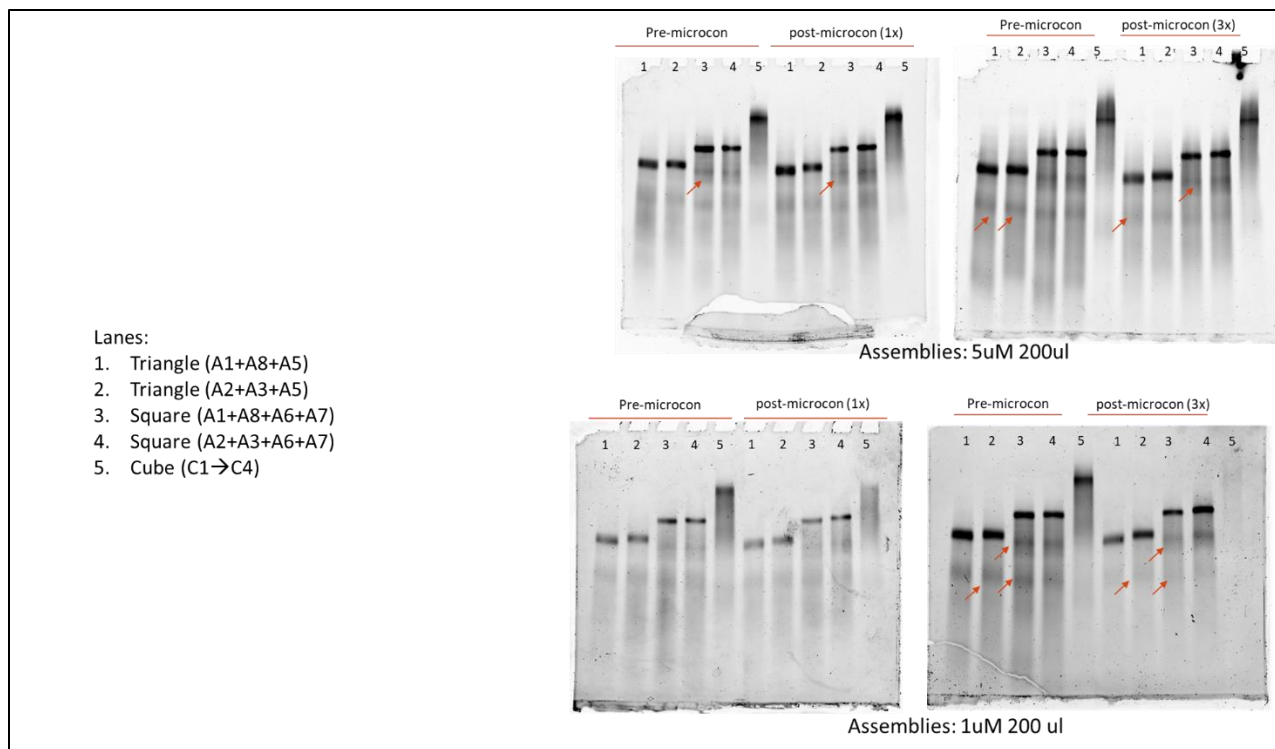


Figure AI. 3. 8% Polyacrylamide native gel showing assembly of triangle, square and cube at 1 μ M and 5 μ M. samples were run for 1.5 hr at 130V in 1xTAMg. Lane 1: triangle against SFLT1, HTT, and PPIB, Lane2: triangle against HTT, Lane 3: square against SFLT1, HTT, and PPIB, lane 4: square against HTT, lane 5: cube. Orange arrows indicate misfolded structures and leftover strands.

AI.3.4. *In vivo* scale assembly and siRNA loading:

Following the positive results for assembly at increased concentration and cleaning up the assembly via size-exclusion filtration centrifugation, we aimed at filling the structures with their complementary sense strands to make them fully double stranded, as well as to try to produce the structures at an *in vivo* relevant concentration. Typically, siRNAs are injected at a dose close to 20nmoles, so we aim to assemble the triangle at 33.35 μM (carries 3 siRNAs), the square at 25 μM (carries 4 siRNAs) and the cube at 12.5 μM (can carry 8 siRNAs), all at a volume of 200 μL .¹³

First, we started by confirming that the structures can be made double-stranded by titrating a triangle that can hold 3 HTT siRNAs with an increasing amount of HTT sense strand. Triangle assemblies with 1x, 2x, 3x (1:1) or 6x the amount of the sense strands were annealed (2 hours) and compared for their mobility shift on a native polyacrylamide gel. In the same gel, we also attempt to assemble the structures at a much higher concentration, that resembles a total of 20nmoles of siRNA. The figure below (**Figure AI. 4.**) shows the decreasing mobility of the triangle when it is increasingly functionalized with sense strands. After 3 sense strands are added, which is a 1:1 ratio between sense and antisense strands, there is no further decrease in mobility at the addition of 6 strands. The unassembled excess components are visible at the bottom of the gel (lane 5, Sybergold staining), indicating the saturation at 1:1 and no need for excess amounts. **Figure AI. 5.** Shows that we also need only 4 copies of sense strands to fully fill the square, as well as the ability to add the sense strands for both at RT instead of annealing them with the structure.

Assembling at 20nmoles siRNA in typical injection volume (100 μL) of the structures was successful as well. For the cube, the band is smeared and there are some aggregates present in the well that do not penetrate the gel, which need to be investigated. Hence in further experiments in animals, the cube was not used. Interestingly as well, in lane 10 in the gel (**Figure AI. 4.**), the triangle was heated at 95 degrees Celsius for 5 minutes and left to cool down, which gave the correct assembly. This is extremely promising for these chemically modified structures, indicating the possibility of skipping

the 2-hour annealing step to get these structures and replacing it by a quick heat and cool step that is more desired in preclinical and clinical settings.

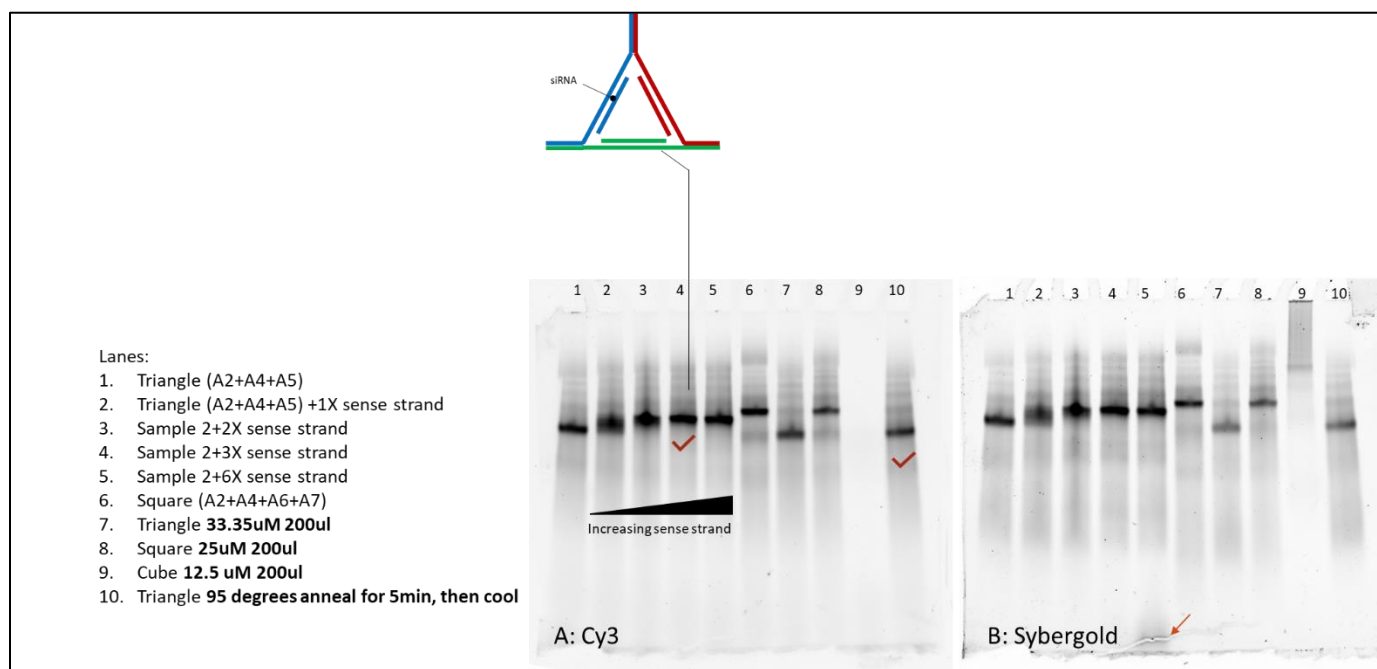


Figure AI. 4. Filling of the triangle with increasing amounts of sense strand, as well as assembling the structures at concentrations representative 20nmoles of siRNA. 8% Polyacrylamide native gel showing assembly of various structures assembled at 5 μ M (lanes 1 to 6). samples were run for 1.10 hr (to see left over, time was decreased) at 130V in 1xTAMg. NOTE: we used a Cy3 labeled A4 strand to visualize in both Cy3 and DNA stain channels

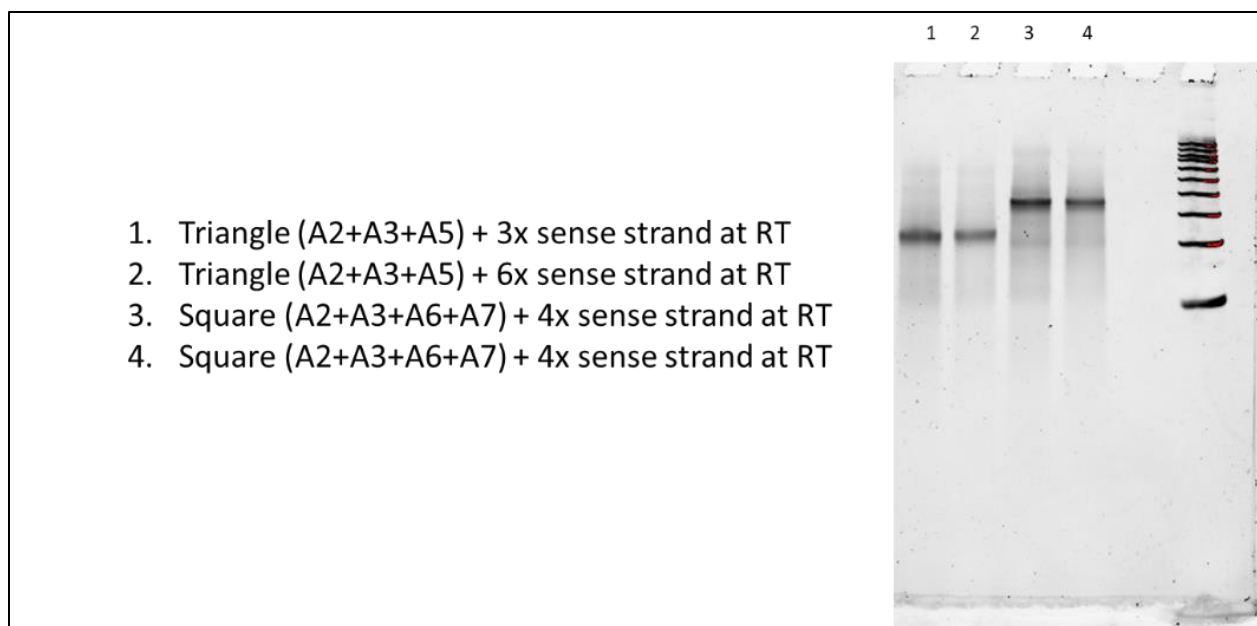


Figure AI. 5. 8% Polyacrylamide native gel showing the triangle and square becoming fully double stranded with 1:1 sense strands, and no need for higher amounts. the addition of the sense strands was done at room temperature following the annealing of the structures, proving that the filling can be done without annealing. samples were run for 1.5 hr at 130V in 1xTAMg

Following the successful assembly at a high concentration for the triangle structures, we aimed to see if we can also make the fully double stranded structures at this concentration. To do this, we took the same samples of triangle and square from the previous figure (lane 7,8; 20nmoles assembled structures at a volume of 100 μ L) and added the complementary sense strands to each structure at a 1:1 ratio at room temperature for a few mins. An aliquot was taken, and then the sample was annealed at 95 degrees for 5 mins, left to cool, and an aliquot of this was also taken. The samples were loaded on a native PAGE gel, which will show us if we can successfully load the sense strands at this concentration of assembly at room temperature, but also if it converts to its target design following a quick anneal protocol (**Error! Reference source not found.**). As evident from the gel, the mobility of the triangle and square decreased as expected indicating formation of the fully double stranded structures (lanes 4,5). Following the quick anneal (lanes 7,8) the structures also formed back with the same mobility as that of lanes 4,5, reconfirming the ability to assemble these structures with a quick anneal step. However, the quality of

the bands following the quick anneal is not as clean. As for the cube (lanes 3,6,9) this is single-stranded cube, where we notice that the aggregate stuck in the well increases in intensity following the quick anneal (lane 9).

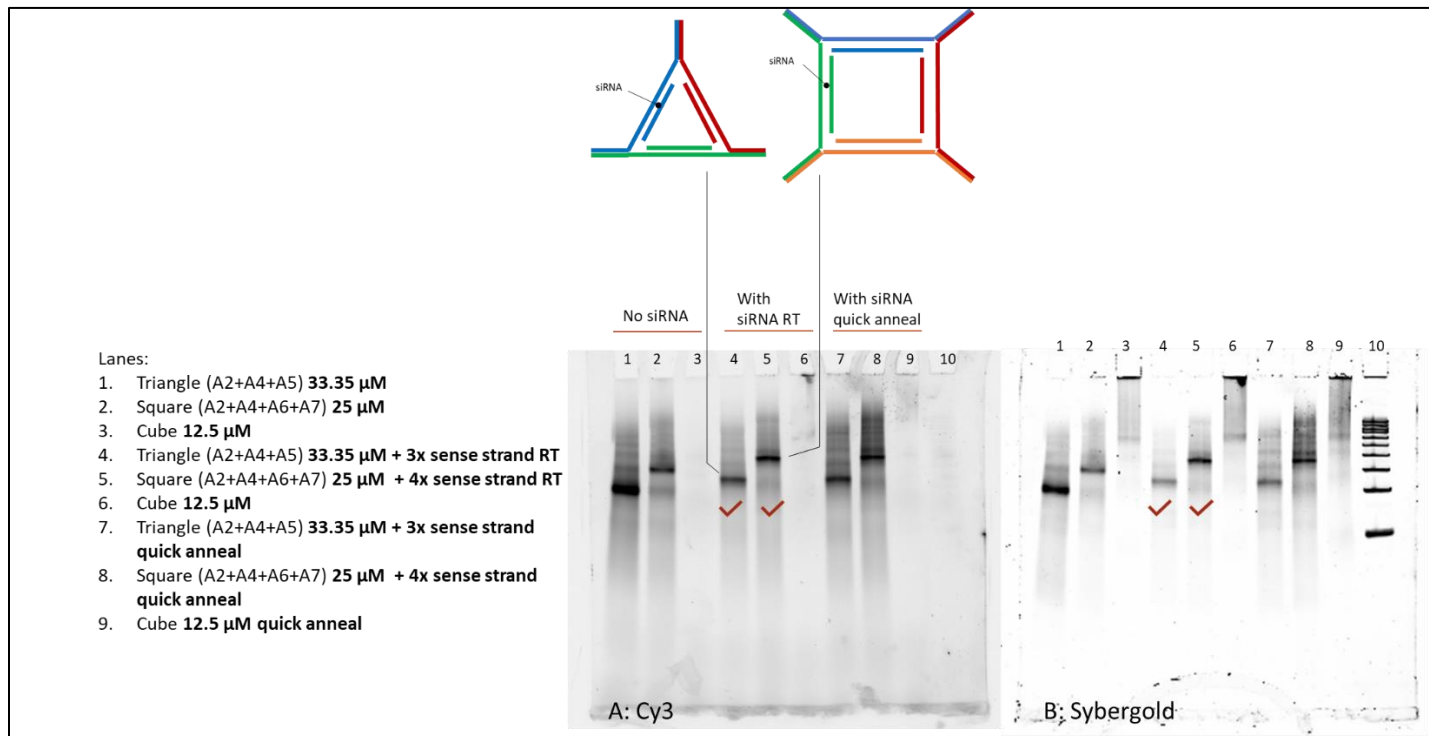


Figure AI. 6 Fully assembling the structures at high concentration (20nmoles of antisense strand). 8% Polyacrylamide native gel showing assembly of various structures assembled 20nmoles of antisense strand (lanes 1,2,3), followed by addition of the sense strands in a 1:1 ratio (lanes 4,5) and quick anneal test (lanes 7,8,9). samples were run for 1.5 hr at 130V in 1xTAMg. NOTE: we used a Cy3 labeled A4 strand to visualize in both Cy3 and DNA stain channels

AI.3.5. *In vivo* Biodistribution profile and toxicity:

After the series of assembly optimizations, we wanted to test how the various size and molecular weight of these structure would impact their *in vivo* behavior. As previously mentioned, these two parameters influence biodistribution, as small material with a size below 5 nm gets filtered by the kidney, while large ones do not.⁵ In addition, their flow in circulation and interaction with components in the body can also differ based on their size and weight.⁵ For this experiment, we injected mice (n=3) intravenously, with either a single

double-stranded arm that makes up a side of the structures, a double stranded triangle, and a double stranded square. All samples had a Cy3 labeled strand, and injections were at 10nmoles final amount with respect to the antisense strand (33.35 μM for triangle, 25 μM for square, and 100 μM for the arm, all at 100 μL). Following 24 hours, the mice were euthanized, and sample major organs were collected (liver, kidney, muscle, spleen, heart, lung) for microscopy imaging, as well as blood collection for initial toxicity screen (blood chemistry and complete blood cells count, CBC).

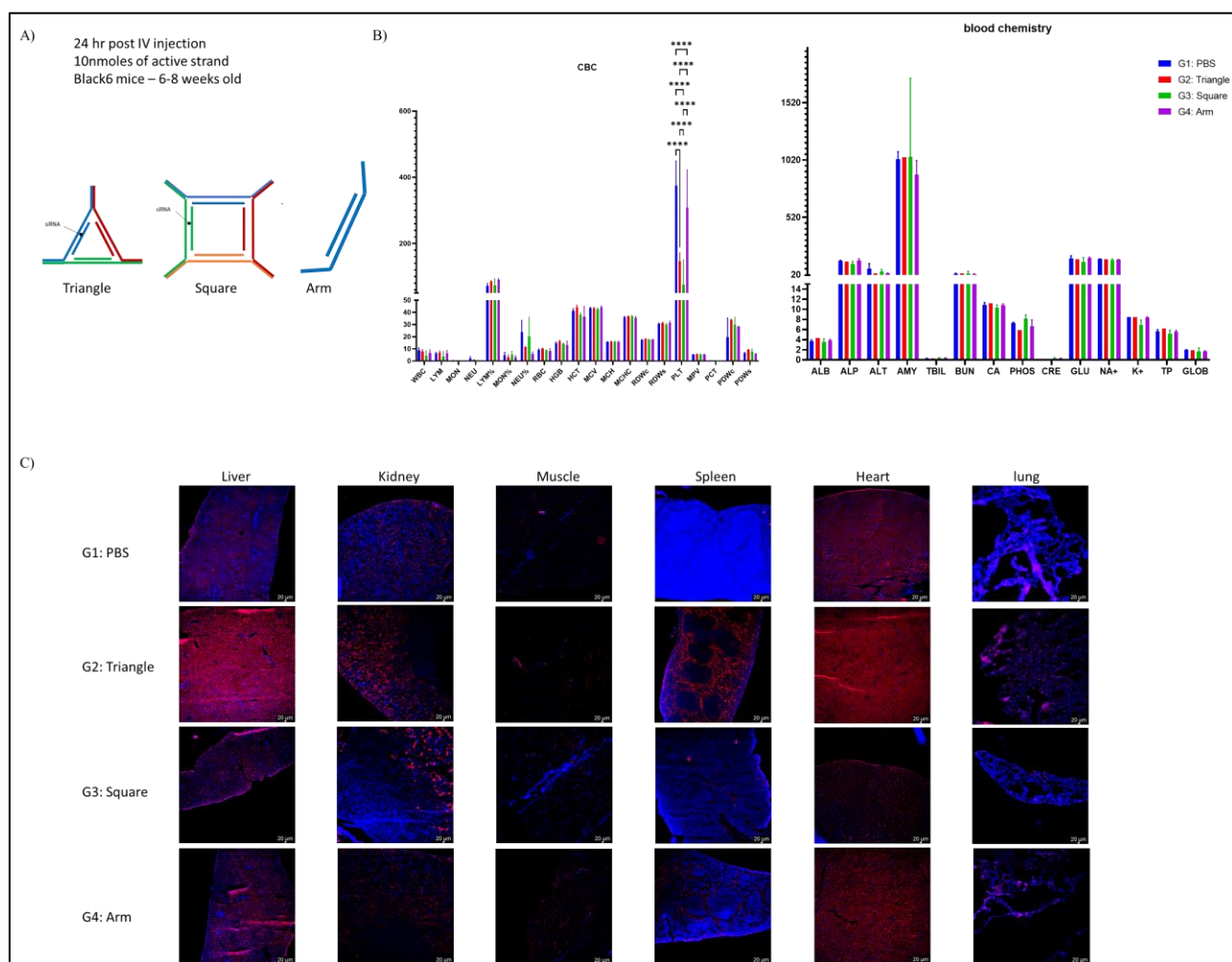


Figure AI. 7. *In vivo* study on the biodistribution and toxicity of various sized structures. A) the samples that were prepared and injected in mice (black6, male, 6-8 weeks old, n=3) via tail vein injection. B) CBC and blood chemistry counts after 24 hours of injection (only significant statistical difference is plotted) and C) representative microscopy images of various organs from different mice groups (blue = DAPI nucleus stain, red = Cy3 fluorescent signal). CBC and blood chemistry abbreviations are defined in experimental data.

The imaging of the organs clearly shows a variation in distribution when the size/weight of the structure varies. For example, the arm sample is mostly cleared following 24 hours of injection, with slight distribution in heart and kidney. As for the triangle, a strong signal is present throughout the liver, and a much stronger signal in the heart, spleen, and lung. The spleen and lung signal however are not evenly distributed, and the signal is specifically residing in certain spots. Surprisingly for the square, the signal in the liver is only in the extremities, and there is no evident signal in any other tissue, which ponders the question if it is still in circulation and such a big size is hindering its efficient uptake into organs. As for the initial toxicity screen, it seems that there is no significant induced toxicity resulting from the structures. The platelets count was the only significant difference, which could either be sample aggregation issue or an indication of a certain toxicity.

This preliminary data clearly confirms that we can skew the distribution of NANPs by simply varying the size/weight and possibly structure. These NANPs are not modified with ligands that are changing their distribution, nor with hydrophobic entities that alter their behavior in circulation as previously reported.^{14,15} These are promising preliminary results, especially with fully chemically modified structures that are stable and do not get degraded. Follow up studies are on-going to study the effect of size/shape on pharmacokinetics and pharmacodynamics of such structures.

AI.3.6. Silencing activity of siRNA loaded structures:

Being part of a such a structure, siRNA activity could either be enhanced or decreased, requiring further investigation. As the active antisense strand is part of the structural strands with no cleavable spots, we hypothesized that siRNA activity will be reduced. To test this, HeLa cells were transfected with either the arm, the triangle, the square, or a control siRNA, all targeting the Huntington gene and then mRNA was quantified using Quantigene bDNA assay 2.0 as previously described and developed.¹⁵ all concentrations indicated are with the respect to the final amount of siRNA used. First, we generated a 7-point dose response study starting from 10nM, and the data showed that the structures were only active at 10nM and not at any lower concentration (**Error! Reference**

source not found. A). This indicates that the activity did decrease in comparison to a free siRNA duplex. We then performed another 7-point dose response study starting with 100nM, and the structures had the same activity in the range of 100-10nM, decreased at 5nM, and were inactive at 2.5nM and lower final concentration. The Square outperforms the triangle in efficacy, which could be due to its increased size and better binding/loading of the antisense strands it carries into the RISC complex. There was no noticeable change of activity between the triangle and the arm.

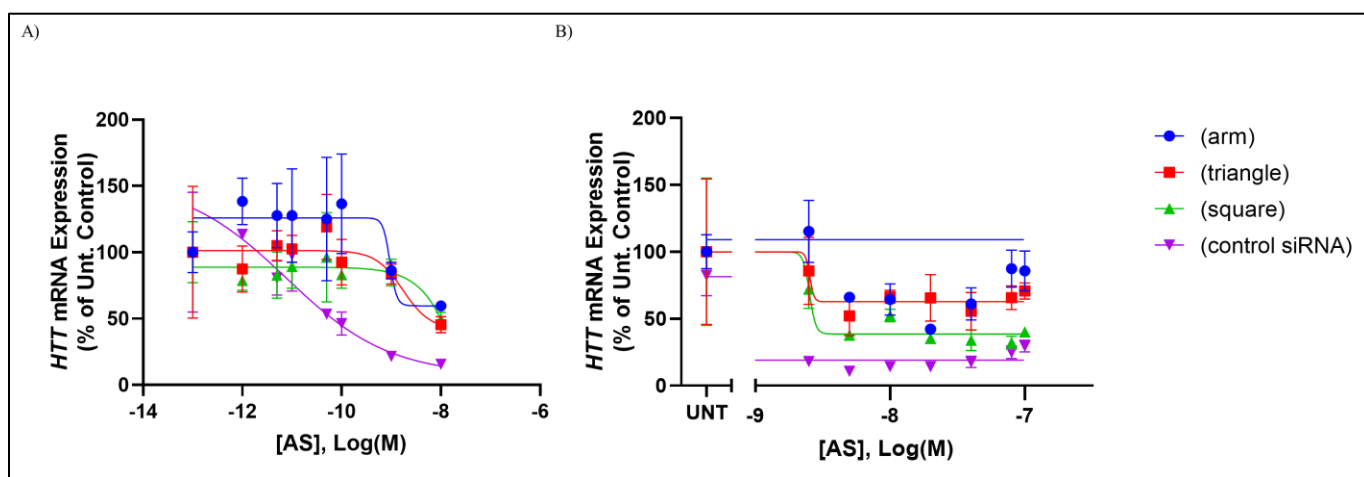


Figure AI. 8. 7-point dose response curve to measure gene silencing activity following RNAimax transfection of various samples into HeLa cells, and gene expression via mRNA quantification using Quantigene bDNA assay 2.0. A) 10nM starting dose and B) 100nM starting dose. All concentrations indicate the final amount of siRNA per sample.

This data shows that the activity of the siRNA, where the antisense is part of the structural strands of the structures, decreases but is still retained at certain concentrations. It has been previously reported in the literature as well as in this thesis Chapter 3 that a cleavable linker is important to release the active strand so it binds its target freely (in this case the antisense strand).^{16,17} Alterations to this design to enhance silencing activity are possible, by either introducing cleavable linkers (short unmodified, single-stranded phosphate DNA) on both sides of the antisense coding sequence in the structures, or by switching the design to include the sense strand in the structure and later freely hybridize the antisense strand to it.

AI.4. Conclusion

In this work, we present our first effort to test the fate of DNA minimal structures *in vivo*. We have demonstrated *in vitro* that these structures are precise, stable, enter cells, and can improve activity of NATs, but *in vivo* studies add another layer of complexity that needs to be studied as well.^{4,8}

We try to take advantage of the ability to produce various sizes and shapes from these particles to study how this impacts biodistribution in animal models. To be able to confidently claim that these structures are intact in such complex media, we had to assemble them from fully chemically modified strands to ensure stability.¹⁸ NANPs, to our knowledge, have never been assembled from fully chemically modified strands, and this work represents the first attempt to do so. We demonstrate that we can assemble these structures from such stable strands, and in fact due to the enhanced binding of these strands long annealing protocols can be avoided in some cases. The designed structures also take advantage of the multivalency of such particles, by having the ability to carry multiple copies of the same NAT, or NATs targeted against multiple genes.

We were able to show as well with preliminary data that we can influence and control biodistribution to certain organs by simply varying the structure size/weight of nucleic acid-based nanoparticles. This was achieved without the use of any hydrophobic conjugates or targeting ligands (antibodies/aptamers) that are usually employed for such result.^{6,7,15} These structures did not show any significant toxicity after 24 hours of injection into mice as well.

The structures can induce gene silencing with the current design, indicating that they do not inhibit activity of NATs. Nonetheless, future work is necessary to redesign the structures to ensure maximal activity of the cargo. Redesign considerations include cleavable/releasable therapeutic cargo.

Work on project is ongoing, to fully study the potential of such nanomaterials in influencing pharmacokinetics/pharmacodynamics of the therapeutics they carry, as well as delivering multiple therapeutics at once.

AI.5. Experimental

AI.5.1. Oligonucleotide synthesis, purification, MS analysis and assembly

Oligonucleotides were synthesized on a Mermade 6/12 synthesizer and Expedite ABI DNA/RNA synthesizer (GE Healthcare Life Sciences, for cube strands) following standard protocols. In brief, strands were synthesized at 5 μ mol scales on a CPG functionalized with Unylinker (ChemGenes, Wilmington, MA, USA). strands were deprotected and cleaved with a solution of 28% aqueous ammonium hydroxide solution for 20 hours at 60°C, followed by drying under vacuum at 60°C, and resuspended in Millipore H₂O. Oligonucleotides were purified using an Agilent Prostar System (Agilent, Santa Clara, CA, USA) over an ion-exchange column. Purified oligonucleotides were desalted by size-exclusion chromatography and characterized by liquid chromatography-mass spectrometry (LC/MS) analysis on an Agilent 6530 accurate-mass quadrupole time-of-flight (Q-TOF) LC/MS (Agilent Technologies, Santa Clara, CA, USA).

To assemble structures, samples were mixed at the desired concentration in Tris-acetic acid-magnesium buffer (1x TAMg buffer, 45 mM Tris, 20 mM acetic acid and 7.6 mM Mg(Cl)₂, pH was adjusted to ~8.0 using glacial acetic acid), diluted with milliQ water, and annealed from 95 to 5 °C over 2 hours using Bio-Rad T100™ thermal cycler.

Concentration of samples and centrifugation filtration (amicon) was done with Amicon® Ultra Centrifugal Filter Units (Millipore sigma), where samples were centrifuged at 4000 rpm for 15-30 mins, always washing with 1xTAMg.

Sequences of the compounds and their modifications are in the table below (#: PS backbone, m: 2'-o-methyl, f: 2'-fluoro)

Strand	Description	sequence	MW expected (g/mol)	MW found (g/mol)
A1	Triangle/square arm 1, 5FLT AS	(mU)#(mC)#(mG)#(fC)(fU)(fU)(mC)(fU)(mA)(fG)(mG)(fA)(mG)(fA)(mU)#(mU)#(mU)#(mU)#(mU)#(mU)#(fA)#(mA)(mA)(mU)(fU)(mU)(mG)(mG)(mA)(mG)(mA)(mU)#(fC)#(mC)#(fG)#(mA)#(mG)#(mA)#(fG)#(mU)#(mU)#(mU)#(mU)#(mU)#(mU)#(fC)(mU)(fU)(mU)(fC)(mA)(fA)(mC)(fU)(mU)(mC)(mA)#(fC)#(fA)#(fC)	19372.31	19356 (-1PS)
A2	Triangle/square arm 1, HTT AS	(mU)#(mC)#(mG)#(fC)(fU)(fU)(mC)(fU)(mA)(fG)(mG)(fA)(mG)(fA)(mU)#(mU)#(mU)#(mU)#(mU)#(mU)#(mU)#(fU)#(mA)(mA)(mU)(fC)(mU)(mC)(mU)(mU)(mU)(mA)(mC)#(fU)#(mG)#(fA)#(mU)#(mA)#(mU)#(mU)#(mU)#(mU)#(mU)#(mU)#(fC)(mU)(fU)(mU)(fC)(mA)(fA)(mC)(fU)(mU)(mC)(mA)#(fC)#(fA)#(fC)	19153.07	19152
A3	Triangle/square arm 2, HTT AS	(mG)#(mU)#(mG)#(fU)(fG)(fA)(mA)(fG)(mU)(fU)(mG)(fA)(mA)(fA)(mG)(mU)#(mU)#(mU)#(mU)#(mU)#(mU)#(mU)#(fU)#(mA)(mA)(mU)(fC)(mU)(mC)(mU)(mU)(mA)(mC)#(fU)#(mG)#(fA)#(mU)#(mA)#(mU)#(mU)#(mU)#(mU)#(mU)#(mU)#(fG)(mU)(fG)(mA)(fU)(mG)(fU)(mC)(fA)(mU)(mC)(mA)#(fA)#(fU)#(fG)	19440.29	19440
A4	Triangle/square arm 2, HTT AS with Cy3	Cy3(mG)#(mU)#(mG)#(fU)(fG)(fA)(mA)(fG)(mU)(fU)(mG)(fA)(mA)(fA)(mG)(mU)#(mU)#(mU)#(mU)#(mU)#(mU)#(mU)#(fU)#(mA)(mA)(mU)(fC)(mU)(mC)(mU)(mU)(mA)(mC)#(fU)#(mG)#(fA)#(mU)#(mA)#(mU)#(mU)#(mU)#(mU)#(mU)#(mU)#(fG)(mU)(fG)(mA)(fU)(mG)(fU)(mC)(fA)(mU)(mC)(mA)#(fA)#(fU)#(fG)	20070.64	20070
A5	Triangle arm 3, HTT AS	(mC)#(mA)#(mU)(fU)(fG)(fA)(mU)(fG)(mA)(fC)(mA)(fU)(mC)(fA)(mC)#(mU)#(mU)#(mU)#(mU)#(mU)#(mU)#(fU)#(mA)(mA)(mU)(fC)(mU)(mC)(mU)(mU)(mU)(mA)(mC)#(fU)#(mG)#(fA)#(mU)#(mA)#(mU)#(mU)#(mU)#(mU)#(mU)#(mU)#(fA)(mU)(fC)(mU)(fC)(mC)(fU)(mA)(fG)(mA)(mA)(mG)(fC)#(fG)#(fA)	19262.21	19262
A6	Square arm 3, HTT AS	(mC)#(mA)#(mU)(fU)(fG)(fA)(mU)(fG)(mA)(fC)(mA)(fU)(mC)(fA)(mC)#(mU)#(mU)#(mU)#(mU)#(mU)#(mU)#(fU)#(mA)(mA)(mU)(fC)(mU)(mC)(mU)(mU)(mU)(mA)(mC)#(fU)#(mG)#(fA)#(mU)#(mA)#(mU)#(mU)#(mU)#(mU)#(mU)#(mU)#(fC)(mA)(fG)(mC)(fA)(mA)(fA)(mC)(fC)(mU)(mU)(mA)#(fC)#(fU)#(fC)	19182.16	19182
A7	Square arm 4, HTT AS	(mG)#(mA)#(mG)#(fU)(fA)(fA)(mA)(fG)(mU)(fU)(mG)(fA)(mA)(fA)(mG)(mU)#(mU)#(mU)#(mU)#(mU)#(mU)#(mU)#(fU)#(mA)(mA)(mU)(fC)(mU)(mC)(mU)(mU)(mU)(mA)(mC)#(fU)#(mG)#(fA)#(mU)#(mA)#(mU)#(fA)#(mU)#(mU)#(mU)#(mU)#(mU)#(mU)#(fA)(mU)(fC)(mU)(fC)(mC)(fU)(mA)(fG)(mA)(mA)(mG)(fC)#(fG)#(fA)	19375.26	19375
A8	Triangle/square arm 2, PPIB AS	(mG)#(mA)#(mU)(fU)(fG)(fA)(mA)(fG)(mU)(fU)(mG)(fA)(mA)(fA)(mG)(mU)#(mU)#(mU)#(mU)#(mU)#(mU)#(mU)#(fU)#(mA)(mA)(mU)(fG)(mU)(fG)(mU)(fG)(mU)(mC)(fA)(mU)(mG)(mA)(mU)(mU)#(mG)#(fC)#(mU)#(mG)#(mU)#(fU)#(mU)#(mU)#(mU)#(mU)#(mU)#(mU)#(fG)(mU)(fG)(mA)(fU)(mG)(fU)(mC)(fA)(mU)(mC)(mA)#(fA)#(fU)#(fG)	19550.38	19550
Sense	HTT sense strand	(mC)#(mA)#(mG)(mU)(fA)(fA)(fA)(mG)(fA)(mG)(mA)(mU)(mU)#(mA)	5057.5	5057
C1	Cube clip 1	(mG)#(mG)#(mA)#(fC)(fA)(fC)(mG)(fU)(mA)(fC)(mC)#(mU)#(mU)#(mU)(mC)(fC)(mU)(fA)(mU)(fA)(mU)(fG)(mG)(fU)(mC)(fA)(mA)(fC)(mU)(fG)(mC)(fU)(mC)(mC)#(mC)#(mU)#(mU)#(mU)#(mU)#(mU)#(mC)(fC)(mU)(mA)(mA)(fG)(fC)(fA)(fA)(fA)(fC)(mU)(mU)(mC)(fC)(mC)(mC)#(mC)#(mU)#(mU)#(fC)(mU)(fC)(mA)(fU)(mA)(fA)(mC)(fA)(mU)(fC)(mC)(fA)(mU)(fA)(mU)(fC)(mC)(fA)(mA)(mC)#(mC)#(mU)#(mU)#(fA)(mG)(fG)(mA)(fA)(fA)(fU)#(mG)#(mG)	31599.57	31599
C2	Cube clip 2	(mG)#(mG)#(mA)#(fG)(fG)(fC)(mG)(fU)(mA)(mC)#(mC)#(mU)#(mU)#(fU)(mC)(fC)(mU)(fA)(mU)(fA)(mU)(fG)(mG)(fU)(mC)(fA)(mA)(fC)(mU)(fG)(mC)(fU)(mC)(mC)#(mC)#(mU)#(mU)#(mG)(fU)(mA)(fC)(mG)(mU)(mG)(fU)(fC)(fC)(fC)(fC)(fC)(mA)(mU)(mU)(mU)(mC)(fC)(mU)(mC)#(mC)#(mU)#(fC)(mU)(fC)(mA)(fU)(mA)(fA)(mC)(fA)(mU)(fC)(mC)(fA)(mU)(fA)(mU)(fC)(mC)(fA)(mA)(mU)#(mU)#(mU)#(fA)(mG)(fG)(mC)(fA)(fC)#(mA)#(mC)#(mU)	31460.34	31460
C3	Cube clip 3	(mC)#(mC)#(mU)#(fG)(fA)(fA)(mG)(fC)(mC)(fA)(mC)#(mC)#(mU)#(mU)#(mU)(mC)(fC)(mU)(fA)(mU)(fA)(mU)(fG)(mG)(fU)(mC)(fA)(mA)(fC)(mU)(fG)(mC)(fU)(mC)(mC)#(mC)#(mU)#(mU)(fA)(mA)(fC)(mG)(mC)(mC)(fU)(fC)(fA)(fG)(fU)(mG)(mG)(mU)(fG)(mC)(fC)(mU)(mC)#(mC)#(mU)#(fC)(mU)(fC)(mA)(fU)(mA)(fA)(mC)(fA)(mU)(fC)(mA)(mU)(fC)(mA)(mC)(fA)(mU)(fC)(mC)(fA)(mA)(mC)(mC)#(mU)#(fU)(mU)(fG)(mC)(fA)(fU)(fU)(mC)#(mA)#(mA)	31428.32	31393 (-2PS?)
C4	Cube clip 4	(mU)#(mG)(mC)(fU)(fU)(fA)(mC)(fG)(mG)(fG)(mC)#(mC)#(mU)#(mU)#(fU)(mC)(fC)(mU)(fA)(mU)(fA)(mU)(fG)(mG)(fU)(mC)(fA)(mA)(fC)(mU)(fG)(mC)(fU)(mC)(mC)#(mC)#(mU)#(mU)(fG)(mG)(fC)(mU)(mU)(mC)(fA)(fG)(fG)(fU)(fU)(fG)(mA)(mA)(mU)(fG)(mC)(fA)(mA)(mC)#(mC)#(mU)#(fC)(mU)(fC)(mA)(fU)(mA)(fA)(mC)(fA)(mU)(fC)(mC)(fA)(mU)(fA)(mU)(fC)(mC)(fA)(mA)(mU)#(mU)#(mC)#(mC)#(fG)(mG)(fU)(mG)(fG)(fA)(fA)#(mG)#(mU)#(mU)	31686.45	31686

Table AI. 1. Table containing all the sequences used in this appendix, with MS data.

AI.5.2. Gel electrophoresis characterization of structures

Assembled structures were loaded on Native Polyacrylamide gel (PAGE) (8%) in 1X TAMg at a constant voltage of 150V for 1.5 hours. Roughly around 2pmoles of strands were ran on the gel, mixed with loading dye and buffer.

AI.5.3. Animal injections

Animal experiments of siRNA conjugates were performed in accordance with animal care ethics approval and guidelines of University of Massachusetts Medical School Institutional Animal Care and Use Committee (IACUC; Protocol #202000010) at the RNA therapeutics institute. 6-8 weeks old black6 male mice (n=3) were injected intravenously via the tail at a concentration of 20nmoles of antisense strand. Blood samples for analysis were collected via cheek incision with a lancet.

AI.5.4. Fluorescence microscopy

Organs were collected from euthanized mice, washed with PBS, and molded with an optimal cutting temperature OCT fixation solution and frozen. Frozen sections are cut using Leica Cryostat CM1950 at 5 μ m thickness, and slides are left to air dry overnight. Then, the slides are hydrated with PBS buffer for 5 mins twice at room temperature, followed by mounting the coverslip on the slides using ProlongTM Gold Antifade Mountant with DAPI staining for nuclei.

AI.5.5. In vitro gene silencing

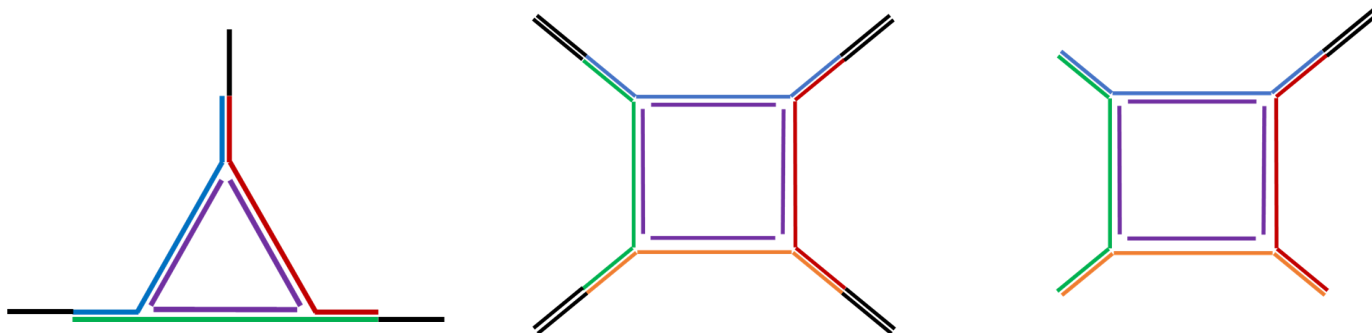
To measure silencing activity, we performed a 7-point dose response, with concentrations ranging from 0 μ M to 100 nM, after 72 h, all being transfected with RNAiMax. These concentrations indicate the final amount of the active strand (antisense). All hsiRNAs use a targeting sequence for huntingtin (HTT) mRNA, which has previously been validated.¹⁹ Briefly, HeLa cells, resuspended in DMEM with 6% FBS and without antibiotics, were added into each well of a 96-well plate with a density of 5,000 cells/50 μ L per well. hsiRNA was diluted to two times final concentration in serum-free OptiMEM, and 50 μ L of compound was added to each well for a final volume of 100 μ L/well and a final concentration of 3% FBS. The mixture was incubated under standard conditions for 72 h and then cells were lysed and processed according to the manufacturer's recommended protocol using the Quantigene bDNA Assay 2.0 (Thermo Fisher QS0011) and were normalized to the housekeeping gene HPRT. Briefly, cells were lysed in 250 μ L diluted lysis mixture (1:2 lysis mixture:water) with 0.167 μ g/ μ L proteinase K (Thermo Fisher QS0103) for 30 min at 55°C. Cell lysates were mixed thoroughly, and 20–80 μ L of lysate were added to a bDNA capture plate along with 0–60 additional diluted lysis mixture without proteinase K to fill up to 80 μ L total volume. Probe sets were diluted as specified in Thermo Fisher protocol, and 20 μ L of either human HTT (Thermo Fisher SA-50339) or HPRT (Thermo Fisher SA-10030) were added to each well of capture plate to a final volume of 100 μ L. Luminescence was detected on a Tecan M 1000.

A1.6. References

- 1 Zhao, Z., Ukidve, A., Krishnan, V. & Mitragotri, S. Effect of physicochemical and surface properties on in vivo fate of drug nanocarriers. *Advanced Drug Delivery Reviews* **143**, 3-21, doi:<https://doi.org/10.1016/j.addr.2019.01.002> (2019).
- 2 Albanese, A., Tang, P. S. & Chan, W. C. W. The Effect of Nanoparticle Size, Shape, and Surface Chemistry on Biological Systems. *Annual Review of Biomedical Engineering* **14**, 1-16, doi:10.1146/annurev-bioeng-071811-150124 (2012).
- 3 Hammond, S. M. *et al.* Delivery of oligonucleotide-based therapeutics: challenges and opportunities. *EMBO Molecular Medicine* **13**, e13243, doi:<https://doi.org/10.15252/emmm.202013243> (2021).
- 4 Seeman, N. C. & Sleiman, H. F. DNA nanotechnology. *Nature Reviews Materials* **3**, 17068, doi:10.1038/natrevmats.2017.68 (2017).
- 5 Mitchell, M. J. *et al.* Engineering precision nanoparticles for drug delivery. *Nature Reviews Drug Discovery* **20**, 101-124, doi:10.1038/s41573-020-0090-8 (2021).
- 6 Weng, Y. *et al.* Improved Nucleic Acid Therapy with Advanced Nanoscale Biotechnology. *Molecular Therapy - Nucleic Acids* **19**, 581-601, doi:<https://doi.org/10.1016/j.omtn.2019.12.004> (2020).
- 7 Tan, X., Jia, F., Wang, P. & Zhang, K. Nucleic acid-based drug delivery strategies. *Journal of Controlled Release* **323**, 240-252, doi:<https://doi.org/10.1016/j.jconrel.2020.03.040> (2020).
- 8 Lacroix, A. & Sleiman, H. F. DNA Nanostructures: Current Challenges and Opportunities for Cellular Delivery. *ACS Nano* **15**, 3631-3645, doi:10.1021/acsnano.0c06136 (2021).
- 9 Bujold, K. E., Lacroix, A. & Sleiman, H. F. DNA Nanostructures at the Interface with Biology. *Chem* **4**, 495-521, doi:<https://doi.org/10.1016/j.chempr.2018.02.005> (2018).
- 10 Fakhoury, J. J., McLaughlin, C. K., Edwardson, T. W., Conway, J. W. & Sleiman, H. F. Development and Characterization of Gene Silencing DNA Cages. *Biomacromolecules* **15**, 276-282, doi:10.1021/bm401532n (2014).
- 11 Wei, M. *et al.* Tetrahedral DNA nanostructures functionalized by multivalent microRNA132 antisense oligonucleotides promote the differentiation of mouse embryonic stem cells into dopaminergic neurons. *Nanomedicine: Nanotechnology, Biology and Medicine* **34**, 102375, doi:<https://doi.org/10.1016/j.nano.2021.102375> (2021).
- 12 McLaughlin, C. K., Hamblin, G. D., Aldaye, F. A., Yang, H. & Sleiman, H. F. A facile, modular and high yield method to assemble three-dimensional DNA structures. *Chemical Communications* **47**, 8925-8927, doi:10.1039/C1CC11726B (2011).
- 13 Biscans, A. *et al.* Docosanoic acid conjugation to siRNA enables functional and safe delivery to skeletal and cardiac muscles. *Molecular Therapy* **29**, doi:10.1016/j.ymthe.2020.12.023 (2020).
- 14 Osborn, M. F. *et al.* Hydrophobicity drives the systemic distribution of lipid-conjugated siRNAs via lipid transport pathways. *Nucleic Acids Res* **47**, 1070-1081, doi:10.1093/nar/gky1232 (2019).

- 15 Biscans, A. *et al.* Diverse lipid conjugates for functional extra-hepatic siRNA delivery in vivo. *Nucleic Acids Research* **47**, 1082-1096, doi:10.1093/nar/gky1239 (2018).
- 16 Fakih, H. H. *et al.* Design and enhanced gene silencing activity of spherical 2'-fluoroarabinose nucleic acids (FANA-SNAs). *Chemical Science* **12**, 2993-3003, doi:10.1039/D0SC06645A (2021).
- 17 Biscans, A. *et al.* The chemical structure and phosphorothioate content of hydrophobically modified siRNAs impact extrahepatic distribution and efficacy. *Nucleic Acids Research* **48**, 7665-7680, doi:10.1093/nar/gkaa595 (2020).
- 18 Lacroix, A., Vengut-Climent, E., de Rochambeau, D. & Sleiman, H. F. Uptake and Fate of Fluorescently Labeled DNA Nanostructures in Cellular Environments: A Cautionary Tale. *ACS Central Science* **5**, 882-891, doi:10.1021/acscentsci.9b00174 (2019).
- 19 Alterman, J. F. *et al.* Hydrophobically Modified siRNAs Silence Huntingtin mRNA in Primary Neurons and Mouse Brain. *Molecular Therapy - Nucleic Acids* **4**, e266, doi:<https://doi.org/10.1038/mtna.2015.38> (2015).

Appendix II | Ultrabright DNA Nanostructures for Biosensing



This work is a collaboration between the Sleiman lab, McGill University, and Quantum Si. Inc., a company providing next generation sequencing on a chip.

Contribution of authors

Hassan H. Fakh helped design the project and primarily contributed to production of experimental data from synthesis, purification, characterization, assembly, and analysis. **Haidong Huang and Robert Boer** synthesized and provided the fluorescent DNA strands and phosphate functionalized DNA strands used in the assemblies. **Quantum Si team (Xinghua Shi and others)** conducted the sequencing experiments, which are confidential and not included in this chapter. **Jeremy Lackey and Xinghua Shi** from Quantum Si initiated the collaboration with **Hanadi F. Sleiman** who conceived the design and idea of the structures to be implemented. The work in this appendix is to be captured and protected by patents.

AII.1. Abstract

Nucleic acid nanostructures provide exceptionally precise control over structural parameters, thanks to the predictable Watson-Crick base pairing that dictates self-assembly. This control, along with ease of manufacturing is attractive for various applications. For biosensing, accurate control over size and shape can resolve many compatibility issues that are faced when aiming to enhance signal readout. For example, adding multiple fluorescent tags to enhance the signal can introduce bulky character which may hinder assays. However, this can be modulated by producing size-controlled compact nucleic acid nanoparticles that are functionalized with the same tags in a more condensed design, thanks to the multivalency of such structures. Quantum Si is interested in improving the fluorescent readout from their semiconductor chip based sequencing platform, with precise and size compatible signalers such as those designed from nucleic acid nanoparticles (NANPs). In this work, we design and optimize a set of wireframe, minimal and ultrabright NANPs with specific sizes, that can be incorporated into their platform.

AII.2. Introduction

Biosensors are systems that can give a signal in the presence of a specific cue with biological relevance.¹ In recent years, single molecule-based sensing platforms, such as fluorescence microscopy, nanopores and mechanochemical instruments (AFM and optical tweezers), have been revolutionizing the sensing field due to their ability to give a signal based on cues at the single molecule level.¹ Such techniques provide unprecedented detection limits and give more informative values than can be obtained with ensemble measurements.¹

Single molecule sensing however suffers from limitations such as low signal-to-noise and poor specificity.¹ In sensing and diagnostics at low amounts of the target in confined spaces such as arrays, the difference in signal between the presence and absence of the cue is very small. This necessitates the need to improve on the molecular probes used in such systems, such as amplifying the signal readout. However, organizing probes in a conventional manner is difficult to integrate into single-molecule detection platforms due to size requirements and specificity towards the target.¹

DNA nanotechnology, a field that exploits the specificity of base-pairing to develop nanostructures with unprecedented control is an attractive strategy to organize matter.² Their well-defined geometries with various shapes and sizes made them excellent scaffolds to organize matter for various applications, such as nanomachines, molecular computing, and targeted drug delivery.³⁻⁶ Using DNA nanotechnology to organize probes is an attractive strategy to enhance single-molecule sensing and imaging.^{2,7} These structures have been used to stabilize nanopores, as rulers in single-molecule imaging, and enhanced throughput and sensitivity in detection.⁸⁻¹¹ DNA nanotechnology also enhances detection and specificity due to the ability of the structures to multiply the signal output and improve on the organization and spatial positioning of the probes.^{1,12,13}

Quantum Si, a company developing next generation sequencing platforms based on single-molecule fluorescence systems, aims at enhancing the signal from their fluorescent probe while still being compatible with their semiconductor arrayed chip system. To do this, the arrangement of bright molecular probes that are precisely controlled in size to ensure compactness and compatibility with the platform is paramount.¹⁴ DNA nanostructures and nanoparticles are promising candidates to achieve this goal, thanks to the programmability of their design and well-defined geometry.² First generation DNA based probes used in this setting are either linear or stem-looped probes.^{13,15} However, more elaborate structures built from DNA can bind and organize multiple probes, and the whole structure used as a single probe entity.^{1,2,9,13,16} Such designs multiplies the intensity observed for a certain event, thanks to the multivalency of DNA nanostructures.² All of this can be achieved while maintaining the compact size necessary for such applications.

In this collaborative work, we fabricate 2D-DNA minimal nanostructures (wireframe triangles and squares) that are cost-effective, compact in size, and ultrabright by carrying multiple fluorescently labeled strands, thanks to their multivalency. The structures are based on a polygon strategy, a design previously developed by our group where they possess multiple single-stranded spots (**Figure AII. 1. A**).¹⁷ These spots are

used to functionalize these structures with fluorescently labeled probe strands, as well as nucleotide-carrying strands. The nucleotide strands will be incorporated into a growing DNA chain being synthesized in the pores where sequencing-by-synthesis is being carried out in the Quantum Si platform. When a base is incorporated, the unique fluorescent signature of that base is signaled by the fluorescent DNA structure connected to it (**Figure AII. 1. B**). Design, assembly, optimization, and validation of the structures as monodispersed and bright probes for nucleotide incorporation is investigated in this appendix.

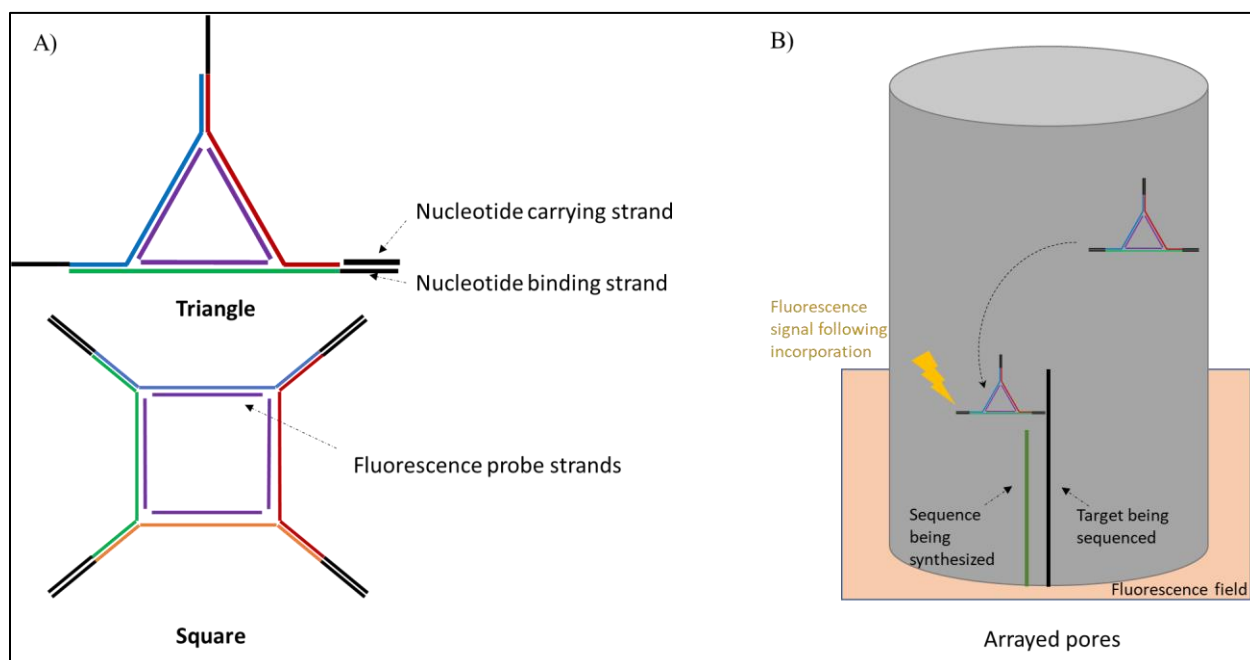


Figure AII. 1. Scheme of the A) the DNA nanostructures developed to incorporate fluorescently labeled strands and nucleotide carrying strands (multiple dye strands are randomly represented with yellow circles) B) sensing system being used: a DNA sequencing of a target (black) is happening by synthesizing its complementary (green). Nucleotides are attached to the fluorescent DNA nanostructures (triangle); when that nucleotide is being incorporated to the growing sequence (green), the triangle enters the fluorescence field (such as total internal reflection evanescent field) and the dyes are excited to emit a fluorescent signal that is being captured to report on the incorporation of that specific nucleotide.

AII.3. Results and Discussion

AII.3.1. Design

To produce triangles and squares from modular strands, we adopted a design developed by our lab, where strands are imagined as sides/arms to the polygons (**Figure AII. 2.**)¹⁷ This design is the same as that used in Appendix I, with small changes. These strands have 5' and 3' regions that are 15bp long and clip onto other strands with complementary sequences on their extremities. On the 5' end of each strand, there is a dithymine (TT) spacer followed by a complementary sequence that will hybridize to nucleotide-carrying strand (nuc). The middle part of these strands is encoded with the sequence that hybridizes to the strand that carries multiple fluorophores (e.g., cyanine dyes), which is synthesized and provided by Quantum Si. 3 arms coming together will yield a triangle with 3 nuc and 3 dye strands called T, and 4 arms coming together will yield a square with 4 nuc and 4 dye strands called S1 (**Figure AII. 2.**).

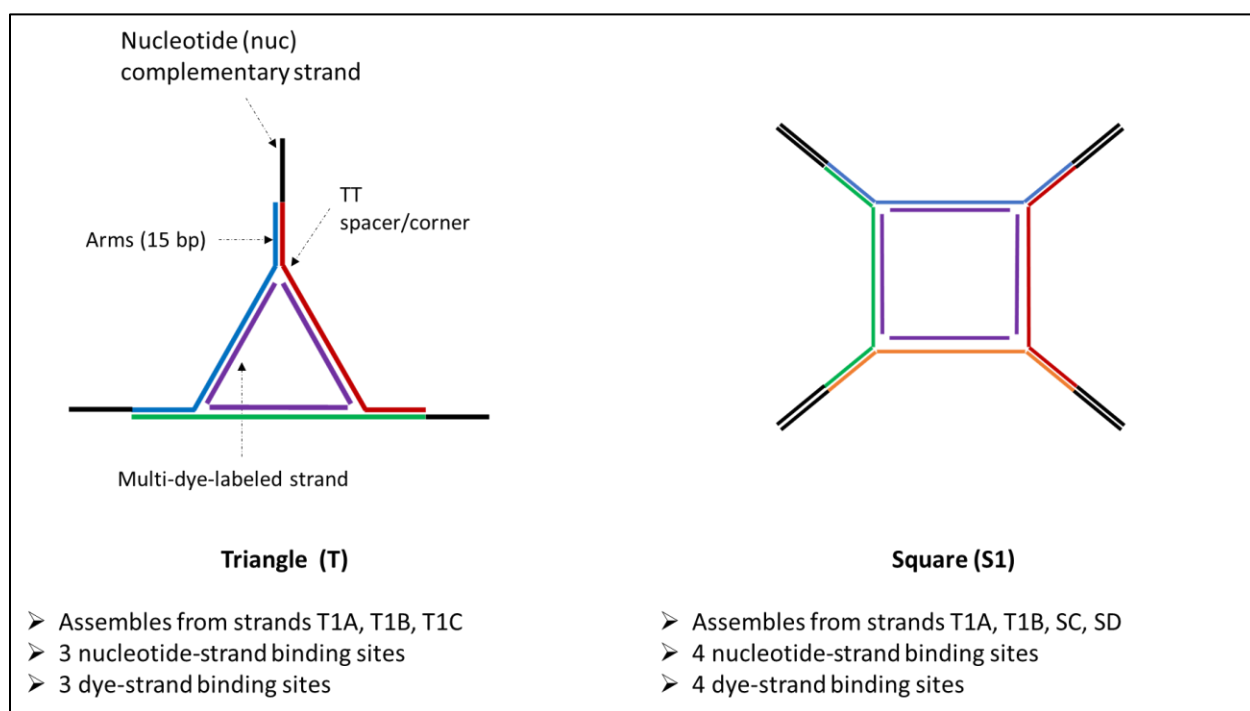


Figure AII. 2. Design of triangle and square that can carry multiple fluorescent probes

AII.3.2. *Assembly optimization and sequencing with triangle*

First, we started by testing the assembly of the triangle and optimizing the conditions. We started by checking if we can assemble the triangle that binds to 3 strands that simulate the dye strands but lack the dye, called “D” strands. To test the assembly, we performed sequential ladder assembly where strands are added one after another to form the structure as previously described in AII. We also tested in this gel if we can get the fully assembled structure without annealing compared to the annealed sample, as well as checking the stability of the structures following 3-day storage post annealing (**Figure AII. 3.**). The gel shows that the assembly of the triangle is much cleaner with annealing (**Figure AII. 3.**) and wasn't impacted following a 3-day storage. In addition, since all 3 triangle strands share the same sequence that binds D, when we add 1 equivalent of D (lane 4) we get a range of 1-bound to 3-bound, and once we add 3 equivalents, we form the final fully double stranded triangle product (lane 5).

This indicated to us that the desired triangular structure is formed, better assembled when annealed, and the cavity can be loaded with the target complementary sequence in all 3 binding sites.

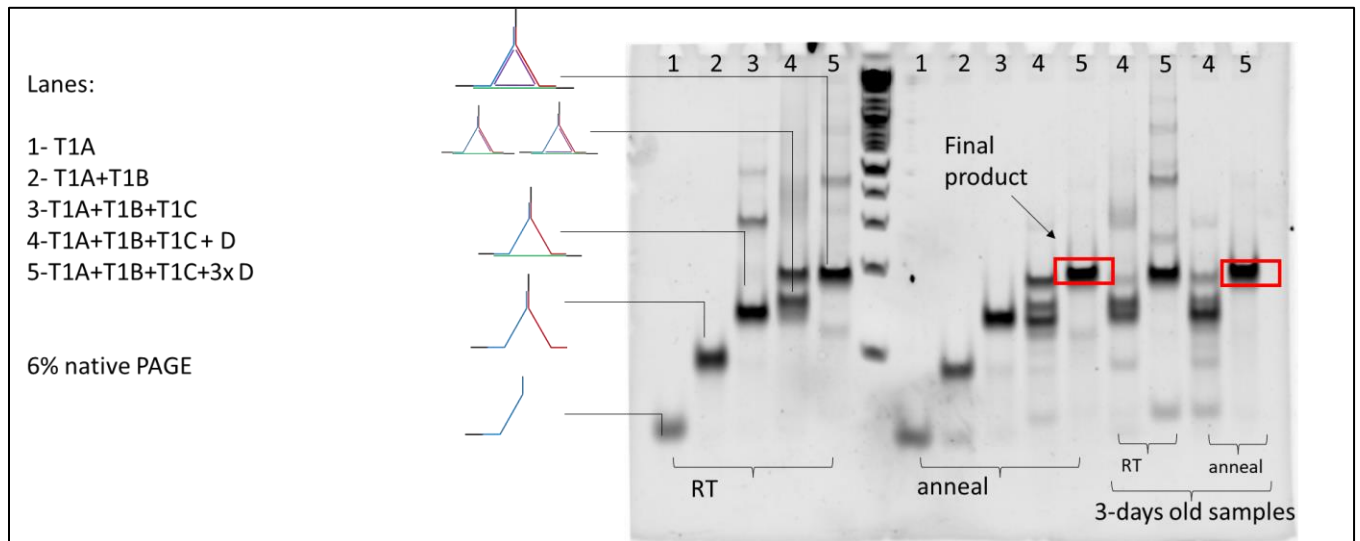


Figure AII. 3. 6% Polyacrylamide native gel showing the sequential assembly of triangle and its loading with D strands at 1 μ M, under different conditions (RT= room temperature, annealed, following 3-day storage at 4 degrees after annealing). samples ran for 1.5 hr at 130V in 1xTAMg.

We then tested the addition of a model nuc strand, that represents the strand holding the nucleotide (but without it). The data showed that the triangle is decreasing in mobility with increasing equivalents of the nuc strand, where it reaches the final product of 3x nuc strand on the triangle in lane 4 (**Figure AII. 4.**)

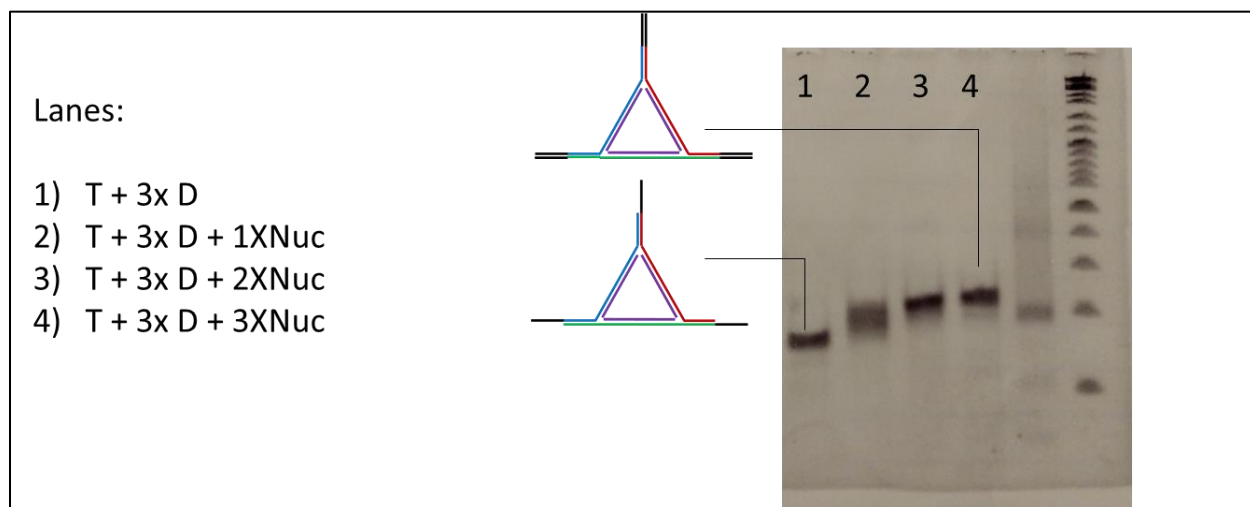


Figure AII. 4. Loading triangle with nuc strands sequentially. 6% Polyacrylamide native gel showing the sequential assembly addition of nuc strands to the triangle at 1uM. Samples were annealed for 2 hours and ran for 1.5 hr at 130V in 1xTAMg.

Following this, we tested the assembly with strands containing the dyes. Quantum Si provided two strands with two different dyes: Q3 and Q4. The structures are not disclosed due to IP purposes. . In this assembly test, we added 3 equivalents of either dye strands to the triangle, at room temperature or annealed with the triangle strands (lanes 1,2,3 for Q3 and lanes 4,5,6 for Q4) and showed that annealing the dye strand with the triangle is more efficient. (**Figure AII. 5 A**). Moving forward, annealing of the dye strands was the method used to form the labeled structure.

We also assembled the triangles with 3 equivalents of the internal strands but varied the number of fluorophores present. We assembled triangles with 1 equivalent Q3/Q4 and 2 equivalents non-labelled D (1/3 labeled strands) (lanes 8,9) and compared its fluorescence signal to that with 3 equivalents of labeled strands (3/3 labeled strands) triangles (lane 3,6). In both triangles loaded with 3 equivalents of the dye strand, we see around 2.4x increase in fluorescent output (expected 3x increase), indicating that as part of the triangle compact structure we still achieve increased fluorescent signal with small amount of quenching as expected due to proximity (**Figure AII. 5. B**).

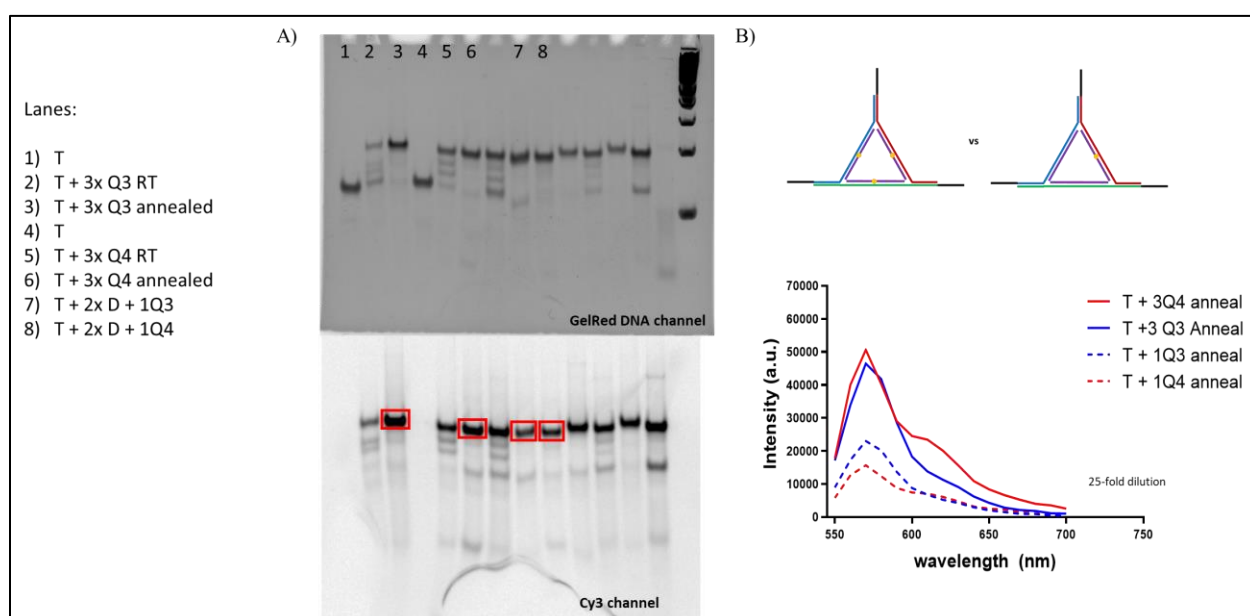


Figure AII. 5. A) 6 % Polyacrylamide native gel showing the assembly of the triangle with fluorescently labeled probe strands Q3 and Q4 at various conditions. **B)** the fluorescent signal increase between a triangle containing 1 labeled strands vs 3 labeled strands, measured on a fluorescence plate reader following 25-fold dilution of 1 μ M samples (n=2). Yellow circles indicate the strands that are labeled with fluorescent dyes.

Following this, we moved to functionalizing the fluorescently labeled strands with the nucleotide carrying strands that are provided by Quantum Si where dC carries a cytosine nucleotide and dG carries guanosine nucleotide.

The assembly test below shows the decreasing mobility of the fluorescently labeled triangle as we add the dC strand to it. However, we needed to add excess copies dC strand to push the assembly of the triangle from carrying 1 or 2 dC strands to 3 dC carrying triangle. The amount sufficient to fully assemble the triangle with 3 nucleotide carrying strands was in between 2:1 and 3:1 nuc strand:triangle ratio (after adding 3:1 ratio, not much change was observed on the gel, lane 5). This could be due to steric hinderance around the triangle with these relatively large moieties and adding excess of the nucleotide carrying strands will require purification of the sample from any excess to avoid interference with the sequencing data. Having leftover nucleotides in the sample that are not coupled to a fluorescent probe to signal its incorporation, can lead to an incorporation that is not fluorescently reported and hence showing up as a deletion in the sequencing run.

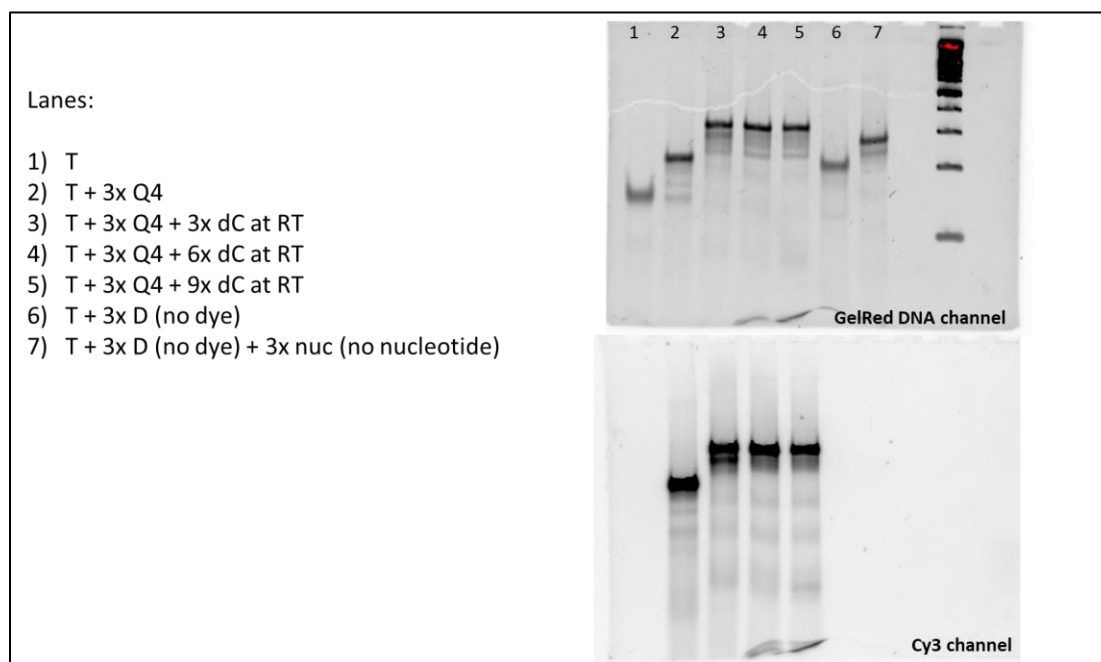


Figure AII. 6. testing the assembly of fluorescently labeled triangle (Q4) with nucleotide functionalized strands (dC). 6 % Polyacrylamide native gel showing the mobility shift of various samples listed in the figure. Samples were annealed for 2 hours at 1 μ M and ran for 1.5 hr at 130V in 1xTAMg.

This indeed is what the Quantum Si team saw, where there was successful incorporation of the structure and roughly around 3x the increase in fluorescent intensity

in comparison to a control that carries 2 fluorescent dyes. However, they also saw slightly increased deletions in the incorporation of dC when it is tagged to a Q3 labeled triangle, and dG when it is tagged to a Q4 labeled triangle.

From this optimization study, we conclude that to get a high yield monodisperse triangle, we will likely need to anneal the dye labeled strands with the triangle assembly strands and excess nucleotide carrying strands at room temperature. We also will need to get rid of any excess non-assembled strands to eliminate their interference with the sequencing process.

AII.3.3. Square 1 (S1) assembly

Much of the assembly conditions developed from the triangle optimization are applied to the square, where the dye strands are annealed with the assembly strands, and the nucleotide carrying strands are added in excess (a little more than 2:1 ratio). To test this, we performed the following test on assembling the square by itself, with dye strands, and with nucleotide strands. The gel below (**Figure AII. 7.**) shows that the square requires excess dye strands (more than 4 copies), as 1:1 dye strands: square (lanes 2,8) showed a secondary faster mobility band right below the fully assembled product (lane 3,9). As for the nucleotide strand addition to the square, we also noticed a secondary band below the final desired product band (lane 4,9), which got fainter with excess nucleotide strand (lanes 5,6,10,11). We also tested annealing the nucleotide strand with the structure which didn't impact the assembly much (lanes 7 and 12).

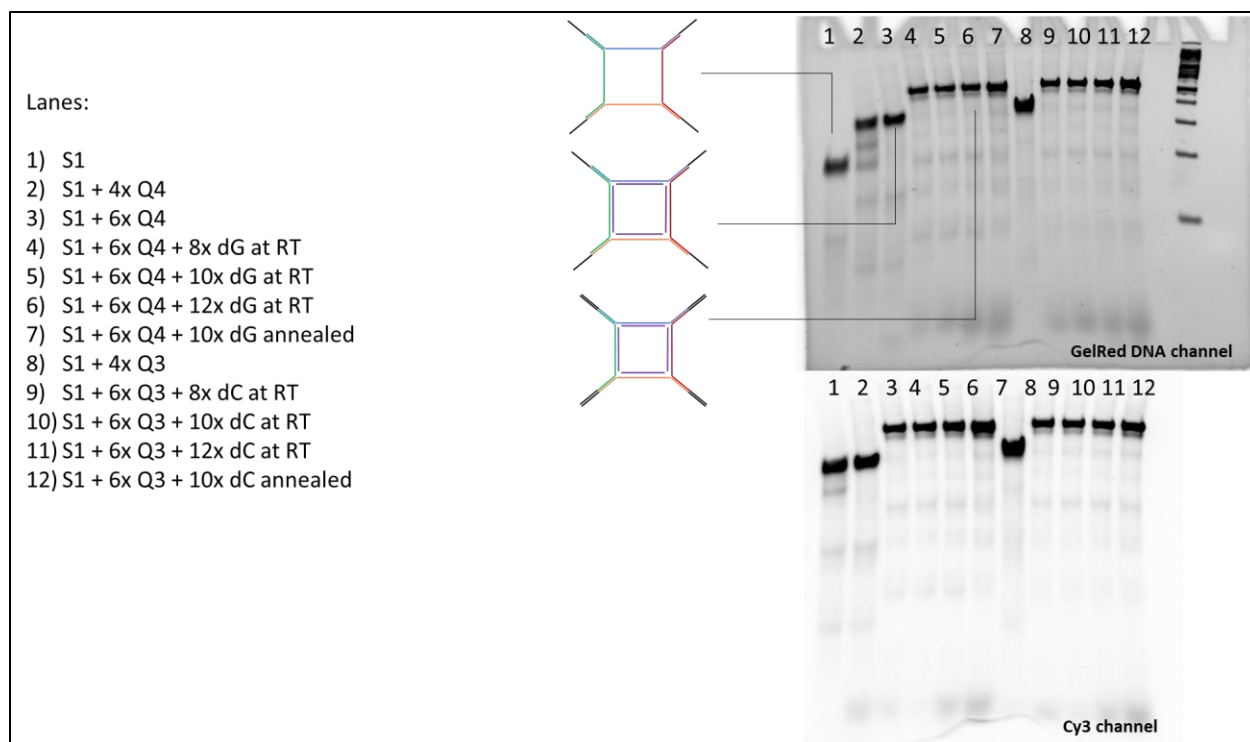


Figure AII. 7. Testing the assembly of the square S1 design with dye and nucleotide strands. 6 % Polyacrylamide native gel showing the mobility shift of various samples listed in the figure. Samples were annealed for 2 hours at 1.5 μ M and ran for 1.5 hr at 130V in 1xTAMg.

This indicates that even a larger structure in the square compared to the triangle, still requires excess of the functionalizing strands due to the sterics inherited from the functional moieties they carry (nucleotide or dye). This was not evident when we tested the triangle with Nuc strand that does not carry the functional moiety on it. Nonetheless the S1 structure adds 4 copies of dye strands, 1.3x more than the triangle, which gives even a higher intensity in sequencing as seen by Quantum Si. Hence after confirming its assembly carrying the fluorescent strands and nucleotide strands, we will focus on it next, where we aim to resolve the leftover excess strands issue.

AII.3.4. Eliminating excess strands by centrifugation filtration

To tackle the issue of leftover strands that are a result of adding excess amounts to push the assembly to completion, we decided to do purify our target structure via separation and isolation based on size (details of method not disclosed due to IP). This will allow us to separate the fully assembled S1 structure from the excess smaller-size molecules. For this, we loaded our samples not only on a 6% native polyacrylamide gel, but also on a 10% gel, to be able to visualize the elimination of the smaller size strands and see if they are retained or removed following this purification strategy.

As evident by the data below (**Figure AII. 8 A**), the square S1 was assembled better when there were excess dye strands (lane 5,10) compared to equimolar dye strands (lane 2,7), using either Q3 or Q4 labeled strands. Following one round of purification, the squares retained their structure as there was no evident deformation of the band even when they were 5 times more concentrated (lanes 3, 6, and 12 in 6% native gel, **Figure AII. 8 A**). If we look at the 10% native gel (**Figure AII. 8 B**) we see that the excess strands indicated by the arrows (blue, orange, and yellow) disappeared following filtration (lanes 3,3', 6, 12,12'). Only in the case of square with Q4 following re-dilution (6') we see an

appearance of the labeled strand as excess (red arrow) which could indicate that it is losing fluorescent strands after re-dilution as lane 6 did not show any excess.

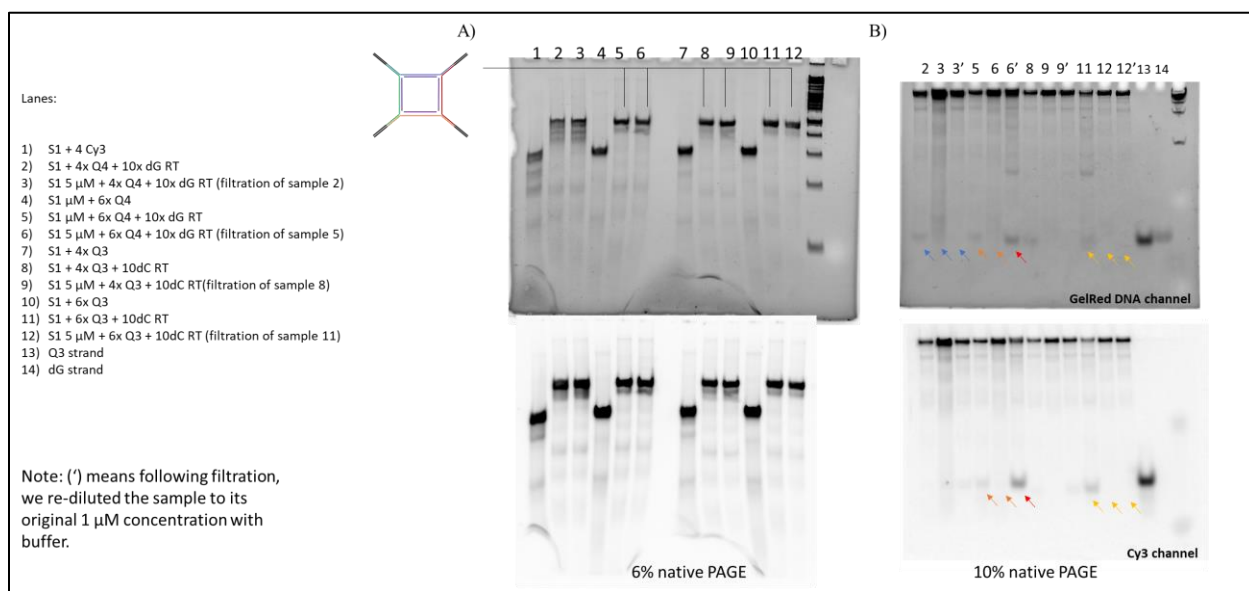


Figure AII. 8. Testing the ability to clean up the square S1 assembly sample by size-exclusion centrifugation filtration by checking assembly on A) 6% native polyacrylamide gel, and B) 10% native polyacrylamide gel to check removal of excess strands. Samples were annealed for 2 hours at 1.5 μ M and ran for 1.5 hr at 130V in 1xTAMg. filtered samples are purified based on size. Samples indicated with “'” are resuspended to their original volume and concentration using 1xTAMg buffer. Cy3 channel is used to image the fluorescently labeled samples.

When these samples were tested by the Quantum Si team for sequencing, the filtration procedure decreased the deletion rate observed, confirming our hypothesis that the release of the nucleotide containing strand from the labeled structure is causing the high deletion rate due to incorporation without signaling. Nonetheless, there were still considerable deletion events compared to the control probes.

AII.3.5. Design of Square 2 (S2) for lower deletion rates

To try to mitigate the deletion issue, we tried to resolve the issue by introducing modifications to our square design. We believe that the deletion rate is high due to need of

excess nucleotide carrying strand to fully functionalize the square. For that, we designed a new square S2. S2 has only 1 arm that binds a nucleotide carrying strand, compared to 4 in design S1. This strategy will hopefully eliminate the need for excess nucleotide carrying strands as there is no crowding anymore with 4 strands (**Figure AII. 9.**).

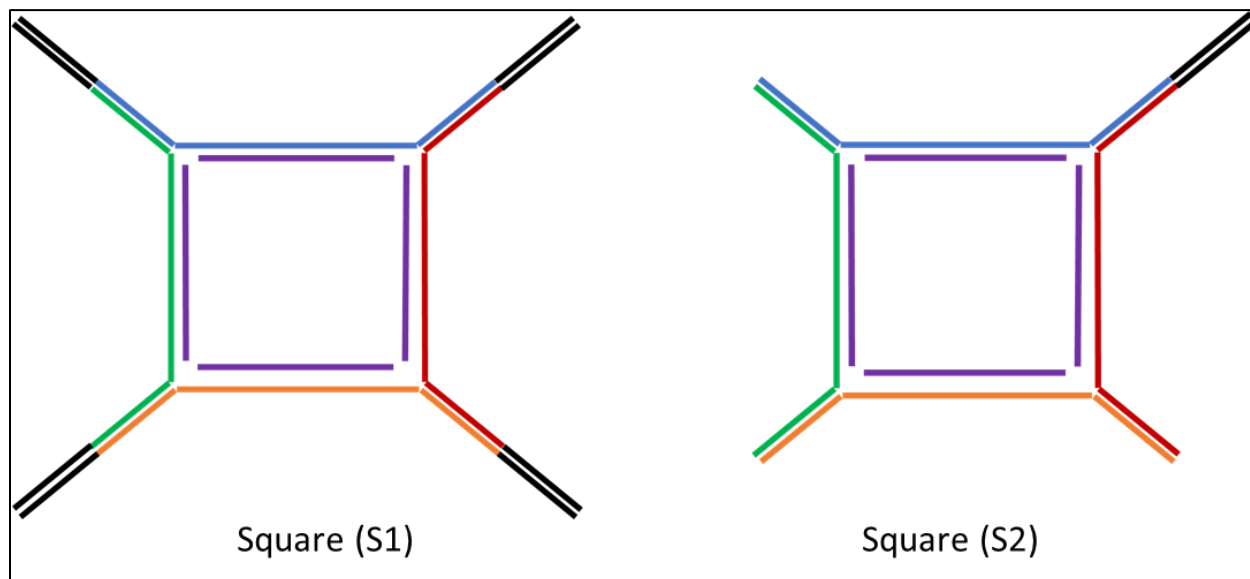


Figure AII. 9. Difference in design between S1 and S2. S1 has 4 regions to bind 4 nucleotide carrying strands, while S2 can only bind one nucleotide strand.

When we tested the assembly of S2 in the best conditions (6x dye strand annealed, 2x nucleotide strand at room temperature) and followed by purification, we obtained the cleanest assembly band of a structure out of all the samples we tried (**Figure AII. 10.**). When this sample was submitted to sequencing, it had a lower deletion rate than S1.

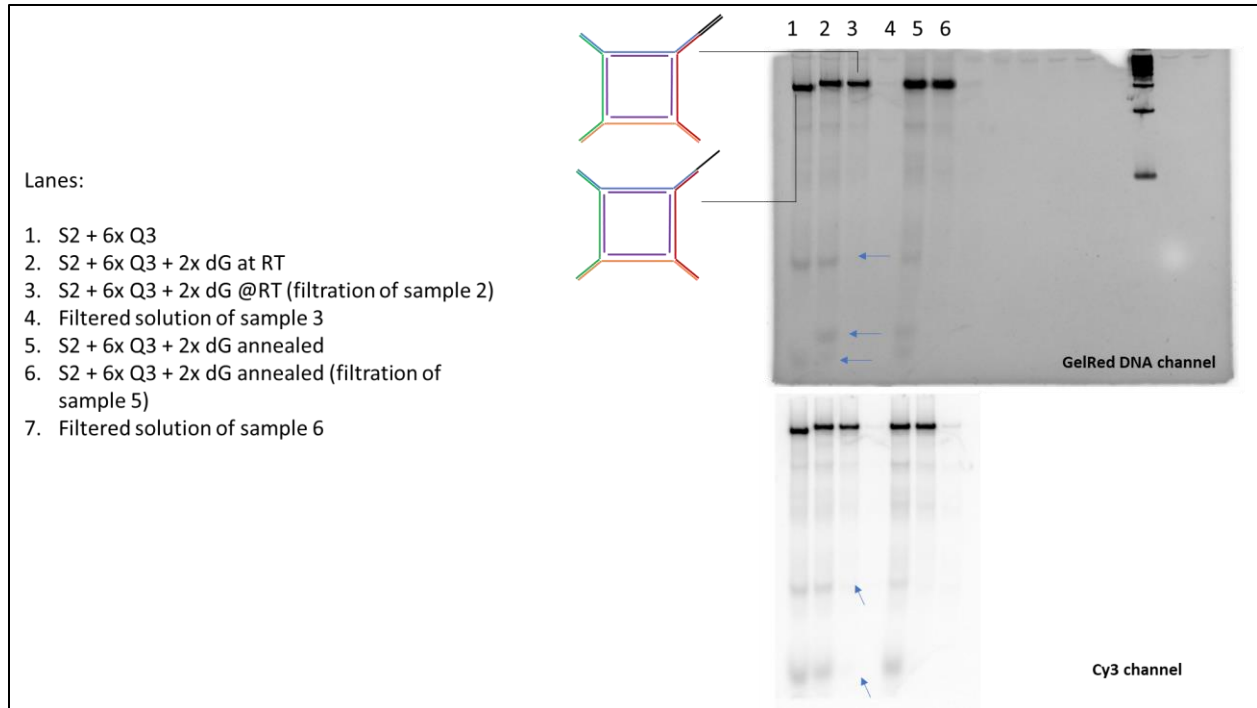


Figure AII. 10. Testing the assembly of Square 2 design, where it carries only 1 nucleotide strand. Samples were annealed for 2 hours at 1.5 μ M and ran for 50 mins at 130V in 1xTAMg. Lane 7 is the eluted buffer from sample 6.

AII.4. Conclusion

In this work, we take advantage of the modularity of the DNA minimal nanostructures produced in Appendix I and redesign them to carry multiple fluorescent strands rather than therapeutics. The multivalency of such structure as well as their compactness finds applications in biosensing as displayed here, where they are designed to produce an ultra-bright fluorescent signal to report on the sensing of biological phenomena (e.g., incorporation of nucleotide into a growing DNA strand being synthesized). This is applied to next generation sequencing methods, where sequencing by synthesis is one modality. In this specific example, the incorporation of a nucleotide is being reported by the production of fluorescence signal that is amplified by the multi-functionalized DNA nanostructures.

We showed that we can expand the multivalency of these structures by going from a triangle to a square that adds 4 dye strands but is still compact and compatible with the array system developed by Quantum Si. In fact, we even recycled 2 of the triangle strands into the design of the square, which is a cost-effective strategy desired for such industrial applications.

There were challenges in decorating the structures with multiple copies of dye strands and nucleotide carrying strands due to their bulkiness, but that was achieved by adding excess strands followed by purification of the sample. Other future directions to avoid this issue is to redesign the structures to have more steric relief on their corners. This could be achieved by increasing the spacer units in between the regions of hybridization of the assembly strands. This work is ongoing, and we are currently testing longer spacer nucleotides and new designs.

AII.5. Experimental

AII.5.1. Oligonucleotide synthesis, purification, and assembly

Oligonucleotide synthesis was performed on a 1 μ mol scale, starting from a universal 1000 Å LCAA-CPG solid-support, on a Mermade 6/12 synthesizer protocols. Strands were deprotected and cleaved with a solution of 28% aqueous ammonium hydroxide solution for 20 hours at 60°C, followed by drying under vacuum at 60°C, and resuspended in Millipore H₂O. Sequences were purified on polyacrylamide/8M urea gel electrophoresis at constant current of 30mA for 1.5 hour (30 min at 250 V followed by 1 hour at 500 V), using the 1x TBE buffer (90 mM Tris, 90 mM boric acid, 2 mM EDTA and the pH is adjusted to 8.0). Following electrophoresis, the plates were wrapped in plastic and placed on a fluorescent TLC plate and illuminated with a UV lamp (254 nm). The bands were quickly excised, and the gel pieces were crushed and incubated in 12 mL of sterile water at 60°C for 12-16 hours. Samples were then dried to 1.0 mL, desalted using size exclusion chromatography (Sephadex G-25), and carefully quantified using UV-Vis spectroscopy (260 nm). Samples were loaded on a 12% polyacrylamide gel in 1X TBE buffer (30 min, 250 V, 1 hour 500 V) and stained with GelRed™. Some strands were ordered from IDT without purification, followed by purification as mentioned above.

To assemble structures, samples were mixed at the desired concentration in Tris-acetic acid-magnesium buffer (1x TAMg buffer, 45 mM Tris, 20 mM acetic acid and 7.6 mM Mg(Cl)₂, pH was adjusted to ~8.0 using glacial acetic acid), diluted with milliQ water, and annealed from 95 to 5 °C over 2 hours using Bio-Rad T100™ thermal cycler.

Concentration of samples and purification was done with size-based separation methods. Details of method are not shown due to pending IP filing. .

The sequences used in this work are tabulated below. NNN are nucleotides that are complementary to the dye strands, and MMM are nucleotides complementary to the nucleotide strands:

	Strand	Sequence (5' to 3')
Triangle assembly	T1a	(MMM)m TT TCGCTTCTAGGAGAT TT (NNN)n TT CTTCAACTTCACAC
	T1b	(MMM)m TT GTGTGAAGTTGAAAG TT (NNN)n TT GTGATGTCATCAATG
	T1c	(MMM)m TT CATTGATGACATCAC TT (NNN)n TT ATCTCCTAGAAGCGA
Square 1 assembly (S1)	T1a	(MMM)m TT TCGCTTCTAGGAGAT TT (NNN)n TT CTTCAACTTCACAC
	T1b	(MMM)m TT GTGTGAAGTTGAAAG TT (NNN)n TT GTGATGTCATCAATG
	SC	(MMM)m TT CATTGATGACATCAC TT (NNN)n TT CAGCAAACCTTACTC
	SD	(MMM)m TT GAGTAAGTTTGCTG (NNN)n TT ATCTCCTAGAAGCGA
Square 2 assembly (S2)	T2A	TCGCTTCTAGGAGAT TT (NNN)n TT CTTCAACTTCACAC
	T2B	GTGTGAAGTTGAAAG TT (NNN)n TT GTGATGTCATCAATG
	SC	(MMM)m TT CATTGATGACATCAC TT (NNN)n TT CAGCAAACCTTACTC
	S2D	GAGTAAGTTTGCTG TT (NNN)n TT ATCTCCTAGAAGCGA
Functionalizing strands	D-strand	(NNN)'n
	Nuc-strand	(MMM)'M

Table AII. 1. Table containing all the sequences used in this appendix. Similar color-highlighted sequences are complementary to each other. (NNN)n represents the sequence complementary to the dye strands, and (MMM)m represents that complementary to the nucleotide strands

AII.5.2. Gel electrophoresis characterization of structures

Assembled structures were loaded on Native Polyacrylamide gel (PAGE) (6-10%) in 1X TAMg at a constant voltage of 130V for 1.5 hours. Roughly around 2pmoles of strands were ran on the gel, mixed with loading dye and buffer.

AII.5.3. Fluorescence spectroscopy

Fluorescence measurements were performed on a SpectraMax i3x Multi-Mode plate reader. Samples were diluted 25-fold from the 1 μ M assembly in 1x TAMg buffer to a final volume of 50 μ L. Measurements were performed at 25 °C (room temperature) in a 384-well plate.

A1.6 References

- 1 Fu, S. *et al.* DNA nanotechnology enhanced single-molecule biosensing and imaging. *TrAC Trends in Analytical Chemistry* **140**, 116267, doi:<https://doi.org/10.1016/j.trac.2021.116267> (2021).
- 2 Seeman, N. C. & Sleiman, H. F. DNA nanotechnology. *Nature Reviews Materials* **3**, 17068, doi:10.1038/natrevmats.2017.68 (2017).
- 3 Adleman, L. M. Molecular Computation of Solutions to Combinatorial Problems. *Science* **266**, 1021-1024, doi:10.1126/science.7973651 (1994).
- 4 BATH, J. & TURBERFIELD, A. J. in *Nanoscience and Technology* 124-133.
- 5 LaBoda, C., Duschl, H. & Dwyer, C. L. DNA-Enabled Integrated Molecular Systems for Computation and Sensing. *Accounts of Chemical Research* **47**, 1816-1824, doi:10.1021/ar500054u (2014).
- 6 Wang, F., Liu, X. & Willner, I. DNA Switches: From Principles to Applications. *Angewandte Chemie International Edition* **54**, 1098-1129, doi:<https://doi.org/10.1002/anie.201404652> (2015).
- 7 Raveendran, M., Lee, A. J., Sharma, R., Wälti, C. & Actis, P. Rational design of DNA nanostructures for single molecule biosensing. *Nature Communications* **11**, 4384, doi:10.1038/s41467-020-18132-1 (2020).
- 8 Spruijt, E., Tusk, S. E. & Bayley, H. DNA scaffolds support stable and uniform peptide nanopores. *Nature nanotechnology* **13**, 739-745 (2018).
- 9 Lim, X. The architecture of structured DNA. *Nature* **546**, 687-689 (2017).
- 10 Fu, J. *et al.* Multi-enzyme complexes on DNA scaffolds capable of substrate channelling with an artificial swinging arm. *Nature Nanotechnology* **9**, 531-536, doi:10.1038/nnano.2014.100 (2014).
- 11 Zhang, H. *et al.* DNA origami-based shape IDs for single-molecule nanomechanical genotyping. *Nature communications* **8**, 1-7 (2017).
- 12 Johnson-Buck, A. *et al.* Kinetic fingerprinting to identify and count single nucleic acids. *Nature Biotechnology* **33**, 730-732, doi:10.1038/nbt.3246 (2015).
- 13 Pei, H. *et al.* A DNA Nanostructure-based Biomolecular Probe Carrier Platform for Electrochemical Biosensing. *Advanced Materials* **22**, 4754-4758, doi:<https://doi.org/10.1002/adma.201002767> (2010).
- 14 Heller, M. J. DNA Microarray Technology: Devices, Systems, and Applications. *Annual Review of Biomedical Engineering* **4**, 129-153, doi:10.1146/annurev.bioeng.4.020702.153438 (2002).
- 15 Fan, C., Plaxco, K. W. & Heeger, A. J. Electrochemical interrogation of conformational changes as a reagentless method for the sequence-specific detection of DNA. *Proceedings of the National Academy of Sciences* **100**, 9134-9137, doi:10.1073/pnas.1633515100 (2003).

- 16 Zhang, S. *et al.* A novel fluorescent biosensor based on dendritic DNA nanostructure in combination with ligase reaction for ultrasensitive detection of DNA methylation. *Journal of Nanobiotechnology* **17**, 121, doi:10.1186/s12951-019-0552-5 (2019).
- 17 McLaughlin, C. K., Hamblin, G. D., Aldaye, F. A., Yang, H. & Sleiman, H. F. A facile, modular and high yield method to assemble three-dimensional DNA structures. *Chemical Communications* **47**, 8925-8927, doi:10.1039/C1CC11726B (2011).